PHOTOCHROMIC N,C-CHELATE 4-COORDINATE ORGANOBORON COMPOUNDS

by

Hazem Amarne

A thesis submitted to the Department of Chemistry

In conformity with the requirements for

the degree of Doctor of Philosophy

Queen's University

Kingston, Ontario, Canada

(August, 2011)

Abstract

The objective of this thesis is to prepare new photochromic N,C-chelate four-coordinate organoboron compounds and investigate their photophysical and photochemical properties.

Phenylpyridine-based organoboron compound ($PhPyBMes_2$) was prepared and studied with NMR, X-ray, and UV-Vis. Experimental and theoretical results established that $PhPyBMes_2$ is photochromic and the photoisomerization process involves a reversible intramolecular C-C bond formation/breaking. The structure of the dark colored isomer of $PhPyBMes_2$ was established by 2D NMR experiments and computational studies. The discovery of the photochromic behavior of $PhPyBMes_2$ led to the investigation of other phenylpyridine-based organoboron compounds.

A series of substituted $PhPyBMes_2$ compounds were synthesized with substituents on the phenyl ring or the pyridine ring of the N,C-chelate. Two other compounds were synthesized by substituting the mesityl rings in $PhPyBMes_2$ with phenyl or pentaflurophenyl rings. The photophysical and photochemical properties of these compounds were studied by NMR, UV-Vis, and DFT/TD-DFT. The studies established that the steric hindrance imposed by the mesityl groups and the nature of substituents on the N,C-chelate have substantial effects on the photoisomerization process.

New organoboron compounds based on N,C-chelates other than phenylpyridine were prepared and their photochemical and photophysical properties studied using NMR, UV-Vis, and DFT/TD-DFT. The phenyl group in the N,C-chelate was replaced by TMS-furan, TMS-thiophene, benzofuran, benzothiophene, and N-phenyl pyridylindole groups.

The conducted studies show that these new compounds have photochromic properties similar to those of phenylpyridine-based compounds. Crystals of the dark isomer of the N-phenyl pyridylindole organoboron compound were successfully grown and the structure of the dark isomer was determined by X-ray diffraction.

New organoboron compounds based on phenyl-benzoxazole and phenyl-benzothiazole have been also prepared and studied. The photoisomerization of these compounds is similar to the other N,C-chelate organoboron compounds but their thermal behavior is different.

Acknowledgements

I would like to sincerely thank my supervisor, Dr. Suning Wang for giving me the chance to be a member of her group; it was a real privilege to work in her lab. Her guidance, support, and patience during my Ph.D studies were unlimited and for that I am so grateful. Her constant dedication and enthusiasm for organoboron chemistry was very inspiring for me and made this project very enjoyable. I would also like to thank her and her husband Dr. Kai Salomma for their hospitality and generosity during dinner and barbeque invitations at their house.

I would also like to thank my research committee members Dr. Donal Macartney and Dr. Anne Petitjean for their help, advice, and valuable time towards my research and thesis. Thanks also goes to Dr. Rui-Yao Wang for his help with X-ray crystallography, Dr. Francoise Sauriol for all of her help in training me and helping me to run NMR experiments, Dr. Jiaxi Wang for his help with mass spectrometry, and Dr. Jean-Michel Nunzi for reading my thesis and for providing access to his lab to perform actinometry experiments. Many thanks go to the department of chemistry staff for all their support and help. I am also grateful to all the members of the Wang group, past and present, for sharing their experience and knowledge and for their friendship during the past four years. Financial support from the Department of Chemistry and Queen's University is also gratefully acknowledged.

Finally, I would like to thank my parents, brothers, sisters, and fiancée, for their unlimited and unconditional support all these years.

Statement of Originality

I hereby certify that all of the work described within this thesis is the original work of the author carried out under the guidance and supervision of Prof. Suning Wang with the following exceptions. Dr. Chul Baik synthesized compounds **3.3**-**3.6**, which he also partially characterized. Any published (or unpublished) ideas and/or techniques from the work of others are fully acknowledged in accordance with the standard referencing practices.

(Hazem Amarne)

(August, 2011)

Table of Contents

List of Tables

List of Figures

List of Symbols and Abbreviations

Å	angstrom
Abs.	absorbance
Anal	analysis
B3LYP	Becke 3-parameter exchange, Lee, Yang and Parr
c	concentration
calcd	calculated
cm	centimeters
CH_3CN	acetonitrile
CH_2Cl_2	dichloromethane
COSY	correlation spectroscopy
CV	cyclic voltammetry
d	doublet
DCM	dichloromethane
dd	doublet of doublets
DFT	density functional theory
DME	dimethoxyethane
DMF	dimethylformamide
EL	electroluminescent
EML	emitting layer
ETM	electron transport material
eV	electron volt

FG	functional group
FWHM	full width at half maximum
Hz	hertz
HMBC	heteronuclear multiple bond correlation
HOMO	highest occupied molecular orbital
HRMS	high resolution mass spectrometry
HTM	hole transport material
ISC	intersystem crossing
J	coupling constant
K	Kelvin
l	path length
LUMO	lowest unoccupied molecular orbital
m	meter, multiplet
M	molar
mA	milliampere
Mes	mesityl
mg	milligram
MHz	megahertz
mL	milliliter
mmol	millimole
MO	molecular orbital
mol	mole

nm	nanometers
NMR	nuclear magnetic resonance
NOESY	Nuclear overhauser effect spectroscopy
OLED	organic light emitting diode
Ph	phenyl
RT	room temperature
s	singlet (NMR), seconds
t	triplet
TBAF	tetra-n-butylammonium fluoride
td	triplet of doublets
THF	tetrahydrofuran
TLC	thin layer chromatography
UV	ultraviolet
UV-Vis	ultraviolet-visible
δ	chemical shift
λ	wavelength
Φ	quantum efficiency
Φ_F	fluorescence quantum efficiency

Chapter 1

Introduction

Organic optoelectronic materials are a very important class of materials, mainly due to their potential applications in OLEDs[1], solar cells[2], and sensors[3]. Researchers in the fields of chemistry, physics, materials sciences, nanotechnology, and electrical engineering have been focusing on the fabrication of the device and the basic science behind it. Among the wide range of organic optoelectronic materials, OLEDs are gaining huge commercial interest which is driven by the worldwide market demand[4]. Currently, OLEDs-based flat panels, mp3 player's screens, cell phone screens, and many more are being sold in the market. Some of the main advantages of OLEDs, compared to the traditional display devices, are: (1) Efficient energy consumption since OLED emits the light and doesn't need a backlight (2) Thinner panels, which means lighter weight, e.g. Sony's XEL1 11" OLED digital television is 3mm thin (3) High brightness, very high contrast ratios and wide viewing angles. On the other hand, the main disadvantage of OLEDs is their relatively higher prices compared to their liquid crystal display (LCDs) counterparts. Nevertheless, one of the most sought goals in the OLEDs technology nowadays is to make them better candidates for efficient and low-cost optoelectronics. In this perspective, chemists have been contributing significantly in the OLED technology, mainly via (1) synthesis of new compounds or polymers leading to higher fluorescence

quantum yields (2) providing scalable and simple synthetic methods (3) optimizing the stability of these compounds in order to maximize the life time of the device.

OLEDs are based on electroluminescence (EL), which is a process where visible light is generated via electrical excitation of molecules and a subsequent radiative relaxation process (light emission). The first organic-based electroluminescence device was reported by Pope and Kallmann in 1963[5], where they demonstrated the use of anthracene crystals as an emitter layer, but the device fluorescence quantum yield (Φ_F) was very low. However, due to the relatively high thickness (20 μm) of the device, high voltages were required. In the following years many devices were fabricated using organic-based molecules or polymers but the problem of thickness vs. high voltages still remained. In 1977 this problem was solved when Kampas and Gouterman[6] fabricated a device using thin organic-based films as emitters, which required only 30 V to operate but at the expense of a lower fluorescence quantum yield (0.05%), but it was not until 1987 when Tang and Van Slyke[7] reported the fabrication of a thin film two-layer device that required only 10 V to produce a fluorescence quantum yield of 1%. Their device consisted of a glass substrate coated with indium-tin-oxide (ITO), which served as the hole-injecting electrode (anode), with two organic layers on top of it: (1) aromatic diamine serving as the hole- transporting layer (HTL) (2) Al(8-hydroxyquinolinate)$_3$ (Alq_3), serving as electron transport layer (ETL) and emissive layer (EML). The top electrode consisted of a magnesium-silver alloy, which served as the electron-injecting electrode (cathode) as shown in Figure 1.1.

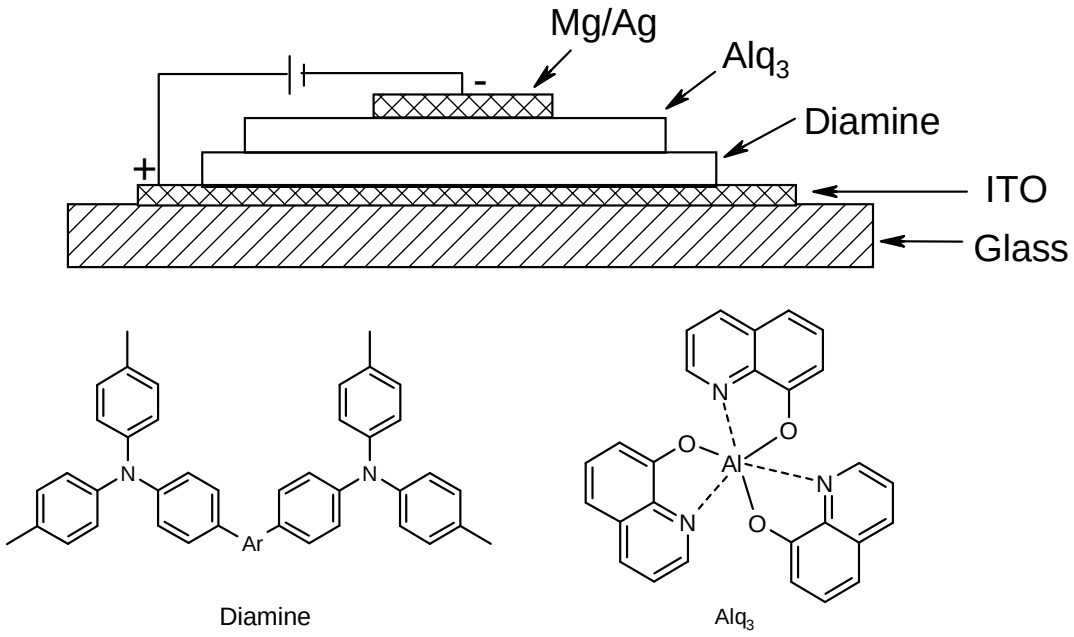

Figure 1.1 Configuration of EL cell and molecular structures of diamine and Alq_3

1.1 4-Coordinate Organoboron Compounds

After the seminal work of Tang and Van Slyke many complexes were synthesized for the same purpose, by replacing Al(III) with other metal ions and by using different chelate ligands[8]. Many of these systems have been studied in our group including those with a boron center instead of a metal. The introduction of the B center generally leads to more covalent character and hence higher stability compared to aluminum compounds. In addition to tridentate ligands, bidentate ligands such as N,O, N,N and N,C are widely used in OLEDs in addition to tridentate ligands.

1.1.1 4-Coordinate Organoboron Compounds with N,O Chelates

The interesting properties of Alq_3 and other derivatives intrigued our group to initiate a study based on the boron analogue BPh_2q (**1.1**). Our group was the first to report these

BPh_2q complexes as OLED materials[9], and subsequently published other reports with modified N,O-chelates[10,11]. They synthesized and studied the photophysical properties of a series of compounds based on quinoline ligand (**1.1**, **1.2**, and **1.3**) as shown in Figure 1.2. When irradiated with UV light, these complexes emit green-blue color at λ_{em} = 495-500 nm. Also, their electroluminescent properties were examined by fabricating EL devices, which were found to have good emission and electron transport properties.

Based on their X-ray diffraction analysis, these N,O organoboron compounds have tetrahedral geometry around boron center. In addition, DFT calculations show that the HOMO is distributed mainly on the phenoxide ring and the LUMO is mainly on the pyridyl ring. They have also shown that, when electron donating groups are attached to the HOMO, the energy of the HOMO increases leading to a red shift in the spectra and when electron donating groups were attached to the LUMO, the energy of the LUMO increased leading to a blue shift.

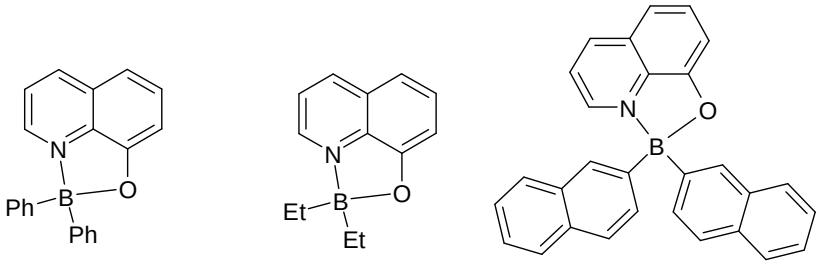

1.1 **1.2** **1.3**

Figure 1.2 Organoboron complexes based on quinoline

Also Lee and co-workers reported N,O-chelate organoboron compounds based on 2-(2-pyridyl)phenol ligand. Compounds **1.4** and **1.5** (Figure 1.3) were prepared by refluxing the pyridyl phenol ligand with triphenyl borane or tris(pentafluorophenyl)borane, respectively, in THF. Based on X-ray structures both compounds had four-coordinate boron centers. While compound **1.4** was formed via a typical bi-dentate chelation, compound **1.5** was mono-dentate. DFT calculations showed that the HOMO-LUMO electronic transitions were ligand-centered with charge transfer from the phenoxide ring to the pyridine ring. The absorption bands in the spectra of these complexes at λ_{max}= 360 and 363 nm, respectively, were assigned to π-π* transitions. Both compounds exhibit bright sky-blue luminescence when exposed to UV light, with λ_{em}= 465 and 485 nm, respectively. The big difference in λ_{em} values compared to λ_{max} values was attributed to the more flexible nature of **1.5**, which might lead to loss of energy in the excited state via vibrational motions. Also, the fluorescence quantum efficiency (Φ_F) values of **1.4** and **1.5**, in chloroform were 0.40 and 0.25, respectively.

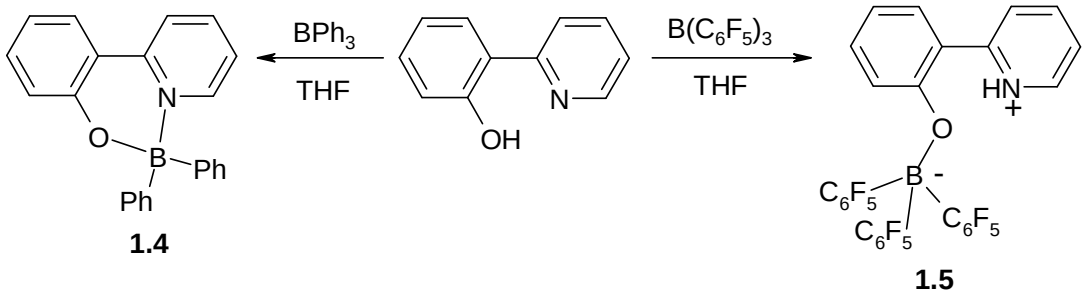

1.4 **1.5**

Figure 1.3 Organoboron complexes based on phenoxy pyridine.

1.1.2 4-Coordinate Organoboron Compounds with N,N Chelates

In this type of compounds, boron is chelated with an N,N ligand, with one of the nitrogens donating its lone pair of electrons in intramolecular fashion. In a series of papers[12-15], our group reported different classes of organoboron compounds chelated with N,N ligands. The boron atom in all cases is bearing two phenyl groups, while the N,N ligands are based on pyridylindole, substituted pyridylindole, pyridyl-7-azaindole, pyridylbenzimidazole, thiazolylindole, 8-quinolylindole, and 8-quinolyl-7-azaindole as shown in Figure 1.4. They have shown that the boron in these complexes is indeed tetra-coordinated with a typical tetrahedral geometry and a coplanar N,N ligand, owing to the intramolecular N-B bond. Based on X-ray data it was found that, the five-membered boron chelates (**1.6**-**1.16**) are more rigid than the six-membered ones (**1.17** and **1.18**). The complexes were found to be stable towards moisture, which was attributed to the presence of the bidentate ligands that saturate the coordination sphere around boron. The main absorption band of these complexes is between 320-390 nm, which was attributed to the ligand-centered π-π^* transitions. All complexes were yellow in color except **1.17** and **1.18** (red and orange, respectively), which showed broad absorption bands in the visible region (360-570 nm). Most of these complexes (**1.6**-**1.16**) exhibited bright luminescent colors in solution (CH_2Cl_2) and in the solid state, ranging from blue to yellowish green. While compounds **1.17** and **1.18** were not luminescent in solution at RT, they exhibited bright red and orange luminescence, respectively, in the solid state and in a poly(vinylcarbazole) matrix. The Φ_F values of **1.6**-**1.16** in CH_2Cl_2 were 0.29, 0.61, 0.33, 0.22, 0.04, 0.32, 0.31, 0.65, 0.60, 0.46, and 0.14, respectively. The HOMO and LUMO

levels for these compounds were assigned using DFT calculations. The HOMO levels for compounds **1.6**-**1.16** were mainly distributed on the (indolyl, 7-azaindolyl, or benzimidazolyl) part of the bidentate ligand. On the other hand, the LUMO levels were mainly composed of the other part of the N,N-chelate. The HOMO levels of complexes **1.17** and **1.18** were distributed over the whole bidentate ligand and their LUMO levels are similar to those of **1.6**-**1.16**. The emission color of the parent compound **1.6** was blue shifted upon the introduction of electron withdrawing groups (Cl, F, N) to the HOMO part of the molecule, which generally leads to stabilization of the HOMO and hence a wider band gap. Upon increasing the number of fluorine substituents from one to four the emission was only shifted from 481 to 467 nm. The only red-shifted emission was observed for compound **1.10**, which has an electron donating group (MeO).

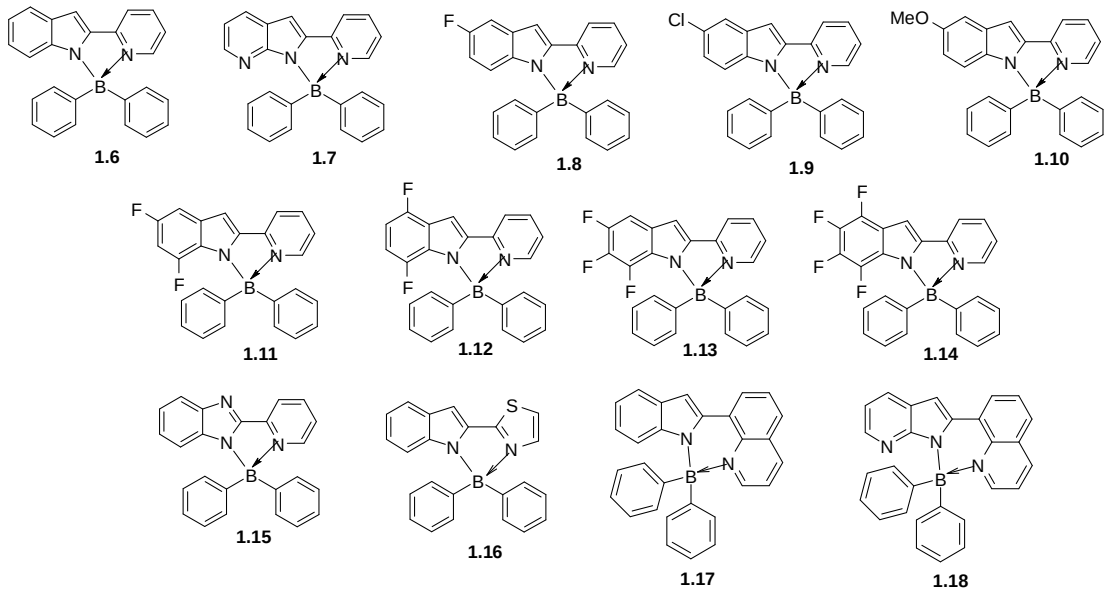

Figure 1.4 Organoboron compounds based on pyridylindole and similar N,N chelates

Also, similar work has been done by Chen and co-workers[16,17] based on naphthoimidazole (Figure 1.5). The HOMO of these complexes was assigned to the imidazole part while the LUMO was assigned to the other part of the bidentate ligand. In dilute DMF solutions ($1x10^{-8}$ M), one emission band was observed for **1.19**, **1.20**, and **1.21** (λ_{em}= 413, 395, and 395 nm, respectively), which was attributed to the ligand-centered π-π* transitions. On the other hand, upon increasing the concentration of these complexes to 10^{-5}M a new red-shifted emission band around λ_{em}= 550 nm appeared, which was attributed to the formation of excimers. When the concentration was further increased (10^{-4} M) the monomer emission band disappeared and only the excimers emission was observed. Also, the Φ_F values of complexes **1.19**, **1.20**, and **1.21** in DMF were 0.8, 0.15, and 0.46, respectively.

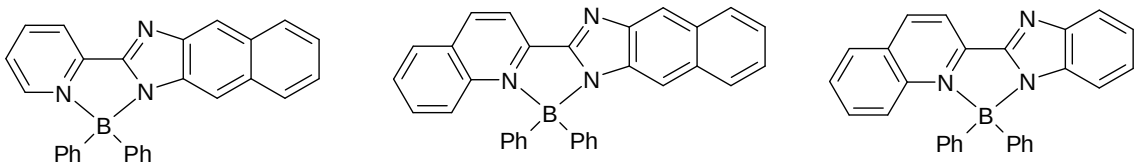

1.19 **1.20** **1.21**

Figure 1.5 Naphthoimidazole-based organoboron complexes

Organoboron complexes based on the pyridylpyrrolide ligand were also reported by Chen *et al.*[18] and others[19]. Chen and co-workers reported the synthesis and photophysical properties of three boron complexes based on this type of ligands (**1.22**, **1.23**, and **1.24**), which are shown in Figure 1.6. The absorption maxima of these

complexes (λ_{max}= 395, 442 and 492 nm, respectively) and the emission maxima (λ_{em}= 490, 510 and 572 nm, respectively) were assigned to π-π* transitions. Also, the HOMO and LUMO were found to be localized on the pyrrolide and pyridine moieties, respectively. In addition, red-shifted absorption and emission were noticed upon increased conjugation and upon the introduction of the electronegative nitrogen atom into the LUMO system, i.e. going from **1.22**, **1.23** to **1.24**. The Φ_F values of **1.22**, **1.23** to **1.24**, in CH_2Cl_2 were 0.52, 0.63, and 0.14, respectively. The lower Φ_F value of **1.24** was attributed to the faster radiationless rate caused by a smaller emission gap, which was supported by the shorter population lifetime for **1.24** (1.9 ns) compared to 11.8 and 8.9 ns for **1.22** and **1.23**, respectively.

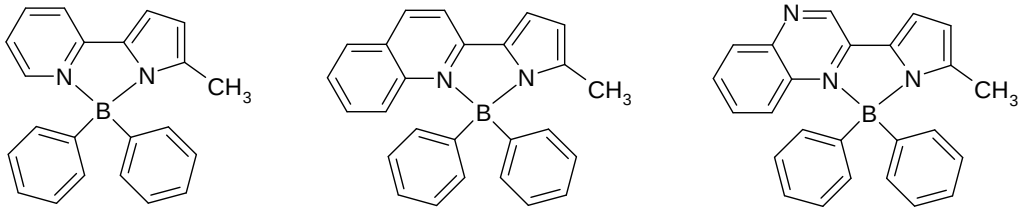

1.22 **1.23** **1.24**

Figure 1.6 Pyridyl pyrrolide-based organoboron complexes

In addition, Gardinier and co-workers[20], reported the synthesis and photophysical properties of a series of 2-pyrazolyl-anilines (Figure 1.7). The stability towards hydrolysis of these complexes was shown to be dependent on the nature of the R group. While compounds with electron withdrawing substituents i.e. **1.29**-**1.31** are very stable in solution or in the solid form, compounds with more electron donating character were much less stable. The X-ray data show that the six-membered ring in these compounds is

puckered and not planar with axial and equatorial phenyl groups on boron. Based on DFT calculations, the HOMO level of these compounds was found to be mainly distributed over the aniline ring including the nitrogen lone pair, while the LUMO was distributed over the pyrazole and the substituted aniline rings. Complexes **1.25-1.31** have intense emission when exposed to a UV light source. The color of emission is in the blue region when R is an electron withdrawing group and yellow-green when R is electron donating group. The Φ_F values of **1.25-1.31** in CH_3CN were 0.002, 0.03, 0.17, 0.51, 0.43, 0.49, and 0.74, respectively. Most interestingly, when the electron withdrawing ability was increased the Φ_F values became higher. This was attributed to the smaller energy gaps in complexes with electron donating substituents, which in turn might lead to increased non radiative decay rates. This was also supported by the excited state life times of **1.25-1.31** (6.0, 7.5, 6.3, 8.8, 10.5, 15.9, 10.5 ns, respectively).

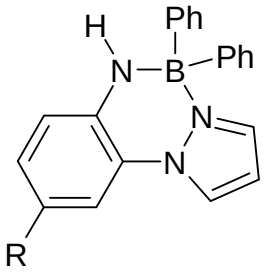

	R
1.25	OMe
1.26	Me
1.27	H
1.28	Cl
1.29	CO_2Et
1.30	CF_3
1.31	CN

Figure 1.7 2-Pyrazolyl-aniline based organoboron complexes

Most of the reported organoboron N,N chelates have a BPh_2 moiety because of the relatively easier synthetic route, where BPh_3 is refluxed with the N,N chelate ligand. In addition, the emission color of these complexes can be easily tuned by manipulating

the energy gap between the HOMO and LUMO. If a red shift is desired the energy gap has to be decreased, which can be done either by attaching electron donating groups to the HOMO or attaching electron withdrawing groups to the LUMO. While if a blue shift is desired, the energy gap should be increased, which can be done by either attaching electron donating groups to the LUMO or attaching electron withdrawing groups to the HOMO. On the other hand, extended π-conjugation of the LUMO leads to a lower LUMO energy and subsequently a smaller energy gap, which leads to a red shift. Furthermore, the addition of electronegative atoms e.g. nitrogen atoms, into the LUMO skeleton might lead to a lower LUMO energy and subsequently a red shift.

1.1.3 4-Coordinate Organoboron Compounds Containing N,C-Chelates

N,C-chelate based ligands have been studied extensively, especially chelates of Ir(III) metal centers because of their use as efficient emitters in OLEDs[21]. On the other hand, there are only few examples of N,C-chelated organoboron compounds[22,23]. Yamaguchi and coworkers[22], reported the synthesis and properties of a number of N,C-chelated (thienyl thiazoles) boron complexes based on **1.32** including dimers as shown in Figure 1.8. Although **1.32** and **1.33** did not exhibit high Φ_F values (< 0.1), the introduction of the $BMes_2$ group led to intramolecular coordination between nitrogen and boron (Lewis base-Lewis acid interaction); consequently, this leads to a planar π-conjug0ated backbone and lower LUMO energies. Based on their reduction potential values (-2.41 and -2.06 V, respectively) compounds **1.32** and **1.33** were suggested as useful candidates for electron transport materials in OLEDs.

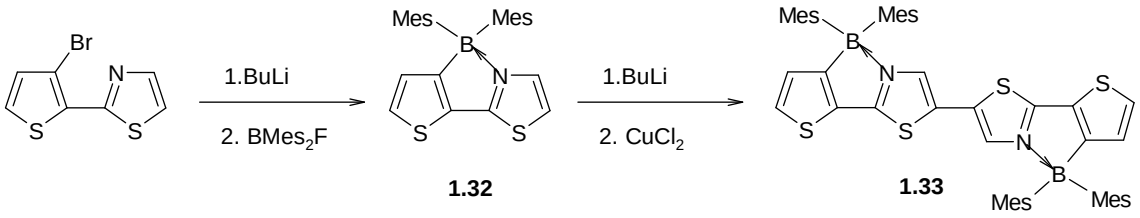

Figure 1.8 Thienyl thiazoles N,C-chelate boron complexes

In addition, Kawashima and co-workers[23] reported a different type of N,C-chelate organoboron compounds, with a nitrogen-boron intramolecular coordination, based on (E)-azobenzene (Figure 1.9). In contrast to most azobenzene compounds, these BAr_2 azobenzene derivatives did not show any photoisomerization when irradiated with UV lamp. Instead, a strong green fluorescence was observed for **1.34** and **1.35** with λ_{em} = 503 and 524 nm, respectively. The fluorescence quantum yields of **1.34** and **1.35** were Φ_F = 0.23 and 0.76, respectively, while almost no fluorescence emission was observed in the case of **1.36**, which was attributed to the substituents on boron. Based on the DFT and TD-DFT calculations done on compounds **1.34**, **1.35**, **1.36**, and the unsubstituted azobenzene (E)-**1.37**; the LUMO and HOMO orbitals of (E)-**1.37** are the π* and n of the azo group, respectively. On the other hand, the π* orbital energy in **1.34**, **1.35**, **1.36** was lowered because of the nitrogen-boron interaction. The HOMO of **1.34** is distributed between Ph-N=N-Ph and the aromatic rings on boron, while for **1.35** the distribution involved MeO-Ph-N=N-Ph, and for **1.36** mainly on the aromatic rings attached to boron atom. Also, the lowest singlet excited state for **1.34** and **1.35** was assigned to the (π-π*) transitions.

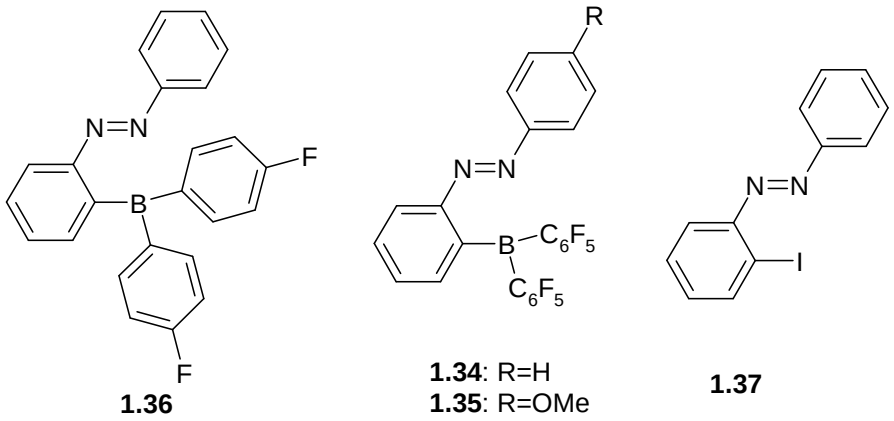

Figure 1.9 N,C-chelate organoboron compounds based on azobenzene

In a more recent work, Kawashima *et al*[24] have also reported a new boron system, similar to the one discussed above, based on N-substituted aldimines as shown in Figure 1.10. A series of 2-borylphenyl substituted imines were synthesized via dehydrative condensation of **1.38** and the corresponding amines. Compared to the non-borylated N-benzylideneaniline, which is not fluorescent, the new borylated compounds are fluorescent with λ_{em} in the range of 398-545 nm. Compounds with more extended π-conjugated systems on the N,C-chelate ligand showed more red-shifted fluorescence.

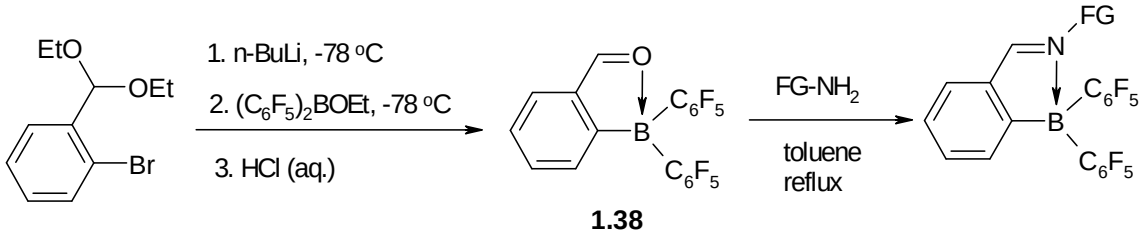

Figure 1.10 N,C-chelate organoboron compounds based on N-substituted aldimines

Most recently, Murakami and co-workers[25] reported a series of N,C-chelate organoboron compounds based on a variety of phenylpyridines and other pyridyl-aryl chelates. The compounds were synthesized via the reaction of dibromoborylaryl pyridine (**1.39**) and triorganoaluminum reagents and diorganozinc reagents as shown in Figure 1.11. Both alkyl and aryl reagents were used, such as Me_3Al, Et_3Al, Ph_3Al, $(i\text{-}Pr)_2Zn$, $(C_6F_5)_2Zn$, $(4\text{-}MeOC_6H_4)_2Zn$, and $(4\text{-}CF_3C_6H_4)_2Zn$. Although reactions using organozinc reagents were slower (12 hrs) than the ones using organoalumiunm reagents (5 min), both gave very good yields. The intermediate reagent **1.39** was prepared via electrophilic aromatic borylation of 2-arylpyridine using BBr_3 and $Et_2N(i\text{-}Pr)$. Interestingly, the intermediate reagent **1.39** was found to be stable enough to be handled in air, which allowed for a facile synthesis of variety of substituted pyridine-boron complexes.

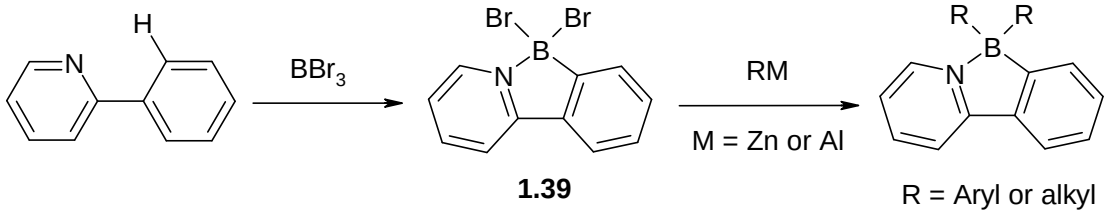

Figure 1.11 Synthetic route to N,C-chelate organoboron compounds via organozinc and organoalumiunm reagents.

On the other hand, our group have found recently that some N,C-chelate boron compounds posses very interesting properties including photochromism[26], hence the focus of this thesis was on studying the photochromic behavior of N,C-chelate boron compounds. The following section will introduce the general concepts of photochromic

phenomena in addition to discussing some representative classes of organic photochromic dyes. Also, the photochemistry of related organoboron compounds will be discussed.

Photochromism is defined as light-induced reversible transformation of a compound between two forms, A and B, which have different absorption spectra[27]. The thermodynamic isomer (A) can be converted to the higher energy isomer (B) by irradiation with UV light, while the reverse reaction can be induced by irradiation with light (normally a longer wavelength) or by heat as shown in Figure 1.12. The latter is defined as photochromism of type T (Thermally reversible), while the former is defined as photochromism of type P (Photochemically reversible).

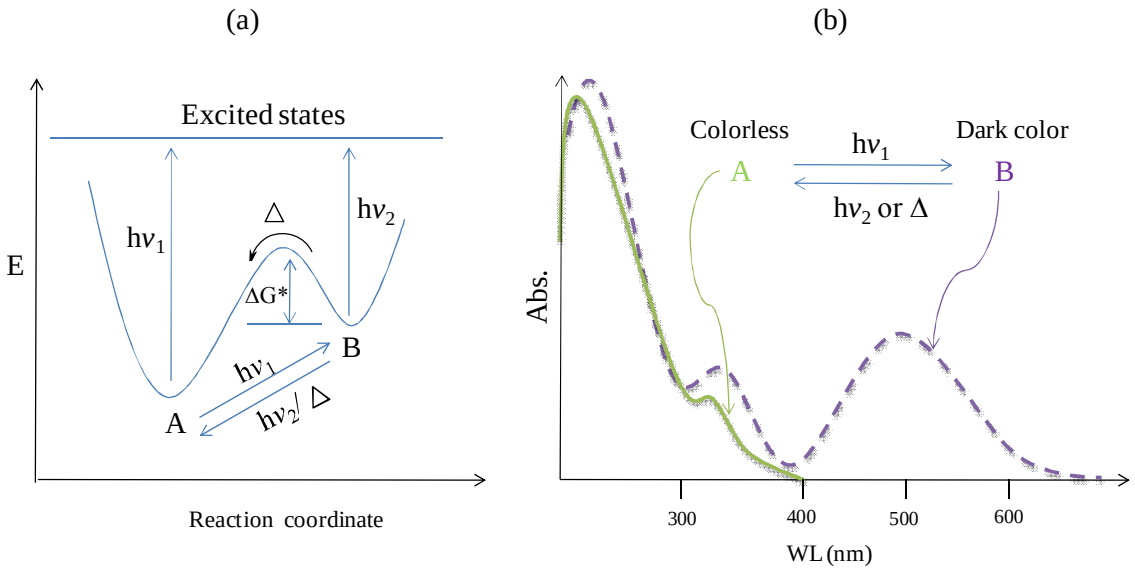

Figure 1.12 Schematic representation of (a) a photochromic system energy profile (b) UV-Vis spectral changes in a photochromic system.

Photochromic reactions are generally associated with significant color change from a colorless or slightly yellowish isomer to a dark colored isomer [A (colorless) → B (colored)]. When the absorption maximum (λ_{max}) of A is smaller than that of B the photochromism is called "positive photochromism". On the other hand, the less common "negative photochromism" is denoted when the opposite case takes place e.g. the absorption maximum (λ_{max}) of A is bigger than that of B. In P-type photochromism isomer B is thermally stable and can only be reverted to isomer A using light, which can be selective and efficient if the absorbance or A and B did not overlap. Some photochromic reactions suffer from photodegradation or fatigue, which is caused by side reactions that decrease the concentration of form A or B and lead to the formation of by-products.

1.2 Representative Classes of Organic Photochromic Systems

The most widely studied classes of photochromic systems are diarylethene derivatives, fulgide/fulgimide derivatives, both of which belong to the P-type photochromic compounds, and spiropyrans, spirooxazines, and benzopyrans, which belong to the T-type.

1.2.1 Diarylethenes

Diarylethenes are structural analogues of stilbenes, which are known to undergo photocyclization reactions to give dihydrophenanthrenes as shown in Figure 1.13. While

this photocyclization reaction is reversible (T-type) if oxygen was excluded from the solution, dihydrophenanthrene reacts irreversibly with oxygen to give phenanthrene.

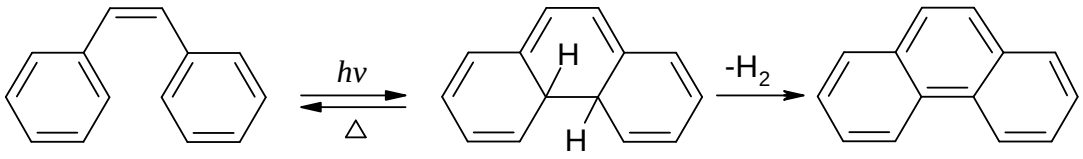

Figure 1.13 Photocyclization reaction of stilbene

Photochromic diarylethenes were reported in the late 60s by Kellogg et al[28], where they replaced the phenyl rings in stilbene by thiophene rings, the effect was a more stable intermediate but the reaction was still reversible (T-type). It was not until 1980s when diarylethenes gained their importance due to the exceptional work done by Irie. In addition to replacing the stilbene rings with thiophene, Irie also replaced the bridging ethylene group by a maleic anhydride, maleimide or perfluorocyclopentene group, as shown in Figure 1.14[29]. The thiophene ring can also be replaced with furan, indole, or thiazole rings.

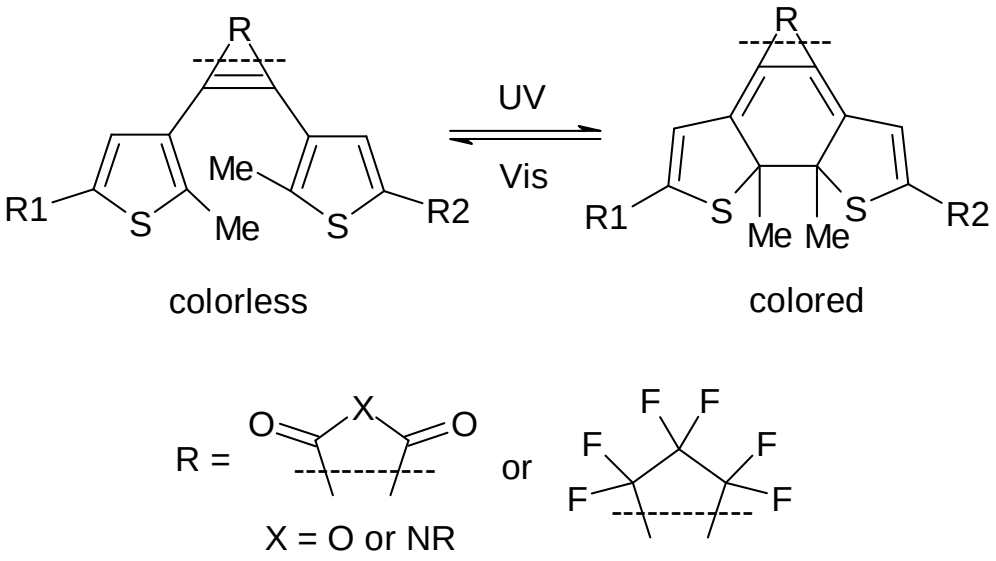

Figure 1.14 Photochromic diarylethenes with different bridging groups.

The new compounds prepared by Irie and others were thermally stable and were only reversible with light (P-type). The thermal stability and the high fatigue resistance of these photochromic compounds made them very important candidates for studies related to optical switches and memories applications.[30]

Diarylethenes can be either symmetrical or non-symmetrical. Extended conjugation at position 2 of diarylethenes generally leads to higher absorption coefficients and red shift in the absorption spectra[31]. On the other hand, larger red shifts are normally observed with non-symmetrical maleic anhydride derivatives or diarylethenes.

1.2.2 Fulgides and Fulgimides

Photochromism of fulgides (Figure 1.15) or aryl-substituted bis-methylene succinic anhydride derivatives was first reported by Stobbe[32]. On the other hand, Becker *et al* were the first to study the mechanism of the reaction leading to the colored species and the effect of substitution on the photochemical and photophysical properties of the fulgides[33]. In their report, they concluded that the photochromic behavior of fulgides is a molecular phenomenon and not a crystalline phenomenon as Stobbe reported earlier. Since then, a wide range of fulgides have been reported and the effect of their different molecular designs been studied extensively[34,35].

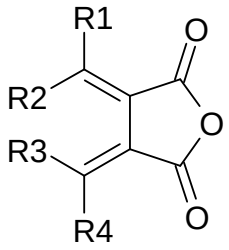

Figure 1.15 General formula of Fulgides

Fulgides are generally synthesized via the Stobbe condensation using an arylaldehyde or arylketone with a substituted methylene succinate followed by hydrolysis and dehydration steps. In order for fulgides to be photochromic they should have at least one aromatic ring on the exo-methylene carbon atom, which leads to the formation of the 1,3,5-hexatriene backbone and consequently can undergo a 6π-electrocyclization process[36].

Fulgides can exist as either *E* or *Z* isomers depending on the arrangement around the double bonds as shown in Figure 1.16. Isomerization of the yellow *Z* form to the *E* form and the subsequent cyclization of the *E* form to give the red C form are accomplished with UV irradiation. The cyclized form C can be converted back to the *E* form by exposure to visible light. The replacement of hydrogen atoms with methyl groups on the closing ring prevents hydrogen-shift side reactions, which reduces fatigue, and prevents the thermal ring opening because of steric effect of the methyl groups.

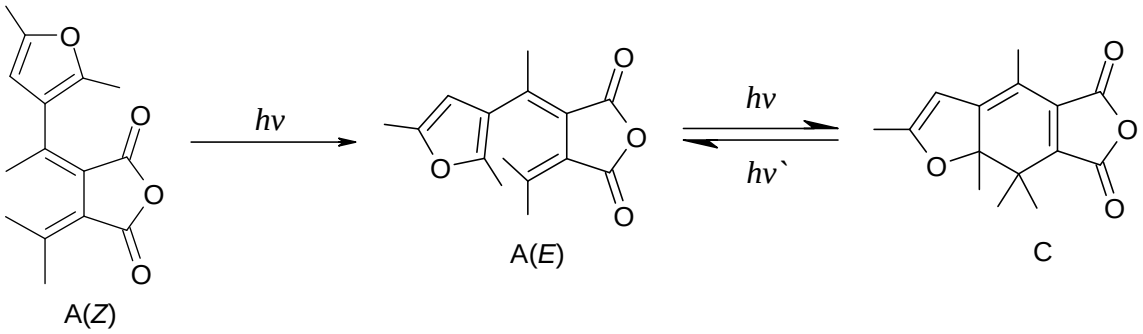

Figure 1.16 Photochromic behavior of Fulgides

Fulgides can be reacted with amines to afford the corresponding fulgimides (Figure 1.17), which have the same photochromic properties of fulgides. Fulgimides are more stable towards hydrolysis[37].

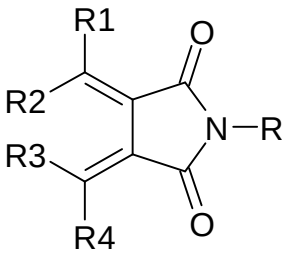

Figure 1.17 General formula of Fulgimides

1.2.3 Spiropyrans, Spirooxazines, and Chromenes

The photochromic properties of spiropyrans were first discovered by Fischer and Hirshberg[38]. Spiropyrans are usually composed of a pyran ring linked via a spiro-carbon atom to another heterocyclic ring as shown in Figure 1.18. The pyran ring is normally a substituted benzopyran or naphthopyran, while the other heterocyclic ring could be a substituted indole, benzoxazole, benzothiazole, quinoline, and other heterocyclic ring systems.

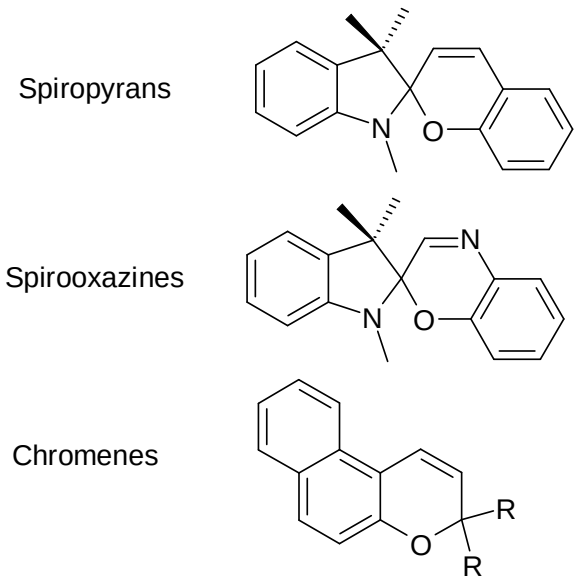

Figure 1.18 General formulas of spiropyrans, spirooxazines, and chromenes

Under thermodynamic conditions, spiropyrans exist in the closed "spiro" form (SP), which is colorless and non-polar with the two ring systems being orthogonal to each other. Upon irradiation with UV light the SP form converts to the open "merocyanine" (MC) form, which is colored, planar, and more conjugated. This is achieved by the

heterolytic cleavage of the C-O spiro bond in the SP form as shown in Figure 1.19. The spiro carbon goes from tetrahedral geometry (sp^3) to planar geometry (sp^2) enabling the two ring systems to become co-planar and conjugated. The extra conjugation of the MC form allows for absorption in the visible region and hence the color change. Upon removal of the UV source, the colored MC form goes back to the colorless thermodynamic SP form via the C-O bond reconnection.

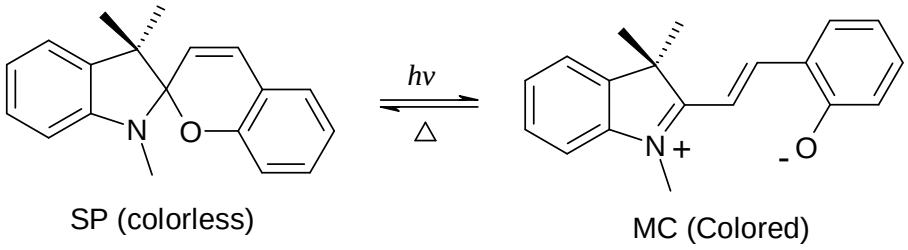

Figure 1.19 Photochromic behavior of spiropyrans

Spirooxazines (Figure 1.18) are structural analogues of spiropyrans and they have very similar photochromic behavior. On the other hand, when the heterocyclic part of spiropyrans is replaced with unconnected alkyl or aryl groups they are called chromenes (Figure 1.18), of which, benzopyrans are the most widely used. The photochromic behavior of chromenes is very similar to that of spiropyrans as shown in Figure 1.20. Under UV irradiation, the C–O bond in the pyran ring is broken leading to the formation of cis-quinoidal which isomerizes to the more stable trans-quinoidal form. Spiropyrans,

spirooxazines, and benzopyrans are generally thermally reversible photochromic systems (T-type).

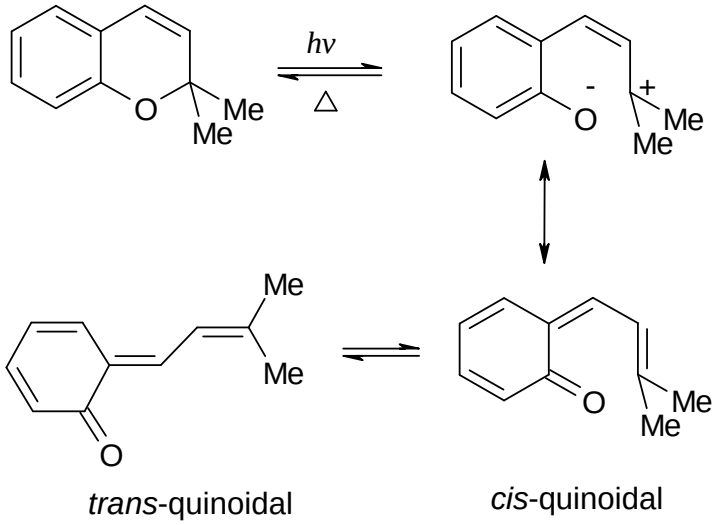

Figure 1.20 Photochromic behavior of chromenes

1.2.4 Azobenzenes

Azobenzenes undergo a *trans* (*E*) → *cis* (*Z*) photoisomerization upon exposure to UV light, which can be reversed back by heating or by exposure to visible light, as shown in Figure 1.21. Most inversions of azobenzenes are not accompanied by significant color change due to the overlap of the absorption bands of the *E* and *Z* isomers. However, when the azo compound is a dye a significant color change, from the highly colored *E* isomer to the less colored *Z* isomer, could take place. On the other hand, the *E*/*Z* isomerization is accompanied by other chemical and physical properties changes, which made azobenzenes suitable candidates for switching applications mainly by incorporating them into polymers[39].

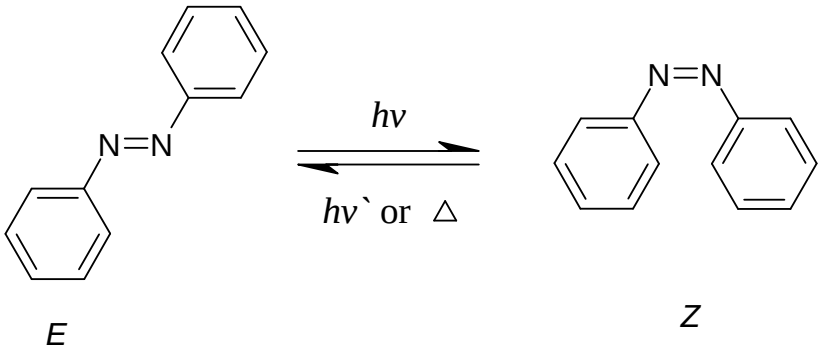

Figure 1.21 Photoisomerization of azobenzenes

1.3 Photochemistry of Organoboron Compounds

In the past few decades the chemistry of boron compounds has been extensively studied. Nevertheless, the photochemistry of boron compounds did not receive much attention and there have been only a few reports discussing this topic.[40] The published studies on boron compounds photochemistry focus on boranes, carboranes, and alkylboranes, and arylborates. The latter is the most relevant to our work and hence the focus of this section will be on aryl borates.

Studies on the photochemistry of tetraarylborates were reported by Williams and others.[40] The irradiation of sodium tetraphenylborate with UV light (254 nm) in a degassed H_2O/DME mixture, has been found to produce 1-phenyl-1,4-cyclohexadiene, biphenyl, and sodium diphenylborinate as shown in Figure 1.22.[40a]

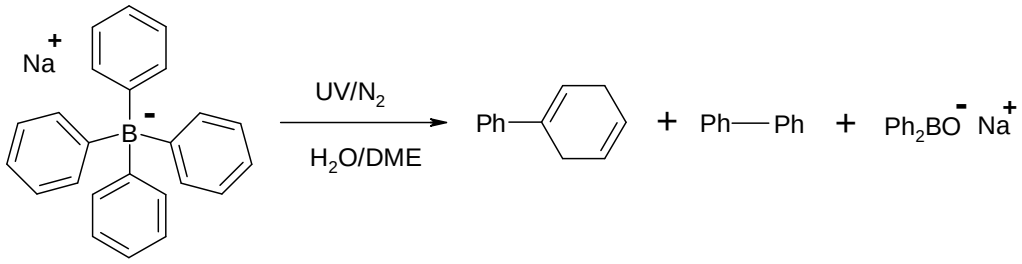

Figure 1.22 Irradiation of sodium tetraphenylborate with UV light (254 nm) under N_2 in a mixture of H_2O and DME.

Williams and co-workers investigated the photolysis of triphenylborane and triphenylborane complexes under the same conditions.[41] Irradiation of a cyclohexane solution of triphenylborane under the same conditions did not yield any hydrocarbon products. On the other hand, irradiation of triphenylborane-methanol, -piperidine, or –pyridine Lewis base adducts furnished the same products produced from the tetraphenylborate. Also, they investigated the mechanism of the photolysis of sodium tetraphenylborate via deuterium labeling and they suggested that it goes through a bicyclic bridged boron intermediates as shown in Figure 1.23. Nevertheless, they were not able to isolate the suggested intermediate.

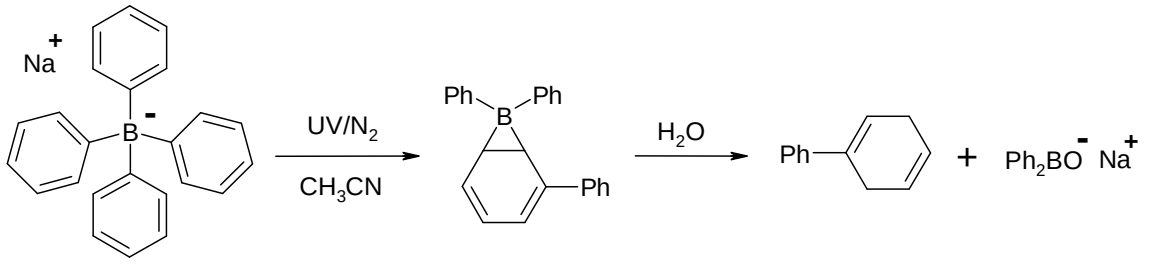

Figure 1.23 Irradiation of sodium tetraphenylborate with UV light (254 nm) under N_2 in CH_3CN.

Later on, Eisch *et al*[42] proposed a different mechanism where the photolysis of tetraphenylborate in degassed THF forms a diphenylborene anion, which was quenched by diphenylacetylene as shown in Figure 1.24.

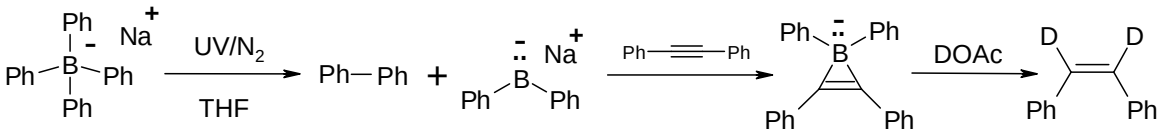

Figure 1.24 Formation of diphenyborene via the irradiation of sodium tetraphenylborate with UV light (254 nm) under N_2 in THF.

On the other hand, Schuster *et al*[43] reinvestigated the photolysis of tetraphenylborate, where they found that irradiation of a degassed THF or acetonitrile solution leads to a red colored solution (^{11}B NMR: -27.3 ppm). Upon adding diphenylacetylene to this red intermediate the color did not change and the ^{11}B NMR did not change. This led them to conclude that the previous conclusion by Eisch was not

correct. On the other hand, their ^{1}H NMR and ^{11}B NMR studies on the red intermediate were consistent with the bicyclic bridged boron intermediate proposed earlier by Williams. In addition, and in a consecutive report[44], they were able to isolate and fully characterize the proposed intermediate by photolysis of (*p*-biphenyl)triphenyl borate (Figure 1.25). The irradiation (254 nm) was done in degassed CH_3CN, where the color of the solution changed from slightly yellowish to red accompanied by a change in ^{11}B NMR from -6.7 to -26.6 ppm. The air-sensitive red solid was isolated in 30% yield by fractional crystallization from a CH_3CN/ether mixture and the structure of the intermediate was unambiguously determined via X-ray crystallography.

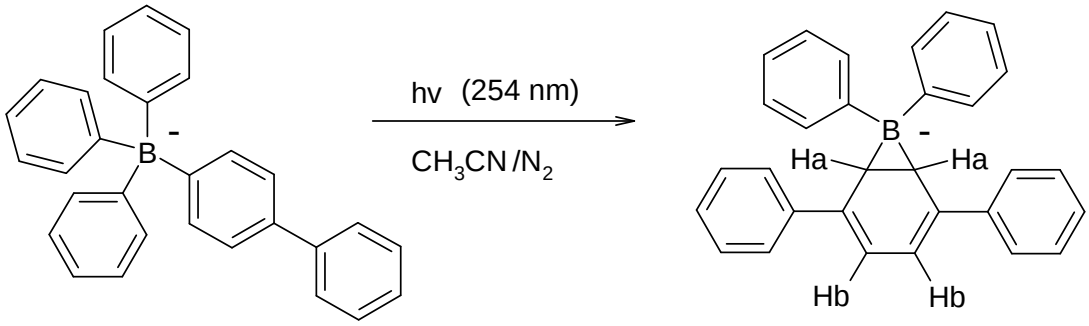

Figure 1.25 Irradiation of (p-biphenyl)triphenyl borate with UV light (254 nm) under N_2 in CH_3CN.

Except for the work published by our lab and by Braunschweig *et al*[45] there have been no reports about photochromic boron compounds, where the boron center is actually involved directly in the photochromic process. Just recently, Braunschweig and co-workers have reported the synthesis and photochemical properties of Lewis base adducts

of pentaphenylborole (**PPB**), namely 4-picoline (**1.40**) and 2,6-lutidine (**1.41**) (Figure 1.26). They found that upon adding 4-picoline to a blue colored solution (CD_2Cl_2) of pentaphenylborole, the color changed to yellow and the ^{11}B NMR signal shifted from 65.4 to 3.5 ppm, which confirmed the formation of a 4-coordinate boron compound (**1.40**). On the other hand, when 2,6-lutidine was added there was no color change and the ^{11}B NMR signal was shifted from 65.4 to 21.0 ppm only.

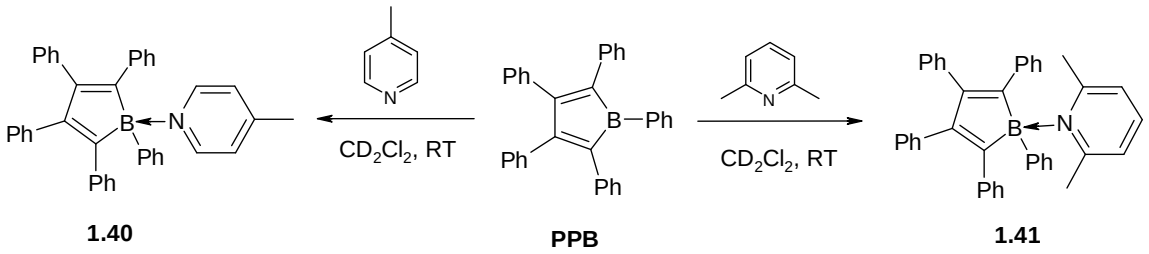

Figure 1.26 Synthesis of pentaphenylborole Lewis base adducts.

Upon cooling (-41°C) a toluene solution of **1.41**, the color changed from blue to yellow and the ^{11}B NMR signal shifted to 3.5 ppm. The previous process was found to be reversible, and hence **1.41** is thermochromic in nature. In addition, they found that irradiation of a solution of **1.41** in toluene-d_8 at -50 °C, using a high energy mercury lamp, leads to a color change from yellow to a dark green. The irradiation process was monitored by ^{1}H NMR, which showed that the conversion of **1.41** to the green compound is associated with the appearance of a new set of peaks representing an isomer of **1.41**. The nature of the new isomer, **1.42**, was further explored by ^{11}B NMR, which showed a peak at 41 ppm corresponding to the formation of a B=C bond. Also, while **1.41** did not

have any detected ^{15}N NMR signals because of the quadrupolar effect of boron, compound **1.42** showed a new ^{15}N NMR signal at -153.0 ppm, which was attributed to the formation of an N-C bond as shown in Figure 1.27.

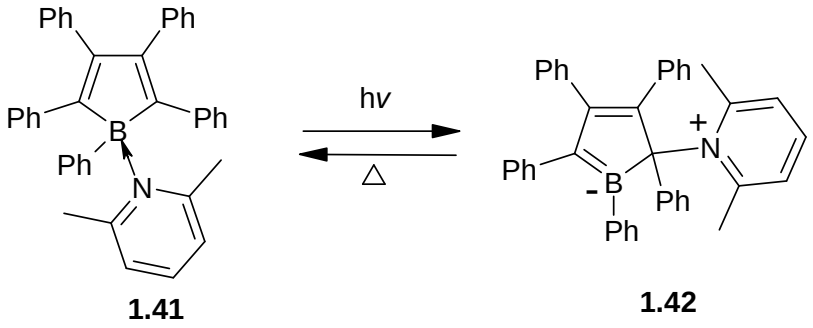

1.41 **1.42**

Figure 1.27 Photolysis of pentaphenylborole 2,6-lutidine adduct.

In addition to the few reports dealing with photochromic boron centers, there have been a few other reports dealing with photochromic systems that contain boron substrates. Branda *et al*[46] recently reported a study about the effect of photochromic switching of dithienylcyclopentenes on the Lewis acidity of an adjacent tricoordinate boron center (Figure 1.28). They found that the Lewis acidity of the boron center in the dioxaborole unit of **1.43** can be modified in a reversible manner using two different wavelengths. The dioxaborole ring in the open form isomer, **1.43**, is aromatic and fulfills Huckel rule with a 4n+2 electrons, which makes the p orbital of the boron atom partially occupied by the delocalized electrons and hence a weaker Lewis acid. Irradiation with UV light leads to cyclization of isomer **1.43** to give isomer **1.44**. In the closed form, oxygen atoms in the borate group are cross-conjugated with the rest of the π backbone of

the molecule. Consequently, the electron density at the boron center is reduced and therefore the Lewis acidity of the boron center is increased.

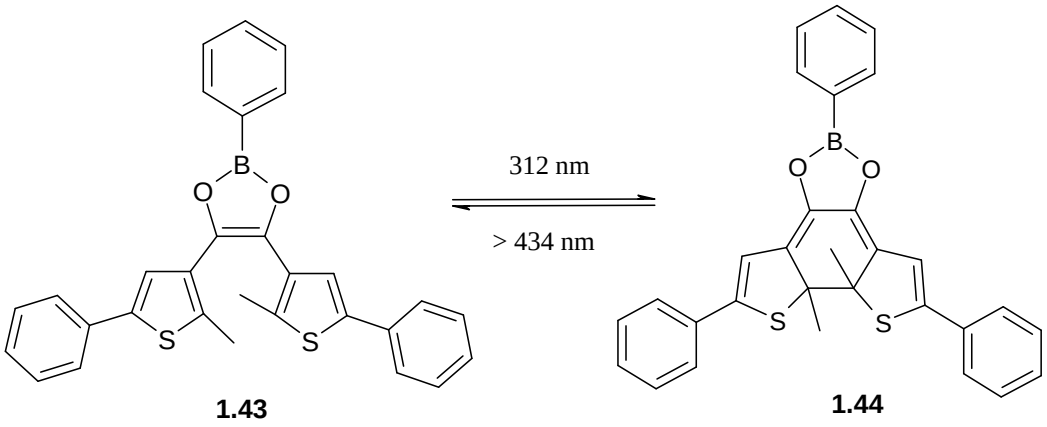

1.43 **1.44**

Figure 1.28 Photochromic switching of dithienylcyclopentenes with a pendant tricoordinate boron center.

In an earlier work, Huang and co-workers[47] reported a similar system based on diarylethenes with an attached 3-coordinate boron center (Figure 1.29). They monitored the change in absorption spectra of the closed (**1.45C**) and open (**1.45O**) isomers before and after adding fluoride ions. The absorption maximum of the closed isomer was red shifted from 655 to 670 nm upon addition of less than 1 equivalent of TBAF in THF. However, when more than 1 equivalent was added, the absorption maximum was blue shifted from 655 to 490 nm, which was attributed to the formation of fluoride adducts. Also, they demonstrated that photochromic switching of **1.45O** and the subsequent addition of fluoride, or vice versa e.g. fluoride addition and subsequent photochromic switching, led to the formation of **1.45C-F.**

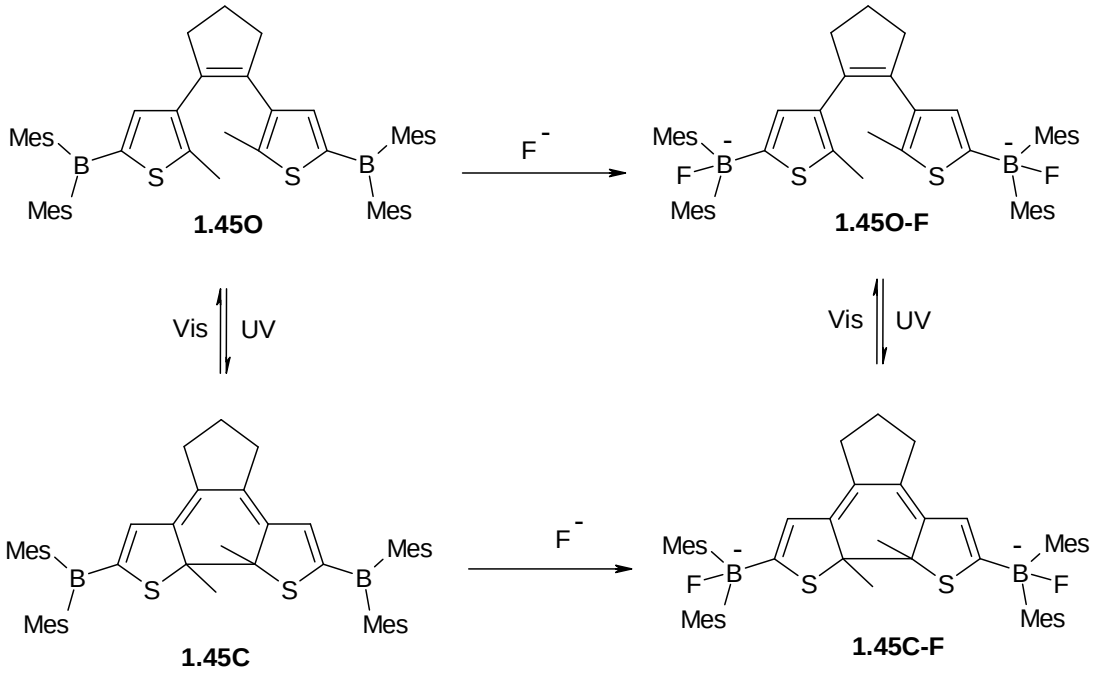

Figure 1.29 Photochromic switching of dithienylcyclopentenes with pendant tricoordinate boron centers in the presence and absence of fluoride.

Most recently, Yam *et al*[48] have recently studied the photophysical and photochromic properties of diarylethenes attached to four coordinate O,O-chelate organoborates (Figure 1.30). Compound **1.46** was prepared via a Suzuki coupling of methyl 4,5-dibromothiophene-2-carboxylate and two equivalents of 2,5-dimethyl-3-thienylboronic acid. Claisen condensation of **1.46** with acetone afforded compound **1.47**. The air-stable diarylethene organoboron final products, **1.48**, **1.49**, and **1.50**, were prepared via a reaction of **1.47** with $BF_3.OEt_2$, $B(C_6F_5)_2F{\cdot}OEt_2$, and BPh_3 respectively.

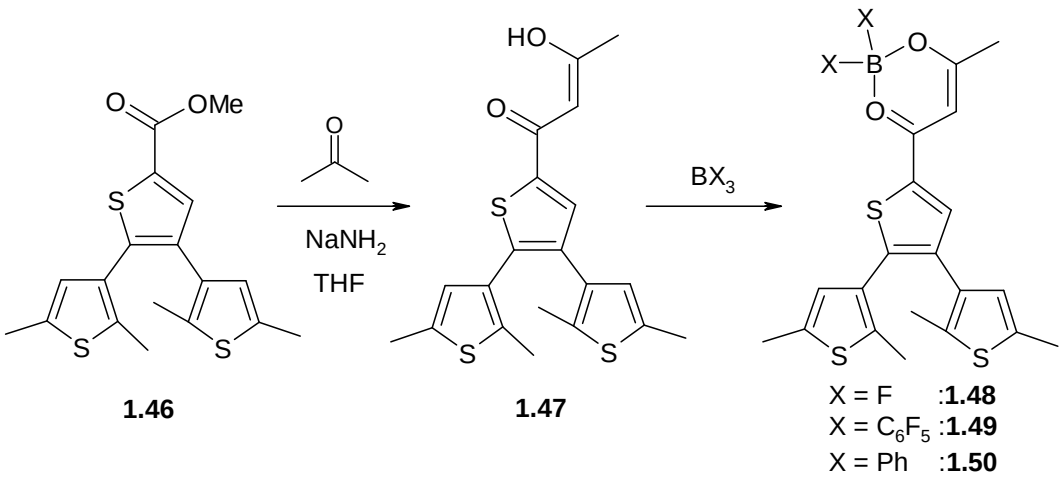

Figure 1.30 Synthesis of photochromic diarylethenes attached to a four coordinate O,O-chelate organoborons.

The absorption maxima of **1.48**, **1.49**, and **1.50** were found to be 417, 434, and 415 nm respectively, compared to 368 nm for **1.47**. Based on TD-DFT, they attributed the red shift of the absorption maxima to the effect of the acac ligand, which stabilizes the LUMO and hence lowers the HOMO-LUMO gap. Upon UV irradiation, **1.47**, **1.48**, and **1.49** were converted to the corresponding closed isomer (Figure 1.31). The cyclization was associated with the appearance of new absorption maxima at 630, 758, and 810 nm, respectively, and quenching of fluorescence. These results show that the photochromic behavior of diarylethenes can be shifted from the visible to the NIR region by the incorporation of the acac-boron moiety. On the other hand, **1.50** did not show any photochromic behavior. Also, the incorporation of the acac-boron enhanced the quantum yield values of the forward and backward reactions. The photocyclization quantum yield

went from 0.17 for compound **1.47**, to 0.39, and 0.35 for compounds **1.48**, and **1.49**, respectively.

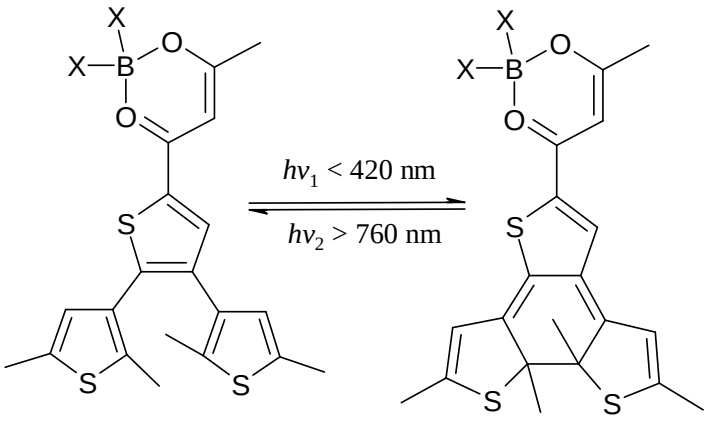

Figure 1.31 Photochromic behavior of diarylethenes attached to a four coordinate O,O-chelate organoborons.

1.4 Applications

1.4.1 General Applications

The design and synthesis of photochromic compounds have been an intense research area because of their potential applications in information storage, smart windows, imaging devices, and ophthalmic lenses.[49]

In order to be useful in commercial applications, photochromic compounds should develop strong colors rapidly upon irradiation with UV light. These colors should cover a wide range of the visible region. In addition, the reversible reaction to the colorless state should be controllable. Also, these compounds should be fatigue resistant.

1.4.1.1 Actinometry

One of the common applications of photochromic compounds is their utilization as chemical actinometers. Actinometry is a very important tool to determine the quantum efficiency of a photochemical reaction (Φ), which is defined as: number of reacted molecules per unit time / number of photons absorbed per unit time. The quantum yield of the unknown sample is determined using a reference compound with a known Φ value. While in absolute actinometry, energy or the number of the incident photons is converted to a quantifiable electrical signal by a photomultiplier or a photodiode. Generally, any photoactive compound with a known quantum yield can be used as an actinometer. Typically, the quantum yield of a useful actinometer should be independent of excitation wavelength, temperature, concentration, trace impurities, and oxygen. Also, the number of reacted molecules per unit time should be easily determined using a convenient analytical method. Chemical actinometers are the most widely used ones, and among these ferrioxalate actinometer[50] is the most reliable and practical actinometer for UV-Vis light (200-500) nm. Upon exposure to light, potassium ferrioxalate decomposes according to the following equations:

$$Fe(C_2O_4)_3^{3-} \xrightarrow{h\nu} Fe^{2+} + C_2O_4^{\cdot -} + 2C_2O_4^{2-}$$

The produced Fe^{2+} ions can be quantified continuously by the in-situ complexation with phenanthroline to yield the colored tris-phenanthroline complex which has a molar absorptivity of (ε = 11100 $L.mol^{-1}.cm^{-1}$ at 510 nm). The number of moles of

Fe^{2+} ions produced in the irradiated solution of a known volume can be calculated using the following equation:

$$\text{moles } Fe^{2+} = [V_1 \times V_3 \times \Delta A(510 \text{ nm})] / [10^3 \times V_2 \times l \times \varepsilon(510 \text{ nm})]$$

where V_1 = volume of the irradiated solution (mL), V_2 = volume of the aliquot of the irradiated solution (mL), V_3 = final volume after complexation with phenanthroline (mL), l = the optical path length of the cell, $\Delta A(510 \text{ nm})$ = the difference in absorbance between the irradiated and the non-irradiated solutions, $\varepsilon(510 \text{ nm})$ = 11100 $L.mol^{-1}.cm^{-1}$. Thus, the moles of photons absorbed by the irradiated solution per time unit ($N h\nu$ / t) are:

$$N h\nu / t = (\text{moles } Fe^{2+}) / (\Phi_\lambda \times t \times F)$$

where Φ_λ = quantum yield of Fe^{2+} ion produced at the specific wavelength used for irradiation, t = irradiation time, and F = the mean fraction of light absorbed by the solution, which can be neglected if the irradiation wavelength was not in the visible region. On the other hand, photochromic actinometers are based on photochromic compounds of the P-type or the T-type. One of the most commonly used actinometers under this category is “Aberchrome 540” which belongs to the fulgides family, as shown in Figure 1.16.

1.4.2 Applications of T-Type Photochromic Compounds

1.4.2.1 Ophthalmic Lenses

P-type photochromic compounds are mostly used in photochromic lenses where they can be coated with on the surface of the lens by means of spin coating or dipping. The coating process must include a resin to provide the flexibility necessary for the photochromic

process to take place. Also, a film containing the photochromic compound can be layered with in multilayer lenses. These two techniques allow for usage of wider range of polymer materials as the lens component including more ridged ones like polycarbonate.[49]

1.4.2.2 Other Applications

T-type photochromic compounds have been also used in specialized printing and surface coatings.[49] Large volume production of photochromic plastics have been achieved by dissolving the photochromic compounds in the molten polymer, which can then be used in many products such as toys, cups, business cards, stickers, utensils, and many more. Similarly, these compounds can be used in textiles for logos on T-shirts and other fashion items like nail polishes and hair dyes. In addition, photochromic materials can be used as security markers on documents, bank notes, and official documents.

1.4.3 Applications of P-Type Photochromic Compounds

In contrast to the T-type photochromic compounds, P-type photochromic compounds have not been commercialized. Nonetheless, the most widely studied P-type photochromic compounds are diarylethenes and fulgides because of their potential use in optical memories and switches[29]. This is mainly because of their thermal stability and the fact that they can photoisomerize in the solid state[51].

1.5 Scope of Thesis

As shown in the previous sections, 4-coordinate N,N- and N,C-chelate organoboron compounds have been widely used in OLEDs, but their stability, especially photostability, have not been investigated. The goal of this thesis was to investigate the stability of N,N and C,N chelate organoboron compounds. During our investigation, it was found that 4-coordinate phenylpyridyl organoboron compounds undergo a reversible photo/thermal switching with the formation/breaking of a C-C bond and a distinct color change. Consequently, the scope of this thesis was focused on understanding this new phenomenon. In order to understand the steric and electronic effects on the photochromic behavior of these C,N chelate organoboron compounds new derivatives of phenylpyridine boron chelates were studied. In addition, the photochromic properties of boron compounds based on new N,C-chelate ligands that contain pyridine as the nitrogen source, were investigated. Also, other N,C-chelates with the nitrogen coming from a five-membered heterocyclic ring, were studied.

In chapter 2, the details of the photochromic behavior of phenylpyridine boron chelate are examined. In chapter 3, the steric and electronic effects of phenylpyridine ligand derivatives and aryl groups attached to boron center are examined. Chapter 4 examines the photochromic properties of a new class of chelates (fused heterocyclic-pyridyl chelates) based on pyridyl-benzothiophene, -benzofuran, and -N-phenylindole boron compounds and the photochromic properties of non-fused pyridyl-heterocyclic chelate boron compounds. In addition, the photochromic behavior of another type of

chelates based on (phenyl-fused heterocyclic) phenyl-benzothiazole and phenyl-benzooxazole chelates is examined. In chapter 5, general summary of the work done in this thesis along with key conclusions and future prospective will be provided.

1.6 References

(1) (a) Entwistle, C. D.; Marder, T. B. *Angew. Chem. Int. Ed.* **2002**, *41*, 2927. (b) Jia, W-L.; Bai, D-R.; McCormick, T.; Liu, Q-D.; Motala, M.; Wang, R. Y.; Seward, C.; Tao, Y.; Wang, S. *Chem. Eur. J.* **2004**, *10*, 994. (c) Sundararaman, A.; Venkatasubbaiah, K.; Victor, M.; Zakharov, L. N.; Rheingold A. L.; Jäkle, F. *J. Am. Chem. Soc.* **2006**, *125*, 16554. (d) Qin, Y.; Kiburu, I.; Shah, S.; Jäkle, F. *Org. Lett.* **2006**, *8*, 5227.

(2) Brabec, C. J.; Sariciftci, N. S.; Hummelen, J. C. *Adv. Funct. Mater.* **2001**, *11*, 15.

(3) (a) Jäkle, F. *Coord. Chem. Rev.* **2006**, *250*, 1107. (b) Wade, C.; Broomsgrove, A.; Aldridge, S.; Gabbai, F. *Chem. Rev.* **2010**, *110*, 3958.

(4) (a) Gevaux, D. *Nature Photonics* **2007**, *1*, 567. (b) Reisch, M. S. *Chemical & Engineering News* **2008**, *86*, 15.

(5) Pope, M., Kallmann, H. *J. Chem. Phys.* **1963**, *38*, 2042.

(6) Kampas, F. J.; Gouterman, M. *Chem. Phys. Lett.* **1977**, *48*, 233.

(7) Tang, C. W.; Van Slyke, S. A. *Appl. Phys. Lett.* **1987**, *51*, 913.

(8) (a) Schmitz, C.; Schmidt, H. W.; Thelakkat, M. *Chem. Mater.* **2000**, *12*, 3012. (b) Chen, B. J.; Sun, X. W.; Li, Y. K. *Appl. Phys. Lett*. **2003**, *82*, 3017. (c) Cui, Y.; Wang, S. *J. Org. Chem.* **2006**, *71*, 6485. (d) McCormick, T.; Liu, Q-D.; Wang, S. *Org. Lett*. **2007**, *9*, 4087.

(9) Wu, Q. G.; Esteghamatian, M.; Hu, N-X.; Popovic, Z.; Enright, G.; Tao, Y.; DIorio, M.; Wang, S. *Chem. Mater*. **2000**, *12*, 79.

(10) Liu, S-F.; Seward, C.; Aziz, H.; Hu, N-X.; Popovic, Z.; Wang, S. *Organometallics* **2000**, *19*, 5709.

(11) Cui, Y.; Liu, Q-D.; Bai, D-R.; Jia, W-L.; Ye, T.; Wang, S. *Inorg. Chem.* **2005**, *44*, 601.

(12) Liu, Q-D.; Mudadu, M. S.; Thummel, R.; Tao, Y.; Wang, S. *Adv. Funct. Mater.* **2005**, *15*, 143.

(13) Liu, Q-D.; Mudadu, M. S.; Schmider, H.; Thummel, R.; Tao, Y.; Wang, S. *Organometallics* **2002**, *21*, 4743.

(14) Liu, S-F.; Wu, Q.; Schmider, H.; Aziz, H.; Hu, N-X.; Popovic, Z.; Wang, S. *J. Am. Chem. Soc.* **2000**, *122*, 3671.

(15) Wang, S. *Coord. Chem. Rev.* **2001**, *215*, 79.

(16) Chen, T-R.; Chien, R-H.; Jan, M-S.; Yeh, A.; Chen, J-D. *J. Organomet. Chem.* **2006**, *691*, 799

(17) Chen, T-R.; Chien, R-H.; Yeh, A.; Chen, J-D. *J. Organomet. Chem.* **2006**, *691*, 1998.

(18) Chen, H-Y.; Chi, Y.; Liu, C-S.; Yu, J-K., Cheng, Y-M.; Chen, K-S.; Chou, P-T.; Peng, S-M.; Lee, G-H.; Carty, A. J.; Yeh, S-J.; Chen, C-T. *Adv. Funct. Mater.* **2005**, *15*, 567.

(19) Klappa, J-J.; Geers,S. A.; Schmidtke, S. J.; MacManus-Spencer, L. A.; McNeill, K. *Dalton Trans.* **2004**, 883.

(20) Liddle, B. J.; Silva, R. M.; Morin, T. J.; Macedo, F. P.; Shukla, R.; Lindeman, S. V.; Gardinier, J. R. *J. Org. Chem.* **2007**, *72*, 5637.

(21) (a) Lamansky, S.; Djurovich, P.; Murphy, D.; Abdel-Razzaq, F.; Lee, H-E.; Adachi, C.; Burrows, P. E.; Forrest, S. R.; Thompson, M. E. *J. Am. Chem. Soc.* **2001**, *123*, 4304. (b) Li, J.; Djurovich, P. I.; Alleyne, B. D.; Yousufuddin, M.; Ho, N. N.; Thomas, J. C.; Peters, J. C.; Bau, R.; Thompson, M. E. *Inorg. Chem.* **2005**, *44*, 1713. (c) Hirani, B.; Li, J.; Djurovich, P. I.; Yousufuddin, M.; Oxgaard, J.; Persson, P.; Wilson, S. R.; Bau, R.; Goddard, W. A.; Thompson, M. E. *Inorg. Chem.* **2007**, *46*, 3865.

(22) Wakamiya, A.; Taniguchi, T.; Yamaguchi, S. *Angew. Chem., Int. Ed.* **2006**, *45*, 3170.

(23) Yoshino, J.; Kano, N.; Kawashima, T. *Chem. Commun*. **2007**, 559.

(24) Yoshino, J.; Kano, N.; Kawashima, T. *J. Org. Chem.* **2009**, *74*, 7496.

(25) Ishida, N.; Moriya, T.; Goya, T.; Murakami, M. *J. Org. Chem.* **2010**, *75*, 8709.

(26) Rao, Y. L.; Amarne, H.; Zhao, S. B.; McCormick, T. M.; Martic, S.; Sun, Y.; Wang, R. Y.; Wang, S. *J. Am. Chem. Soc.* **2008**, *130*, 12898.

(27) Bouas-Laurent, H.; Durr, H. *Pure Appl. Chem.* **2001**, *73*, 639.

(28) Kellogg, R. M.; Groen, M. B.; Wynberg, H. *J. Org. Chem.* **1967**, *32*, 3093.

(29) Irie, M. *Chem. Rev.* **2000**, *100*, 1685.

(30) Fukaminato, T.; Doi, T.; Tamaoki, N.; Okuno, K.; Ishibashi, Y.; Miyasaka, H.; Irie, M. *J. Am. Chem. Soc*. **2011**, *133*, 4984.

(31) Irie, M. In *Organic Photochromic and Thermochromic Compounds*, Volume 1, *Main Photochromic Families*, Ed. Crano, J. C.; Guglielmetti, R. J., Plenum Press, New York, 1999, pp. 207-222.

(32) Exelby, R.; Grinter, R. *Chem. Rev.* **1965**, *65*, 247.

(33) Santiago, A.; Becker, R. S. *J. Am. Chem. Soc.* **1968**, *52*, 3654.

(34) Heller, H. G.; Hughes, D. S.; Hursthouse, M. B.; Rowles, N. G. *Chem. Commun*. **2000**, 1397.

(35) Liang, Y.; Dvornikov, A. S.; Rentzepis, P. M. *Macromolecules* **2002**, *35*, 9377.

(36) Feringa, B. L. *Molecular Switches*; Wiley-VCH: Weinheim, Germany, 2001, pp. 108-113.

(37) Yokoyama, Y. *Chem. Rev.* **2000**, *100*, 1717.

(38) Fischer, E.; Hirshberg, Y. *J. Chem. Soc*. **1952**, 4522.

(39) (a) Delaire, J. A.; Nakatani, K. *Chem. Rev*. **2000**, *100*, 1817. (b) Natansohn, A.; Rochon, P. *Chem. Rev*. **2002**, *102*, 4139.

(40) (a) Pelter, A.; Pardasani, R. T.; Pardasani, P. *Tetrahedron* **2000**, *56*, 7339. (b) Porter, R. F.; Turbini, L. P. *Top. Curr. Chem.* **1980**, *96*, 1. (c) Billing, R.; Rohorek, D.; Hennig, H. *Top. Curr. Chem.* **1990**, *158*, 151.

(41) Williams, J. L. R.; Grisdale, P. J.; Doty, J. C. *J. Am. Chem. Soc.* **1967**, *89*, 4538.

(42) Eisch, J. J.; Tamao, K.; Wilcsek, R. J. *J. Am. Chem. Soc.* **1975**, *97*, 895.

(43) Wilkey, J. D.; Schuster, G. B. *J. Org. Chem.* **1987**, *52*, 2117.

(44) Wilkey, J. D.; Schuster, G. B. *J. Am. Chem. Soc.* **1988**, *110*, 7569.

(45) Ansorg, K.; Braunschweig, H.; Chiu, C.; Engels, B.; Gamon, D.; Hugel, M.; Kupfer, T.; Radacki, K. *Angew. Chem. Int. Ed.* **2011**, *50*, 2833.

(46) Lemieux, V.; Spantulescu, M. D.; Baldridge, K. K.; Branda, N. R. *Angew. Chem. Int. Ed.* **2008**, *47*, 5034.

(47) Zhou, Z.; Xiao, S.; Xu, J.; Liu, Z.; Shi, M.; Li, F.; Yi, T.; Huang, C. *Org. Lett.* **2006**, *8*, 3911.

(48) Poon, C. T.; Lam, W. H.; Wong, H. L.; Yam, V. W. *J. Am. Chem. Soc.* **2010**, *132*, 13992.

(49) Bamfield, P. *Chromic Phenomena*; RSC, Cambridge, 2001, pp. 28-33.

(50) Kuhn , H. J.; Braslavsky, S. E.; Schmidt, R. *Pure Appl. Chem.* **2004**, *76*, 2105.

(51) Irie, M.; Kobatake, S.; Horichi, M. *Science* **2001**, *291*, 1769.

Chapter 2

Photochromic behavior of phenylpyridine-$BMes_2$

2.1 Introduction

Four-coordinate organoboron compounds have been widely investigated in the field of organic electronics, especially as emissive and electron transport materials in organic light emitting diodes (OLEDs)[1], which is attributed to their high thermal and chemical stability which is in turn attributed to the stabilization of the boron center by the intramolecular coordination from a Lewis-basic atom e.g. nitrogen or oxygen. The chelation of the boron center also enhances the conjugation of the compound and lowers the LUMO level energy[2].

In the past few years our group reported that some four-coordinate organoborons could be photochromic, which might be utilized in photochromic materials. The studies reported by our group showed that some four-coordinate N,C-chelate organoboron compounds such as phenylpyridine-$BMes_2$ (**2.1**) (Mes = mesityl), are not only emissive but also photochromic. Upon exposure to UV light, compound **2.1** undergoes a thermally reversible photochromic conversion to **2.1a** (T-type photochromism) as shown in Figure 2.1. Also, the dark isomer **2.1a** resulting from photolysis of compound **2.1** is very reactive towards oxygen and gives a new compound (**2.1b**) through coupling of two aromatic carbon atoms. The possible photochromic applications stemming from this class of organoboron compounds motivated us to investigate their structure-property

relationship. In this chapter, the synthesis, photophysical properties, and photochromic behavior of compound **2.1** are discussed.

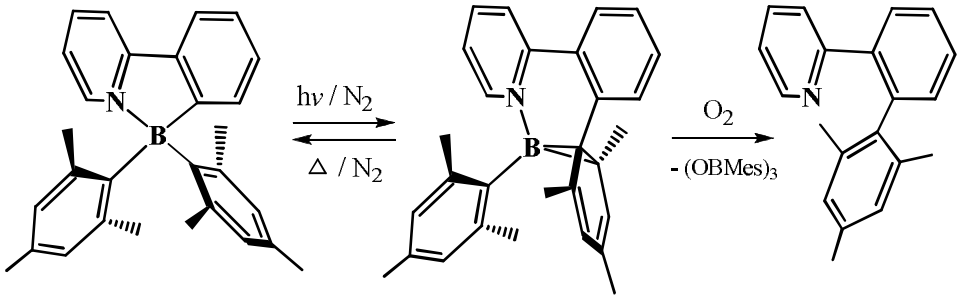

2.1 **2.1a** **2.1b**

Figure 2.1 Photolysis of compound **2.1** under nitrogen and the subsequent reaction of **2.1a** with O_2

2.2 Experimental

2.2.1 General

Starting materials were purchased from Aldrich Chemical Co. and were used without further purification. Solvents were dried using activated alumina column system, PURE SOLV, purchased from Innovative Technology Inc., while C_6D_6 was dried over CaH_2 in a glove box. All reactions were carried out under an atmosphere of dry nitrogen using standard Schlenk techniques. Purifications using column chromatography were performed using ultra pure silica gel (70-230 Mesh) 60 Å, purchased from Silicycle. NMR spectra (^1H,^{13}C, and ^{11}B) were recorded at room temperature on a Bruker Avance 400 or 500 MHz. Chemical shifts, ^1H and ^{13}C, were reported with respect to solvent peaks as internal standard and $BF_3.Et_2O$ was used as reference for ^{11}B NMR. Coupling

constants (J) were recorded in Hertz (Hz). Excitation and emission spectra were recorded on a Photon Technologies International QuantaMaster Model C-60 spectrometer. UV-Vis spectra were recorded on an Ocean Optics Model CHEMUSB4-UV/VIS. Elemental analyses were performed by Canadian Microanalytical Services, Delta, BC, Canada. High resolution mass spectra (HRMS) were obtained using a Waters/Micromass GC-TOF spectrometer (EI mode). Cyclic voltammetry was performed using a BAS CV-50W analyzer with a scan rate of 200 mV/s and sample concentrations of 5 mg/3.0 mL DMF, using 0.10 M NBu_4PF_6 (TBAP) as supporting electrolyte and Ag/AgCl reference electrode. The ferrocenium/ferrocene couple was used as the internal standard (E^o = 0.56 V). 2-(2-Bromophenyl)pyridine[3] was synthesized based on literature methods.

2.2.2 Synthesis of $BMes_2$(2-(2´-pyridyl)benzene) (2.1)

To a solution of 2-(2-bromophenyl)pyridine (0.47 g, 2.0 mmol) in THF (30 mL), at -78°C, n-BuLi (1.6 M in hexane, 1.25 mL, 2.0 mmol) was added slowly and mixed for 30 min. The resulting solution was transferred to a THF (20 mL) solution of $BMes_2F$ (0.59 g, 2.0 mmol) via cannula at -78°C and stirred overnight. The solution was filtered and the solvents were removed under reduced pressure. The resulting mixture was purified over silica gel by flash column chromatography using CH_2Cl_2/hexanes (1:1) mixture. The resulting white solid was recrystallized from CH_2Cl_2/pentane to give yellow crystals of **2.1** (0.50 g, 62%). Anal. Calcd (%) for $C_{29}H_{30}BN$: C, 86.35; H, 7.50; N, 3.47. Found: C, 85.47; H, 7.45; N, 3.31. ^{1}H NMR (CD_2Cl_2, 25 °C, δ, ppm): 8.60 (d, 1H, ^3J = 6.0 Hz), 8.06-8.01 (m, 2H), 7.92 (d, 1H, ^3J = 6.8 Hz), 7.76 (d, 1H, ^3J = 6.8 Hz), 7.36-7.25 (m,

3H), 6.65 (s, 4H), 2.18 (s, 6H), 1.79 (s, 12H). ^{13}C NMR (CD_2Cl_2, 25 °C, δ, ppm): 159.5, 146.3, 140.9, 135.1, 134.0, 131.2, 131.0, 130.0, 125.5, 122.0, 121.9, 118.2, 25.0, 20.6. ^{11}B NMR (C_6D_6, 25 °C, δ, ppm): 5.02.

2.2.3 Isolation and Characterization of 2-(2-mesitylphenyl)pyridine (2.1b)

The C-C coupling product was obtained by photolysis of a toluene solution of $BMes_2$(2-(2´-pyridyl)benzene) (**2.1**) using UV light (365 nm) under an atmosphere of oxygen at RT for 1 h. Solvents were removed under reduced pressure and the crude product was purified using a preparative TLC plate using a mixture of CH_2Cl_2/Hexane (1:1) to afford **2.1b** as a white solid (yield 93%, based on ^{1}H NMR). HRMS, calcd. for $C_{20}H_{19}N$: m/z 273.1528; found: 273.1517. ^{1}H NMR (CD_2Cl_2, 25 °C, δ, ppm): 8.58 (d, 1H, ^3J = 4.5 Hz), 7.84-7.78 (m, 1H), 7.52-7.42 (m, 2H), 7.39 (t, 1H, ^3J = 7.7 Hz), 7.20-7.11 (m, 1H), 7.10 (t, 1H, ^3J = 6.0 Hz), 6.65 (d, 1H, ^3J = 8.0 Hz), 6.85 (s, 2H), 2.29 (s, 3H), 1.91 (s, 6H). ^{13}C NMR (CD_2Cl_2, 25 °C, δ, ppm): 158.9, 149.6, 139.4, 138.2, 136.9, 136.3, 135.5, 130.9, 130.6, 128.8, 128.4, 127.6, 123.8, 121.7, 21.1, 20.8.

2.2.4 Isolation and Characterization of Boroxine $(MesBO)_3$

The byproduct resulting from the exposure of **2.1a** to oxygen [boroxine $(MesBO)_3$] was isolated from a C_6D_6 solution of **2.1** after exposure to UV light in the presence of O_2. The precipitated $(MesBO)_3$ was characterized by ^{1}H NMR and HRMS. ^{1}H NMR (CD_2Cl_2, δ, ppm): 6.67 (6H, s), 2.49 (18H, s), 2.14 (9H, s). HRMS calcd. for $C_{27}H_{33}B_3O_3$: m/z 438.2723; found: 438.2715. These values are similar to those reported previously in literature[4].

2.2.5 Fluorescence Quantum Yield Measurements

Fluorescence quantum yield of dilute degassed toluene solutions (Abs. = ~0.1) were measured at room temperature using the relative quantum yield method using 9,10-diphenylanthracene as the reference standard ($\Phi_F = 0.90$).[5]

2.2.6 General Procedure Used for Monitoring Photolysis Process via ^{1}H NMR

Samples were dissolved in dry C_6D_6 in an NMR tube under inert atmosphere. To remove any traces of oxygen that might be present in the NMR tube, 3 freeze-thaw cycles were performed using liquid N_2. The photolysis was then performed using a UV source (365 nm) at room temperature, followed by recording ^{1}H NMR after different time periods. The same sample was used for the consecutive UV exposure/NMR cycles and the exposure times were added up.

2.2.7 General Procedure Used for Monitoring Photolysis Process via UV-Vis spectroscopy

Samples were dissolved in dry degassed toluene in a quartz cuvette (~10^{-5} M), under inert atmosphere in a glove box. After wrapping the quartz cuvette with aluminum foil, it was transferred out and photolysis was then performed, using a hand-held UV lamp (365 nm) at room temperature. The UV-Vis spectra were recorded after each exposure time and the exposure times were added up.

2.2.8 Density Functional Theory Calculations

Gaussian 2003 program was used for all theoretical calculations, which were carried out at the B3LYP level of theory with 6-311G* as the basis set.[6] For compounds with

available X-ray structures, geometric parameters were used as starting points for the geometry optimizations, while *GaussView* software package was used for compounds with no X-ray data available.

2.2.9 Photoisomerization Quantum Yield Measurements

All preparation and measurements were done under dark light conditions and with freshly prepared and mixed solutions. Phenanthroline and $K_3[Fe(C_2O_4)_3].3H_2O$ are light sensitive and were kept in the dark at all times. The quantum yield of the photoisomerization of **2.1** to **2.1a** was determined using potassium ferrioxalate $K_3[Fe(C_2O_4)_3].3H_2O$ actinometry based on Hatchard-Parker method.[7] The absorbance of the Fe(II)-1,10-phenanthroline complex was measured at 510 nm in a buffered acidic solution, while the absorbance of **2.1a** was measured in degassed toluene at 599 nm. The absorbance was measured using an Ocean Optics fiber optic spectrophotometer connected to a Quantum Northwest four-way temperature-controlled cuvette holder via 400 μm fiber optic. The irradiation source was a Photon Technologies International 200 W Hg/Xe lamp equipped with a monochromator.

2.2.10 X-ray Crystallography

Single-crystals of compound **2.1** were obtained as described above. Crystals were mounted on glass fiber and data collection was done using a Siemens P4 single-crystal X-ray diffractometer, equipped with a Smart CCD-1000 detector and graphite-monochromated Mo Kα radiation operating at 50 kV and 35 mA. Data were processed on a PC using Bruker SHELXTL software package.[8]

Table 2.1 Crystallographic data of compound **2.1**

	2.1
Formula	$C_{29}H_{30}BN$
Fw	403.35
space group	P2(1)/c
a/Å	11.3972(7)
b/Å	12.7454(8)
c/Å	15.7096(10)
α, deg	90
β, deg	92.6770(10)
γ, deg	90
V/Å^3	2279.5(2)
Z	4
D_c/(g cm^{-3})	1.175
μ/mm^{-1}	0.066
$2\theta_{max}$/deg	56.52
reflns measured	25495
reflns used (R_{int})	5304 (0.0255)
final R [I > 2σ (I)]	R_1[a] = 0.0475 wR_2[b] = 0.1303
R (all data)	R_1[a] = 0.0669 wR_2[b] = 0.1436
goodness-of-fit on F^2	1.073

[a] $R_1 = \Sigma[|F_o| - |F_c|]/\Sigma|F_o|$. [b] $wR_2 = \{\Sigma[w(F_o^2 - F_c^2)]/ \Sigma(wF_o^2)\}^{1/2}$.

$\omega = 1/[\sigma^2(F_o^2) + (0.075P)^2]$, where $P = [\max.(F_o^2,0) + 2F_c^2]/3$.

Table 2.2 Selected bond lengths (Å) and angles (°) for compound **2.1**

N(1)-C(1)	1.3558(19)	C(1)-N(1)-C(5)	118.71(13)
N(1)-C(5)	1.3636(18)	C(1)-N(1)-B(1)	129.24(12)
N(1)-B(1)	1.6531(19)	C(5)-N(1)-B(1)	111.98(11)
B(1)-C(11)	1.625(2)	C(11)-B(1)-C(12)	105.63(11)
B(1)-C(12)	1.644(2)	C(11)-B(1)-N(1)	95.13(10)
B(1)-C(21)	1.654(2)	C(12)-B(1)-N(1)	116.76(11)
C(1)-C(2)	1.370(2)	C(11)-B(1)-C(21)	119.69(11
C(2)-C(3)	1.378(3)	C(12)-B(1)-C(21)	114.91(11)
C(3)-C(4)	1.373(3)	N(1)-B(1)-C(21)	103.60(10)

2.3 Results and Discussion

2.3.1 Synthesis and Characterization

The N,C-chelate ligand, 2-(2-bromophenyl)pyridine, was synthesized using a modified Suzuki coupling reaction[3] of 2-bromophenylboronic acid and 2-bromopyridine, using 5 mol % of $Pd(PPh_3)_4$ as the catalyst. Compound **2.1** was prepared by lithiation of the N,C ligand in THF followed by the addition of $BMes_2F$ as shown in Figure 2.2. The crude product was purified on silica gel using flash chromatography and crystallized by slow evaporation of pentane into a CH_2Cl_2 solution (62% yield). Compound **2.1** was characterized by ^{1}H, ^{13}C, ^{11}B NMR, elemental analysis, and X-ray crystallography.

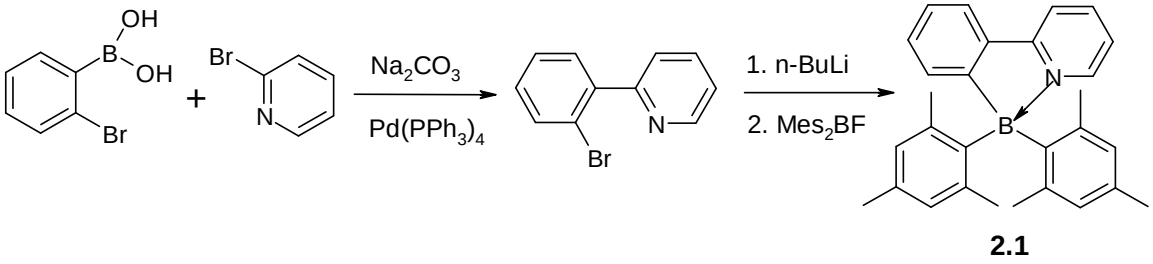

2.1

Figure 2.2 Synthesis of compound **2.1**

2.3.2 Crystal Structure

The crystal structure of **2.1** was determined by single crystal X-ray diffraction as shown in Figure 2.3. The boron center adopts a tetrahedral geometry because of the intramolecular N(1) to B(1) coordination, which leads to a dihedral angle of 7.6° between the phenyl and the pyridine planes. The N-B-$C_{chelate}$ bond angle is 95.13(1)°, while the C_{Mes}-B-C_{Mes} bond angle is 114.91(1)° .The B-N bond length (1.653(2) Å) and B-C bonds length (1.625(2) - 1.654(2) Å) are similar to those of previously reported for tetrahedral boron molecules[9]. Also, the mesityl groups are arranged asymmetrically around the boron center with respect to the phenylpyridine chelate ring, where one mesityl group is closer to the phenyl ring, represented by C(11), than the other. The distance C(11)···C(12) = 2.604 Å is much shorter than C(11)···C(21) = 2.836 Å, which might be attributed to the steric congestion imposed by the mesityl groups.

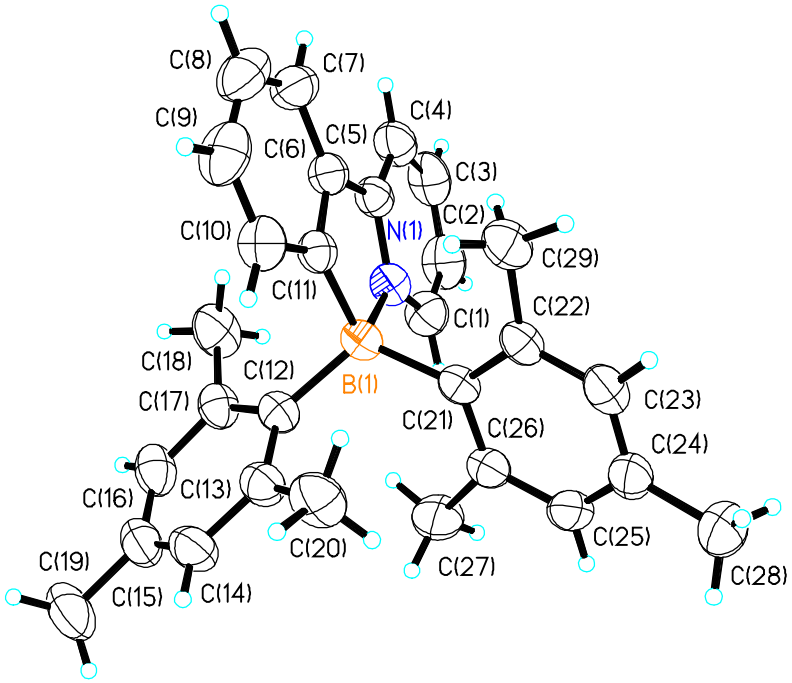

Figure 2.3 Crystal structure of compound **2.1** with 50% thermal ellipsoids

2.3.3 UV-Vis Absorption and Luminescence Properties of 2.1

The UV-Vis absorption spectrum of compound **2.1** (Figure 2.4), shows a strong absorption band at (λ_{max} = 314 nm, ε = 7600 $M^{-1}.cm^{-1}$), which can be attributed to ligand-centered transition (phenylpyridine). In addition, it shows a low-energy shoulder at (λ_{max} = 357 nm, ε = 3200 $M^{-1}.cm^{-1}$), which can be attributed to a charge transfer transition from a mesityl group (HOMO) to the phenylpyridine chelate (LUMO). This is also supported by the solvent dependent emission of **2.1** (Figure 2.5), where the emission is red-shifted about 20 nm when the solvent is changed from toluene (non-polar) to DCM (polar). In addition, compound **2.1** displays a strong sky-blue fluorescence in DCM with λ_{max} = 475 nm and a fluorescence quantum efficiency Φ_F = 0.1.

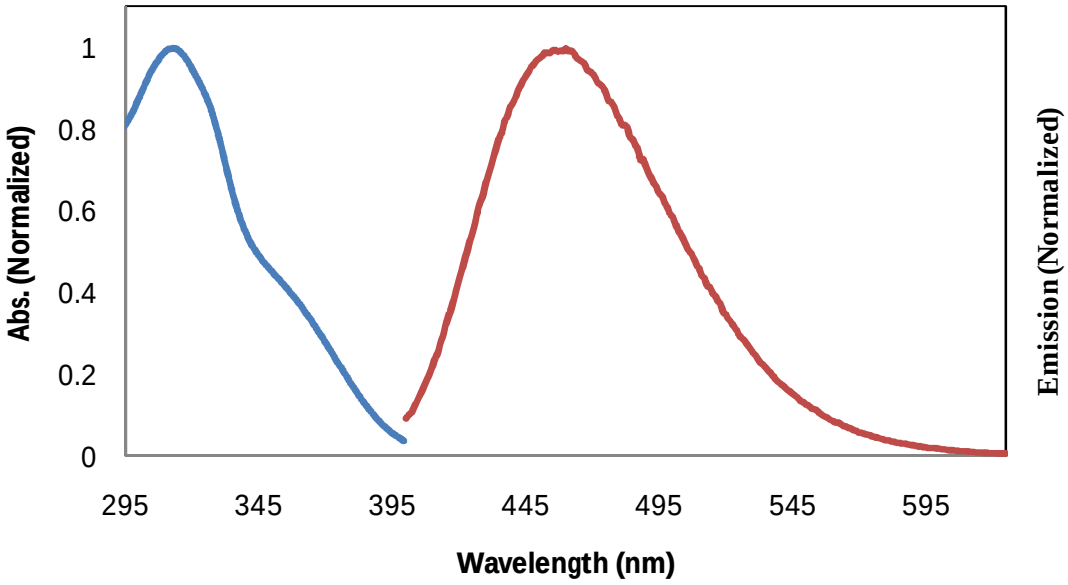

Figure 2.4 Normalized absorption and fluorescence of **2.1** in toluene (~10^{-5} M)

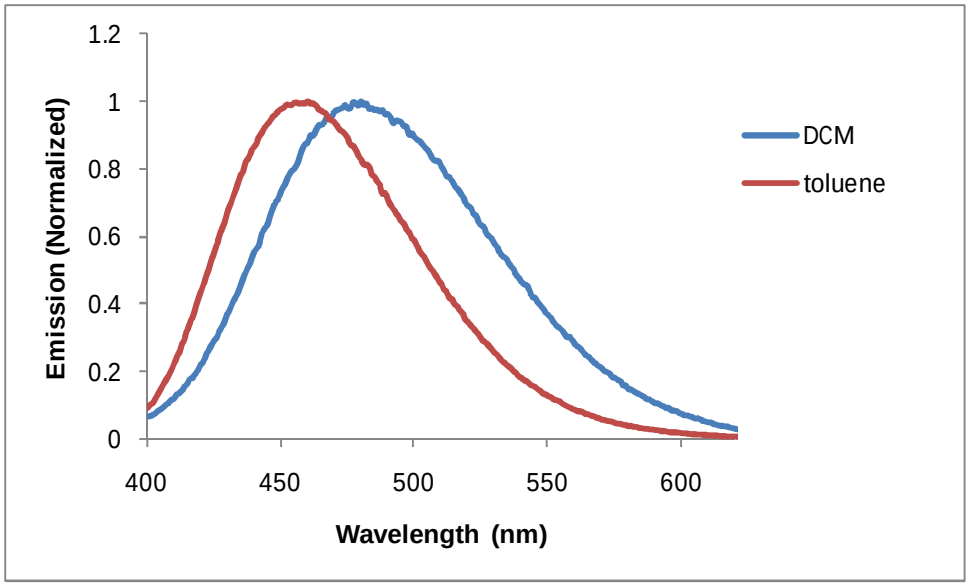

Figure 2.5 Emission spectra of compound **2.1** in toluene and DCM.

2.3.4 Electrochemical Properties

Compound **2.1** displays an irreversible reduction peak at – 2.30 V (vs. $FeCp_2^{+/0}$ in DMF) (Figure 2.6), corresponding to a LUMO energy level of -2.45 eV, which can be attributed to the reduction of the π* orbital of the phenylpyridine ligand. The reduction peak of **2.1** is more negative than those of similar triarylboron compounds,[10] which means triarylborons are better electron acceptors.

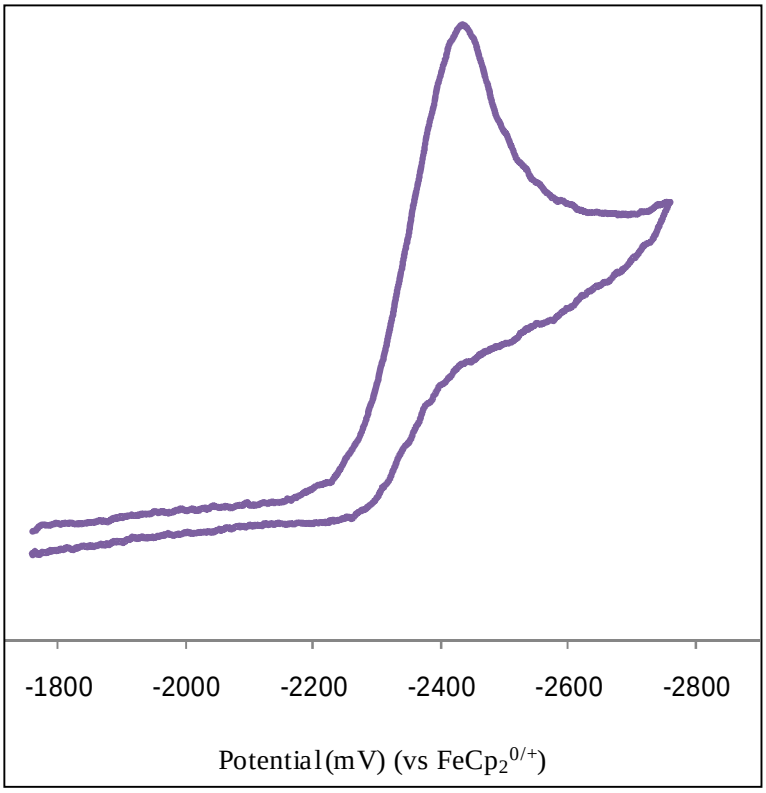

Figure 2.6 CV diagram showing the reduction peak of **2.1** recorded in DMF with scan rate 300 mV/s

In addition, the experimental optical energy gap calculated based on the absorption edge (3.1 eV) is in agreement with the HOMO-LUMO gap calculated based on DFT calculations (3.51 eV).

2.3.5 DFT Calculations

DFT and TD-DFT calculations were performed on compound **2.1** and it was established that the lowest energy transition observed in the absorption and emission spectra originates from the HOMO-LUMO transition. The HOMO and LUMO diagrams are shown in Figure 2.7. The HOMO is mainly dominated by the mesityl group closer to the phenyl ring of the phenylpyridine and the C_{phenyl}-B, while the LUMO is mainly dominated by the phenylpyridine π^* orbital.

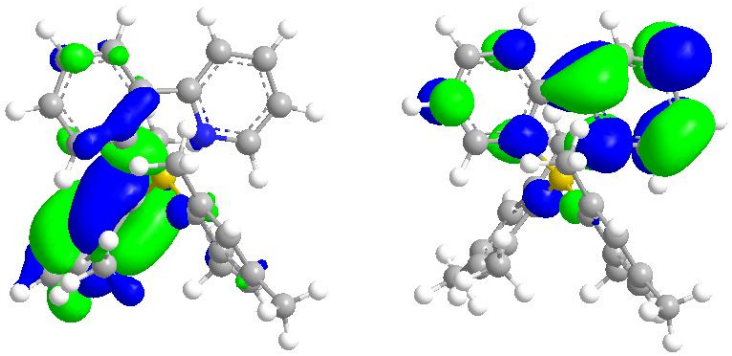

HOMO LUMO

Figure 2.7 HOMO and LUMO diagrams of compound **2.1** with a surface isocontour value of 0.03.

Also, TD-DFT calculations supports that the lowest energy transition is mainly a HOMO-LUMO one with oscillator strength of 0.0127 (Figure 2.8). The calculated UV-

Vis spectrum of **2.1** has similar features as those of the experimental one with about 70 nm shift, which might be attributed to the fact that DFT calculations were performed based on the gas phase.

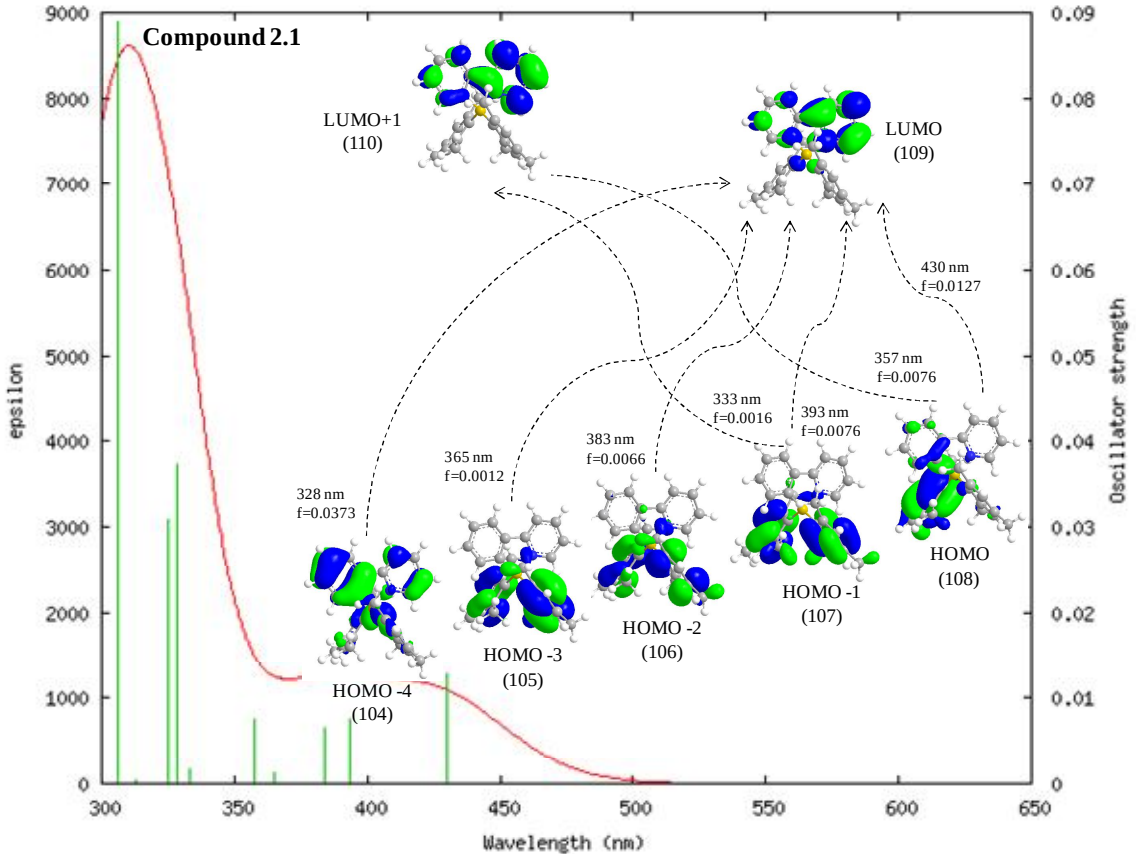

Figure 2.8 Calculated UV-Vis spectrum of **2.1** with characteristic electronic transitions calculated at the TD-DFT (B3LYP/6-311G*) level. Produced using GaussSum program V.2.2.2 with FWHM = 3000 cm^{-1}

Table 2.3 Selected data of electronic transitions in **2.1** by TD-DFT method at the B3LYP/6-311G* level.

State	λ(nm)	f [(a)]	Composition of band	CI [(b)] coefficients
1	430.25	0.0127	108→109	0.69980
2	393.47	0.0076	106→109 107→109	0.36893 0.59580
3	383.99	0.0066	106→109 107→109	0.59757 -0.37205
4	365.17	0.0012	105→109	0.70407
5	357.31	0.0076	108→110	0.69910
6	333.06	0.0016	106→110 107→110	0.39405 0.57878
7	328.26	0.0373	104→109 106→110 107→110	0.55900 -0.32832 0.20462
8	324.94	0.0308	103→109 104→109 106→110 107→110	0.11193 0.35617 0.47484 -0.34260
9	312.58	0.0005	105→110	0.70226
10	306.02	0.0889	103→109 104→110	0.64416 0.12220

(a) f = oscillator strength (b) CI = configuration interaction

2.3.6 Photochromic Behavior of Compound 2.1

During our investigation of the properties of compound **2.1** we discovered that it is photochromic in nature and belongs to the T-type photochromic systems. Upon irradiation of a toluene solution of **2.1** with UV light (365 nm) under an atmosphere of N_2, the color changes from colorless/slightly yellowish to dark blue. Simultaneously, the initial strong sky-blue fluorescence starts to lose its intensity and eventually disappears. On the other hand, by heating the same solution the dark blue color fades out and the solution goes back to its initial colorless state. The photochromic conversion was monitored using UV-Vis spectroscopy as shown in Figure 2.9. Upon irradiation of a toluene solution of **2.1** with UV light (365 nm) under an atmosphere of N_2, a new intense broad band with λ_{max} = 599 nm (ε = 5000 $M^{-1}.cm^{-1}$) appears and grows rapidly. The quantum efficiency of the photoisomerization of **2.1** to **2.1a** was determined to be 0.88 in toluene at 298 K, with λ_{ex} = 365 nm using ferrioxalate actinometry, which the highest recorded for this type of compounds as will be discussed in chapter 3.

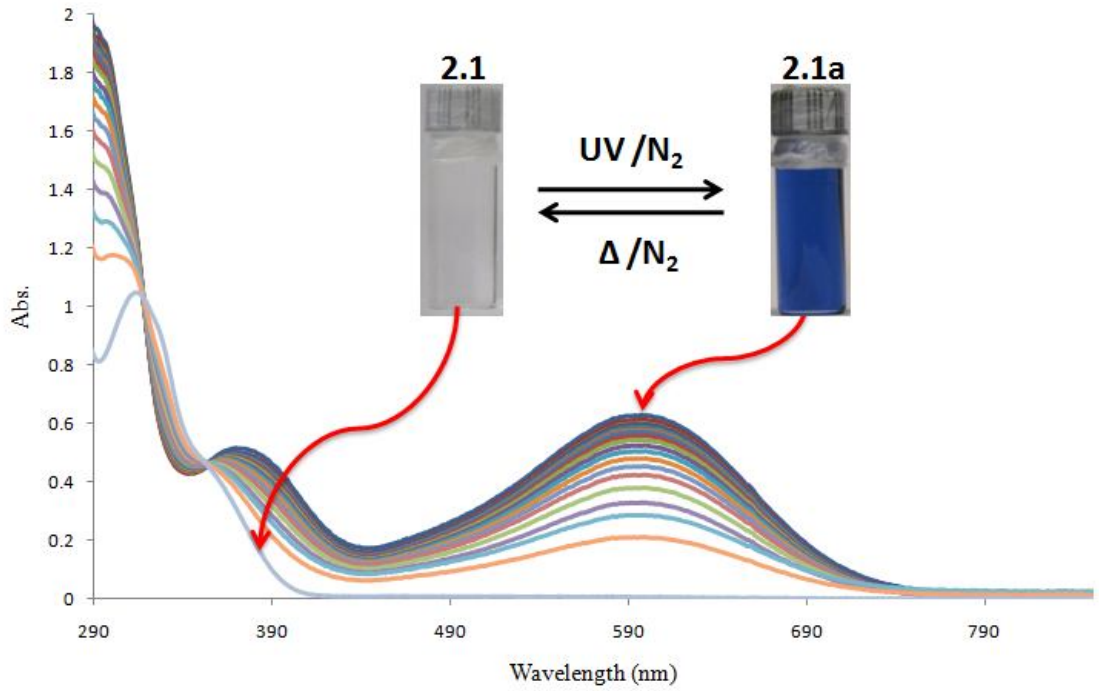

Figure 2.9 UV-Vis spectral changes of **2.1** under N_2 in toluene upon UV irradiation at 365 nm. Inset, photographs of **2.1** showing the color change before and after irradiation.

Similarly, a thin film of PMMA containing **2.1** prepared by slow evaporation, under inert atmosphere, of a DCM solution of both PMMA and **2.1** shows a similar behavior, which indicates that **2.1** is also photochromic in the solid state (Figure 2.10)

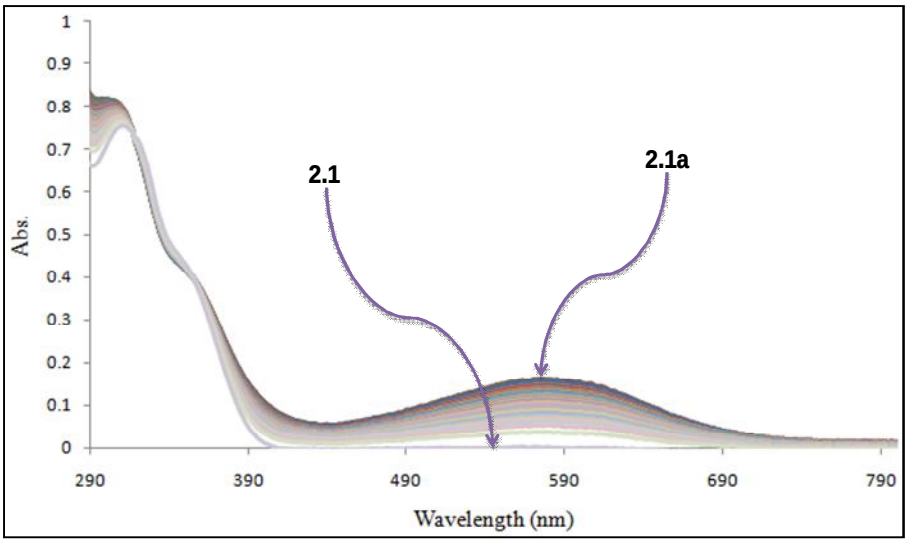

Figure 2.10 UV-Vis spectral changes of **2.1**, in a PMMA matrix, under N_2 in toluene upon UV irradiation at 365 nm.

2.3.7 Elucidation of the Dark Isomer Structure (2.1a)

The proposed **2.1a** structure was suggested based on ^{1}H NMR, ^{11}B NMR, and 2D NMR experiments and based on a previously reported X-ray structure of a similar system, namely the (p-biphenyl)triphenyl borate reported by Schuster *et al*[11] (Figure 1.24). The photolysis of (p-biphenyl)triphenyl borate performed by Schuster *et al* led to a color change from slightly yellowish to red, which is consistent with observed color change in our case.

2.3.7.1 Elucidation of the Dark Isomer Structure (2.1a) using ^{1}H NMR and ^{11}B NMR

The photochromic behavior of **2.1** was monitored using ^{1}H NMR spectroscopy. Upon irradiation of a C_6D_6 solution of **2.1** with UV light (365 nm) under N_2, the ^{1}H NMR spectra of **2.1** displays a new set of peaks that represent the dark isomer (**2.1a**). With

more UV exposure time the peaks of **2.1a** gained more intensity and the peaks of **2.1** diminished gradually as shown in Figure 2.11. Upon conversion of **2.1** to **2.1a** the singlet representing the four aryl protons of the two mesityl groups (H_{Ar}) splits in to four distinct singlet peaks (H_a, H_b, H_c, and H_d), and the two singlet peaks representing the six methyl groups in **2.1** ($Me_{\textit{para}}$ and $Me_{\textit{ortho}}$) splits in to six distinct methyl peaks (Me_a, Me_b, Me_c, Me_d, Me_f, and Me_e) as shown in Figure 2.12, which indicates a restricted rotation around the B-C_{Mes} bonds in **2.1a**.

The singlet aryl proton peaks of one of the two mesityl groups in **2.1a** (H_a and H_b) shows a distinct up-field shift. Similarly, one of the *ortho* methyls (Me_a) shifts to 0.55 ppm, which represents the chemical shift of a methyl group that's attached to an sp^3 carbon, indicating loss of aromaticity.

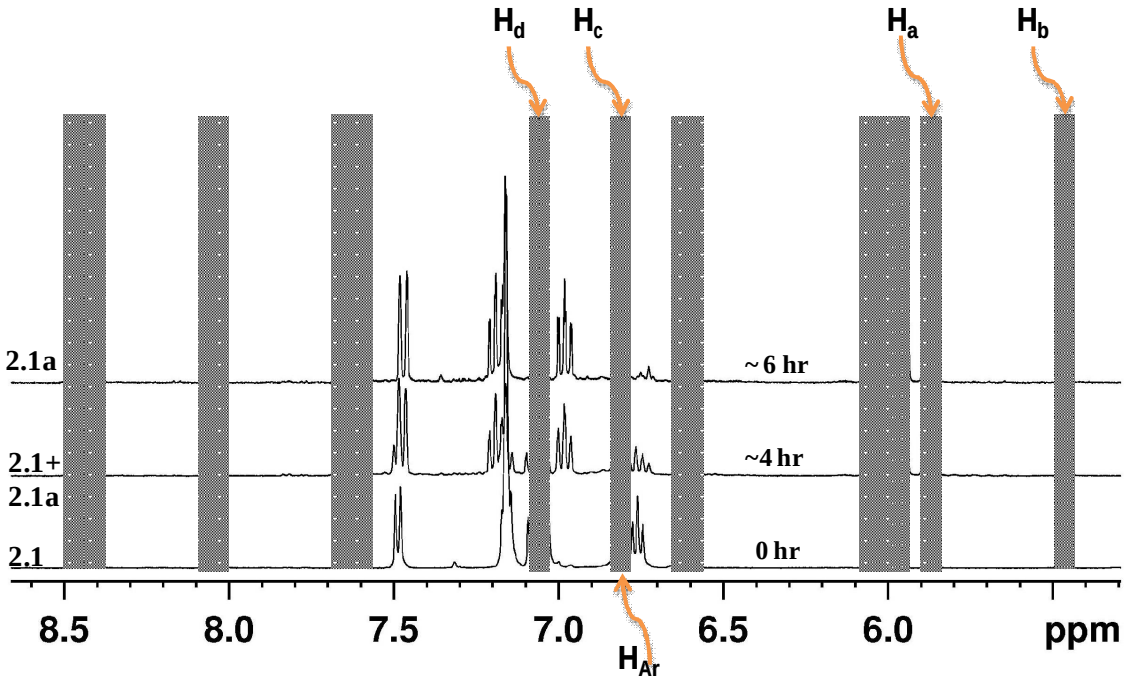

Figure 2.11 ^{1}H NMR spectral changes (aromatic region) of **2.1** in C_6D_6 under N_2 upon irradiation at 365 nm. Violet: **2.1** and green: **2.1a**.

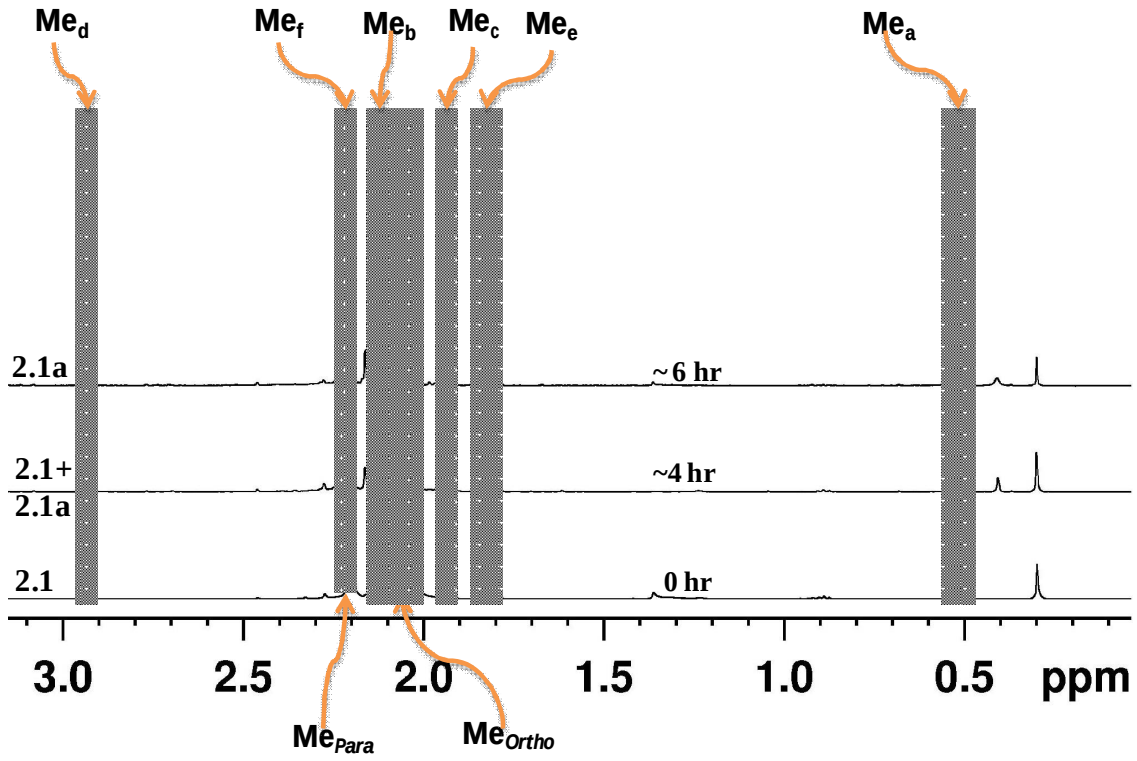

Figure 2.12 ^{1}H NMR spectral changes (aliphatic region) of **2.1** in C_6D_6 under N_2 upon irradiation at 365 nm. Highlights show mesityl protons. Violet: **2.1** and green: **2.1a**.

Also, upon photolysis of compound **2.1** the ^{11}B NMR signal of the tetrahedral B center of **2.1** at 5.02 ppm shifts to -9.91 ppm (**2.1a**) (Figure 2.13), which indicates a change of chemical environment around the B center with retention of the tetrahedral geometry.

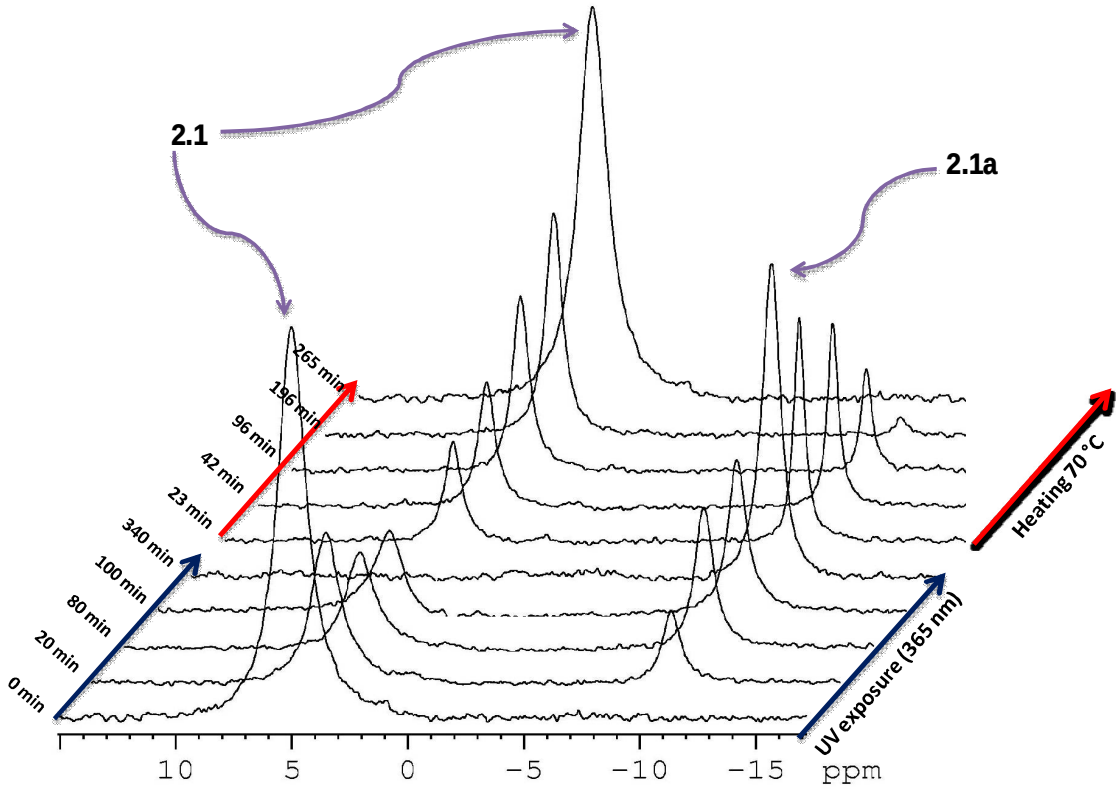

Figure 2.13 ^{11}B NMR spectral changes of **2.1** in C_6D_6 under N_2 upon irradiation at 365 nm and the subsequent heating at 70 °C of **2.1a** back to **2.1**.

The characteristic peaks of **2.1a** in both ^{1}H NMR and ^{11}B NMR spectra are similar to those reported by Schuster and co-workers. Their proposed dark isomer, which was unambiguously confirmed by X-ray analysis, has similar characteristic ^{1}H NMR peaks at 5.55 ppm representing Hb and at 1.39 ppm representing Ha (Figure 1.25). They have also observed a distinct up field shift of 20 ppm in the ^{11}B NMR (-6.7 to -26.6 ppm) suggesting a similar boron environment for their dark isomer with compound **2.1a**. These similarities led us to believe that the dark isomer (**2.1a**) has the proposed structure that's

showed in Figure 2.1. Based on ^{1}H NMR and 2D NMR experiments done on **2.1a** (2D-NMR experiments were performed by my colleague Sanela Martic) the ^{1}H NMR peaks of **2.1a** were assigned as shown in Figure 2.14 and Figure 2.15.

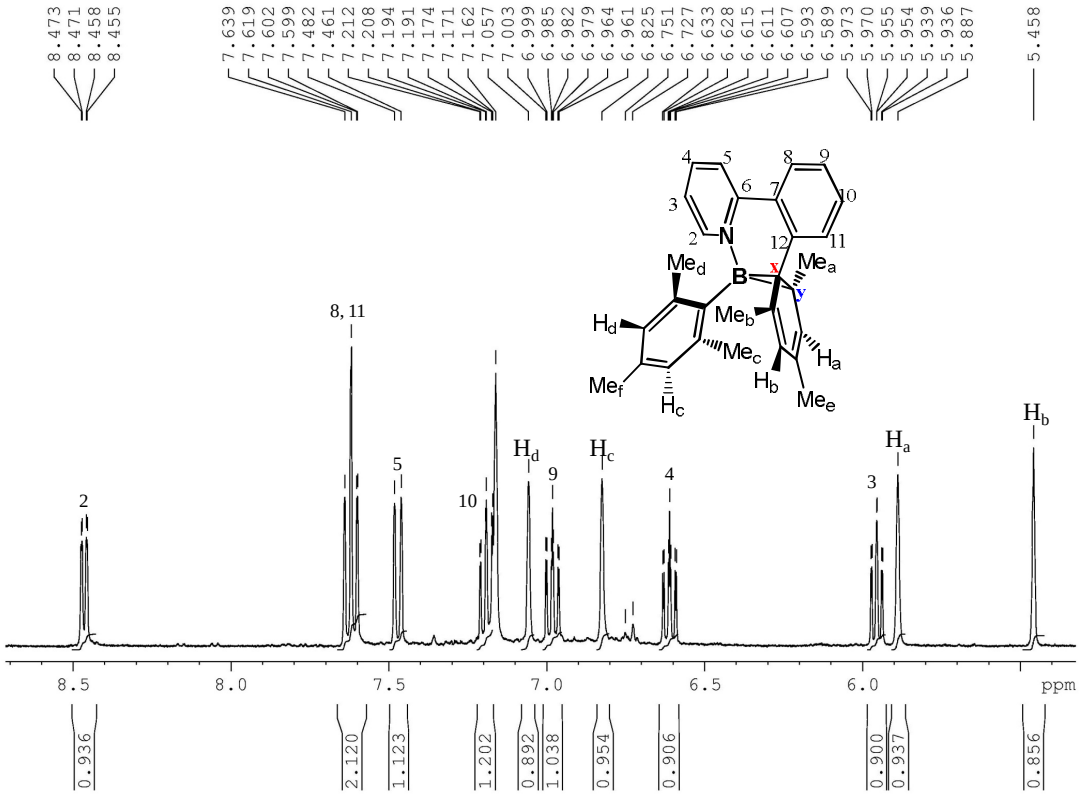

Figure 2.14 ^{1}H NMR spectral assignments of the aromatic region of **2.1a** in C_6D_6 at RT

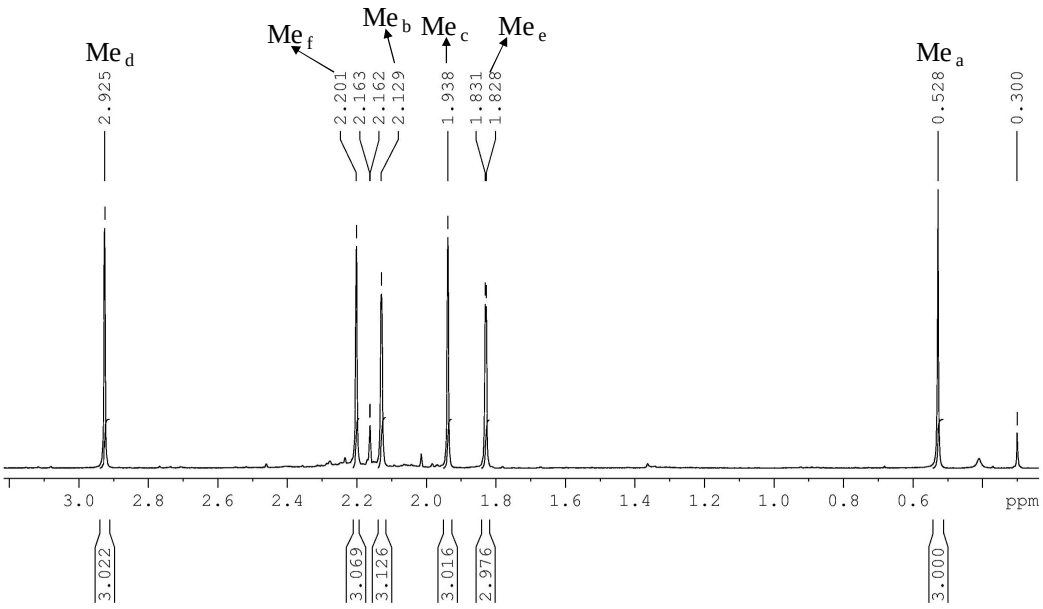

Figure 2.15 ^{1}H NMR spectral assignments of the aliphatic region of **2.1a** in C_6D_6 at RT

Peak assignments of 2.1a protons were also supported by COSY NMR data, which are shown in Figure 2.16 and Figure 2.17.

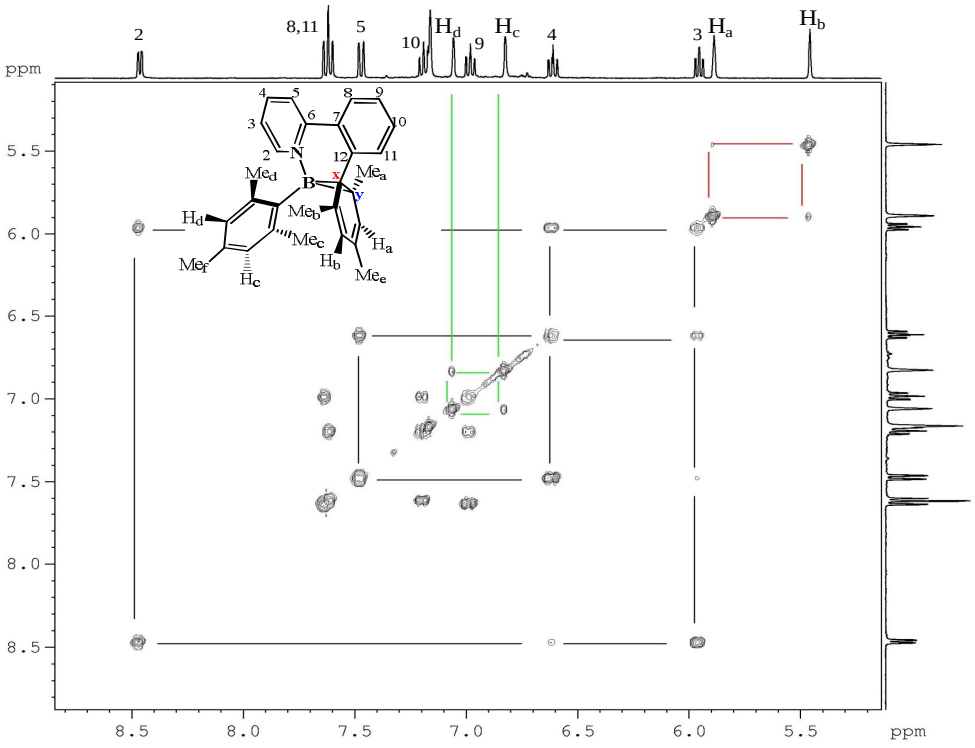

Figure 2.16 COSY spectrum of **2.1a** showing the correlation between the protons of the aromatic region, in C_6D_6 at RT

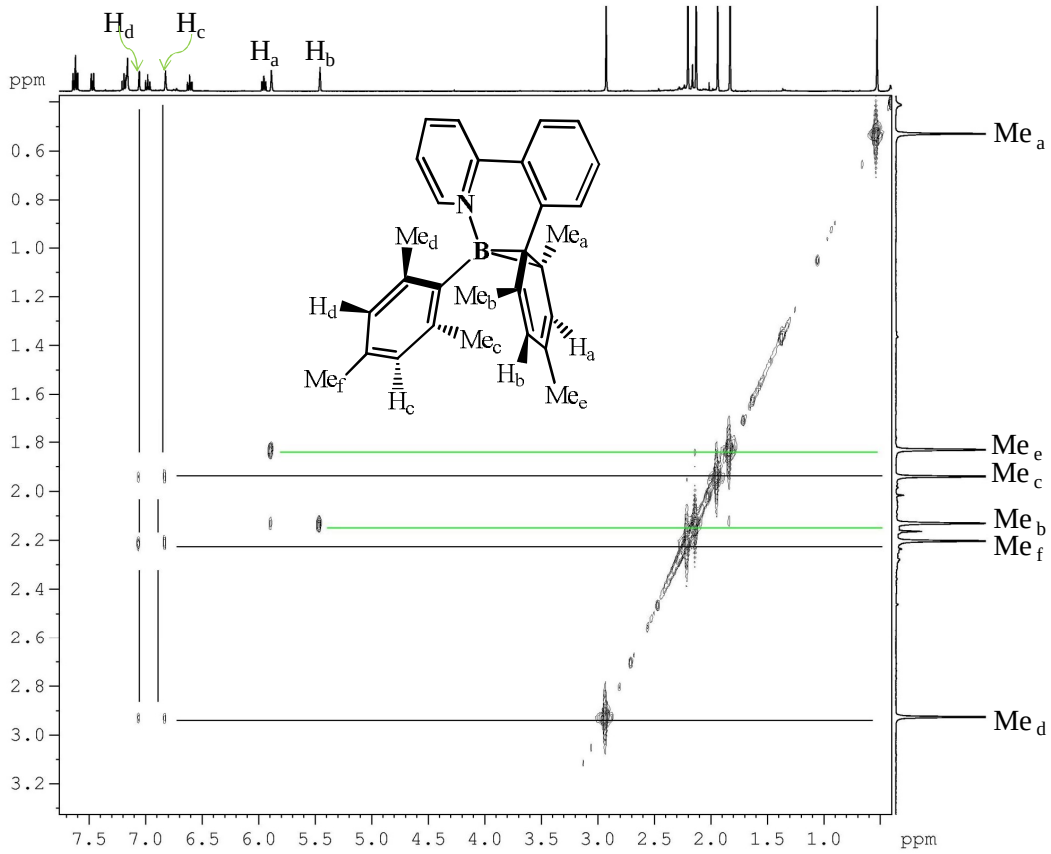

Figure 2.17 COSY spectrum of **2.1a** showing the correlation between the protons of the aromatic region and the methyl protons in the aliphatic region, in C_6D_6 at RT

2.3.7.2 Elucidation of the Dark Isomer Structure (2.1a) using ^{13}C NMR and HMBC NMR

The structural elucidation of **2.1a** was also supported by the HMBC NMR spectra as shown in Figure 2.18 and Figure 2.19, where C_x exhibits $^3J_{C\text{-}H}$ coupling with H_a, H_b, H_{11}, Me_a, and Me_b protons and C_y exhibits a $^2J_{C\text{-}H}$ coupling with H_a and Me_a protons. These correlations are consistent with the presence of a C_x-C_y bond.

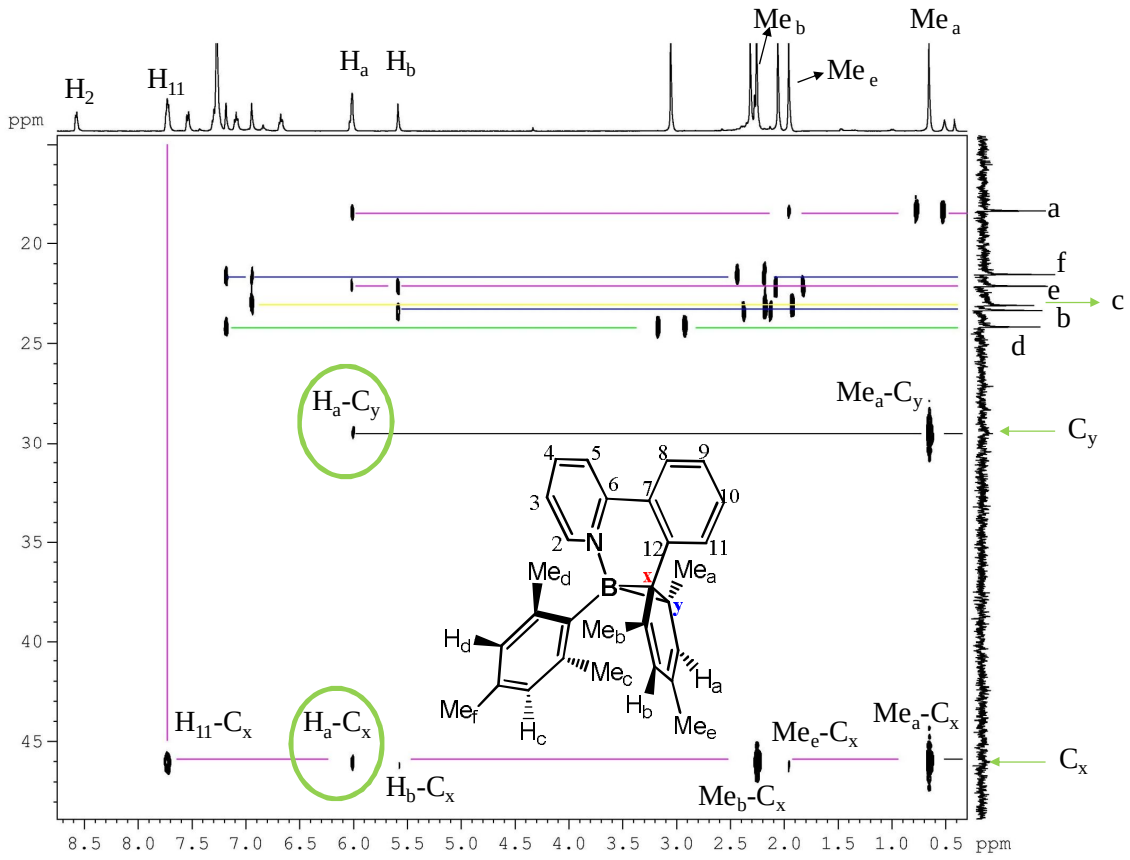

Figure 2.18 HMBC spectrum of **2.1a** showing the correlation between all protons and carbons of the aliphatic region, in C_6D_6 at RT

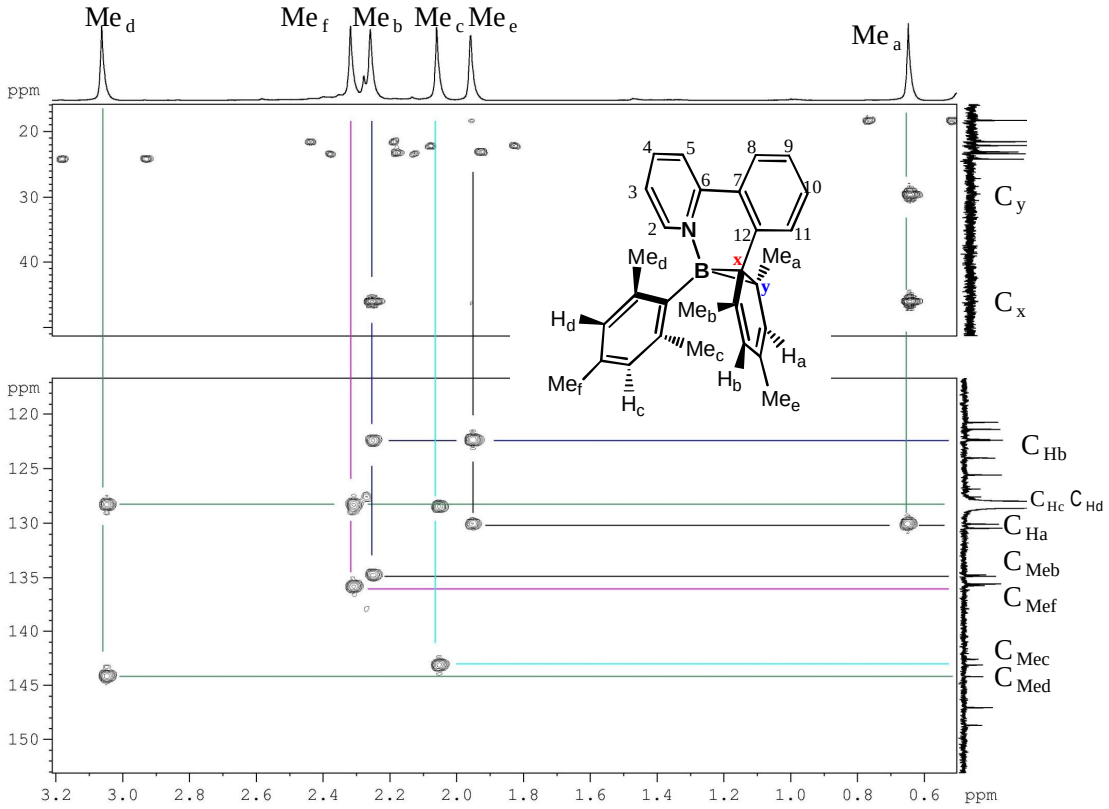

Figure 2.19 HMBC spectrum of **2.1a** showing the correlation between the protons of the aliphatic region and all carbons, in C_6D_6 at RT

In addition, the ^{13}C chemical shifts (Figure 2.20 and Figure 2.21) of the quaternary C_x and C_y atoms (46.0 and 29.5 ppm) indicate that both are aliphatic carbons, further supporting the proposed structure of **2.1a**.

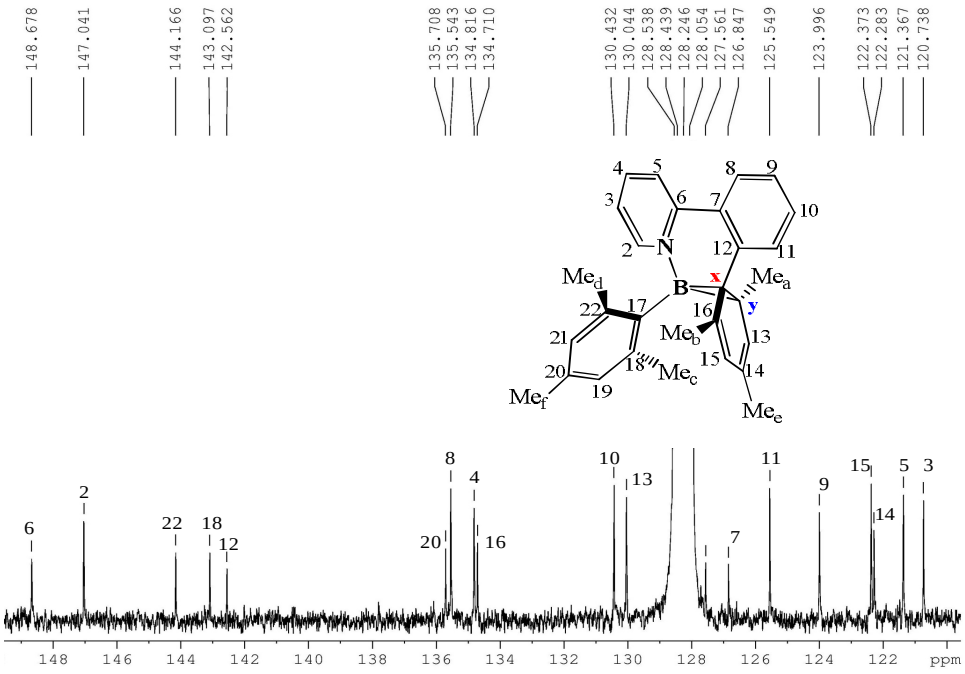

Figure 2.20 ^{13}C NMR spectral assignments of the aromatic region of **2.1a** in C_6D_6 at RT

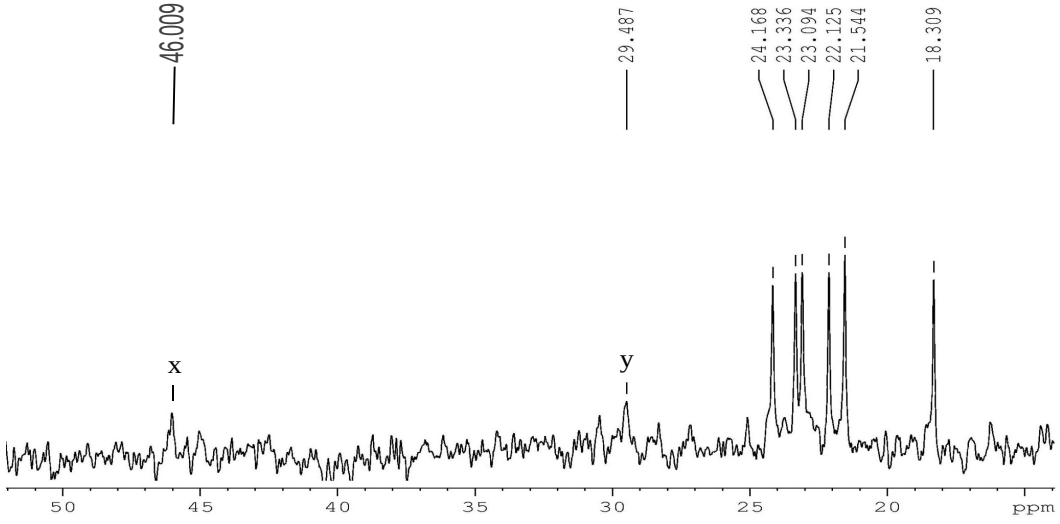

Figure 2.21 ^{13}C NMR spectral assignments of the aliphatic region of 2.1a in C_6D_6 at RT

In addition to the through-space interaction between protons that the NOESY spectra provided (Figure 2.22 - Figure 2.24), the aromatic region of the NOESY spectrum shows strong chemical exchange cross-peaks between (H_a-H_b), and (H_c-H_d). Also, the aliphatic region of the NOESY shows similar cross-peaks between (Me_a-Me_b), and (Me_c-Me_d). The exchange between both (H_c-H_d) and (Me_c-Me_d) indicates that there is a degree of free rotation around the (B-C_{17}) bond, e.g. rotation of the mesityl group. On the other hand, the exchange between both (H_a-H_b) and (Me_a-Me_b) indicates that the cyclohexadiene ring is rotating, which possibly could go through a B-C_y bond breaking associated with rotation around C_x and movement of the conjugated π electrons towards C_y.

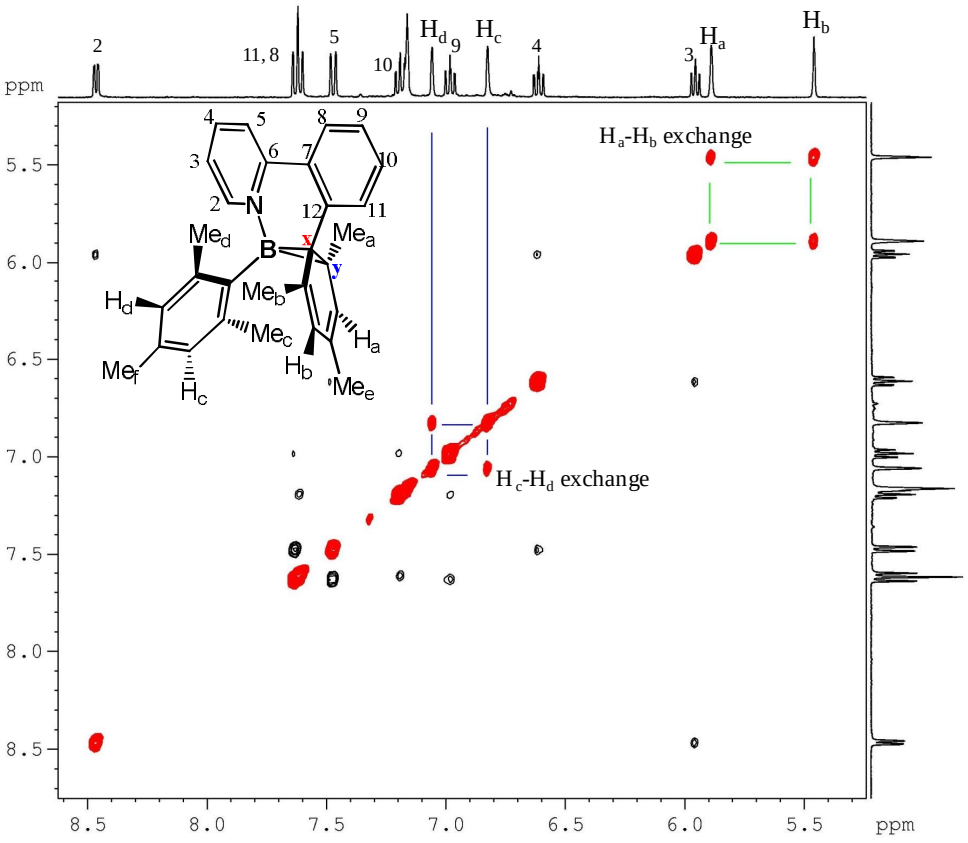

Figure 2.22 NOESY spectrum of **2.1a** showing the through-space interaction between the protons of the aromatic region (red color indicates exchange cross-peaks), in C_6D_6 at RT

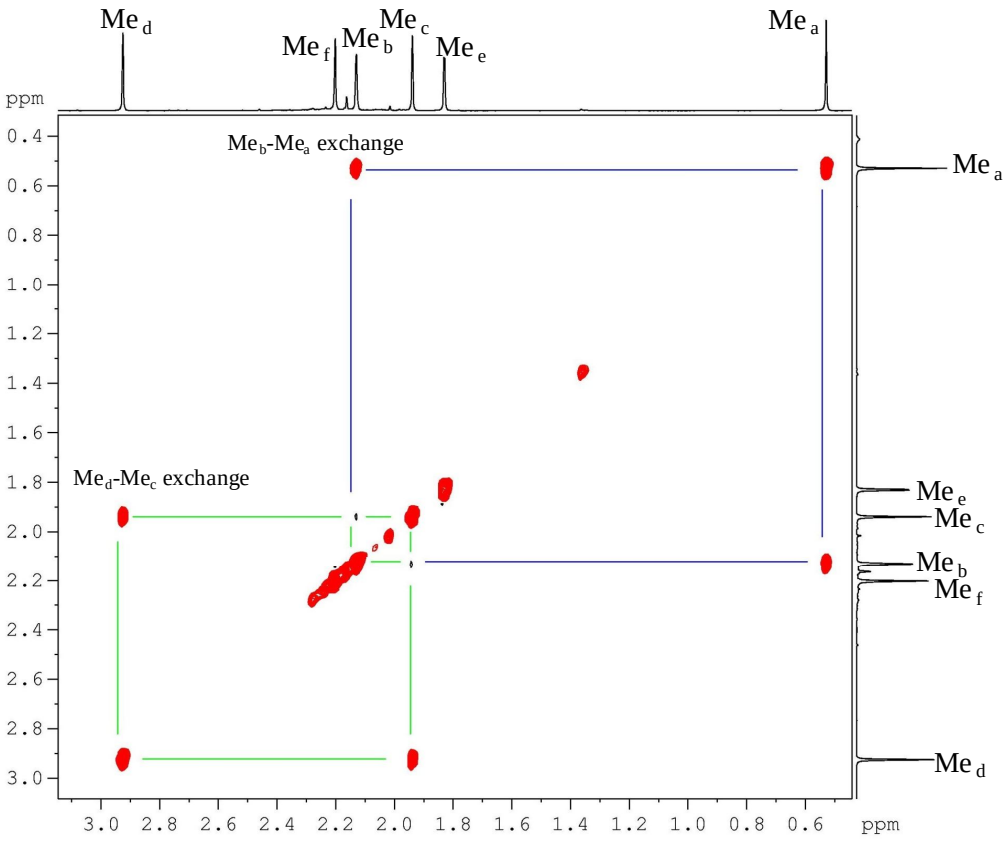

Figure 2.23 NOESY spectrum of **2.1a** showing the through-space interaction between the methyl groups (red color indicates exchange cross-peaks), in C_6D_6 at RT

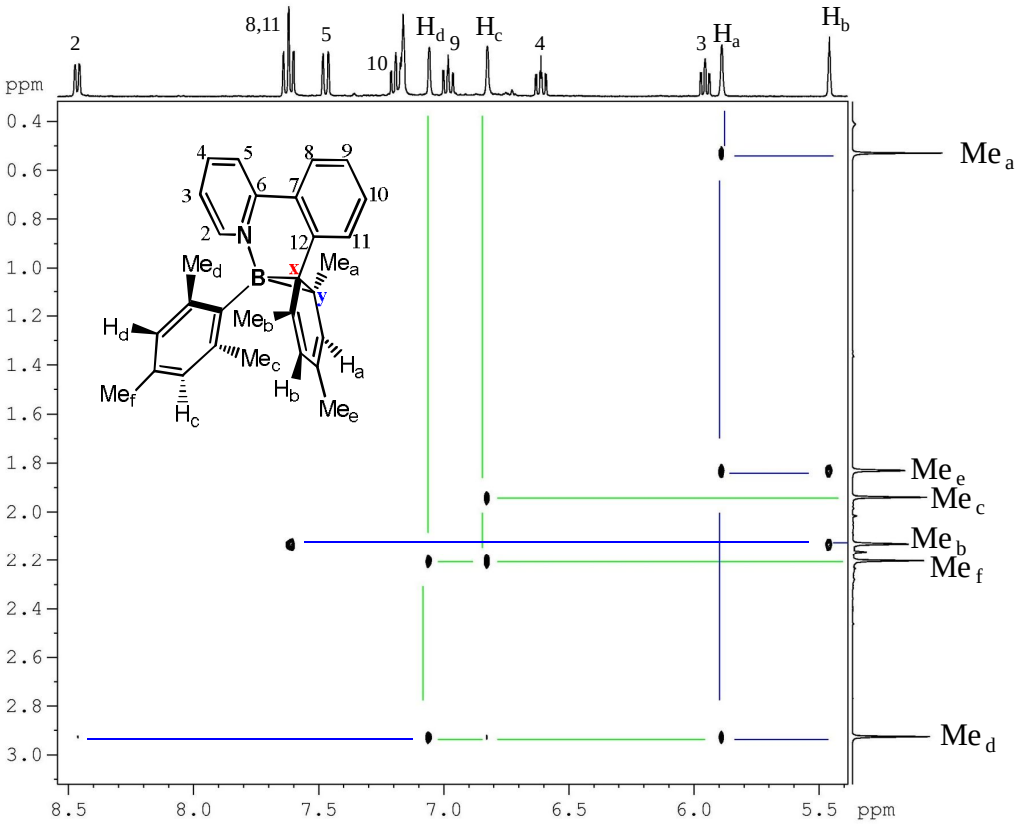

Figure 2.24 NOESY spectrum of **2.1a** showing the through-space interaction between the protons of the aromatic region and the methyl groups, in C_6D_6 at RT

Schuster and co-workers proposed that a di-π-borate rearrangement leads to the formation of compound 3 (Figure 2.26), which is analogous to the di-π-methane rearrangement[12] (Figure 2.25)

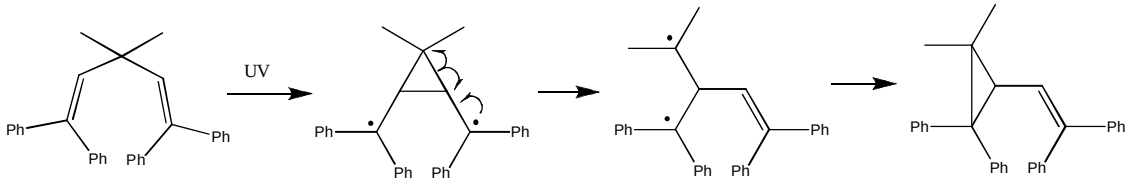

Figure 2.25 General mechanism of di-π-methane rearrangement.

The possible products (**1**, **2**, and **3**) from the di-π-borate rearrangement of (p-biphenyl)triphenyl borate (Figure 2.26), were identified in the reaction mixture immediately after irradiation using ^{1}H NMR but only **3** was successfully crystallized.

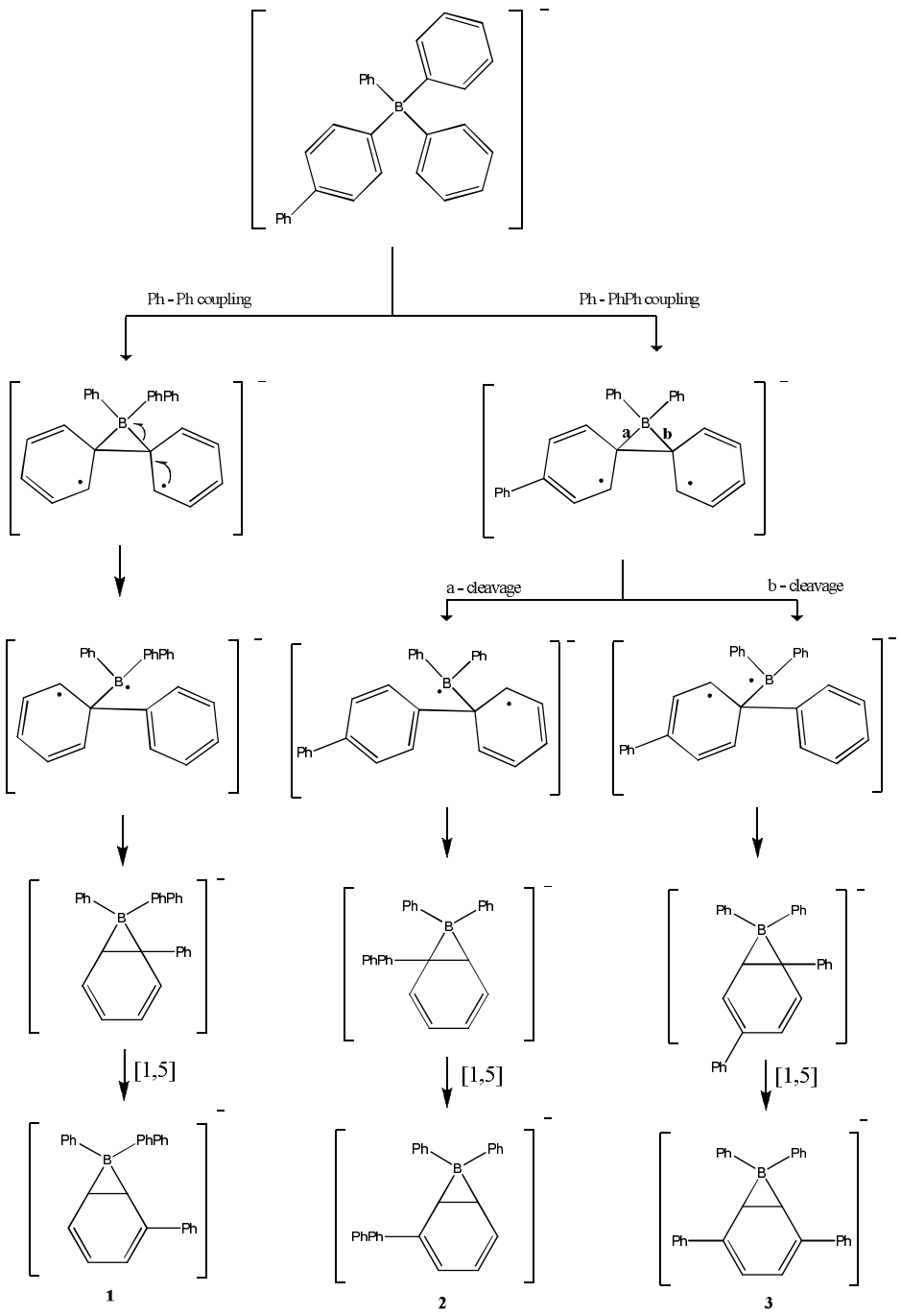

Figure 2.26 Suggested mechanism of di-π-borate rearrangement of (p-biphenyl)triphenyl borate .

Based on the di-π-borate rearrangement we anticipated the formation of two different products **2.1a** and **2.1c** (Figure 2.27), but our NMR studies strongly support the formation of **2.1a**. In addition, the X-ray crystal structure of a similar N,C-chelate (will be discussed in chapter 3) also proves the formation of the **2.1a** photoproduct.

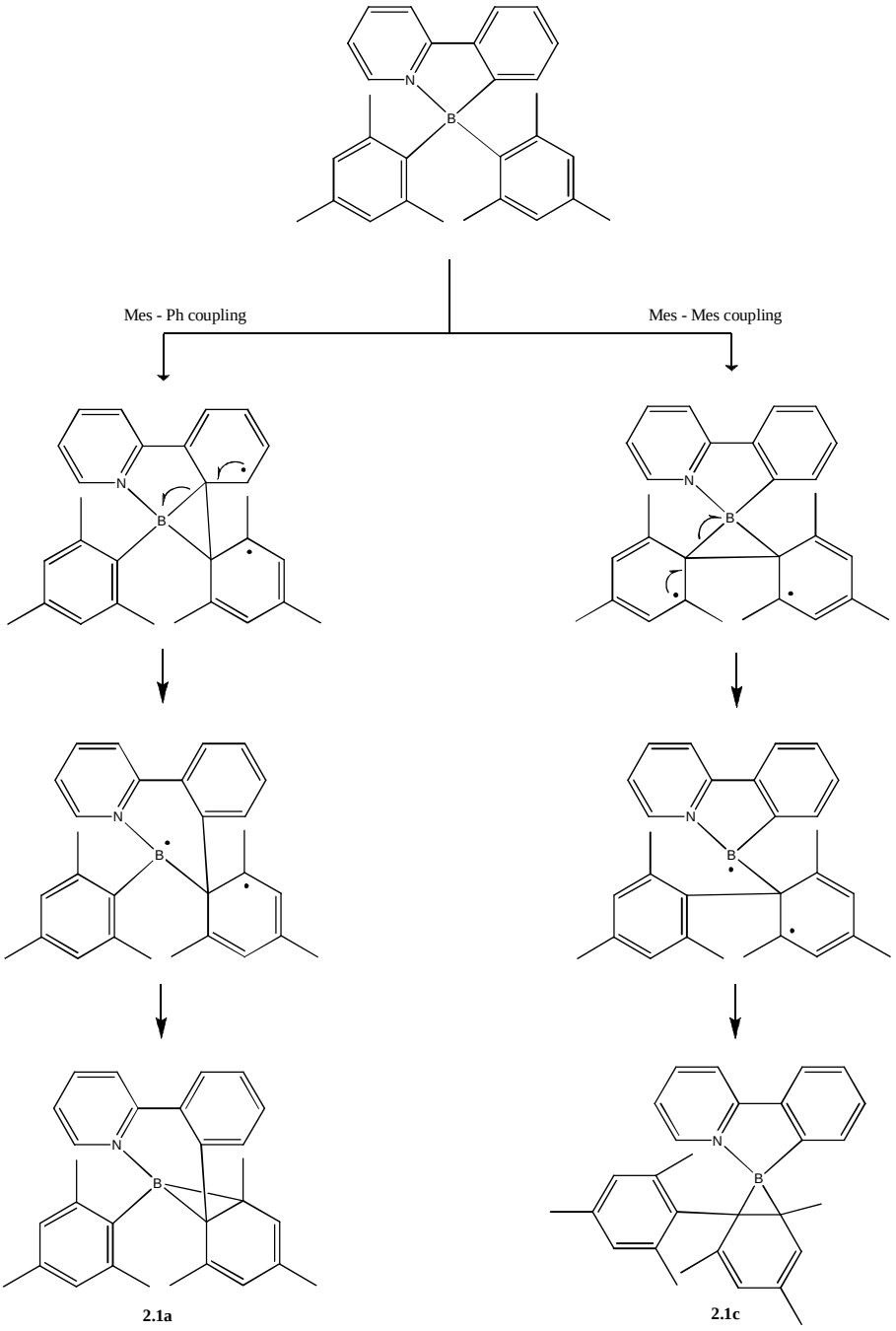

Figure 2.27 Suggested mechanism of di-π-borate rearrangement of $PhPyBMes_2$.

2.3.8 Thermal Conversion of the Dark Colored Isomer (2.1a) to the Colorless Isomer 2.1

The dark blue colored isomer (**2.1a**) can be converted back to the colorless isomer (**2.1**) upon heating (T-type). Figure 2.13 above shows the complete conversion of **2.1a** to **2.1** in C_6D_6 monitored by ^{11}B NMR at 70 °C. The thermal conversion was also studied using ^{1}H NMR at different temperatures as shown in Table 2.4, and the activation energy (109 kJ/mol) was estimated using an Arrhenius plot (Figure 2.28). The ^{1}H NMR spectra of thermal conversion at 70 °C of **2.1a** to **2.1** is shown in Figure 2.29.

Table 2.4 Activation energy data of the thermal conversion of **2.1a** to **2.1** using ^{1}H NMR

T (K)	1/T (K^{-1})	k (min^{-1})	ln(k)
298	0.003356	0.00005	-9.90
323	0.003096	0.0015	-6.50
330	0.00303	0.0047	-5.36
340	0.002941	0.0104	-4.57

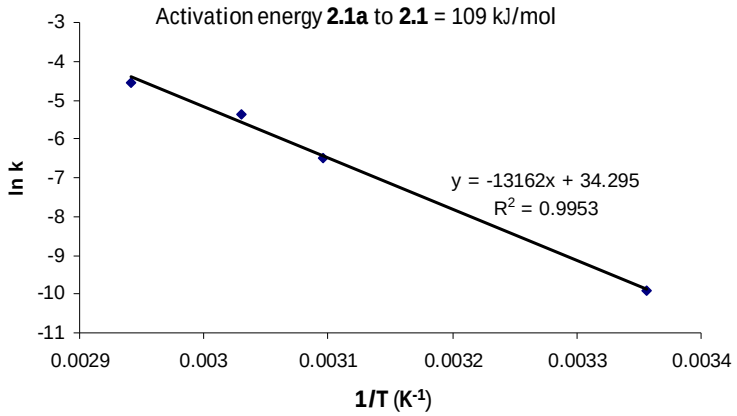

Figure 2.28 Activation energy of the thermal conversion of **2.1a** to **2.1** using Arrhenius plot.

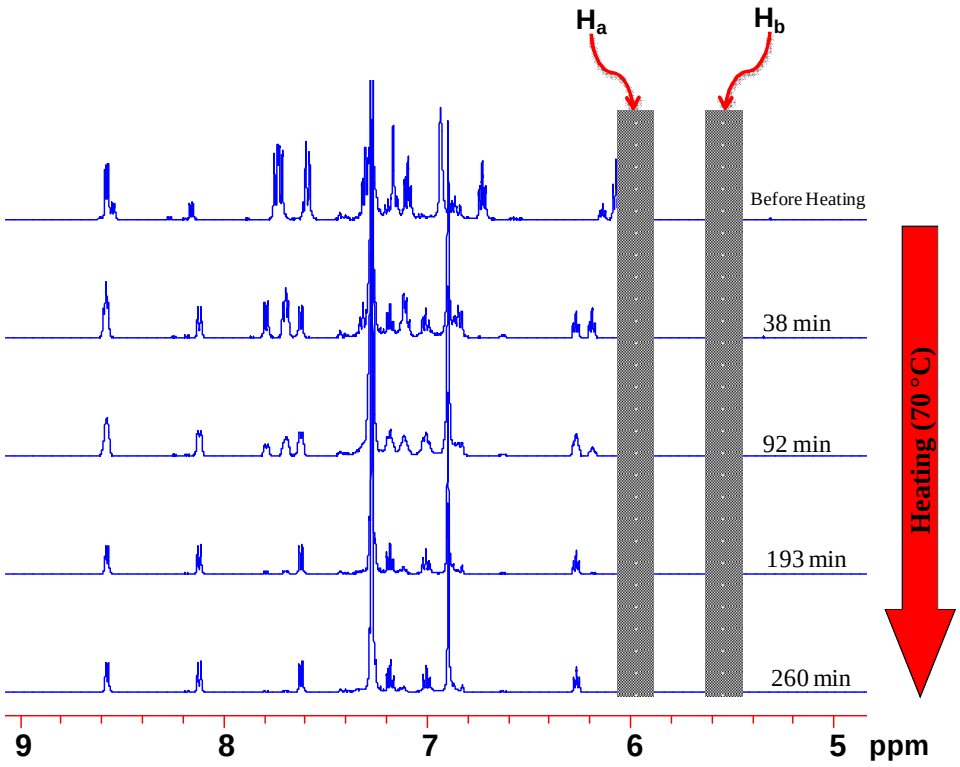

Figure 2.29 Thermal conversion of **2.1a** to **2.1** under nitrogen in C_6D_6 at 70 °C. The highlights show the disappearance of the aromatic singlet peaks (H_a and H_b) of **2.1a**.

2.3.9 Sensitivity of the Dark Isomer (2.1a) Towards Oxygen

The dark isomer **2.1a** is highly reactive towards oxygen and the blue colored **2.1a** C_6D_6 solution loses color immediately when exposed to O_2, which leads to the formation of compound **2.1b**. The photolysis of **2.1** under an atmosphere of oxygen was monitored using ^{1}H NMR as shown in Figure 2.30. The formation of compound **2.1b** was quantitative and it was isolated and characterized using ^{1}H NMR, ^{13}C NMR, and HRMS. In addition, the boron content of **2.1b** was recovered as boroxine $(MesBO)_3$, which precipitated out of the C_6D_6 solution.

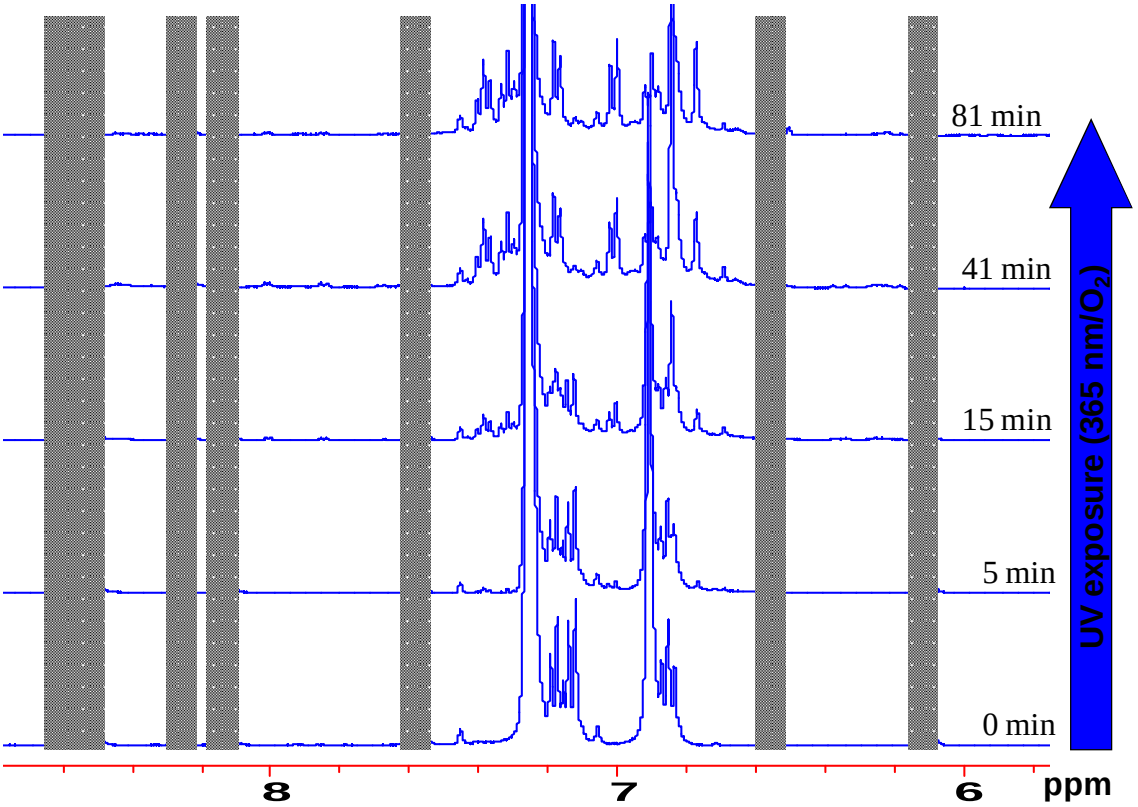

Figure 2.30 UV irradiation at 365 nm of compound **2.1** under oxygen in C_6D_6. Violet: **2.1** and yellow: **2.1b**.

2.3.10 Calculated Structural Parameters and DFT Calculations of 2.1a

The high oxygen-sensitivity of **2.1a** and the high solubility in both polar and non-polar solvents, in addition to the competing thermal reversibility rendered the crystallization of **2.1a** impossible to achieve. Hence, the proposed structure was built using Gaussian program and was optimized using DFT calculations, which was performed by my colleague Theresa McCormick.

The optimized structural model of **2.1a** agrees very well with the interpretations made based on the NMR data. Based on the calculated structure of **2.1a** (Figure 2.31), the 6-membered chelating ring is co-planar with the phenyl-pyridine rings and at 115° of the 3-membered ring composed of CBC. Also, the calculated (C_{Ph}-C_x) bond length is 1.48 Å, while the bond lengths of the 3-membered ring are 1.66 Å and 1.63 Å for the two B-C bonds, and 1.56 Å for the C-C bond. In addition, the through-space distance between H_a and the protons of Me_d is very short (2.5 Å), which is consistent with the strong cross-peak correlations between them in the NOESY spectrum.

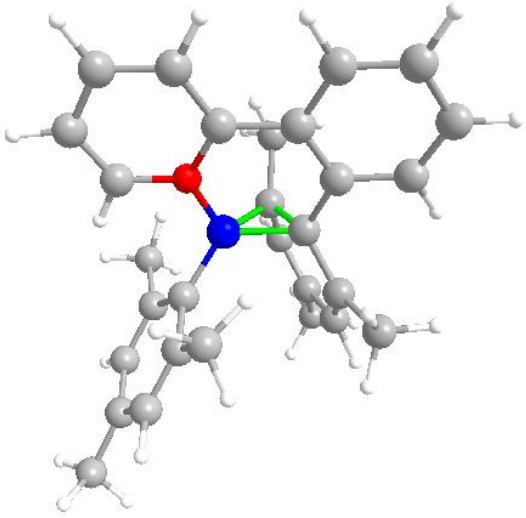

Figure 2.31 Calculated structure of compound **2.1a**

Furthermore, the calculated UV-Vis spectra of **2.1a** obtained from TD-DFT calculations using the GaussSum[13] program, has the same spectral features as the experimental one as shown in Figure 2.32 and Figure 2.33, which further supports that the proposed structure of **2.1a**. Also, the HOMO-LUMO gap of **2.1a** (1.14 eV) is less than that of **2.1** (3.51 eV), which is consistent with the optical energy gaps difference of **2.1a** (1.61 eV) and **2.1** (3.1 eV) obtained from UV-Vis spectra as shown in Table 2.5.

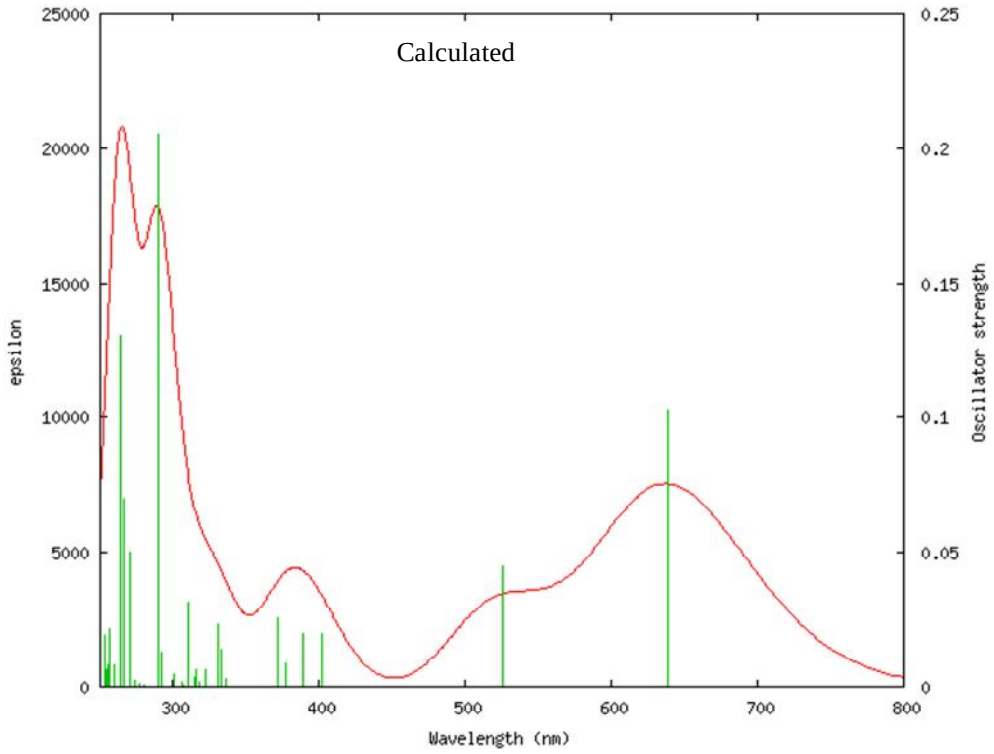

Figure 2.32 Calculated UV-Vis spectrum of **2.1a** based on TD-DFT calculations

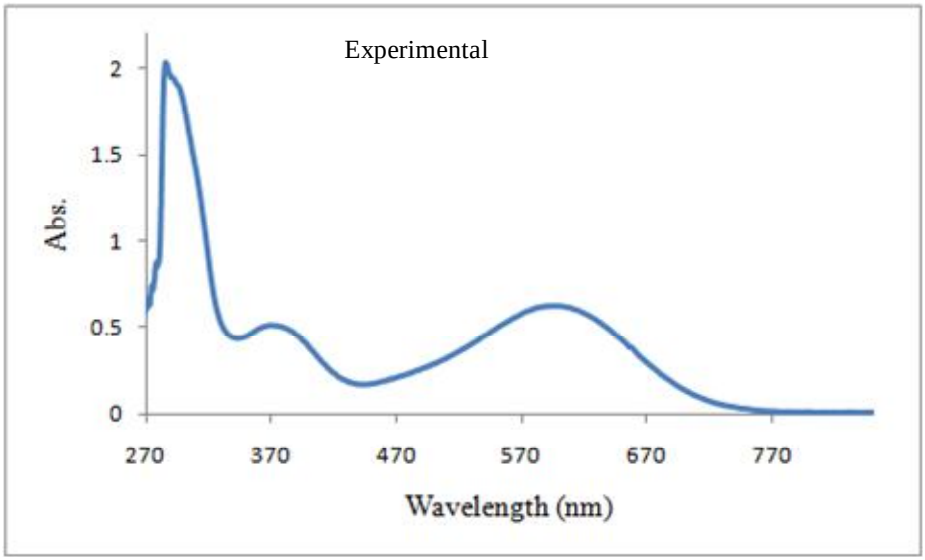

Figure 2.33 Experimental UV-Vis spectrum of **2.1a** in toluene.

Table 2.5 Photophysical and electrochemical properties of compounds **2.1** and **2.1a**

	Absorption λ_{max} (nm)[a]	λ_{em} (nm)	ΔE_{DFT} (eV)	$\Delta E_{Optical}$ (nm/eV)	$E_{1/2}^{ox}$ (V)[b]	$E_{1/2}^{red}$ (V)[b]	$\Delta E_{Electrochemical}$ (eV)
2.1	357	458	3.51	400/3.10	N/A	-2.30	N/A
2.1a	605	N/A	1.14	770/1.61	-0.54	-2.30	1.76

[a] Recorded in toluene (~10^{-5}M). [b] Recorded in DMF, relative to the potential of $FeCp_2^{+/0}$.

The DFT calculations of **2.1a** show that the HOMO is mainly dominated by the cyclohexadienyl ring and both B-C_x and B-C_y bonds with contribution from the π orbitals of the phenylpyridine rings. On the other hand, the LUMO of **2.1a** is mainly dominated by the π* orbital of the phenylpyridine rings and the σ* of both B-C_x and B-C_y, with some contribution from the diene π* orbitals, as shown in Figure 2.34. Hence, the intense low-energy band of **2.1a** responsible for the dark blue color can be attributed to a low-energy charge transfer transition from HOMO to the LUMO.

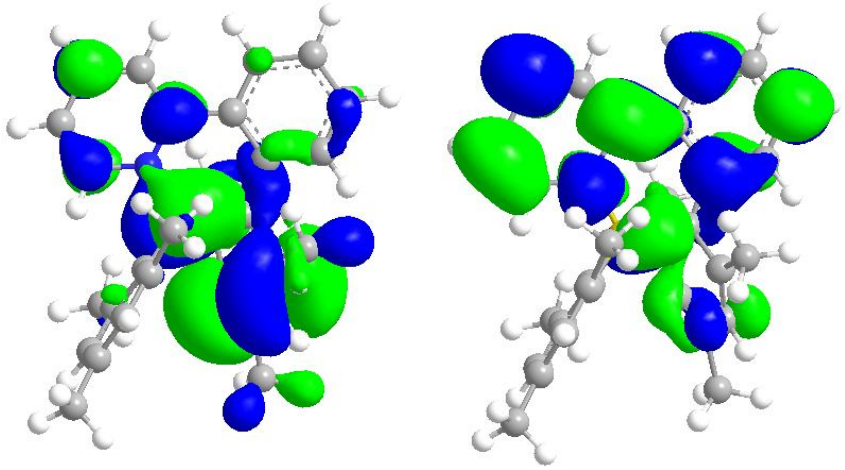

HOMO LUMO

Figure 2.34 HOMO and LUMO of **2.1a** with a surface isocontour value of 0.03

The lowest electronic transition of **2.1** is a charge transfer from the mesityl group, which becomes cyclohexadiene after photolysis, to the phenylpyridine rings. Hence, the photoisomerization process is expected to be a photoinduced internal charge transfer, which is stabilized by hyperconjugation[16] with the CH_3 groups on the cyclohexadiene allowing the proposed di-π-borate rearrangement to take place over the expected equilibrium process to the initial state[17].

2.4 Conclusion

A new photochromic of type-T compound has been synthesized and its photophysical/photochemical properties studied. The new 4-coordinate N,C-chelate organoboron compound can be photoisomerized using UV light. The photoisomerization process is believed to go through a light induced internal charge transfer, followed by a di-π-borate rearrangement.

Although organic photochromic systems including ones that contain peripheral organoboron substituents have been known and studied extensively, compound **2.1a** and closely related 4-coordinate N,C-chelate organoborons are the first examples of organoboron-based photochromic systems that actually involve the boron center in the photochromic process. The N,C-chelate and the mesityl groups play an important role in this reversible photo-thermal isomerization process.

2.5 References

(1) (a) Wang, S. *Coord. Chem. Rev.* **2001**, *215*, 79. (b) Cui, Y.; Wang, S. *J. Org. Chem.* **2006**, *71*, 6485. (c) Fukazawa, A.; Yamada, H.; Yamaguchi, S. *Angew. Chem. Int. Ed.* **2008**, *47*, 5582.

(2) Wakamiya, A.; Taniguchi, T.; Yamaguchi, S. *Angew. Chem. Int. Ed*. **2006**, *45*, 3170.

(3) Huo, S.; Deaton, J.; Rajeswaran, M.; Lenhart, W. *Inorg. Chem.* **2006**, *45*, 3155.

(4) Cole, S. C.; Coles, M. P.; Hitchcock, P. B. *Dalton Trans.* **2003**, 3663.

(5) (a) Demas, N. J.; Crosby, G. A. *J. Am. Chem. Soc.* **1970**, *92*, 7262. (b) Fery-Forgues, S.; Lavabre, D. *J. Chem. Ed.* **1999**, *9*, 1260.

(6) Frisch, M. J.; et al. *Gaussian 03*, revision C.02; Gaussian, Inc.: Wallingford, CT, 2004.

(7) (a) Parker, C. A. Proc. R. Soc. London A 1953, 220, 104. (b) Abdallah, D.; Whelan, J.; Dust, J. M.; Hoz, S.; Buncel, E. *J. Phys. Chem. A.* **2009**, *113*, 6640.

(8) SHELXTL Version 6.14, Bruker AXS, 2000-2003.

(9) (a) Wakamiya, A.; Taniguchi, T.; Yamaguchi, S. *Angew. Chem., Int. Ed.* **2008**, *47*, 834. (b) Liu, Q. D.; Mudadu, M. S.; Thummel, R.; Tao, Y.; Wang, S. *Adv. Funct. Mater.* **2005**, *15*, 143. (c) Liu, S. F.; Wu, Q.; Schmider, H. L.; Aziz, H.; Hu, N. X.; Popovic, Z.; Wang, S. *J. Am. Chem. Soc.* **2000**, *122*, 3671. (d) Wu, Q.; Esteghamatian, M.; Hu, N. X.; Popovic, Z.; Enright, G.; Breeze, S.; Wang, S. *Angew. Chem. Int. Ed.* **1999**, *38*, 985. (e) Chen, H. Y.; Chi, Y.; Liu, C. S.; Yu, J. K.; Cheng, Y. M.; Chen, K. S.; Chou, P. T.; Peng, S. M.; Lee, G. H.; Carty, A. J.; Yeh, S. J.; Chen, C. T. *Adv. Funct. Mater.* **2005**, *15*, 567.

(10) Rao, Y. L.; Wang, S. *Inorg. Chem.* **2009**, *48*, 7698.

(11) (a) Wilkey, J. D.; Schuster, G. B. *J. Org. Chem.* **1987**, *52*, 2117. (b) Wilkey, J. D.; Schuster, G. B. *J. Am. Chem. Soc.* **1988**, *110*, 7569.

(12) Zimmerman, H. E. *Rearrangements in Ground and Excited States*; de Mayo, P., Ed.; Academic Press. NY, 1980; Vol. 3, pp: 131.

(13) O'Boyle, N. M.; Tenderholt, A. L.; Langner, K. M. *J. Comp. Chem.* **2008**, *29*, 839.

Chapter 3

Substituted Phenylpyridine-Based N,C-Chelate Organoboron Compounds

3.1 Introduction

The interesting photochromic behavior of certain N,C-chelate 4-coordinate organoboron compounds, discussed in chapter 2, and the importance of organic photochromic systems in general,[1] intrigued us to further study their properties. To gain insight about the steric and electronic factors influencing the photochromic properties of N,C-chelate 4-coordinate organoboron compounds, we have synthesized two different types of substituted phenylpyridine-based compounds (Figure 3.1). The first type was synthesized via introducing different substituents on the phenylpyridine chelate ring (**3.1**-**3.5**) in order to examine the effect of electron donating and electron withdrawing groups. Also the effect of adding conjugated groups on the phenylpyridine N,C-chelate was examined. The second type of these N,C-chelate organoboron compounds was designed via changing the aryl groups attached to the boron center (**3.6** and **3.7**) in order to examine the different steric and electronic effects imposed by replacing the mesityl groups with phenyl or pentafluorophenyl groups. The effects of these substitutions on the photophysical and photoisomerization properties were studied.

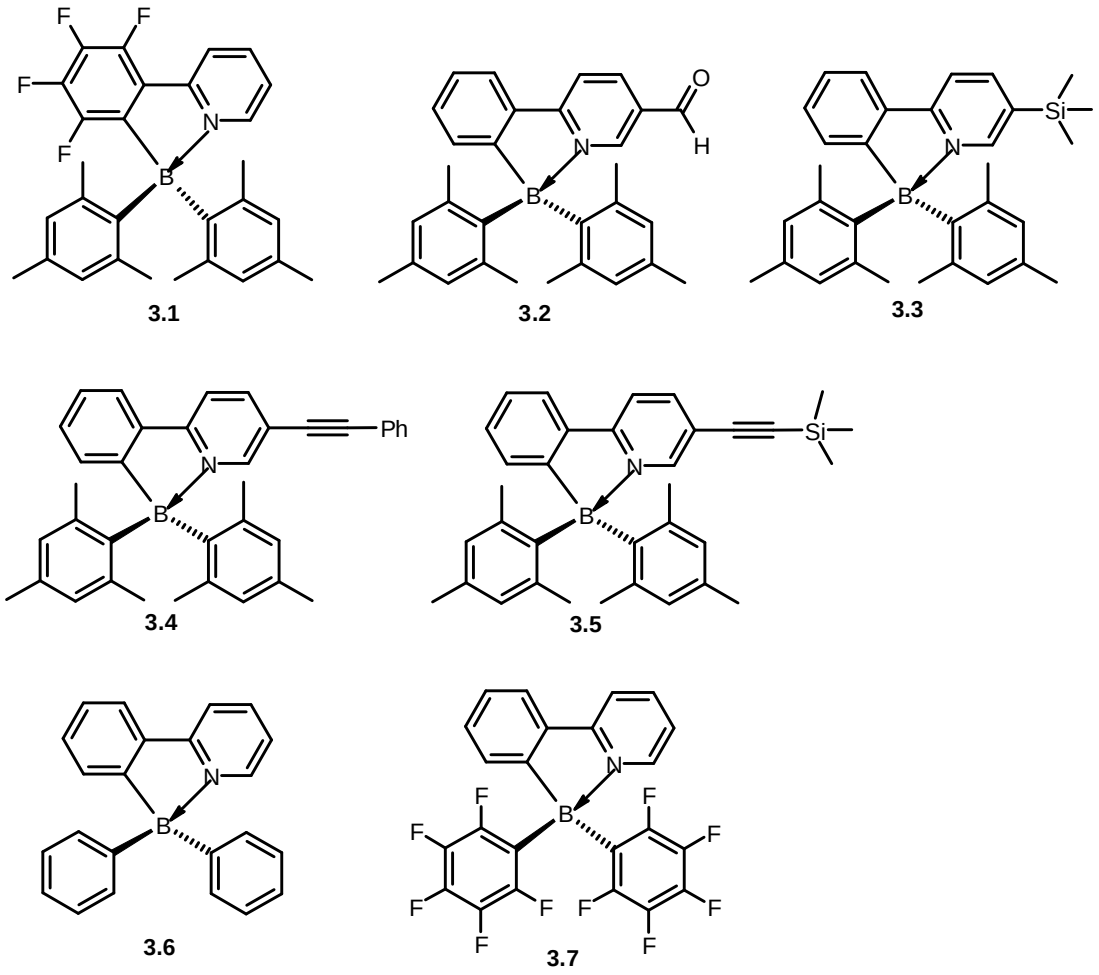

Figure 3.1 Structures of different phenylpyridine-based N,C-chelate organoboron compounds **3.1**-**3.7**.

3.2 Experimental

3.2.1 General

Starting materials were purchased from Aldrich Chemical Co. and were used without further purification. Solvents were dried using activated alumina column system, PURE SOLV, purchased from Innovative Technology Inc., while C_6D_6 was dried over CaH_2 in a

glove box. All reactions were carried out under an atmosphere of dry nitrogen using standard Schlenk techniques. Purifications using column chromatography were performed using ultra pure silica gel (70-230 Mesh) 60 Å, purchased from Silicycle. NMR spectra (^{1}H,^{13}C, ^{11}B and ^{19}F) were recorded at room temperature on a Bruker Avance 400 or 500 MHz. Proton and ^{13}C chemical shifts were reported with respect to solvent peaks as internal standard, while $BF_3.Et_2O$ and $CFCl_3$ were used as references for ^{11}B and ^{19}F NMR respectively. Coupling constants (*J*) were recorded in Hertz (Hz). Excitation and emission spectra were recorded on a Photon Technologies International QuantaMaster Model C-60 spectrometer. UV-Vis spectra were recorded on an Ocean Optics Model CHEMUSB4-UV/VIS. Elemental analyses were performed by Canadian Microanalytical Services Ltd., Delta, BC. High resolution mass spectra (HRMS) were obtained using a Waters/Micromass GC-TOF spectrometer (EI mode). Cyclic voltammetry was performed using a BAS CV-50W analyzer with a scan rate of 200 mV/s and sample concentrations of 5 mg / 3.0 mL DMF, using 0.10 M NBu_4PF_6 (TBAP) as supporting electrolyte and Ag/AgCl reference electrode. The ferrocenium/ferrocene couple was used as the internal standard ($E°$ = 0.56 V). 2-Bromopyridine, 2,3,4,5-tetrafluorophenylboronic acid, 2-bromophenylboronic acid, and $BMes_2F$ were purchased from Aldrich. 2-(2-Bromophenyl)pyridine[2], 2-bromo-5-(trimethylsilyl)pyridine[3], 2-bromo-5-((trimethylsilyl)ethynyl)pyridine[4], BPh_2Cl[5], $B(C_6F_5)_2F$[6] and compounds **3.2**[7], **3.4**[7] were synthesized based on reported literature procedures.

3.2.2 Synthesis and characterization of N,C ligands (3.1L, 3.3L, and 3.5L)

3.2.2.1 Synthesis and characterization of 2-(2,3,4,5-tetrafluorophenyl)pyridine (3.1L)

To a N_2-bubbled (30 min) mixture of THF (15 mL) and H_2O (15 mL), 2-bromopyridine (0.16 g, 0.1 mL, 1.0 mmol), 2,3,4,5-tetrafluorophenylboronic acid (0.194 g, 1.0 mmol), and K_2CO_3 (0.69 g, 5.0 mmol), were added. After bubbling N_2 again for 10 min, $Pd(PPh_3)_4$ (0.034 g, 0.03 mmol) was added and the mixture was heated to 55 °C and stirred overnight. The THF layer was separated and the aqueous layer was washed with CH_2Cl_2 (30 mL x 3). The organic layers were combined and dried over $MgSO_4$ and solvents were removed under reduced pressure, then the crude product was purified by column chromatography using a mixture of CH_2Cl_2/hexanes (1:1) to give yellow oil of **3.1L** (0.09 g, 40%). HREI-MS $(M)^+$: m/z Calcd. for $C_{11}H_5F_4N$, 227.0358. Found: 227.0365. ^{1}H NMR (CD_2Cl_2, 25 °C, δ, ppm): 8.73 (d, 1H, ^3J = 4.4 Hz), 7.85-7.78 (m, 3H), 7.36-7.33 (m, 1H). ^{13}C NMR (CD_2Cl_2, 25 °C, δ, ppm): 150.5-150.1 (m), 148.7-148.6 (m), 147.6-147.4 (m), 146.3-146.2 (m), 145.1-145.0 (m), 142.7-141.9 (m), 140.2-139.9 (m), 137.1, 124.5-124.2 (m), 123.7, 112.0-111.4 (m). ^{19}F NMR (CD_2Cl_2, 25 °C, δ, ppm): -140.9~-141.1(m, 1F), -144.5~-144.6 (m, 1F), -157.1~-157.3 (m, 1F), -157.7 (t, 1F, J_F = 19.8 Hz).

3.2.2.2 Synthesis and characterization of 2-(2-bromophenyl)-5-(trimethylsilyl)pyridine (3.3L)

A mixture of 2-bromophenylboronic acid (1.65 g, 8.25 mmol), 2-bromo-5-(trimethylsilyl)pyridine (1.90 g, 8.25 mmol) and $Pd(PPh_3)_4$ (0.27 g, 0.247 mmol) was

added to a degassed mixture of THF (30 mL) and aqueous K_2CO_3 (1M, 25 mL). The mixture was refluxed overnight and the crude product obtained after work-up, was purified by column chromatography using CH_2Cl_2/hexanes (1:2) mixture to give colorless oil of **3.3L** (2.17 g, 86%). HREI-MS $(M)^+$: m/z Calcd for $C_{14}H_{16}BrNSi$, 305.0235. Found: 305.0241. ^1H NMR ($CDCl_3$, 25 °C, δ, ppm): 8.81 (s, 1H), 7.87 (d, 1H, ^3J = 7.5 Hz), 7.66 (d, 1H, ^3J = 7.5 Hz), 7.59 (d, 1H, ^3J = 8.0 Hz), 7.55 (d, 1H, ^3J = 8.0 Hz), 7.39 (t, 1H, ^3J = 7.5 Hz), 7.23 (t, 1H, ^3J = 7.5 Hz), 0.36 (s, 9H). ^{13}C NMR ($CDCl_3$, 25 °C, δ, ppm): 158.8, 153.9, 141.7, 141.3, 134.1, 133.7, 131.9, 130.1, 127.9, 124.4, 122.2, -0.8.

3.2.2.3 Synthesis and characterization of 2-(2-bromophenyl)-5 ((trimethylsilyl)ethynyl)-pyridine (3.5L)

A mixture of 2-bromophenylboronic acid (0.32 g, 1.57 mmol), 2-bromo-5-((trimethylsilyl)ethynyl)pyridine (0.40 g, 1.57 mmol) and $Pd(PPh_3)_4$ (0.087 g, 0.078 mmol) were added to a degassed mixture of THF (30 mL) and aqueous 1M K_2CO_3 (25 mL). The mixture was refluxed overnight, then the solution was extracted with diethyl ether and the crude product was purified by column chromatography to afford **3.5L** (0.25 g, 48%). HREI-MS $(M)^+$: m/z Calcd for $C_{16}H_{16}BrNSi$, 329.0235. Found: 329.0241. ^1H NMR (CD_2Cl_2, 25 °C, δ, ppm): 8.76 (s, 1H), 7.84 (d, 1H, ^3J = 8.0 Hz), 7.71 (d, 1H, ^3J = 8.0 Hz), 7.60 (d, 1H, ^3J = 7.6 Hz), 7.55 (d, 1H, ^3J = 7.6 Hz), 7.45 (t, 1H, ^3J = 7.6 Hz), 7.31 (t, 1H, ^3J = 7.6 Hz), 0.28 (s, 9H). ^{13}C NMR (CD_2Cl_2, 25 °C, δ, ppm): 157.5, 152.4, 141.0, 138.8, 133.6, 131.8, 130.3, 127.8, 124.3, 121.8, 119.2, 101.7, 98.9, -0.2.

3.2.3 Synthesis and characterization of compounds 3.1, 3.3, 3.5, 3.6, and 3.7

All compounds were prepared according to the following general procedure:

n-BuLi (1.1 eq., 1.6 M in hexane) was added slowly to a solution of the phenylpyridine ligands (1 eq.) in THF (or Et_2O), at -78 °C and the resulting solution was stirred for about 1 hour at -78 °C. Then, diaryl boron halide (1 eq.) was added under a stream of nitrogen and the solution was stirred at the same temperature for about 2 hours and then stirred overnight at ambient temperature. Then, solvents were removed under reduced pressure and the resulting solid was dissolved in about 60 mL of CH_2Cl_2 and quenched with 10 mL of H_2O. The organic layer was separated and dried over $MgSO_4$ and filtered. After CH_2Cl_2 was removed under reduced pressure, the residue was purified over silica gel by flash column chromatography using CH_2Cl_2/ hexanes mixture to afford the pure product.

3.2.3.1 Synthesis and characterization of 2-(2-(dimesitylboryl)-3,4,5,6 tetrafluorophenyl)-pyridine (3.1)

2-(2,3,4,5-Tetrafluorophenyl)pyridine (**3.1L**) (0.087 g, 0.38 mmol) in THF (30 mL), n-BuLi (0.24 mL, 0.38 mmol), and $BMes_2F$ (0.114 g, 0.38 mmol) were treated according to the general procedure and purified by chromatography using CH_2Cl_2/hexanes (1:2). The resulting product was redissolved in CH_2Cl_2 and layered with hexanes to give yellow crystals of **3.1** (0.07 g, 39%). HREI-MS $(M)^+$: m/z Calcd for $C_{29}H_{26}BF_4N$, 475.2028. Found: 475.2093. Anal. Calcd for $C_{29}H_{26}BF_4N$: C, 73.28; H, 5.51; N, 2.95. Found: C, 73.08; H, 5.61; N, 2.91. ^{1}H NMR (CD_2Cl_2, 25 °C, δ, ppm): 8.72 (d, 1H, ^3J = 6.0 Hz), 8.29 (d, 1H, ^3J = 8.0 Hz), 8.12 (t, 1H, ^3J = 7.8 Hz), 7.41 (t, 1H, ^3J = 6.6 Hz), 6.69 (s, 4H), 2.19 (s, 6H), 1.80 (s, 12H). ^{13}C NMR (CD_2Cl_2, 25 °C, δ, ppm): 154.2, 148.4-148.3 (m),

146.3, 146.0-146.1(m), 143.9-143.8(m), 141.9, 140.6, 137.9-137.8(m), 134.9, 130.4, 123.4, 122.6 (d, J_{C-F} = 12.6 Hz), 24.6, 20.6. ^{19}F NMR (CD_2Cl_2, 25 °C, δ, ppm): -129.9 (t, 1F, J_F = 20.9 Hz), -144.4 (td, 1F, J_F = 20.5 Hz, 4.9 Hz), -152.2~-152.4 (m, 1F), -161.6 (t, 1F, J_F = 19.4 Hz). ^{11}B NMR (CD_2Cl_2, 25 °C, δ, ppm): 8.08.

3.2.3.2 Synthesis and characterization of 2-(2-(dimesitylboryl)phenyl)-5-(trimethylsilyl)-pyridine (3.3)

2-(2-Bromophenyl)-5-(trimethylsilyl)pyridine (**3.3L**) (0.64 g, 2.10 mmol) in Et_2O (40 mL), n-BuLi (1.43 mL, 2.30 mmol), and $BMes_2F$ (0.71 g, 2.64 mmol) were treated according to the general procedure and purified by chromatography using CH_2Cl_2/hexanes (1:4) to give a white powder of **3.3**, which was crystallized from CH_2Cl_2 and hexanes to give colorless crystals of **3.3** (0.81 g, 81%). HREI-MS $(M)^+$: m/z Calcd for $C_{32}H_{38}BNSi$, 475.2867. Found: 475.2867. Anal. Calcd for $C_{32}H_{38}BNSi$: C, 80.82; H, 8.05; N, 2.95. Found: C, 80.70; H, 7.99; N, 2.97. ^{1}H NMR (CD_2Cl_2, 25 °C, δ, ppm): 8.68 (s, 1H), 8.09 (d, 1H, ^3J = 8.0 Hz), 8.00 (d, 1H, ^3J = 8.0 Hz), 7.91 (d, 1H, ^3J = 6.8 Hz), 7.74 (d, 1H, ^3J = 6.8 Hz), 7.31 (m, 2H), 6.65 (s, 4H), 2.17 (s, 6H), 1.79 (s, 12H), 0.28 (s, 9H). ^{13}C NMR ($CDCl_3$, 25 °C, δ, ppm): 159.2, 150.0, 145.6, 140.0, 135.4, 133.9, 133.7, 131.2, 130.1, 125.5, 122.0, 117.6, 24.9, 20.7, -1.67. ^{11}B NMR (CD_2Cl_2, 25 °C, δ, ppm): 7.21.

3.2.3.3 Synthesis and characterization of 2-(2-(dimesitylboryl)phenyl)-5-((trimethylsilyl)-ethynyl)pyridine (3.5)

2-(2-Bromophenyl)-5-((trimethylsilyl)ethynyl) pyridine (**3.5L**) (0.25 g, 0.76 mmol), in Et_2O (40 mL), n-BuLi (0.57 mL, 0.91 mmol), and $BMes_2F$ (0.27 g, 1 mmol) were treated according to the general procedure and purified by chromatography using CH_2Cl_2/hexanes (1:2) to give a yellow powder of **3.5**, which was crystallized from CH_2Cl_2 and hexanes to give yellow crystals of **3.5** (0.31 g, 83%). HREI-MS $(M)^+$: m/z Calcd for $C_{34}H_{38}BNSi$, 499.2867. Found: 499.2891. Anal. Calcd for $C_{34}H_{38}BNSi$: C, 81.74; H, 7.67; N, 2.80. Found: C, 82.91; H, 7.81; N, 2.83. ^{1}H NMR ($CDCl_3$, 25 °C, δ, ppm): 8.69 (s, 1H), 7.98 (d, 1H, ^3J = 8.0 Hz), 7.90 (d, 1H, ^3J = 8.0 Hz), 7.81 (d, 1H, ^3J = 7.2 Hz), 7.79 (d, 1H, ^3J = 7.2 Hz), 7.32 (d, 1H, ^3J = 7.2 Hz), 7.27 (d, 1H, ^3J = 7.2 Hz), 6.68 (s, 4H), 2.21 (s, 6H), 1.79 (s, 12H), 0.27 (s, 9H). ^{13}C NMR ($CDCl_3$, 25 °C, δ, ppm): 166.7, 158.7, 149.4, 145.5, 143.5, 140.6, 134.8, 134.4, 132.2, 131.6, 130.3, 125.9, 122.3, 118.5, 117.6, 100.9, 100.1, 25.4, 21.2, 0.1. ^{11}B NMR (CD_2Cl_2, 25 °C, δ, ppm): 7.93.

3.2.3.4 Synthesis and characterization of 2-(2-(diphenylboryl)phenyl)pyridine (3.6)

2-(2-Bromophenyl)pyridine (1.17 g, 5.0 mmol) in THF (50 mL), n-BuLi (3.13 mL, 5.0 mmol), and BPh_2Cl (1.1 g, 5.0 mmol) were treated according to the general procedure and purified by chromatography using CH_2Cl_2/hexanes (1:1). The resulting yellow solid was recrystallized from THF/hexanes to give colorless crystals of **3.6** (0.52 g, 33%). HREI-MS $(M)^+$: m/z Calcd for $C_{23}H_{18}BN$, 319.1532. Found: 319.1530. Anal. Calcd for $C_{23}H_{18}BN$: C, 86.54; H, 5.68; N, 4.39. Found: C, 86.46; H, 5.81; N, 4.42. ^{1}H NMR

(CD_2Cl_2, 25 °C, δ, ppm): 8.52 (d, 1H, ^3J = 5.6 Hz), 8.20-8.05 (m, 2H), 7.96 (d, 1H, ^3J = 8.0 Hz), 7.71 (d, 1H, ^3J = 7.2 Hz), 7.55-7.42 (m, 2H), 7.38 (td, 1H, ^3J = 7.4 Hz, ^4J = 1.2 Hz), 7.30-7.10 (m, 10H). ^{13}C NMR (CD_2Cl_2, 25 °C, δ, ppm): 158.6, 144.3, 141.2, 136.4, 133.2, 131.3, 130.7, 127.6, 126.3, 125.9, 122.5, 122.1, 118.7. ^{11}B NMR (CD_2Cl_2, 25 °C, δ, ppm): 6.48.

3.2.3.5 Synthesis and characterization of 2-(2-(bis(pentafluorophenyl)boryl)phenyl)pyridine (3.7)

2-(2-Bromophenyl)pyridine (0.58 g, 2.5 mmol) in THF (50 mL), n-BuLi (1.56 mL, 2.5 mmol), and $B(C_6F_5)_2F$ (used without purification) (2.5 mmol based on 100% yield) were treated according to the general procedure and purified by chromatography using EtOAc/hexanes (2:1). The resulting brownish solid was recrystallized from toluene/hexanes to give colorless crystals of **3.7** (0.20 g, 16%). HREI-MS $(M)^+$: m/z Calcd for $C_{23}H_8BF_{10}N$, 499.0590. Found: 499.0584. Anal. Calcd for $C_{23}H_8BF_{10}N$: C, 55.35; H, 1.62; N, 2.81. Found: C, 55.51; H, 1.90; N, 2.76. ^{1}H NMR (CD_2Cl_2, 25 °C, δ, ppm): 8.61 (d, 1H, ^3J = 5.6 Hz), 8.21 (td, 1H, ^3J = 7.8 Hz, ^4J = 1.2 Hz), 8.12 (d, 1H, ^3J = 8.4 Hz), 7.94 (d, 1H, ^3J = 6.8 Hz), 7.75 (d, 1H, ^3J = 7.2 Hz), 7.40-7.53 (m, 3H). ^{13}C NMR (CD_2Cl_2, 25 °C, δ, ppm): 159.2, 149.2-149.3 (m), 147.0-147.1 (m), 144.9, 142.9, 141.0-141.1 (m), 138.7-138.8 (m), 136.2-136.3 (m), 135.7, 132.1, 130.4, 127.5, 123.0, 122.2, 118.9. ^{19}F NMR (CD_2Cl_2, 25 °C, δ, ppm): -133.41 (dd, 4F, J_F = 25.2 Hz, 9.2 Hz), -159.87 (t, 2F, J_F = 20.1 Hz), -165.16 ~ -165.29 (m, 4F). ^{11}B NMR (CD_2Cl_2, 25 °C, δ, ppm): δ 0.77.

3.2.4 Fluorescence Quantum Yield Measurements

Fluorescence quantum yields of dilute degassed toluene solutions (Abs. = ~0.1) were measured at room temperature using the relative quantum yield method using 9,10-diphenylanthracene as the reference standard ($\Phi_F = 0.90$).[8]

3.2.5 General Procedure Used for Monitoring Photolysis Process via ^{1}H NMR

Samples were dissolved in dry C_6D_6 in an NMR tube under inert atmosphere. To remove any traces of oxygen that might be present in the NMR tube, three freeze/pump/thaw cycles were performed using liquid N_2. The photolysis for all compounds except **3.6** was then performed with either a Rayonet photochemical reactor with irradiation at 350 nm or a UVP UVGL-25 compact hand-held UV lamp at 365 nm at room temperature, followed by recording the ^{1}H NMR spectra after different time periods. For compound **3.6**, the photolysis was performed in C_6D_6 with a Spectroline UV lamp at 312 nm.

3.2.6 General Procedure Used for Monitoring Photolysis Process via UV-Vis Spectroscopy

Samples were dissolved in dry degassed toluene in a quartz cuvette (~10^{-5} M), under inert atmosphere in a glove box. After wrapping the cuvette with aluminum foil, it was transferred out and photolysis was then performed using a UVP UVGL-25 compact UV lamp (365 nm) at room temperature. On the other hand, the photolysis of compound **3.6** was performed with a Spectroline UV lamp at 312 nm. The UV-Vis spectra were recorded after each exposure time and the exposure times were added up.

3.2.7 Density Functional Theory Calculations

Gaussian 03 program was used for all theoretical calculations, which were carried out at the B3LYP level of theory with 6-311G* as the basis set.[9] For compounds with available X-ray structures, geometric parameters were used as starting points for the geometry optimizations, while *GaussView* software package was used for obtaining geometric parameters of compounds that do not have X-ray structural data.

3.2.8 Photoisomerization Quantum Yield Measurements

All work was done under dark light conditions and freshly prepared and mixed solutions were used in all experiments. Phenanthroline and $K_3[Fe(C_2O_4)_3].3H_2O$ are light sensitive and were kept in the dark at all times. The quantum yield of the photoisomerization of (**3.3→3.3a**) was determined using potassium ferrioxalate $K_3[Fe(C_2O_4)_3].3H_2O$ actinometry based on Hatchard-Parker method[10]. The absorbance of the Fe(II)-1,10-phenanthroline complex was measured at 510 nm in a buffered acidic solution, while the absorbance of **3.3a** at 600 nm was measured in degassed toluene. The absorbance was measured using an Ocean Optics fiber optic spectrophotometer connected to a Quantum Northwest four-way temperature-controlled cuvette holder via 400 μm fiber optic. The irradiation source was a Photon Technologies International 200 W Hg/Xe lamp with a monochromator.

3.2.9 X-ray Crystallography

Single-crystals of compounds **3.1**, **3.3**, **3.5**, **3.6**, and **3.7**, were obtained as described above. Crystals were mounted on glass fiber and data collection was done using a

Siemens P4 single-crystal X-ray diffractometer, equipped with a Smart CCD-1000 detector and graphite-monochromated Mo Kα radiation operating at 50 kV and 35 mA. Data were processed on a PC using Bruker SHELXTL software package[11].

Table 3.1 Crystallographic data of **3.1**, **3.3**, **3.5**, **3.6**, and **3.7**.

	3.1	**3.3**	**3.5**
Formula	$C_{29}H_{26}BF_4N$	$C_{32}H_{38}BNSi$	$C_{34}H_{38}BNSi$
Fw	475.32	475.53	499.55
space group	P2(1)/c	P2(1)/c	P2(1)/c
a/Å	11.514(3)	21.482(5)	13.160(2)
b/Å	12.665(3)	16.869(4)	21.360(3)
c/Å	15.632(4)	16.514(4)	10.8191(17)
α, deg	90	90	90
β, deg	92.628(3)	111.182(4)	105.673(2)
γ, deg	90	90	90
V/Å^3	2277.1(10)	5580(2)	2928.1(8)
Z	4	8	4
D_c/(g cm^{-3})	1.386	1.132	1.133
μ/mm^{-1}	0.102	0.104	0.103
$2\theta_{max}$/deg	52.28	54.48	54.16
reflns measured	22576	24642	14723
reflns used (R_{int})	4493 (0.1286)	12357 (0.1108)	6349 (0.0523)
final R [I > 2σ (I)]	R_1[a] = 0.0648 wR_2[b] = 0.1652	R_1[a] = 0.0815 *w*R2 = 0.1723	R_1[a] = 0.0751 wR_2[b] = 0.1711
R (all data)	R_1[a] = 0.1260	R_1[a] = 0.1977	R_1[a] = 0.1344

	wR_2[b] = 0.1988	wR_2[b] = 0.2213	wR_2[b] = 0.1984
goodness-of-fit on F^2	1.025	0.981	1.062

[a] $R_1 = \Sigma[|F_o| - |F_c|]/\Sigma|F_o|$. [b] $wR_2 = \{\Sigma[w(F_o^2 - F_c^2)]/ \Sigma(wF_o^2)\}^{1/2}$.

$\omega = 1/ [\sigma^2(F_o^2) + (0.075P)^2]$, where $P = [\max.(F_o^2,0) + 2F_c^2]/3$.

Table 3.1 Crystallographic data of **3.1**, **3.3**, **3.5**, **3.6**, and **3.7** (cont'd)

	3.6	**3.7**
formula	$C_{23}H_{18}BN$	$C_{23}H_8BF_{10}N$
Fw	319.19	499.11
space group	P-1	P2(1)/n
a/Å	9.0519(15)	9.5920(2)
b/Å	9.1725(16)	13.1877(2)
c/Å	12.263(2)	15.6344(3)
α, deg	74.459(2)	90
β, deg	79.441(2)	104.3860(10)
γ, deg	61.063(2)	90
V/Å^3	856.8(3)	1915.68(6)
Z	2	4
D_c/(g cm^{-3})	1.237	1.731
μ/mm^{-1}	0.070	0.169
$2\theta_{max}$/deg	54.10	54.38
reflns measured	9573	14180
reflns used (R_{int})	3708 (0.0300)	4236 (0.0289)
final R [I > 2σ (I)]	R_1[a] = 0.0536 wR_2[b] = 0.1328	R_1[a] = 0.0380 wR_2[b] = 0.0969

R (all data)	R_1[a] = 0.0801 wR_2[b] = 0.1479	R_1[a] = 0.0527 wR_2[b] = 0.1058
goodness-of-fit on F^2	1.058	1.078

[a] $R_1 = \Sigma[|F_o| - |F_c|]/\Sigma|F_o|$. [b] $wR_2 = \{\Sigma[w(F_o^2 - F_c^2)]/ \Sigma(wF_o^2)\}^{1/2}$.

$\omega = 1/[\sigma^2(F_o^2) + (0.075P)^2]$, where $P = [\max.(F_o^2,0) + 2F_c^2]/3$.

Table 3.2 Selected bond lengths (Å) and angles (º) of **3.1**, **3.3**, **3.5**, **3.6**, and **3.7**.

Compound	B-N (Å)	B-$C_{chelate}$ (Å)	B-C_{Ar} (Å)	N-B-$C_{chelate}$ (°)	C_{Ar}-B-C_{Ar} (°)
3.1	1.661(4)	1.628(5)	1.629(5) 1.636(5)	94.5(2)	116.1(3)
3.3	1.643(6)	1.641(6)	1.633(6) 1.661(5)	95.1(3)	116.3(3)
3.5	1.667(4)	1.621(4)	1.632(5) 1.643(5)	95.2(4)	115.6(2)
3.6	1.618(3)	1.628(3)	1.611(3) 1.616(3)	95.58(13)	113.48(15)
3.7	1.612(2)	1.610(2)	1.635(2) 1.639(2)	97.63(11)	114.34(12)

3.3 Results and Discussion

3.3.1 Synthesis and Characterization

The organoboron compounds in this chapter can be divided into two groups based on the BAr_2 group attached to the N,C-chelate: (1) Compounds **3.1**-**3.5** with Ar = Mes group. This group enabled us to examine the effect of different types of substituents on the photophysical and photochromic properties on the organoboron compounds. (2) Compounds **3.6** and **3.7** with Ar = Ph and C_6F_5, respectively. These two compounds enabled us to examine the effect imposed by the Ar group on the photophysical and photochromic properties of the organoboron compounds under investigation.

Compounds **3.1**, **3.3**, and **3.5** were prepared according to Figure 3.2. The ligand 2-(2,3,4,5-tetrafluorophenyl)pyridine **3.1L** was synthesized using a Suzuki-Miyaura coupling protocol of 2-bromopyridine with and 2,3,4,5-tetrafluorophenylboronic acid. Lithiation of **3.1L** followed by the addition of $BMes_2F$ produced **3.1** in 39% yield. The ligands 2-(2-bromophenyl)-5-(trimethylsilyl)pyridine (**3.3L**) and 2-(2-bromophenyl)-5-((trimethylsilyl)ethynyl)pyridine **3.5L** were also synthesized via Suzuki-Miyaura coupling of 2-bromophenylboronic acid with 2-bromo-5-(trimethylsilyl)pyridine and 2-bromo-5-((trimethylsilyl)ethynyl)pyridine, respectively. Lithiation of **3.3L** and **3.5L** followed by the addition of $BMes_2F$ produced **3.1** and **3.5** in (81% and 83%) yields, respectively.

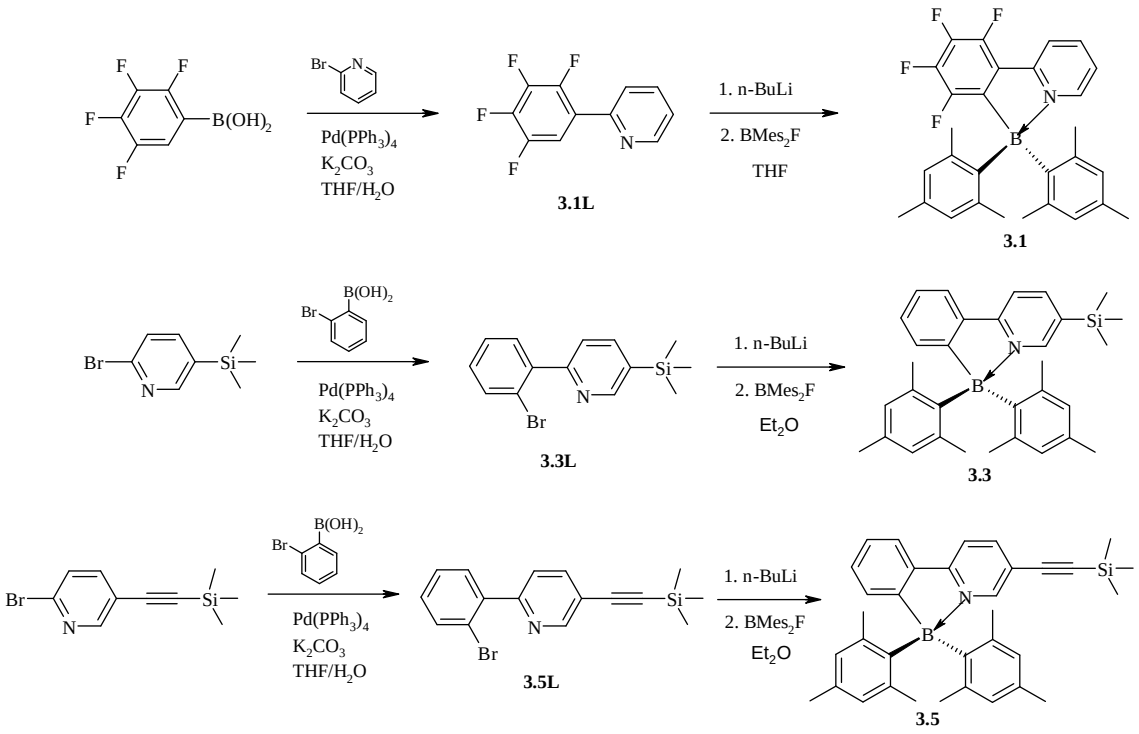

Figure 3.2 Synthetic routes for compounds **3.1**, **3.3**, and **3.5**.

Compounds **3.6** and **3.7** were prepared according to Figure 3.3. Lithiation of 2-(2-bromophenyl)pyridine and the subsequent addition of BPh_2Cl and $B(C_6F_5)_2F$ produced **3.6** and **3.7** in (33% and 16%) yields, respectively. All compounds were fully characterized by NMR, HRMS, elemental analysis, and single crystal X-ray diffraction.

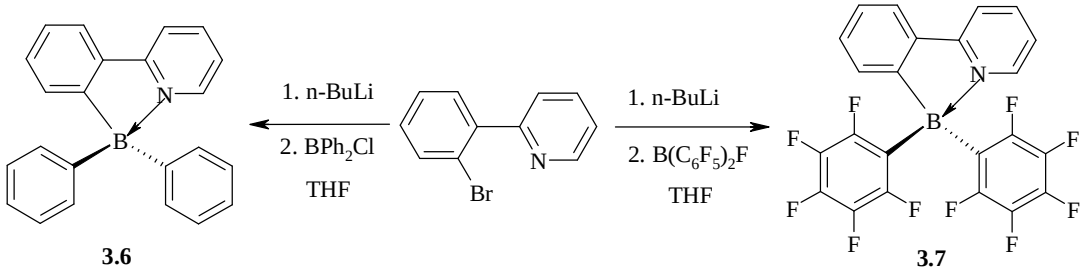

Figure 3.3 Synthetic routes for compounds **3.6** and **3.7**.

3.3.2 Crystal Structures

Crystal structures of compounds **3.1**, **3.3**, **3.5**, **3.6**, and **3.7** were determined by single crystal X-ray diffraction as shown in Figure 3.4 - Figure 3.8, respectively. The important bond angles and bond lengths for compounds **3.1**, **3.3**, **3.5**, **3.6**, and **3.7** are listed in Table 3.2.

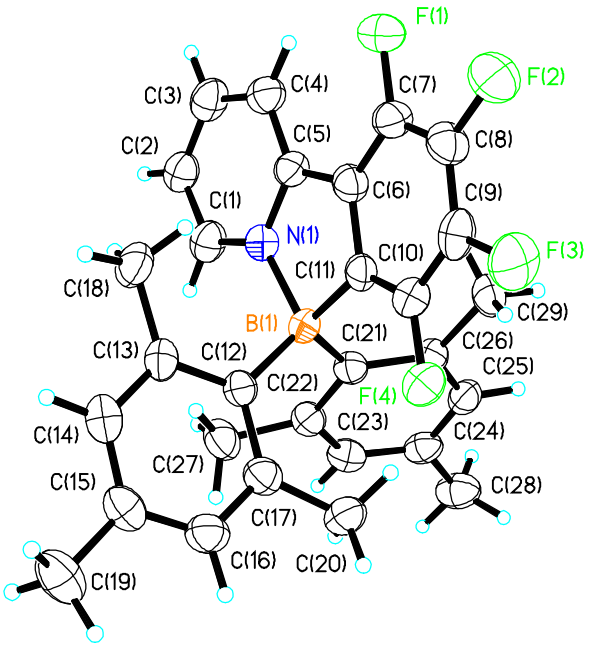

Figure 3.4 Crystal structure of compound **3.1** with 50% thermal ellipsoids

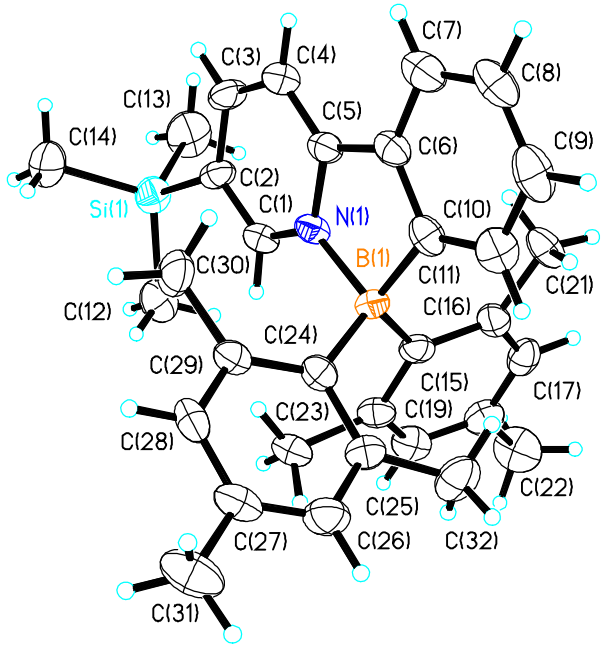

Figure 3.5 Crystal structure of compound **3.3** with 50% thermal ellipsoids

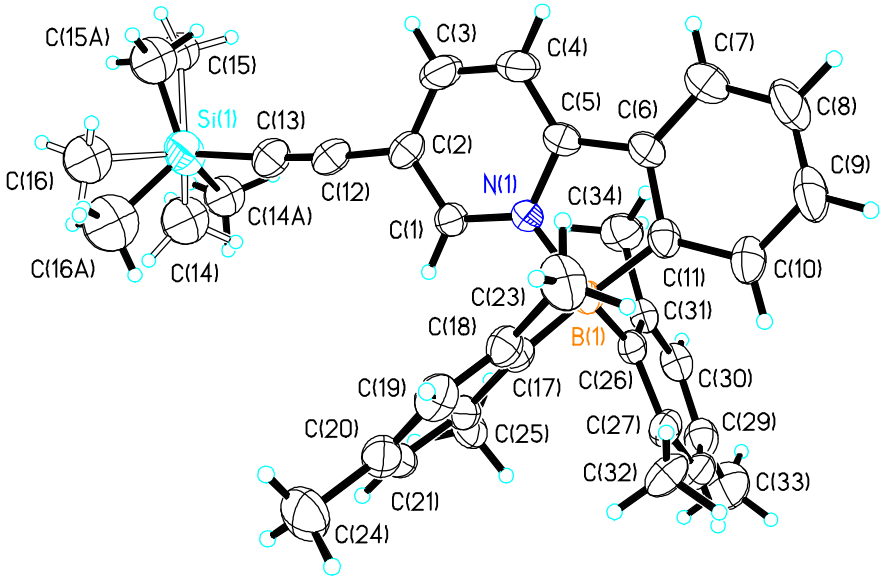

Figure 3.6 Crystal structure of compound **3.5** with 50% thermal ellipsoids (showing two sets of the disordered $SiMe_3$ group)

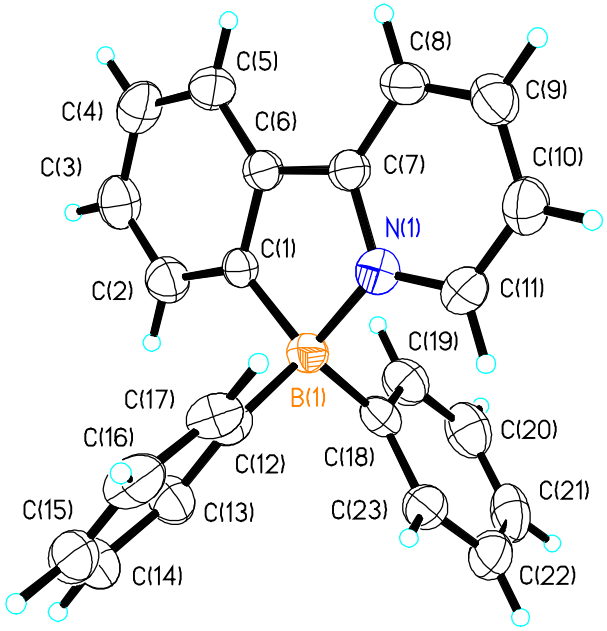

Figure 3.7 Crystal structure of compound **3.6** with 50% thermal ellipsoids

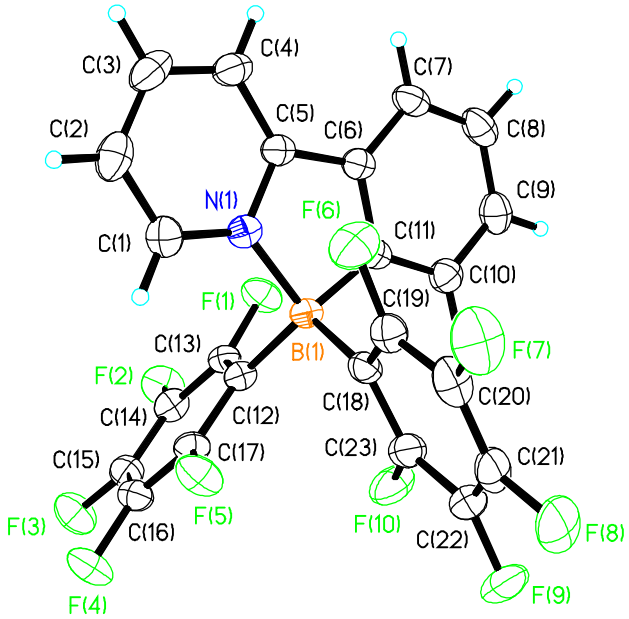

Figure 3.8 Crystal structure of compound **3.7** with 50% thermal ellipsoids

Compounds **3.1**, **3.3**, **3.5**, **3.6**, and **3.7** have the phenylpyridine group or substituted phenylpyridine as the chelate ring. There are however significant variations in B-N and B-C bond lengths among these compounds. Comparison of structural data of compound **2.1** (chapter 2) with those of **3.6** shows that the bulky mesityl groups in **2.1** clearly destabilizes the compound, as evidenced by the much longer B-N (1.653(2) Å) and B-C_{Ar} bond lengths (1.649(2) Å in average) of **2.1** versus those of **3.6** (1.618(3) Å and 1.613(3) Å, in average). The C_6F_5 group in **3.7** also destabilizes the molecule by weakening the B-C_{Ar} bond (1.637(2) Å in average), compared to the phenyl group in **3.6**, which can be attributed to the electron-withdrawing nature of the C_6F_5 group. The electron donating group $SiMe_3$ in **3.3**, the phenylacetylene group in **3.4**[12], and the $SiMe_3$-acetylene group in **3.5** on the pyridine ring of the phenylpyridine chelate do not have significant impact on the B-C_{Mes} bond length, but increase the B-$C_{chelate}$ bond length to some extent. In contrast, the electron-withdrawing fluoride atoms on the phenyl ring of **3.1** do shorten the B-C_{Mes} bonds considerably (1.632(5) Å in average in **3.1**) but this does not have a significant impact on the B-$C_{chelate}$ bond.

The crystal structural data of compounds **3.6** and **3.7**, which contain phenyl and pentafluorophenyl groups as the Ar group, shows that the boron center retains a four-coordinate environment in the solid state. Also, compounds **3.1**-**3.5** have a four coordinate boron center despite the presence of the bulky mesityl groups. In addition, all compounds retain a four-coordinate geometry in solution, which is confirmed by the ^{11}B NMR chemical shifts (0.77 - 8.08 ppm) compared to ((-20) - 30 ppm) range for four-

coordinate organoboron compounds in general[13]. The crystal data also confirm that the substituent groups on the phenylpyridine chelate and the nature of the aryl groups have an impact on the B-N and B-C bond lengths and angles, which may in turn influence the stability/reactivity of the boron center.

3.3.3 UV-Vis Absorption and Luminescence Properties of 3.1-3.7

The UV-Vis absorption spectra for compounds **3.1**-**3.7** are shown in Figure 3.9 and the λ_{max} of the lowest energy absorption band, the absorption edge (optical energy gap), and the λ_{em} spectra along with fluorescence quantum efficiencies are provided in Table 3.3. All compounds have intense absorption bands in the region 290-400 nm. Compounds **3.1**, **3.3**, **3.6**, and **3.7** have no significant absorption in the visible region (400-800 nm), which is consistent the fact that these compounds are colorless in solution and in the solid state. On the other hand, compounds **3.2**, **3.4**, and **3.5** have absorption shoulders in the 400-460 nm range; hence they have a yellow color in both solution and solid states.

Compounds **3.1**-**3.5**, which have mesityl groups attached to the boron center, have a low energy shoulder band in the 350-470 nm region that can be attributed to a charge transfer transition from one of the mesityl groups to the phenylpyridine N,C-chelate. The latter is supported by DFT calculations, which shows that the HOMO is mainly localized on one of the mesityl groups and the LUMO is mainly localized on the phenylpyridine chelate. The fact that this low energy shoulder band is absent in the absorption spectra of compounds **3.6** and **3.7**, which have Ph and C_6F_5 groups attached to the boron center, is consistent with this assignment.

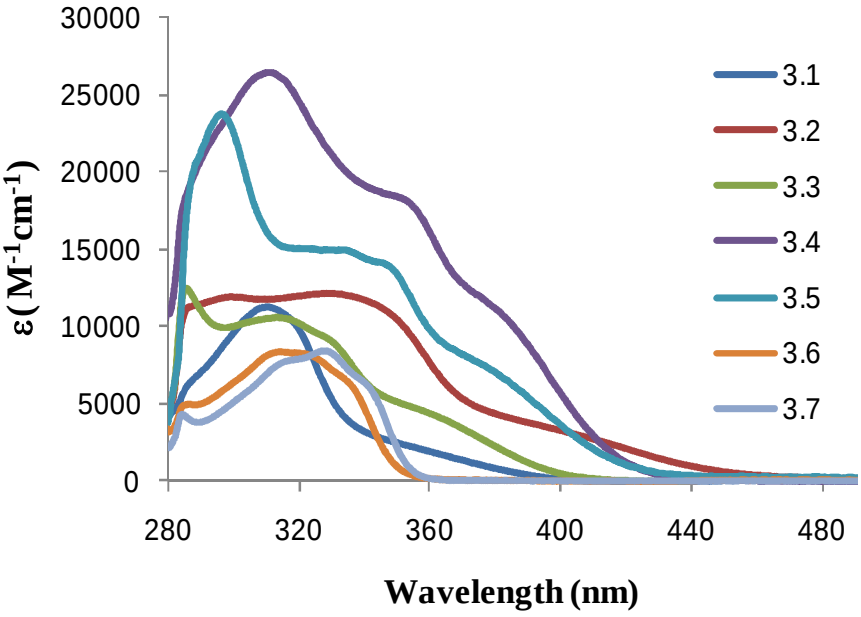

Figure 3.9 Absorption spectra of compounds **3.1**-**3.7** in toluene (~10^{-5} M)

The optical energy gaps for compounds **3.1**-**3.7** (Table 3.3) were estimated using the absorption edge. The smaller energy gaps of **3.2**, **3.4**, and **3.5** may be attributed to the conjugation of the carbonyl and acetylene groups to phenylpyridine chelate, which in turn lowers the LUMO energy and subsequently lowers the HOMO-LUMO gap.

Table 3.3 Photophysical and electrochemical properties of compounds **3.1-3.7**

Compound	Absorption λ_{max} (nm) (ε, $M^{-1}cm^{-1}$)	λ_{em} (nm)	Φ_F in toluene[a]	$\Delta E_{Optical}$ (eV)	$E_{1/2}^{red}$ (V)[b]
3.1	349 (2400)	470	0.05	3.13	-2.09
3.2	390 (3800)	523	0.15	2.70	-1.68
3.3	355 (4700)	418	0.12	3.08	-2.32
3.4	377 (12000)	488	0.37	2.90	-2.03
3.5	371 (8200)	491	0.28	2.93	-2.04
3.6	334 (6500)	413	0.31	3.52	-2.28
3.7	341 (6200)	356	0.22	3.48	-2.09

[a] Standard reference 9,10-diphenylanthracene (Φ_F = 90%). [b] From CV diagrams recorded in DMF, relative to the potential of $FeCp_2^{+/0}$.

Upon irradiation with UV light, compounds **3.1**-**3.7** emit a bright blue (**3.3**, **3.6**, and **3.7**), green (**3.4** and **3.5**), or yellow (**3.2**) light in toluene with λ_{em} ranging from 360-527 nm, while **3.1** emits a weak blue color as shown in Figure 3.10. Compared to compound **2.1** (the non-substituted phenylpyridine analogue), the emission energy of compounds **3.1**-**3.5** are in the following order: **3.3** (λ_{em}= 418 nm) > **2.1** (λ_{em}= 458 nm) > **3.1** (λ_{em}= 470 nm) > **3.4** (λ_{em}= 488 nm) ~ **3.5** (λ_{em}= 491 nm) > **3.2** (λ_{em}= 523 nm) which supports the earlier suggested charge transfer transition from the mesityl group π to the phenylpyridine chelate π^* level. Compound **3.3** contains an electron donating group ($SiMe_3$) which destabilizes the π^* level of the phenylpyridine chelate and hence increases

its energy. On the other hand, the π* level of the phenylpyridine chelate in all the other compounds is stabilized by extended π-conjugation or inductive effect from an electron withdrawing group. In compound **3.2** the carbonyl is conjugated to the N,C-chelate ring and since it's polarized in nature it also imposes an electron withdrawing effect, which significantly decreases the energy of the charge transfer transition as evidenced by the much longer emission wavelength of **3.2**. The π* level in both **3.4** and **3.5** is also stabilized by extended conjugation to the acetylene group attached to phenylpyridine. In addition, the π* level of **3.1** is stabilized by the inductive effect of the fluoride atoms attached to the N,C-chelate.

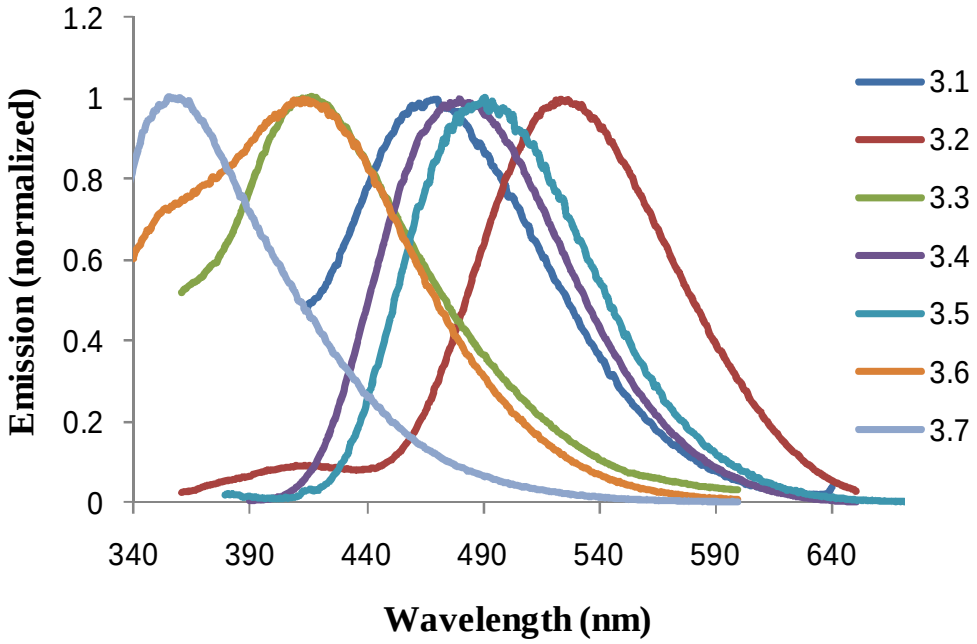

Figure 3.10 Normalized emission of compounds **3.1-3.7** in toluene (~10^{-5} M)

3.3.4 Electrochemical Properties

In DMF solution, compounds **3.1-3.7** display an irreversible reduction peak at -2.09 V (**3.1**), -1.68 V (**3.2**), -2.32 V (**3.3**), -2.03 V (**3.4**), -2.04 V (**3.5**), -2.28 V (**3.6**), and -2.09 V (**3.7**), which can be attributed to an addition of an electron to the π* orbital of the N,C-chelate ligand. The cyclic voltammetry diagrams are shown in Figure 3.11. Compared to the parent non-substituted compound (**2.1**), compounds **3.1**, **3.2**, **3.4**, and **3.5** display more positive reduction potentials, which indicates that they have a relatively lower energy LUMO level, most likely due to the presence of electron withdrawing groups (**3.1** and **3.2**) and/or conjugation to the acetylene moiety (**3.4** and **3.5)**. On the other hand, compound **3.3** shows a more negative potential, due to the presence of the electron donating $SiMe_3$ group. These observations are all consistent with the LUMO level being the π* orbital of the phenylpyridine chelate. In addition, compound **3.7** has a much more positive reduction potential than **3.6** due to the presence of the electron withdrawing fluoride substituents, which lowers the LUMO energy considerably. Also, **3.7** has a much more positive reduction potential when compared to compound **2.1**. This can be attributed to the greater σ-donation of the phenylpyridine to the boron center in **3.7**, as evident by the shorter B-$C_{chelate}$ bond of **3.7** (1.610(2)) compared to that of **2.1** (1.625(2)). The later is a direct effect of the electron withdrawing nature of the C_6F_5 moieties, which makes the boron center more electron deficient which in turn affects the energy of the π* level of the N,C-chelate ligand.

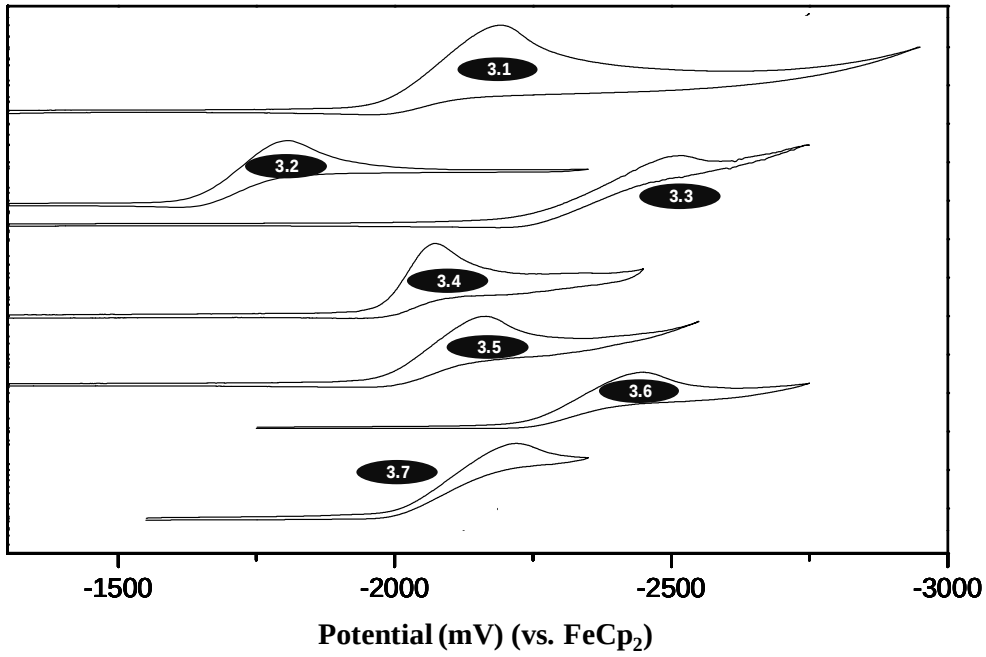

Figure 3.11 CV diagrams showing the reduction peak of **3.1-3.7** recorded in DMF with scan rate 200-300 mVs^{-1}.

3.3.5 DFT Calculations

Both DFT and TD-DFT calculations were performed on compounds **3.1-3.7**. The HOMO in compounds **3.1-3.5** is mainly composed of the mesityl group closer to the phenyl ring of the phenylpyridine chelate with contribution from the C_{phenyl}-B σ-bond and the phenyl ring itself, while the LUMO is mainly dominated by the phenylpyridine π* orbital with small contribution from the B-C_{Mes} bonds, Figure 3.12 and Figure 3.13. Based on TD-DFT calculations, the lowest energy transition of **3.1-3.5** is mainly a HOMO-LUMO transition with oscillator strength (transition probability) values of 0.0082, 0.0196, 0.0180, 0.0390, and 0.0244, respectively (Table 3.4). The HOMO and LUMO orbitals in

3.1-3.5 partially overlap around the $C_{chelate}$ moiety, suggesting a possible pathway of a charge transfer interaction through the phenyl ring.

The LUMO in compounds **3.6** and **3.7** is almost entirely composed of phenylpyridine π* orbital, while the HOMO of **3.6** is mainly composed of one of the phenyl rings with some contribution from the second phenyl ring and the $C_{chelate}$-B σ-bond. On the other hand, the HOMO of **3.7** is dominated by the phenylpyridine chelate with considerable contribution from one of the C_6F_5 rings. Based on TD-DFT calculations, the lowest energy transition of **3.6** is a HOMO-LUMO transition with oscillator strength (transition probability) of 0.0063. In addition, the lowest energy transition of **3.7** is indeed a HOMO-LUMO transition with oscillator strength of 0.0358 but since the major contributor of the HOMO is the phenylpyridine chelate the transition is mainly a $\pi \rightarrow \pi^*$ one. The large HOMO-LUMO gap in **3.6** and **3.7** is caused by the relative stability of the HOMO levels resulting from replacing the mesityl groups with phenyl and pentafluorophenyl groups, which can be attributed to the presence of the electron-withdrawing fluoride atoms in **3.7** and the "neutral" hydrogen atoms in **3.6** instead of the electron-releasing CH_3 groups on the mesityls.

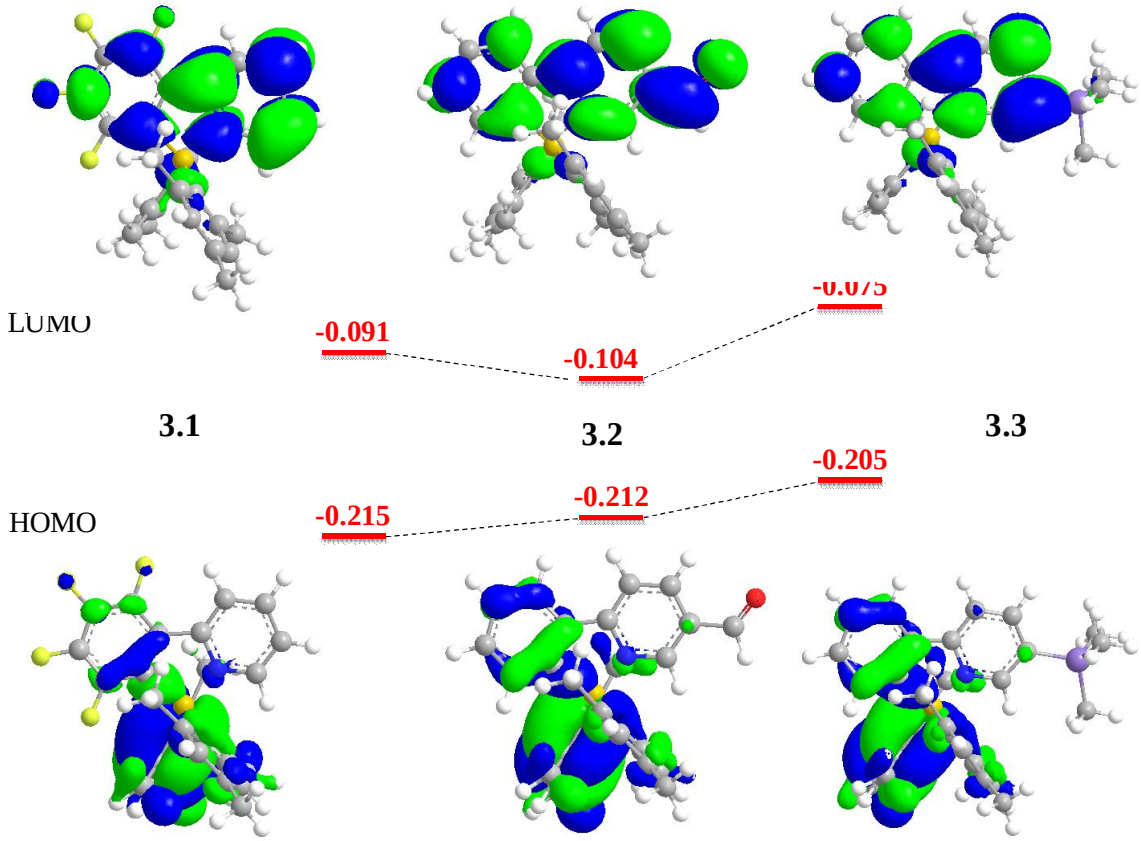

Figure 3.12 HOMO and LUMO diagrams of compounds **3.1-3.3** with calculated energy levels shown in Hartree (1 Hartree = 27.2107 eV) and surface isocontour value of 0.02.

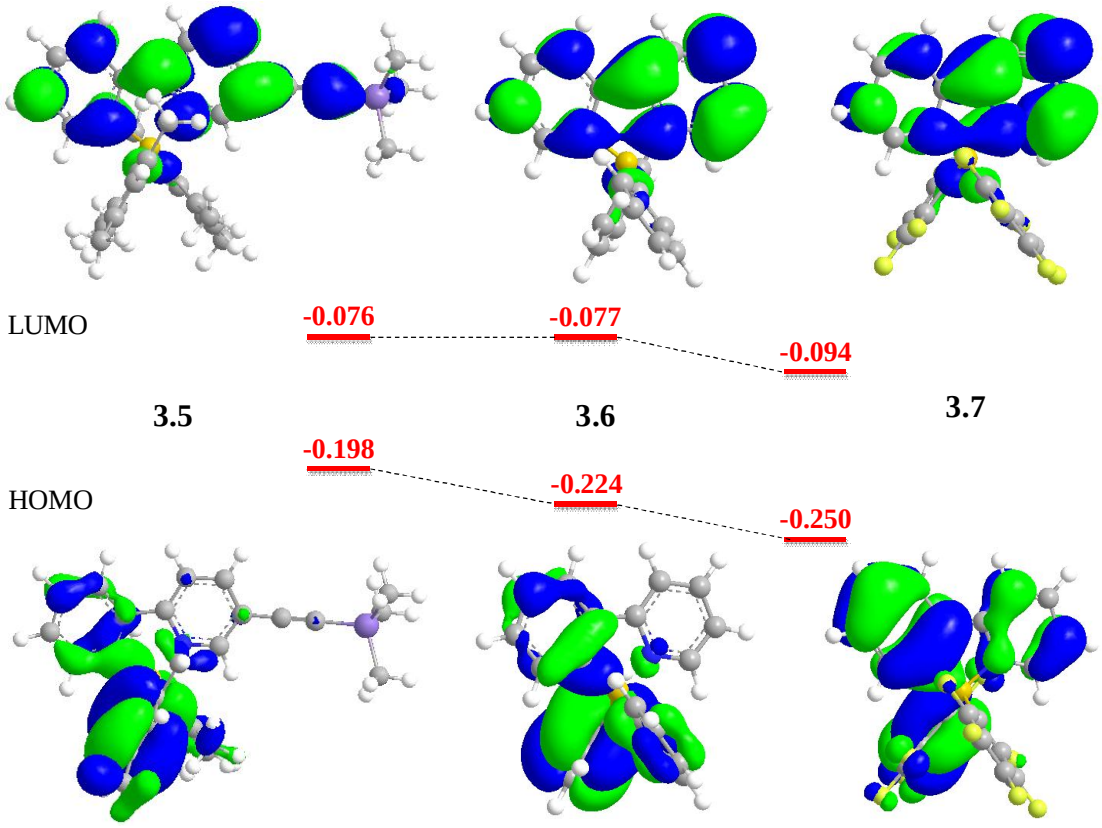

Figure 3.13 HOMO and LUMO diagrams of compounds **3.5-3.7** with calculated energy levels shown in Hartree (1 Hartree = 27.2107 eV) and surface isocontour value of 0.02.

The experimental values of the HOMO-LUMO energy levels and gaps of all compounds, calculated using the optical energy gaps and the reduction potentials, were compared to those obtained using DFT calculations as shown in Figure 3.14. Although the calculated band gap values deviate from those obtained experimentally, the general trends of the HOMO-LUMO band gaps obtained from both methods are consistent.

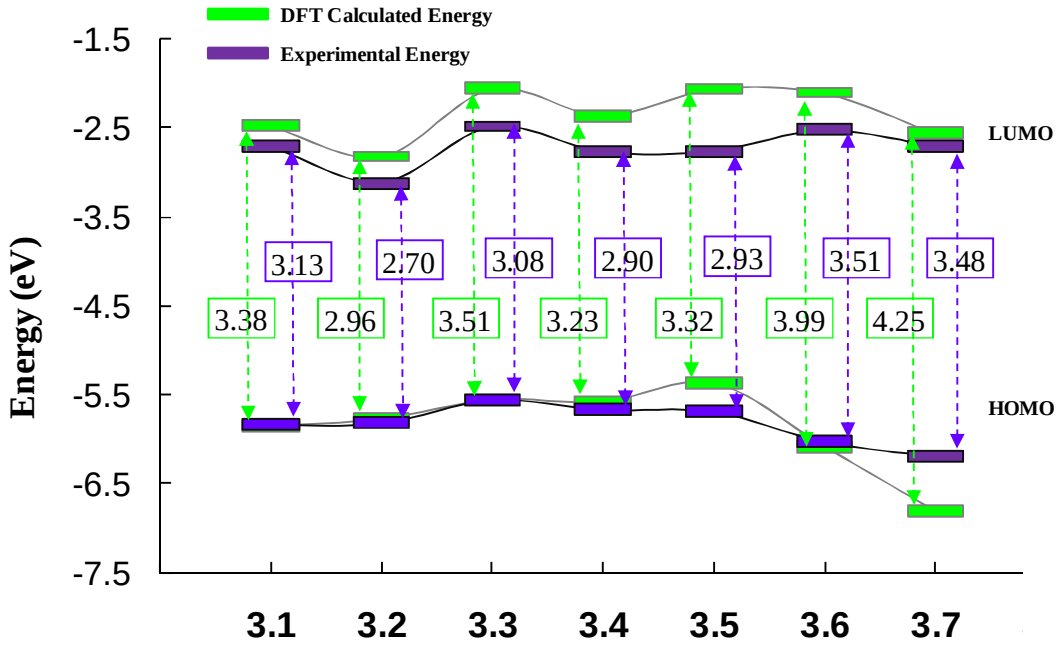

Figure 3.14 DFT-calculated and experimental HOMO-LUMO energy levels

Table 3.4 Selected data of electronic transitions for compounds **3.1-3.7** calculated using TD-DFT method at the B3LYP/6-311G* level. First excited state is a HOMO→LUMO transition in all compounds (*f* = oscillator strength)

	3.1	**3.2**	**3.3**	**3.4**	**3.5**	**3.6**	**3.7**
Excited State	Transition λ (nm) *f*	Transition λ (nm) *f*	Transition λ (nm) *f*	Transition λ (nm) *f*	Transition λ (nm) *f*	Transition λ (nm) *f*	Transition λ (nm) *f*
1	124→125 449.98 0.0082	115→116 513.09 0.0196	128→129 428.50 0.0180	134→135 460.99 0.0390	134→135 454.16 0.0244	84→85 372.02 0.0063	124→125 342.77 0.0358
2	123→125 417.66 0.0015	114→116 464.89 0.0062	127→129 390.19 0.0075	133→135 419.51 0.0091	133→135 414.77 0.0081	83→85 349.38 0.0106	123→125 329.81 0.0030
3	122→125 410.86 0.0097	113→116 453.99 0.0089	126→129 381.18 0.0079	132→135 411.24 0.0205	132→135 405.52 0.0113	82→85 336.04 0.0005	122→125 324.26 0.0142
4	121→125 388.63 0.0023	112→116 429.82 0.0004	125→129 362.58 0.0014	131→135 390.98 0.0015	131→135 385.82 0.0005	81→85 326.06 0.0010	121→125 318.59 0.0293
5	124→126 360.78 0.0044	115→117 394.74 0.0003	128→130 354.85 0.0058	134→136 387.48 0.0020	134→136 381.48 0.0035	84→86 320.70 0.0040	120→125 309.48 0.0361

6	123→126 341.60 0.0002	114→117 369.01 0.0003	127→130 330.50 0.0012	130→135 363.79 0.4332	133→136 357.61 0.0001	80→85 316.80 0.0622	119→125 301.38 0.0201
7	122→126 337.25 0.0012	111→116 363.07 0.0723	124→129 328.52 0.0980	133→136 361.59 0.2183	132→136 349.36 0.0298	83→86 305.59 0.0252	124→126 286.89 0.0693
8	120→125 328.38 0.0575	113→117 358.13 0.0187	126→130 322.57 0.0190	132→136 352.65 0.0742	130→135 343.24 0.2459	79→85 299.92 0.0754	123→126 280.26 0.0043
9	121→126 322.64 0.0023	109→116 345.10 0.0010	125→130 310.16 0.0016	131→136 338.22 0.0009	131→136 333.88 0.0010	82→86 292.93 0.0080	122→126 275.93 0.0177
10	119→125 309.07 0.1373	112→117 343.62 0.0014	123→129 306.44 0.1233	129→135 330.73 0.1601	129→135 321.03 0.1752	81→86 285.77 0.0043	121→126 271.08 0.0797

The calculated absorption spectra of **3.1**-**3.7** were obtained using TD-DFT calculations at the (B3LYP/6-311G*) level after geometry optimization at the same level of theory using DFT calculations. The TD-DFT-based UV-Vis spectra of **3.1**-**3.7** are shown in Figure 3.15 - Figure 3.21. The important energy transitions, including the lowest energy transitions, of **3.1**-**3.7** are shown on the figures, along with the involved

orbital diagrams, oscillator strengths, and the wavelength at which the transition took place.

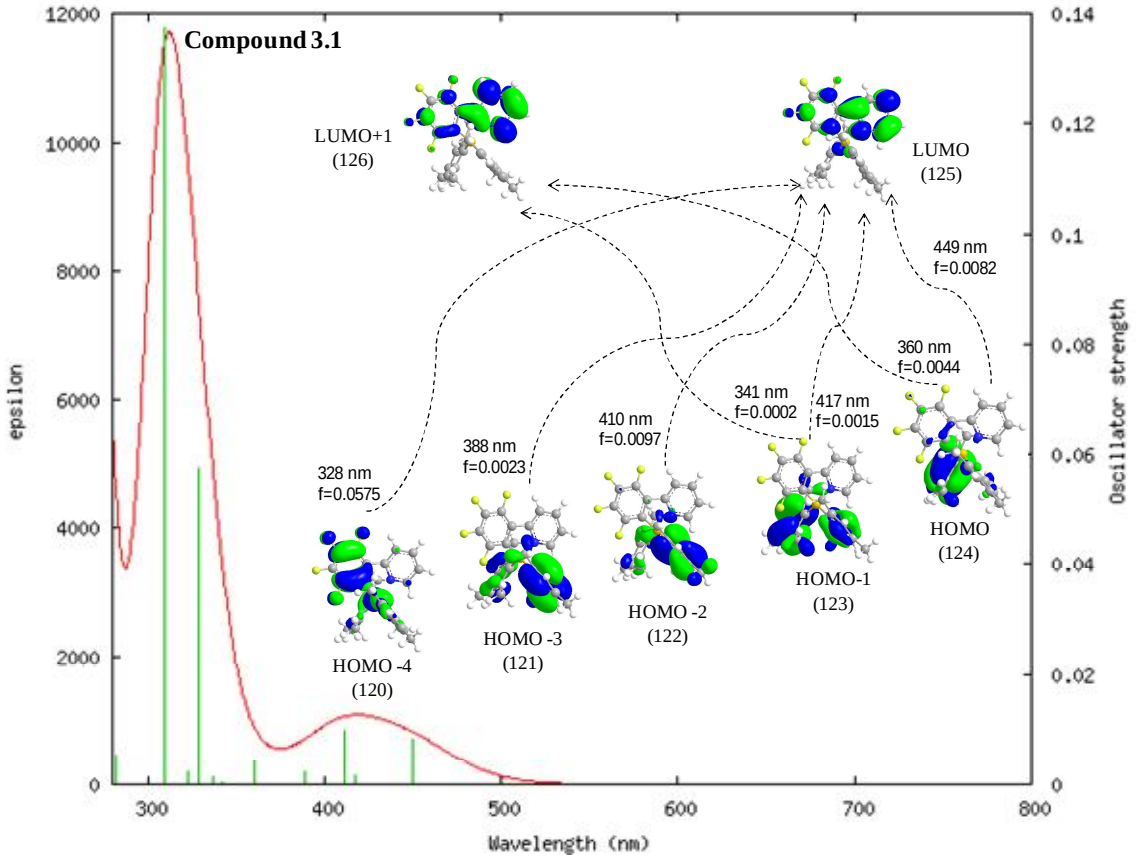

Figure 3.15 Calculated UV-Vis spectrum of **3.1** with characteristic electronic transitions calculated at the TD-DFT (B3LYP/6-311G*) level. Produced using GaussSum program V.2.2.2 with FWHM = 3000 cm^{-1}

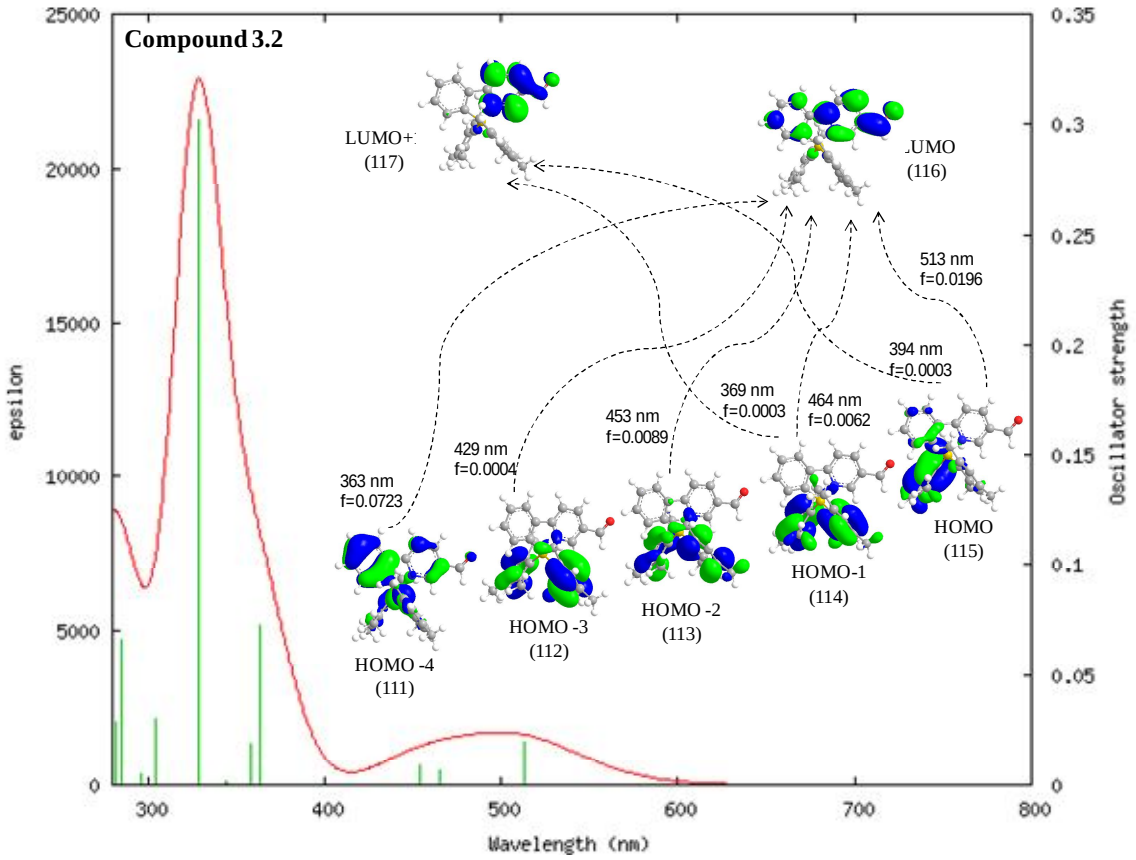

Figure 3.16 Calculated UV-Vis spectrum of **3.2** with characteristic electronic transitions calculated at the TD-DFT (B3LYP/6-311G*) level. Produced using GaussSum program V.2.2.2 with FWHM = 3000 cm^{-1}

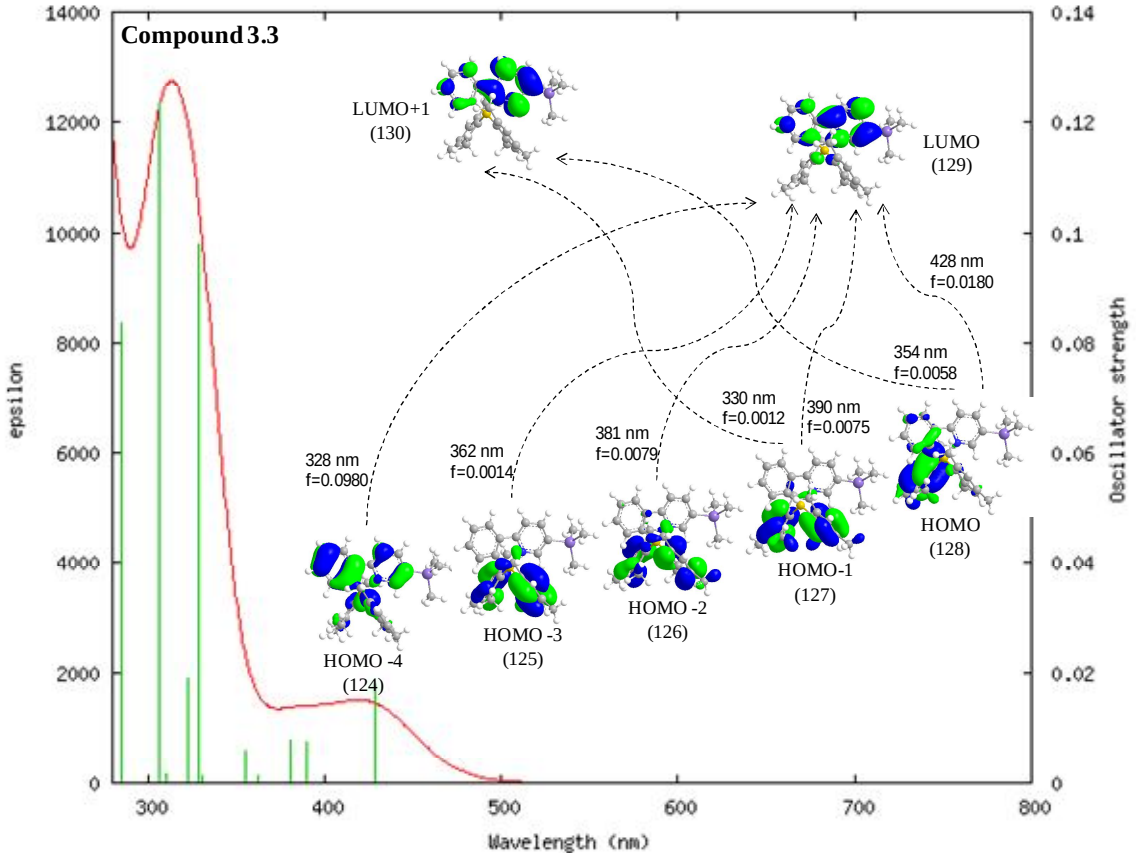

Figure 3.17 Calculated UV-Vis spectrum of **3.3** with characteristic electronic transitions calculated at the TD-DFT (B3LYP/6-311G*) level. Produced using GaussSum program V.2.2.2 with FWHM = 3000 cm^{-1}

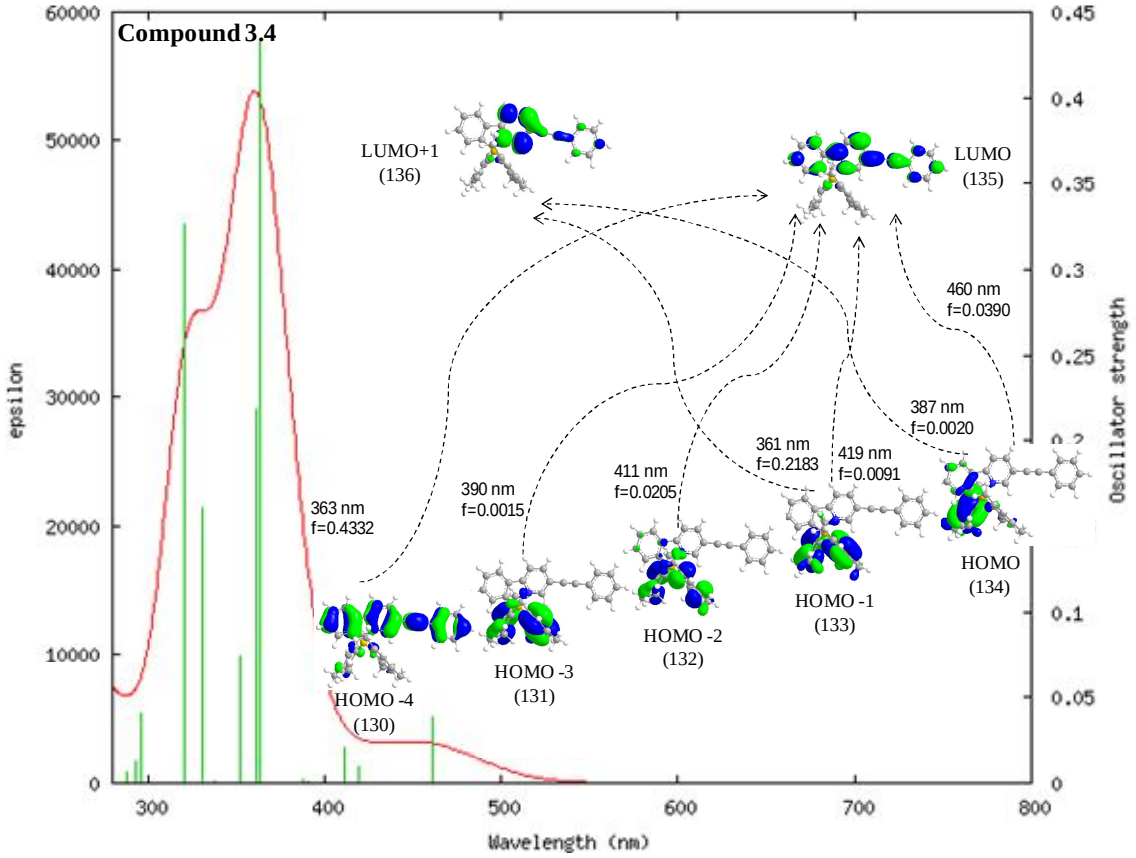

Figure 3.18 Calculated UV-Vis spectrum of **3.4** with characteristic electronic transitions calculated at the TD-DFT (B3LYP/6-311G*) level. Produced using GaussSum program V.2.2.2 with FWHM = 3000 cm^{-1}

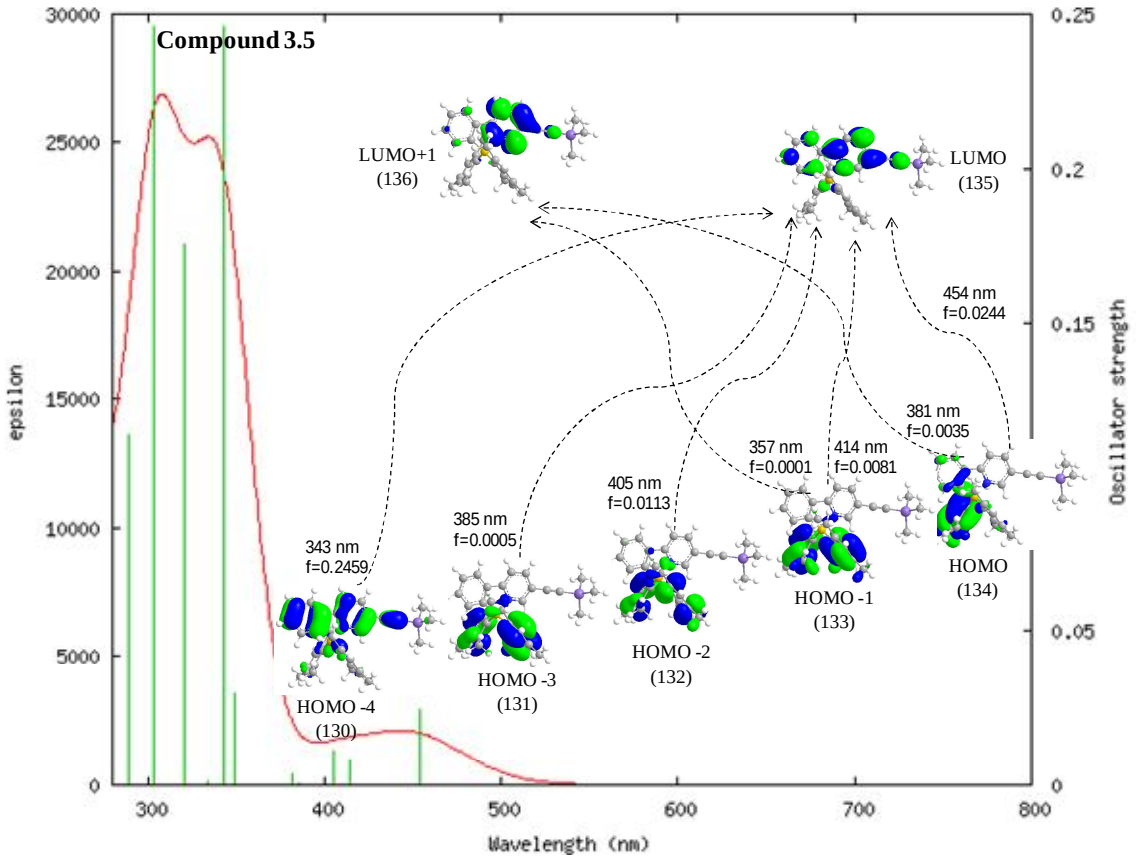

Figure 3.19 Calculated UV-Vis spectrum of **3.5** with characteristic electronic transitions calculated at the TD-DFT (B3LYP/6-311G*) level. Produced using GaussSum program V.2.2.2 with FWHM = 3000 cm^{-1}

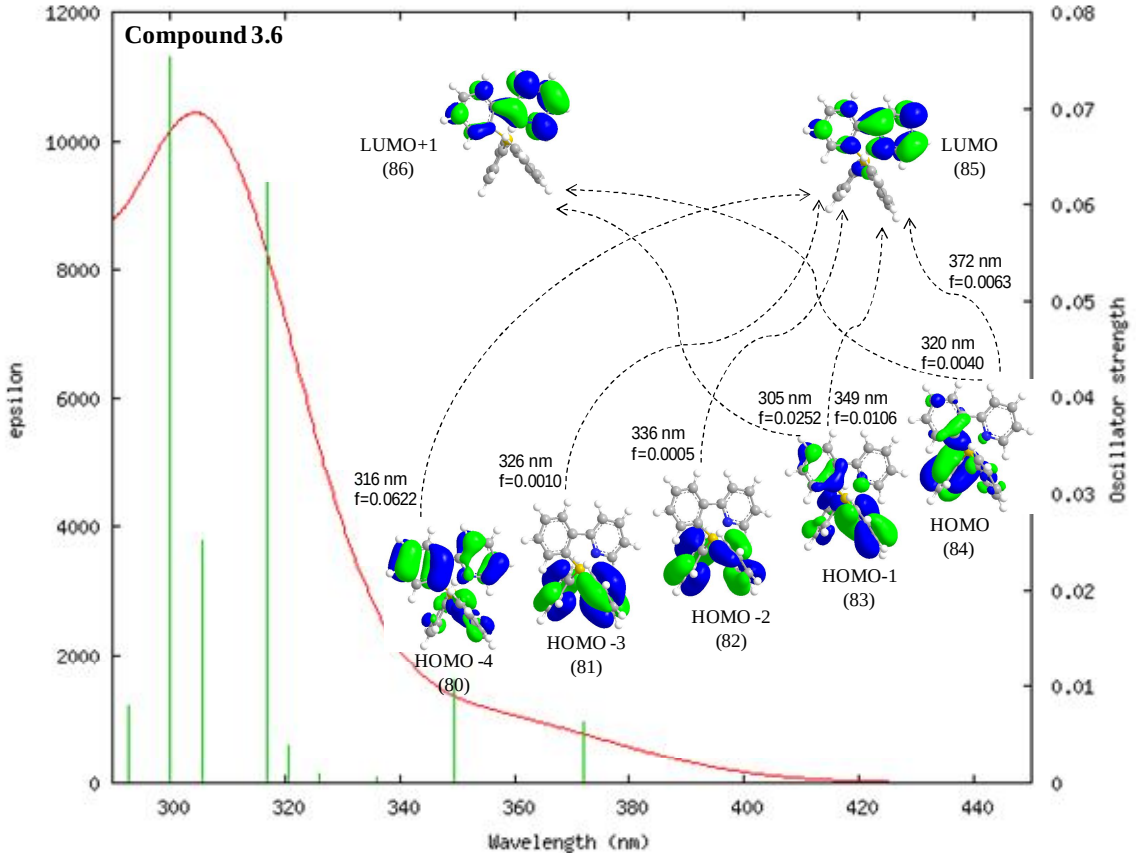

Figure 3.20 Calculated UV-Vis spectrum of **3.6** with characteristic electronic transitions calculated at the TD-DFT (B3LYP/6-311G*) level. Produced using GaussSum program V.2.2.2 with FWHM = 3000 cm^{-1}

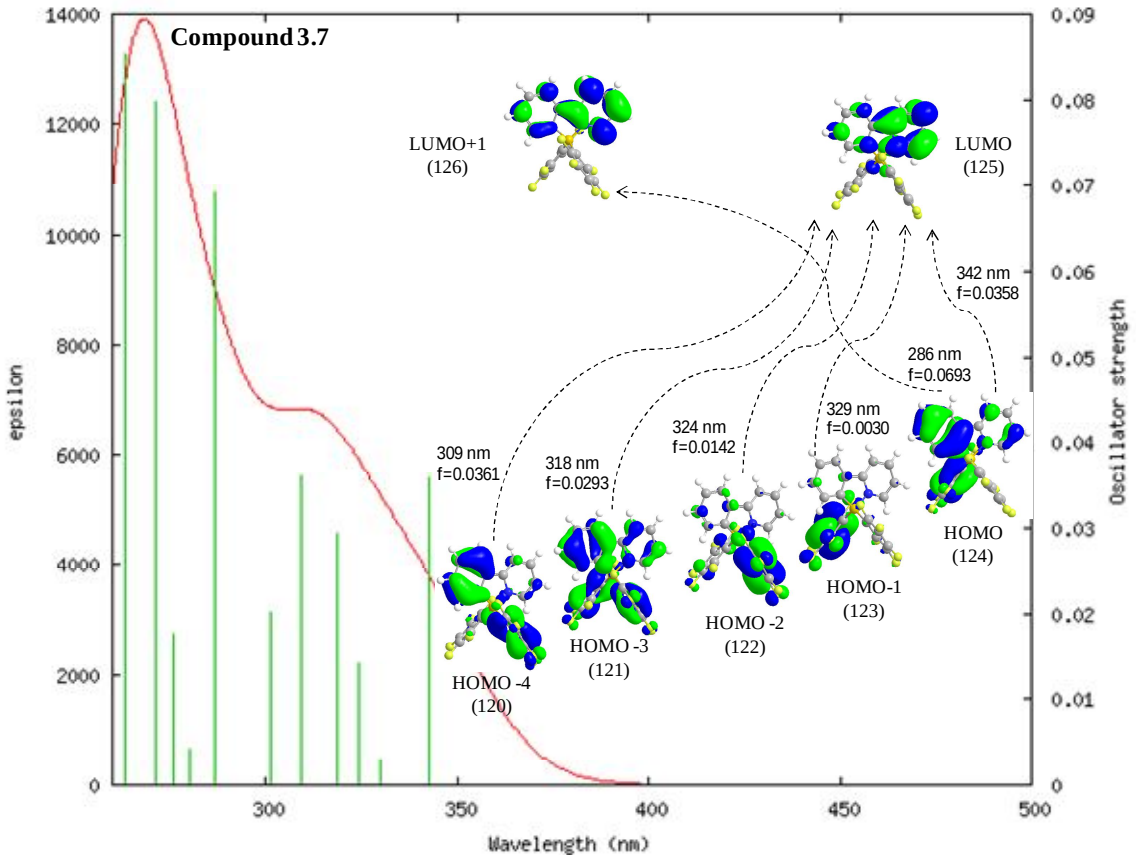

Figure 3.21 Calculated UV-Vis spectrum of **3.7** with characteristic electronic transitions calculated at the TD-DFT (B3LYP/6-311G*) level. Produced using GaussSum program V.2.2.2 with FWHM = 3000 cm^{-1}

3.3.6 Photochromic Behavior of Compounds 3.1-3.7

Compounds **3.2-3.5** have similar photochromic properties to those observed in compound **2.1**. Upon exposure to UV light (365 nm or 350 nm) under nitrogen atmosphere the colorless/yellowish toluene solution becomes dark blue, yellow, or green as shown in Figure 3.22. On the other hand, compounds **3.1** and **3.7** were unstable towards photolysis and did not show photochromic properties, which may be attributed to the presence of fluoride atoms. In addition, compound **3.6** did not show any response towards UV light even when irradiated at its absorption maximum (312 nm), which suggests that the steric congestion imposed by the two mesityl groups plays an important role in the photoisomerization process. This is supported by the fact that the HOMO and LUMO energy levels of **3.6** are very similar to those of **2.1**; hence the photoisomerization process cannot be explained based on electronic factors alone.

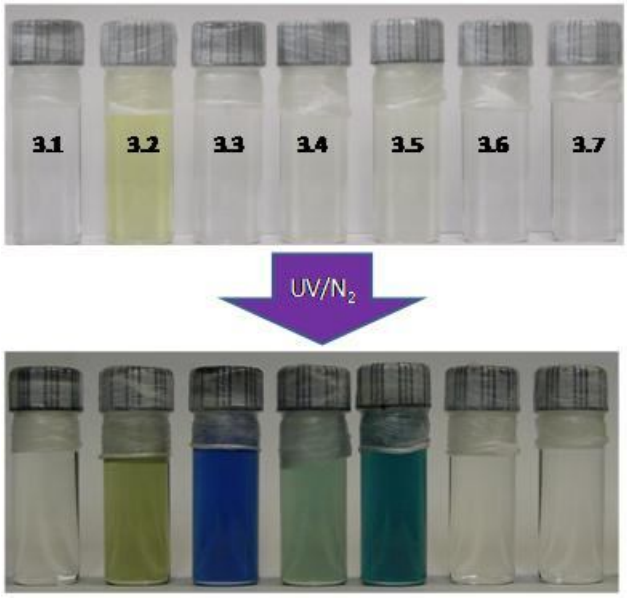

Figure 3.22 Color changes of **3.1-3.7** upon exposure to UV light

Further important points about the steric effect imposed by the two mesityl groups can be inferred by comparing the X-ray structure data of **2.1** and **3.6**. Both compounds have the same N,C-chelate back-bone with different aryl groups attached to the boron center (Mes and Ph, respectively). Based on crystal structure data the B-Mes bonds (1.644 and 1.654 Å) in **2.1** are much longer, hence weaker, than the B-Ph bonds (1.611 and 1.616 Å) in **3.6**, which is attributed to the larger steric demand required by the Mes groups. Also the Mes groups are less symmetrically arranged around the boron center than the phenyl groups are as shown in Figure 3.23, where one Mes group is closer to the $C_{Chelate}$ atom than the other (2.60 vs. 2.83 Å). The weaker B-Mes bond and the asymmetric arrangement of the Mes groups seem to be behind this unusual photochromic behavior. In addition, a comparison between the photochemically stable compound **3.6** and photochemically reactive BPh_4^- suggests that the N,C-chelate is making compound **3.6** more thermodynamically stable. Nevertheless, N,C-chelation accompanied with the presence of the bulky mesityl groups still leads to photoresponsive behavior, further suggesting that the mesityl groups are essential for the photochromic process to take place.

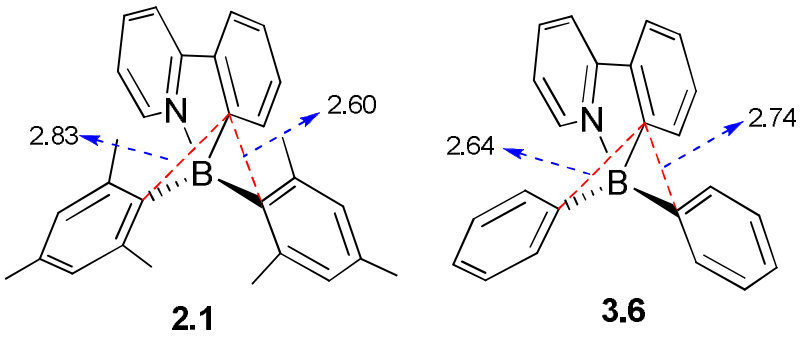

Figure 3.23 Comparison of through-space distance (Å) between C_{Mes}-$C_{Chelate}$ of **2.1** and **3.6**.

The photochromic conversions of **3.2**, **3.3**, **3.4**[12], and **3.5** were monitored using UV-Vis and ^{1}H NMR spectroscopy techniques. Upon irradiation of a toluene solution of **3.2**, **3.3**, or **3.5** with UV light (365 nm) under an atmosphere of N_2, a new intense broad band appears and grows rapidly (λ_{max} = 728, 605, and 650 nm, respectively) as shown in Figure 3.24 - Figure 3.26, which follows a similar trend compared to the λ_{em} of these compounds. The quantum efficiency of the photoisomerization process of **3.3** and **3.4**[12] determined using the ferrioxalate actinometry was 0.51 and 0.33 compared to 0.88 for compound **2.1** (the non-substituted compound). The lower photoisomerization quantum efficiency of **3.4** is associated with a higher fluorescence quantum yield of 0.37 compared to 0.1 and 0.12 for **2.1** and **3.3**, respectively, which may be attributed to the extended π conjugation of **3.4**.

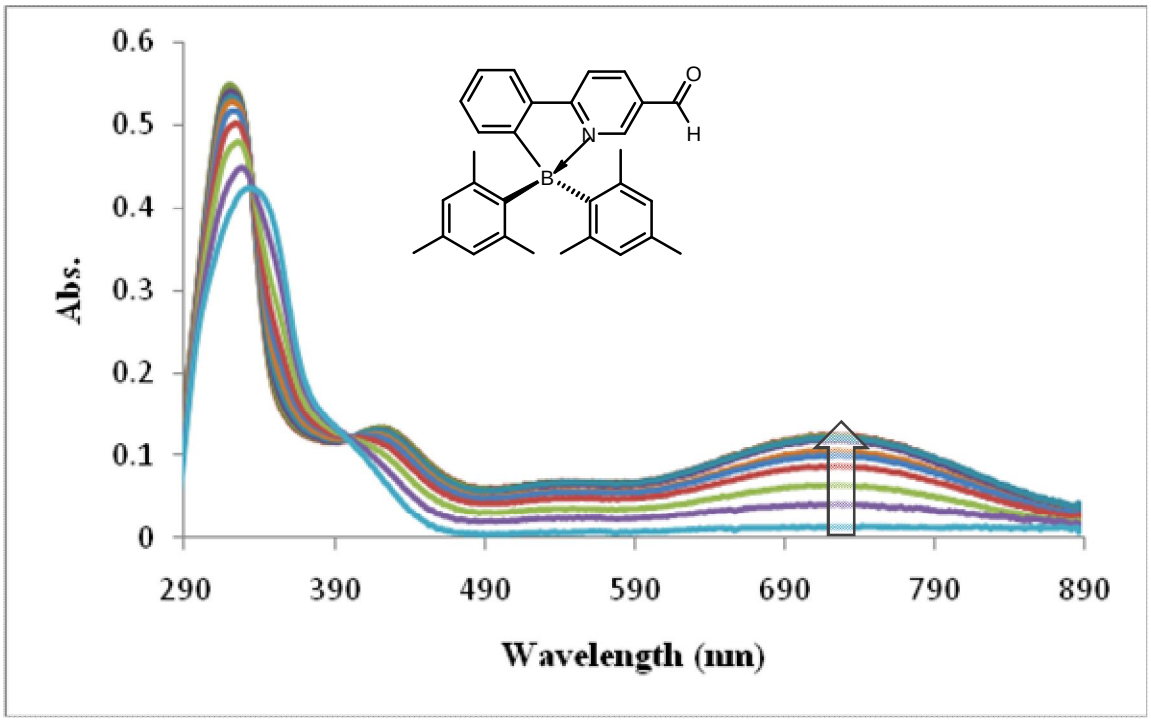

Figure 3.24 UV-Vis spectral changes of **3.2** in toluene upon irradiation by UV light (365 nm) under nitrogen at RT, recorded at ~10^{-5} M with 5 s intervals of UV exposure.

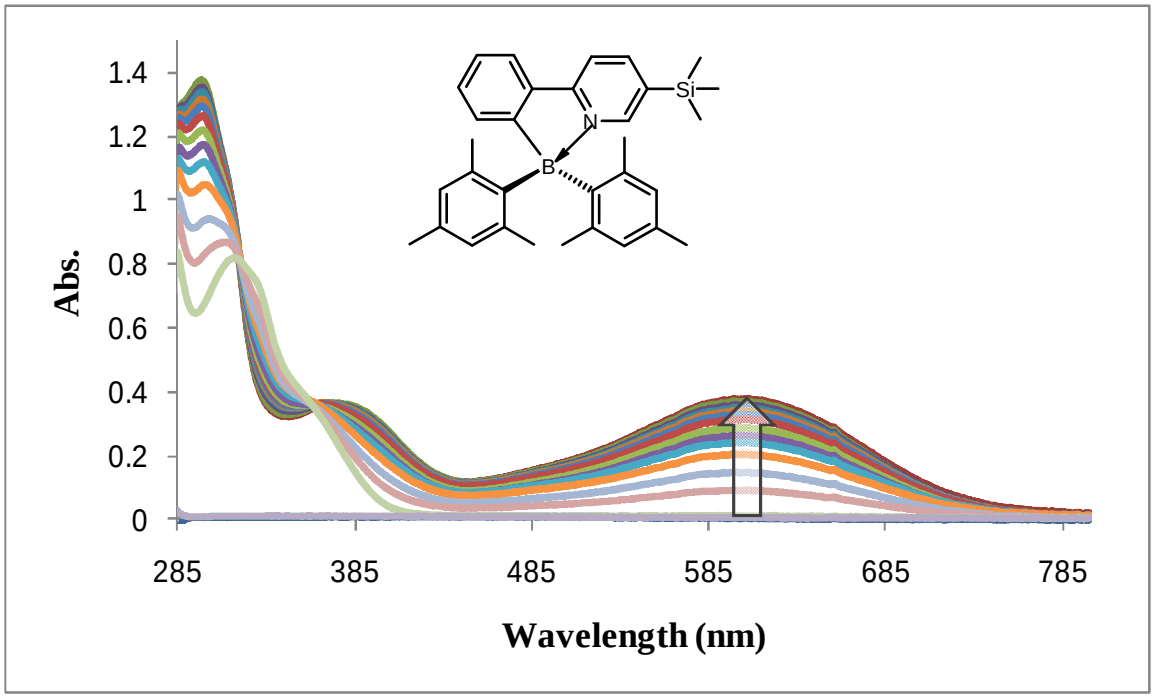

Figure 3.25 UV-Vis spectral changes of **3.3** in toluene upon irradiation by UV light (365 nm) under nitrogen at RT, recorded at ~10^{-5} M with 5 s intervals of UV exposure.

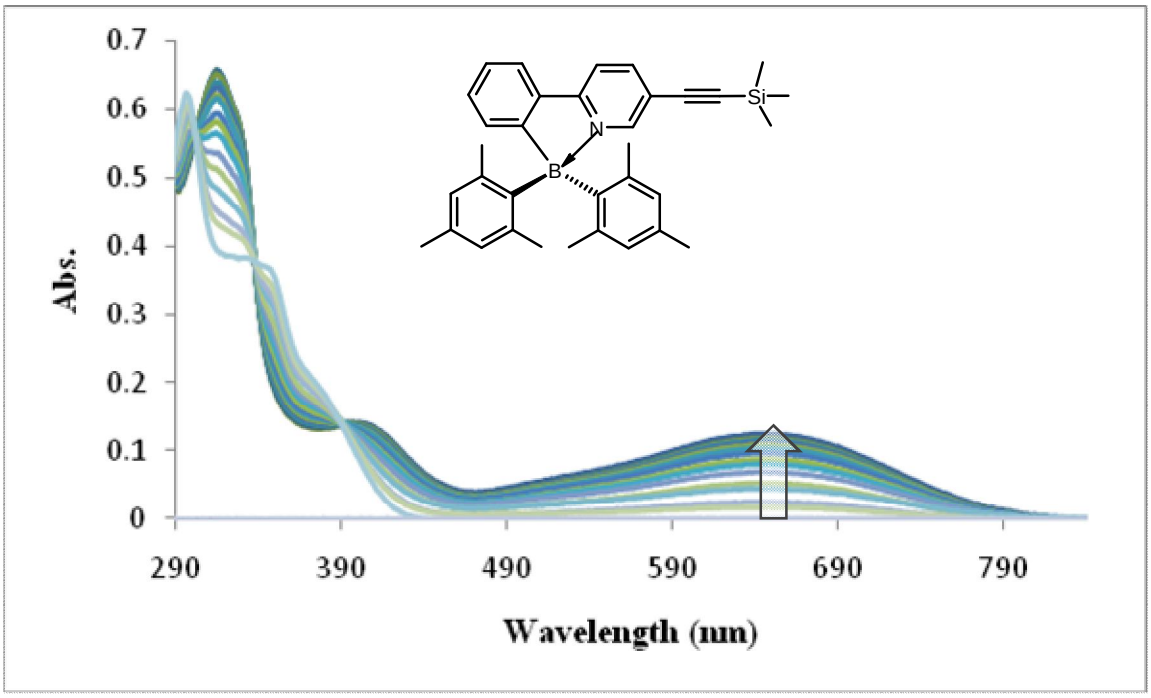

Figure 3.26 UV-Vis spectral changes of **3.5** in toluene upon irradiation by UV light (365 nm) under nitrogen at RT, recorded at ~10^{-5} M with 3 s intervals of UV exposure.

The photochromic behavior of **3.2**, **3.3**, and **3.5** was also monitored using ^{1}H NMR spectroscopy, Figure 3.27 - Figure 3.29. Upon irradiation of a C_6D_6 solution of these compounds with UV light (365 nm) under N_2, the ^{1}H NMR spectra display a new set of peaks that represent the corresponding dark isomers. Similar to the photo conversion of compound **2.1** to **2.1a**, the singlet representing the four aryl protons of the two mesityl groups (H_{Ar}) splits in to four distinct singlet peaks and the two singlet peaks representing the six methyl groups splits in to six distinct methyl peaks.

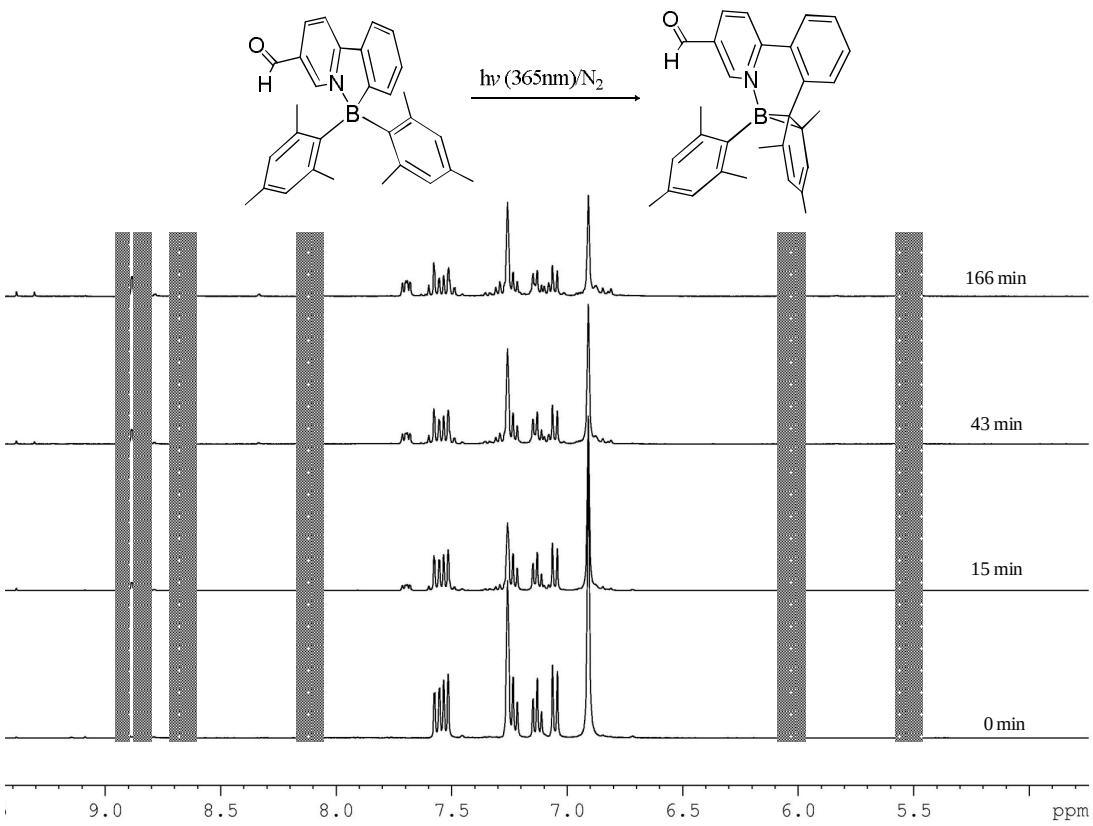

Figure 3.27 ^{1}H NMR spectral changes (aromatic region) of **3.2** in C_6D_6 under N_2 upon irradiation at 365 nm. Violet: **3.2** and green: **3.2a**.

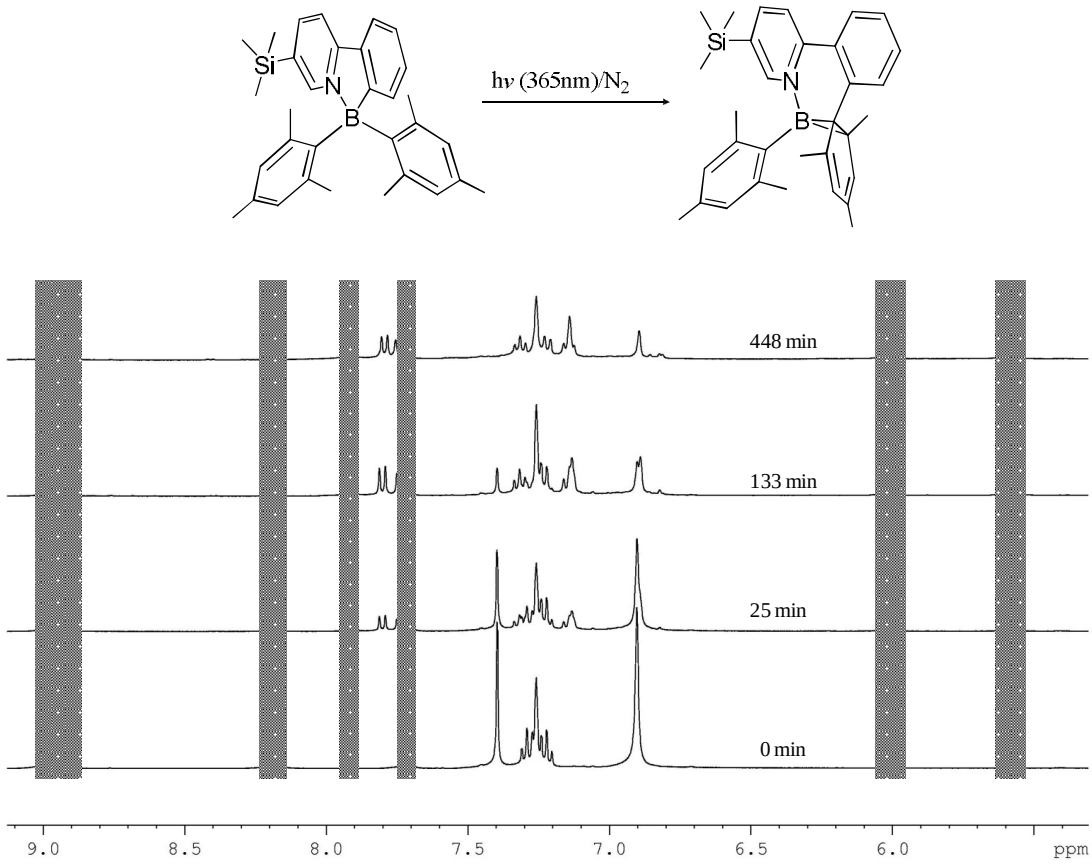

Figure 3.28 ^{1}H NMR spectral changes (aromatic region) of **3.3** in C_6D_6 under N_2 upon irradiation at 365 nm. Violet: **3.3** and green: **3.3a**.

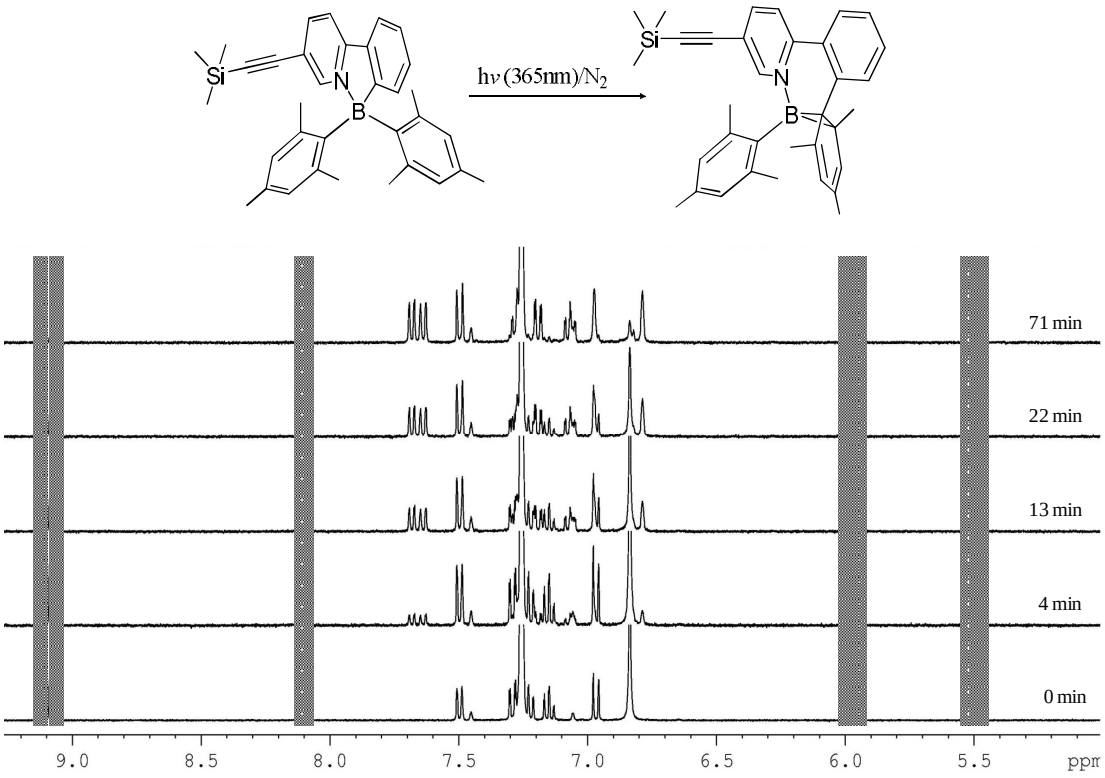

Figure 3.29 ^{1}H NMR spectral changes (aromatic region) of **3.5** in C_6D_6 under N_2 upon irradiation at 365 nm. Violet: **3.5** and green: **3.5a**.

3.3.7 Relative Photoisomerization Rate Studies

The photoisomerization rates of **3.2**, **3.3**, **3.4**[12], and **3.5** relative to **2.1** were studied using ^{1}H NMR spectroscopy as shown in Figure 3.30 – Figure 3.32, where the effect of the different substituents on the phenylpyridine chelate was investigated. The photoisomerization of **3.2**, which contains the –COH electron-withdrawing group, is slower than that of **2.1** (k(**2.1**)/k(**3.2**) = 1.2), which might be attributed to the stabilization of the π* and the excited state in **3.2** by the -COH group, which seems to slow down the

photoisomerization. On the contrary, the electron-donating ability of the -$SiMe_3$ group in **3.3** destabilizes the π* and the excited state, which is believed to be responsible for the faster isomerization rate of **3.3** (k(**2.1**)/k(**3.3**) = 0.8). The photoisomerization rates of **3.4** and **3.5** related to **2.1** are k(**2.1**)/k(**3.4**) = 20 and k(**2.1**)/k(**3.5**) = 0.8. The much slower isomerization rate of **3.4** can be attributed to the extended π-conjugation of the N,C-chelate with the Ph-acetylene moiety, which leads to the stabilization of the π* and the excited state. On the other hand, although compound **3.5** has a conjugated acetylene group attached to the N,C-chelate its photoisomerization rate is much faster than that of **3.4**, which might be attributed to the dominant effect of the electron-releasing $SiMe_3$ group capping the acetylene leading to a higher π* (LUMO) level as depicted by DFT calculations.

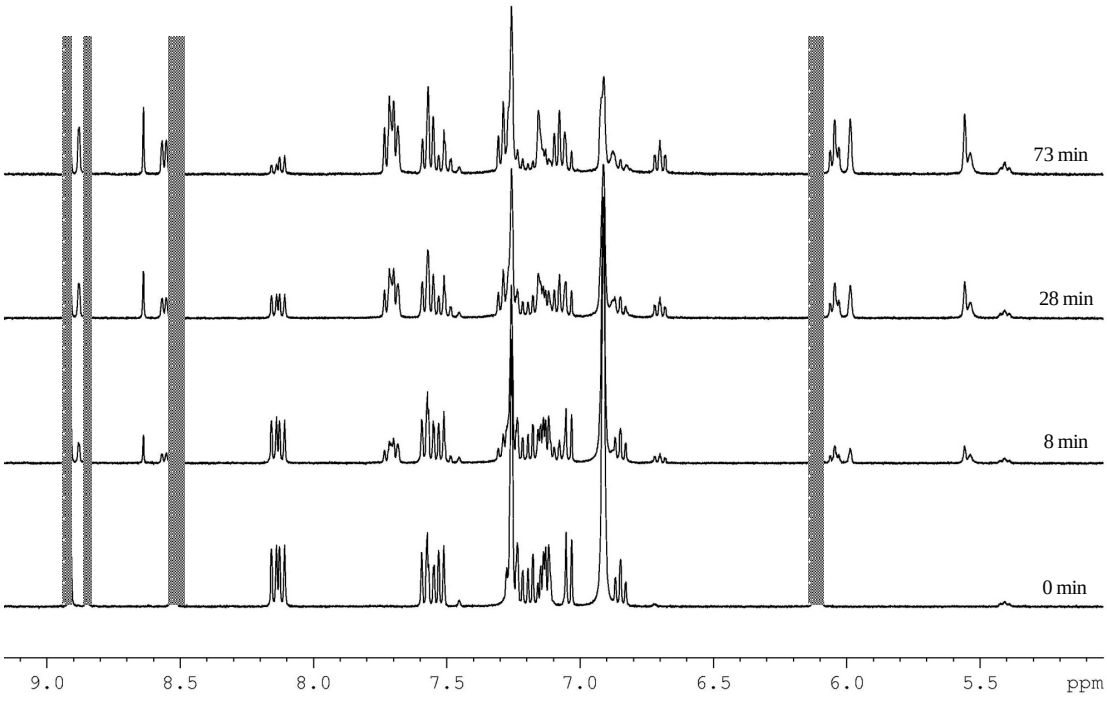

Figure 3.30 ^{1}H NMR spectra of **3.2** and **2.1**(reference) showing the relative conversion rate to **3.2a** and **2.1a** after irradiation with UV (365 nm) in C_6D_6 under N_2 .Color code: **3.2**(Violet) and **2.1** (Orange)

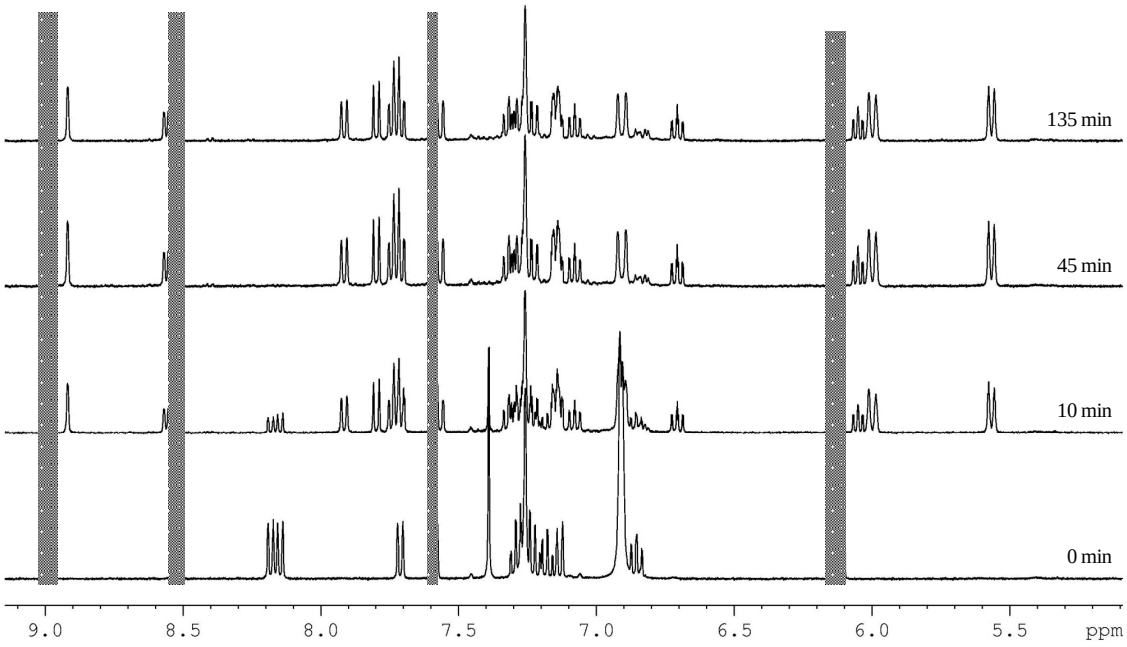

Figure 3.31 ^{1}H NMR spectra of **3.3** and **2.1**(reference) showing the relative conversion rate to **3.3a** and **2.1a** after irradiation with UV (365 nm) in C_6D_6 under N_2 .Color code: **3.3**(Violet) and **2.1** (Orange)

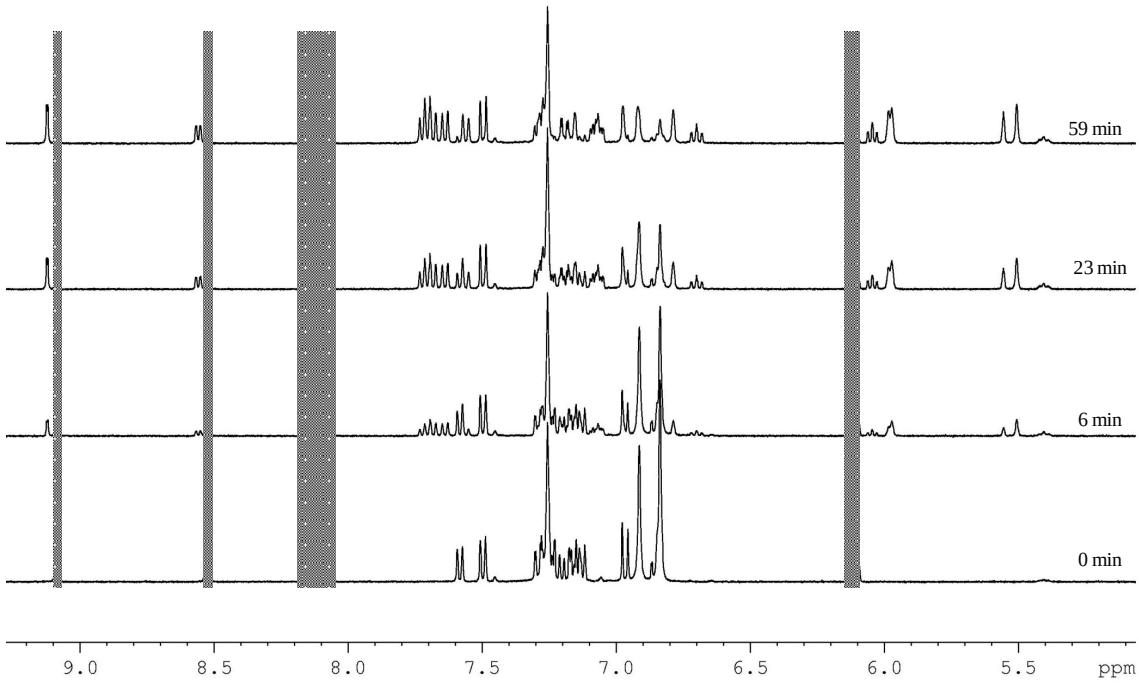

Figure 3.32 ^{1}H NMR spectra of **3.5** and **2.1**(reference) showing the relative conversion rate to **3.5a** and **2.1a** after irradiation with UV (365 nm) in C_6D_6 under N_2 .Color code: **3.5**(Violet) and **2.1** (Orange)

Similar to the dark isomer **2.1a**, the dark isomers **3.3a** and **3.5a** can be converted back to the colorless original state **3.3** and **3.5** upon heating to 50-70 °C or very slowly at room temperature. The thermal reversal of **3.3a** and **3.5a** was monitored by ^{1}H NMR as shown in Figure 3.33 and Figure 3.34. Reversing the dark isomers using visible light was not effective, which supports that this class of compounds are of the T-type photochromic compounds. On the other hand, the thermal conversion of **3.2a** was not attempted because compound **3.2** cannot be fully converted to **3.2a** and decomposes under the general experimental conditions used, which can be explained by the reactivity of the –COH group.

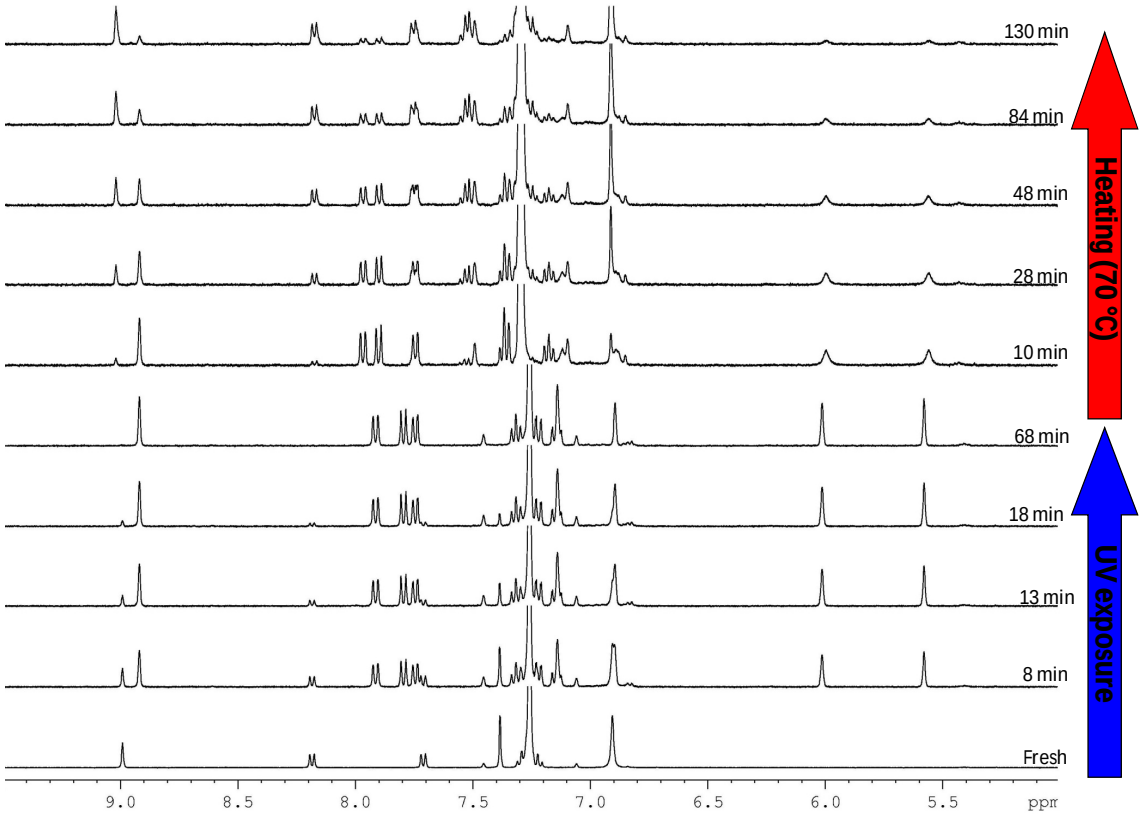

Figure 3.33 Photolysis of **3.3** to **3.3a** and subsequent thermal conversion of **3.3a** to **3.3** under nitrogen in C_6D_6 at 50 °C.

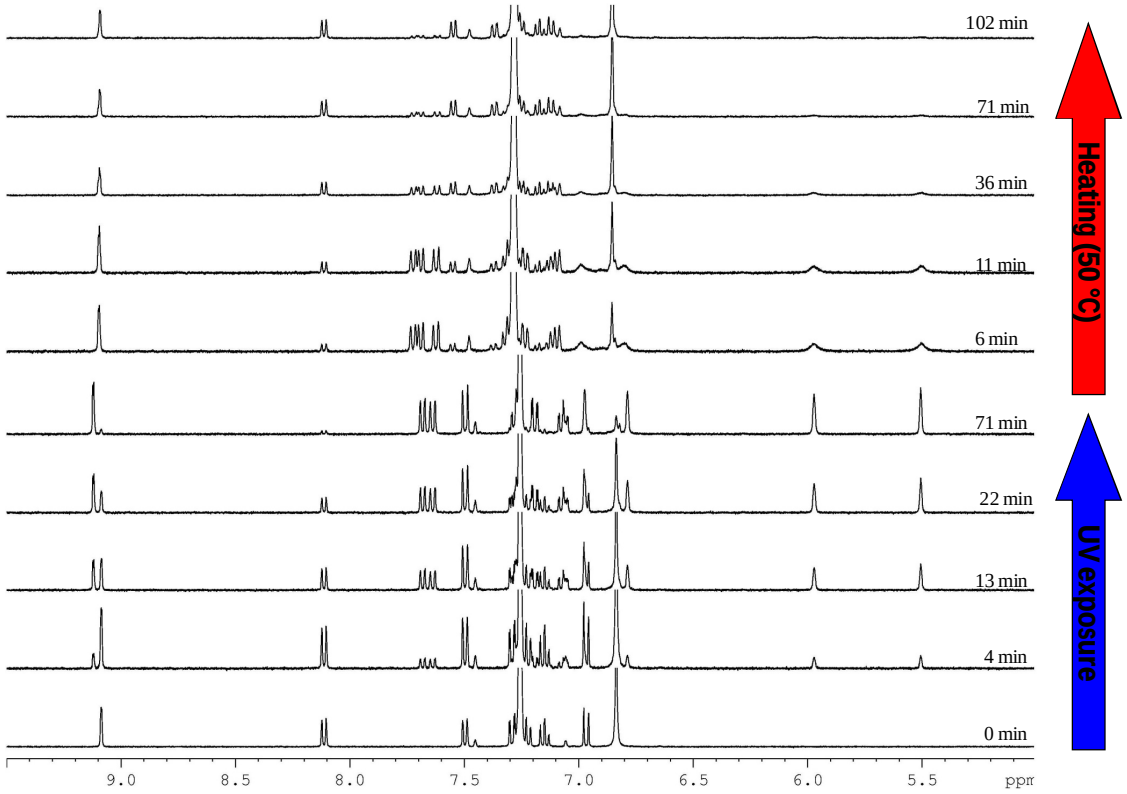

Figure 3.34 Photolysis of **3.5** to **3.5a** and subsequent thermal conversion of **3.5a** to **3.5** under nitrogen in C_6D_6 at 50 °C.

The dark isomers **3.2a**, **3.3a**, **3.4a**, and **3.5a** are also oxygen-sensitive, similar to **2.1a**, and yield the corresponding C-C coupled products **3.2b**, **3.3b**, **3.4b**, and **3.5b**, which can be obtained by exposing the dark isomer solutions to air/oxygen or by irradiating the solutions in the presence of O_2. The C-C coupled products were identified and characterized by HRMS spectroscopy. The similar thermal behavior and oxygen-sensitivity of these dark isomers to **2.1a**, further supports that all these compounds undergo photoisomerization in the same manner.

3.4 Conclusion

The new substituted 4-coordinate N,C-chelate organoborons enabled us study the steric and electronic effects of the substituents on the phenylpyridine chelate and on the boron center. The following points can be concluded: (1) The photoisomerization of the phenylpyridine-based organoboron compounds is expected to be initiated by a photo-induced charge transfer from the HOMO localized on the mesityl group closer to the $C_{Chelate}$ to the LUMO localized on the N,C-chelate moiety, which is followed by a di-π-borate rearrangement (Zimmerman rearrangement). (2) The presence of the bulky mesityl groups is a key factor in the photoisomerization process, which stems from their role in destabilizing the HOMO level. Although other bulky aryl groups have not been investigated it is anticipated that these could have a similar effect. (3) Electron-releasing substituents on the LUMO e.g. $SiMe_3$ appear to accelerate the photoisomerization rate via their destabilizing effect on the excited state. (4) Stabilizing the excited sate using extended π-conjugated substituents e.g. phenylacetylene appears to slow down the photoisomerization rate (5) Fluorinated N,C-chelates or fluorinated aryl groups attached to the boron center should be avoided when designing new members of this photochromic class, as these compounds tend to decompose upon irradiation with UV light. (6) The non-substituted phenylpyridine compound (**2.1**) has higher photoisomerization efficiency than all the studied substituted ones.

3.5 References

(1) (a) Durr, H.; Bouas-Laurent, H. In *Photochromism: Molecules and Systems*, 2nd ed.; Elsevier: Amsterdam, The Netherlands, 2003; and references therein. (b) Berkovic, G.; Krongauz, V.; Weiss, V. *Chem. Rev.* **2000**, *100*, 1741. (c) Crano, J. C.; Guglielmetti, R. J. In *Organic Photochromic and Thermochromic Compounds*; Plenum Press: NewYork, 1999.

(2) Huo, S.; Deaton, J.; Rajeswaran, M.; Lenhart, W. *Inorg. Chem.* **2006**, *45*, 3155.

(3) Stange, A. F.; Tokura, S.; Kira, M. *J. Organomet. Chem.* **2000**, *612*, 117.

(4) Grave, C.; Lentz, D.; Schafer, A.; Samori, P.; Rabe, J. P.; Franke, P.; Schluter, A. D. *J. Am. Chem. Soc.* **2003**, *125*, 6907.

(5) Koster, R.; Binger, P. *Inorg. Synth.* **1974**, *15*, 149.

(6) (a) Duchateau, R.; Lancaster, S. J.; Thornton-Pett, M.; Bochmann, M. *Organometallics* **1997**, *16*, 4995. (b) Yoshino, J.; Kano, N.; Kawashima, T. *Chem. Commun*. **2007**, 559.

(7) Baik, C.; Hudson, Z. M.; Amarne, H.; Wang, S. *J. Am. Chem. Soc.* **2009**, *131*, 14549.

(8) (a) Demas, N. J.; Crosby, G. A. *J. Am. Chem. Soc.* **1970**, *92*, 7262. (b) Fery-Forgues, S.; Lavabre, D. *J. Chem. Ed.* **1999**, *9*, 1260.

(9) Frisch, M. J.; et al. *Gaussian 03*, revision C.02; Gaussian, Inc.: Wallingford, CT, 2004.

(10) (a) Parker, C. A. Proc. R. Soc. London A 1953, 220, 104. (b) Abdallah, D.; Whelan, J.; Dust, J. M.; Hoz, S.; Buncel, E. *J. Phys. Chem. A.* **2009**, *113*, 6640.

(11) SHELXTL Version 6.14, Bruker AXS, 2000-2003.

(12) Baik, C.; Hudson, Z. M.; Amarne, H.; Wang, S. *J. Am. Chem. Soc.* **2009** *131*, 14549.

(13) Wrackmeyer, B. *Annu. Rep. NMR Spectrosc.* **1988**, *20*, 61.

Chapter 4

Heterocycle-Based N,C-Chelate Organoboron Compounds

4.1 Introduction

The rich chemistry of photochromic compounds in general and their potential applications in molecular switches, optical memory devices, and ophthalmic glasses, on one hand,[1] and the discovery of the phenylpyridine-based organoboron photochromic compounds on the other, encouraged us to investigate new N,C-chelate organoboron compounds. To establish whether the photoisomerization of the N,C-chelate-$BMes_2$ system is only limited to phenylpyridines or not, we have designed and synthesized a series of heterocyclic-based N,C-chelates to be used with the bulky $BMes_2$ groups instead of phenylpyridine as shown in Figure 4.1. Compounds **4.1**-**4.5** are based on Het-pyridine as the N,C-chelates, where Het = TMS-furan, TMS-thiophene, benzofuran, benzothiophene, and N-PhIndole, respectively. On the other hand, compounds **4.6** and **4.7** are based on Het-phenyl (Het = benzothiazole or benzoxazole). These compounds enabled us to study the effect of the different hetero atoms and the different steric demands of the N,C-chelates on the photochemical stability and photoisomerization rates compared to the phenylpyridine-based compounds.

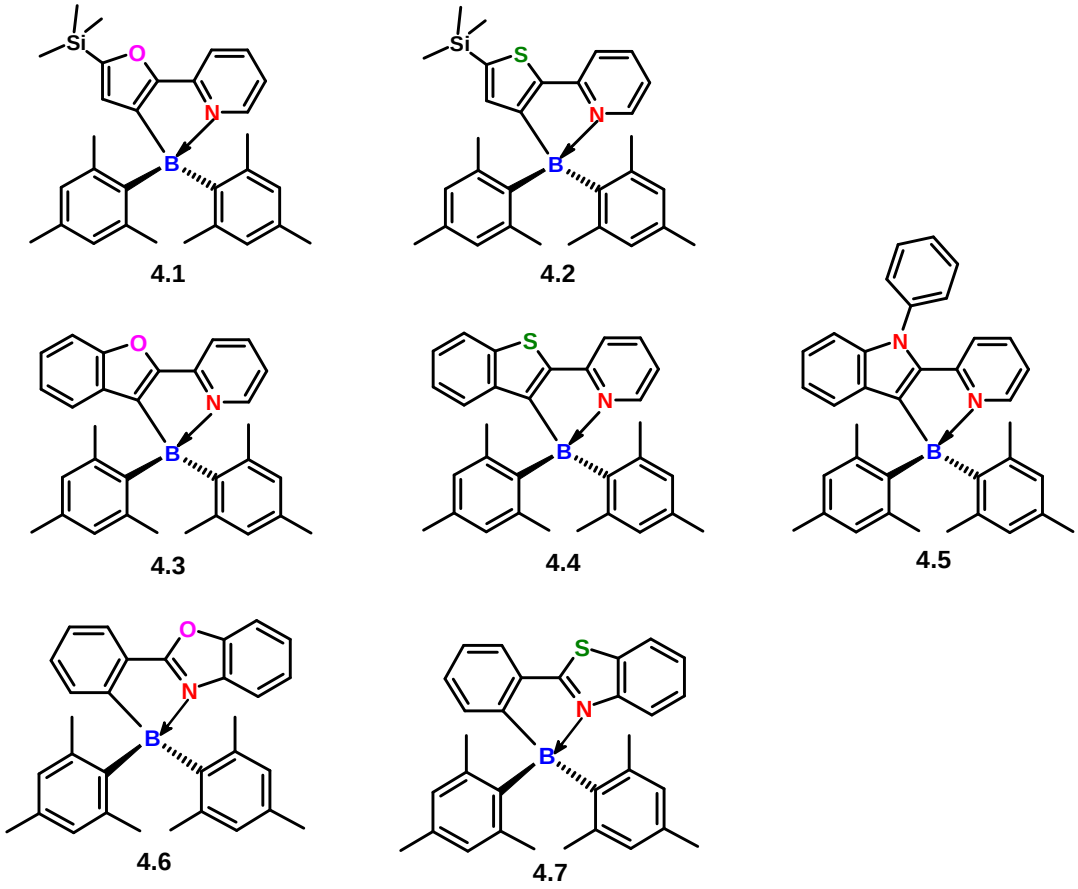

Figure 4.1 Structure of heterocycle-based N,C-chelate organoboron compounds **4.1**-**4.7**

4.2 Experimental

4.2.1 General

Starting materials were purchased from Aldrich Chemical Co. and were used without further purification. Solvents were dried using activated alumina column system, PURE SOLV, purchased from Innovative Technology Inc., while C_6D_6 was dried over CaH_2 in a glove box. All reactions were carried out under an atmosphere of dry nitrogen using standard Schlenk techniques. Purifications using column chromatography were

performed using ultra pure silica gel (70-230 Mesh) 60 Å, purchased from Silicycle. NMR spectra (^{1}H,^{13}C, and ^{11}B) were recorded at room temperature on a Bruker Avance 400 or 500 MHz. Proton and ^{13}C chemical shifts were reported with respect to solvent peaks as internal standard, while $BF_3.Et_2O$ was used as reference for ^{11}B NMR. Coupling constants (*J*) were recorded in Hertz (Hz). Excitation and emission spectra were recorded on a Photon Technologies International QuantaMaster Model C-60 spectrometer. UV-Vis spectra were recorded on a Cary 50 spectrometer. Elemental analyses were performed by Canadian Microanalytical Services, Delta, BC and Elemental Analysis Service at the University of Montreal. High resolution mass spectra (HRMS) were obtained using a Waters/Micromass GC-TOF spectrometer (EI mode). 2-Bromopyridine, 2-bromophenylboronic acid, 2-(2-thienyl)pyridine, 2-chlorobenzoxazole, and 2-chlorobenzothiazole were purchased from Aldrich; benzofuran-2-ylboronic acid and benzothiophen-2-ylboronic acid were purchased from Boron Molecular company; 2-(2-furyl)pyridine[2], 2-(5-(trimethylsilyl)furan-2-yl)pyridine (**4.1L**)[3], 2-(5-(trimethylsilyl)thiophen-2-yl)pyridine (**4.2L**)[3], 2-(Benzofuran-2-yl)pyridine (**4.3L**)[4], 2-(benzothiophen-2-yl)pyridine (**4.4L**)[5], 1-phenyl-2-(pyridin-2-yl)indole (**4.5L**)[6], 2-(2-bromophenyl)benzoxazole (**4.6L**)[7], and 2-(2-bromophenyl)benzothiazole (**4.7L**)[7] were prepared based on literature procedures.

4.2.2 Synthesis and Characterization of Compounds 4.1-4.7

Compounds **4.1**-**4.7** were prepared according to the following general procedure:

n-BuLi (1 eq., 1.6 M in hexane) was added slowly to a solution of the heterocyclic chelate ligands (1 eq.) in THF at -78 °C and the resulting solution was stirred for about 1 hour at -78 °C. Then, $BMes_2F$ (1 eq.) was added under a stream of nitrogen and the solution was stirred at the same temperature for about 2 hours and then stirred overnight at ambient temperature. Then, solvents were removed under reduced pressure and the resulting solid was dissolved in 50 mL of CH_2Cl_2 and quenched with 10 mL of H_2O. The organic layer was separated and dried over $MgSO_4$ and filtered. After CH_2Cl_2 was removed under reduced pressure, the residue was purified over silica gel by flash column chromatography using a CH_2Cl_2/hexanes mixture to afford the pure product. Preparation, workup, and purification of **4.1**, **4.2**, **4.6**, and **4.7** were done in the absence of ambient light by wrapping the flasks and columns with aluminum foil.

4.2.3 Synthesis and Characterization of 2-(3-(dimesitylboryl)-5-(trimethylsilyl)furan -2-yl)pyridine (4.1)

2-(5-(Trimethylsilyl)furan-2-yl)pyridine (**4.1L**) (0.3 g, 1.38 mmol) in THF (40 mL), n-BuLi (0.88 mL, 1.4 mmol), and $BMes_2F$ (0.42 g, 1.4 mmol) were treated according to the general procedure and purified by chromatography (CH_2Cl_2:hexanes = 1:4) to give a yellow powder, which was crystallized from CH_2Cl_2/hexanes to give yellow crystals of **4.1** (0.31 g, 48%). HREI-MS $(M)^+$: m/z Calcd for $C_{30}H_{36}BNOSi$, 465.2659. Found: 465.2672. Anal. Calcd for $C_{30}H_{36}BNOSi$: C, 77.40; H, 7.79; N, 3.01. Found: C, 76.52; H,

8.35; N, 2.83. ^{1}H NMR (CD_2Cl_2, 25 °C, δ, ppm): 8.41 (d, 1H, ^{3}J = 4.8 Hz), 7.91 (t, 1H, ^{3}J = 7.6 Hz), 7.60 (d, 1H, ^{3}J = 8.0 Hz), 7.02 (t, 1H, ^{3}J = 6.6 Hz), 6.82 (s, 1H), 6.65 (s, 4H), 2.19 (s, 6H), 1.84 (s, 12H), 0.33 (s, 9H). ^{13}C NMR (CD_2Cl_2, 25 °C, δ, ppm): 168.4, 155.2, 149.4, 147.4, 141.4, 140.6, 134.2, 129.8, 123.9, 118.6, 115.0, 24.3, 20.7, -1.6. ^{11}B NMR (CD_2Cl_2, 25 °C, δ, ppm): 6.44.

4.2.3.1 Synthesis and Characterization of 2-(3-(dimesitylboryl)-5-(trimethylsilyl)thiophen-2-yl)pyridine (4.2)

2-(5-(Trimethylsilyl)furan-2-yl)pyridine (**4.2L**) (1.4 g, 6.0 mmol) in THF (50 mL), n-BuLi (6.0 mL, 3.8 mmol), and $BMes_2F$ (1.8 g, 6.0 mmol) were treated according to the general procedure and purified by chromatography (CH_2Cl_2:hexanes = 1:4) to give a yellow powder, which was crystallized from CH_2Cl_2/hexanes to give yellow crystals of **4.2** (1.35 g, 47%). HREI-MS $(M)^+$: m/z Calcd for $C_{30}H_{36}BNSSi$, 481.2431. Found: 481.2445. Anal. Calcd for $C_{30}H_{36}BNSSi$: C, 74.82; H, 7.53; N, 2.91. Found: C, 74.71; H, 7.75; N, 2.88. ^{1}H NMR (CD_2Cl_2, 25 °C, δ, ppm): 8.47 (d, 1H, ^{3}J = 6.0 Hz), 7.92 (t, 1H, ^{3}J = 7.5 Hz), 7.62 (d, 1H, ^{3}J = 8.0 Hz), 7.41 (s, 1H), 7.10 (t, 1H, ^{3}J = 6.5 Hz), 6.69 (s, 4H), 2.25 (s, 6H), 1.85 (s, 12H), 0.39 (s, 9H). ^{13}C NMR (CD_2Cl_2, 25 °C, δ, ppm): 155.3, 149.9, 146.7, 141.2, 140.5, 139.2, 136.8, 134.2, 129.9, 119.3, 117.6, 24.4, 20.7, -0.04. ^{11}B NMR (CD_2Cl_2, 25 °C,δ, ppm): 6.51.

4.2.3.2 Synthesis and Characterization of 2-(3-(dimesitylboryl)benzofuran-2-yl)pyridine (4.3)

2-(Benzofuran-2-yl)pyridine (**4.3L**) (0.4 g, 2.0 mmol) in THF (50 mL), n-BuLi (1.25 mL, 2.0 mmol), and $BMes_2F$ (0.6 g, 2.0 mmol) were treated according to the general procedure and purified by chromatography (CH_2Cl_2:hexanes = 1:2) to give a yellow powder, which was crystallized from CH_2Cl_2/hexanes to give yellow crystals of **4.3** (0.58 g, 66%). HREI-MS $(M)^+$: m/z Calcd for $C_{31}H_{30}BNO$, 443.2420. Found: 443.2436. Anal. Calcd for $C_{31}H_{30}BNO$: C, 83.97; H, 6.82; N, 3.16. Found: C, 81.72; H, 7.31; N, 2.88. ^1H NMR (CD_2Cl_2, 25 °C, δ, ppm): 8.57 (d, 1H, ^3J = 5.6 Hz), 8.00 (t, 1H, ^3J = 7.7 Hz), 7.79-7.77 (m, 2H), 7.56 (d, 1H, ^3J = 8.4 Hz), 7.35 (t, 1H, ^3J = 7.6 Hz), 7.24-7.15 (m, 2H), 6.68 (s, 4H), 2.19 (s, 6H), 1.92 (s, 12H). ^{13}C NMR (CD_2Cl_2, 25 °C, δ, ppm): 160.5, 151.9, 149.9, 147.3, 141.3, 140.1, 134.5, 130.3, 130.0, 126.2, 124.2, 123.5, 120.1, 116.2, 112.2, 24.7, 20.7. ^{11}B NMR (CD_2Cl_2, 25 °C, δ, ppm): 7.93.

4.2.3.3 Synthesis and Characterization of 2-(3-(dimesitylboryl)benzothiophen-2-yl)pyridine (4.4)

2-(Benzothiophen-2-yl)pyridine (**4.4L**) (0.42 g, 2.0 mmol) in THF (50 mL), n-BuLi (1.25 mL, 2.0 mmol), and $BMes_2F$ (0.6 g, 2.0 mmol) were treated according to the general procedure and purified by chromatography (CH_2Cl_2:hexanes = 1:2) to give a yellow powder, which was crystallized from CH_2Cl_2/hexanes to give yellow crystals of **4.4** (0.56 g, 61%). HREI-MS $(M)^+$: m/z Calcd for $C_{31}H_{30}BNS$, 459.2192. Found: 459.2198. Anal. Calcd for $C_{31}H_{30}BNS$: C, 81.04; H, 6.58; N, 3.05. Found: C, 81.68; H, 6.81; N, 2.99. ^1H NMR (CD_2Cl_2, 25 °C, δ, ppm): 8.65 (d, 1H, ^3J = 5.6 Hz), 8.04 (d, 1H, ^3J = 7.6 Hz), 7.98-

7.89 (m, 2H), 7.66 (d, 1H, ^3J = 8.0 Hz), 7.35-7.27 (m, 2H), 7.18 (t, 1H, ^3J = 6.6 Hz), 6.68 (s, 4H), 2.18 (s, 6H), 1.90 (s, 12H). ^{13}C NMR (CD_2Cl_2, 25 °C, δ, ppm): 155.6, 146.1, 146.0, 141.4, 141.2, 140.3 134.5, 134.1, 130.4, 126.9, 126.2, 125.8, 125.4, 125.0, 123.8, 120.4, 118.5, 24.9, 20.7. ^{11}B NMR (CD_2Cl_2, 25 °C, δ, ppm): δ 7.96.

4.2.3.4 Synthesis and Characterization of 3-(dimesitylboryl)-1-phenyl-2-(pyridin-2-yl)-indole (4.5)

1-Phenyl-2-(pyridin-2-yl)-indole (**4.5L**) (0.54 g, 2.0 mmol) in THF (50 mL), n-BuLi (1.25 mL, 2.0 mmol), $BMes_2F$ (0.6 g, 2.0 mmol) were treated according to the general procedure and purified by chromatography (CH_2Cl_2:hexanes = 1:1) to give a yellow powder, which was crystallized from THF/hexanes to give bright yellow crystals of **4.5** (0.40 g, 39%). HREI-MS $(M)^+$: m/z Calcd for $C_{37}H_{35}BN_2$, 518.2893. Found: 518.2901. Anal. Calcd for $C_{37}H_{35}BN_2$: C, 85.71; H, 6.80; N, 5.40. Found: C, 85.58; H, 6.62; N, 5.29. ^{1}H NMR (CD_2Cl_2, 25 °C, δ, ppm): 8.54 (d, 1H, ^3J = 6.0 Hz), 7.82 (d, 1H, ^3J = 8.0 Hz), 7.65-7.61 (m, 3H), 7.57-7.54 (m, 1H), 7.48-7.47 (m, 2H), 7.18-7.17 (m, 2H), 7.05-7.02 (m, 1H), 7.00-6.97 (m, 1H), 6.83 (d, 1H, ^3J = 8.0 Hz), 6.66 (s, 4H), 2.16 (s, 6H), 1.94 (s, 12H). ^{13}C NMR (CD_2Cl_2, 25 °C, δ, ppm): 151.8, 147.2, 145.6, 140.4, 140.2, 138.2, 136.5, 134.1, 130.1, 129.1, 128.5, 128.2, 124.8, 124.4, 120.7, 119.0, 117.1, 111.1, 25.0, 20.7. ^{11}B NMR (C_6D_6, 25 °C, δ, ppm): 8.34.

4.2.3.5 Synthesis and Characterization of 2-(2-(dimesitylboryl)phenyl)benzooxazole (4.6)

2-(2-Bromophenyl)benzoxazole (**4.6L**) (1.15 g, 4.19 mmol) in THF (50 mL), n-BuLi (2.63 mL, 4.2 mmol), $BMes_2F$ (1.26 g, 4.2 mmol) were treated according to the general

procedure and purified by chromatography (CH_2Cl_2:hexanes = 1:4) to give a white powder of **4.6** (0.68 g, 41%). HREI-MS $(M)^+$: m/z Calcd for $C_{31}H_{30}BNO$, 443.2420. Found: 443.2432. Anal. Calcd for $C_{31}H_{30}BNO$: C, 83.97; H, 6.82; N, 3.16. Found: C, 83.45; H, 7.06; N, 3.09. ^{1}H NMR (CD_2Cl_2, 25 °C, δ, ppm): 7.99 (d, 1H, ^3J = 7.0 Hz), 7.85 (d, 1H, ^3J = 7.5 Hz), 7.76 (d, 1H, ^3J = 8.0 Hz), 7.65 (d, 1H, ^3J = 7.5 Hz), 7.50-7.37 (m, 4H), 6.69 (s, 4H), 2.19 (s, 6H), 1.91 (s, 12H). ^{13}C NMR (CD_2Cl_2, 25 °C, δ, ppm): 169.8, 153.2, 134.6, 134.4, 133.4, 131.8, 130.1, 127.1, 126.3, 126.2, 124.1, 123.2, 117.2, 112.8, 111.3, 25.4, 20.8. ^{11}B NMR (CD_2Cl_2, 25 °C, δ, ppm): 3.43.

4.2.3.6 Synthesis and Characterization of 2-(2-(dimesitylboryl)phenyl)benzothiazole (4.7)

2-(2-Bromophenyl)benzothiazole (**4.7L**) (1.45 g, 5.0 mmol) in THF (50 mL), n-BuLi (3.2 mL, 5.0 mmol), and $BMes_2F$ (1.5 g, 5.0 mmol) were treated according to the general procedure and purified by chromatography (CH_2Cl_2:hexanes = 1:4) to give a yellow powder of **4.7** (1.4 g, 61%). HREI-MS $(M)^+$: m/z Calcd for $C_{31}H_{30}BNS$, 459.2192. Found: 459.2209. Anal. Calcd for $C_{31}H_{30}BNS$: C, 81.04; H, 6.58; N, 3.05. Found: C, 80.75; H, 6.69; N, 3.02. ^{1}H NMR (CD_2Cl_2, 25 °C, δ, ppm): 7.97-7.92 (m, 2H), 7.88 (t, 2H, ^3J = 7.5 Hz), 7.49-7.40 (m, 3H), 7.33 (t, 1H, ^3J = 7.5 Hz), 6.69 (s, 4H), 2.20 (s, 6H), 1.89 (s, 12H). ^{13}C NMR (CD_2Cl_2, 25 °C, δ, ppm): 175.5, 145.7, 134.5, 133.4, 132.7, 132.4, 130.5, 130.3, 128.5, 126.2, 126.0, 124.2, 124.0, 120.2, 25.0, 20.8. ^{11}B NMR (CD_2Cl_2, 25 °C, δ, ppm): 4.48.

4.2.4 Fluorescence Quantum Yield Measurements

Fluorescence quantum yields of dilute degassed toluene solutions (Abs. = ~0.1) were measured at room temperature using the relative quantum yield method using 9,10-diphenylanthracene as the reference standard ($\Phi_F = 0.90$).[8]

4.2.5 General Procedure Used for Monitoring Photolysis Process via ^{1}H NMR

Samples were dissolved in dry C_6D_6 in an NMR tube under inert atmosphere. To remove any traces of oxygen that might be present in the NMR tube, three freeze/pump/thaw cycles were performed using liquid N_2. The photolysis was performed using either a Rayonet photochemical reactor with irradiation at 350 nm or a UVP UVGL-25 compact hand-held UV lamp at 365 nm at room temperature, followed by recording the ^{1}H NMR spectra after different time periods.

4.2.6 General Procedure Used for Monitoring Photolysis Process via UV-Vis Spectroscopy

Samples were dissolved in dry degassed toluene in a quartz cuvette (~10^{-5} M), under inert atmosphere in a glove box. After wrapping the cuvette with aluminum foil, it was transferred out and photolysis was then performed using a UVP UVGL-25 compact UV lamp (365 nm) at room temperature. The UV-Vis spectra were recorded after each exposure time and the exposure times were added up.

4.2.7 Density Functional Theory Calculations

Gaussian 03 program was used for all theoretical calculations, which were carried out at the B3LYP level of theory with 6-311G* as the basis set.[9] For compounds with available

X-ray structures, geometric parameters were used as starting points for the geometry optimizations, while *GaussView* software package was used for obtaining geometric parameters of compounds that do not have X-ray structural data.

4.2.8 Photoisomerization Quantum Yield Measurements

All work was done under dark light conditions and freshly prepared and mixed solutions were used in all experiments. Phenanthroline and $K_3[Fe(C_2O_4)_3].3H_2O$ are light sensitive and were kept in the dark at all times. The quantum yield of the photoisomerization of (**4.1→4.1a**), (**4.2→4.2a**), (**4.5→4.5a**), (**4.6→4.6a**), and (**4.7→4.7a**) were determined using potassium ferrioxalate $K_3[Fe(C_2O_4)_3].3H_2O$ actinometry based on Hatchard-Parker method[10]. The absorbance of the Fe(II)-1,10-phenanthroline complex was measured at 510 nm in a buffered acidic solution, while the absorbance of **4.1a** (566 nm), **4.2a** (568 nm), **4.5a** (606 nm), **4.6a** (600 nm), and **4.7a** (650 nm), were measured in degassed toluene. The absorbance was measured using an Ocean Optics fiber optic spectrophotometer connected to a Quantum Northwest four-way temperature-controlled cuvette holder via 400 μm fiber optic. The irradiation source was a Photon Technologies International 200 W Hg/Xe lamp with a monochromator.

4.2.9 X-ray Crystallography

Single-crystals of compounds **4.1**-**4.5** were obtained as described above, while single-crystals of **4.5a** (the dark isomer of **4.5**) were obtained (by Dr. Chul Baik) from a hexane solution at -50 °C. Crystals were mounted on glass fiber and data collection was done using a Siemens P4 single-crystal X-ray diffractometer, equipped with a Smart CCD-

1000 detector and graphite-monochromated Mo Kα radiation operating at 50 kV and 35 mA. Data were processed on a PC using Bruker SHELXTL software package[11].

Crystals of **4.5a** were obtained by photoisomerization of **4.5** (5 mg) in degassed hexanes (50 mL) in a Schlenk flask. To exclude any traces of oxygen, 3 freeze/pump/thaw cycles were performed using liquid N_2. Then, the flask was irradiated at 365 nm in a UV reactor at ambient temperature for 2 days. The solubility of compound **4.5** in hexanes is poor and the solution displays very bright yellow emission. With continuous irradiation the emission color and the precipitate disappeared. The volume of the dark turquoise-green solution was reduced to about 10 mL in *vacuo* and left standing at -50°C for about a month, after which dark turquoise-green crystals were formed and isolated from this solution. The dark crystals of **4.5a** are very soluble in hexanes, paraffin oil, and grease at room temperature, hence, the solution was immediately decanted after removing the flask from the freezer to prevent the crystals from re-dissolving. A single crystal was then quickly covered by epoxy glue to prevent decomposition in air during mounting of the crystal.

Table 4.1 Crystallographic data of compounds **4.1**-**4.5** and **4.5a**

	4.1	**4.2**	**4.3**
formula	$C_{30}H_{36}BNOSi$	$C_{30}H_{36}BNSSi$	$C_{31}H_{30}BNO$
Fw	465.50	481.56	443.37
space group	C2/c	Pn	P2(1)/c
a/Å	38.5770(14)	8.2220(3)	7.6702(14)
b/Å	7.9170(3)	9.0601(3)	17.780(3)
c/Å	37.8145(15)	18.3261(7)	19.155(4)
α, deg	90	90	90
β, deg	97.380(3)	99.563(2)	112.918(13)
γ, deg	90	90	90
V/Å^3	11453.4(8)	1346.18(8)	2406.1(8)
Z	16	2	4
D_c/(g cm^{-3})	1.080	1.188	1.224
μ/mm^{-1}	0.103	0.184	0.072
$2\theta_{max}$/deg	54.28	54.22	54.06
reflns measured	25915	8934	12065
reflns used (R_{int})	12559 (0.0820)	5056 (0.0484)	5250 (0.2852)
final R [I > 2σ (I)]	R_1[a] = 0.0733 wR_2[b] = 0.1661	R_1[a] = 0.0534 wR_2[b] = 0.0954	R_1[a] = 0.1009 wR_2[b] = 0.2094
R (all data)	R_1[a] = 0.1599 wR_2[b] = 0.2015	R_1[a] = 0.0937 wR_2[b] = 0.1103	R_1[a] = 0.3037 wR_2[b] = 0.3165
goodness-of-fit on F^2	0.891	0.996	0.931

[a] $R_1 = \Sigma[|F_o| - |F_c|]/\Sigma|F_o|$. [b] $wR_2 = \{\Sigma[w(F_o^2 - F_c^2)]/\Sigma(wF_o^2)\}^{1/2}$.

$\omega = 1/[\sigma^2(F_o^2) + (0.075P)^2]$, where $P = [\max.(F_o^2,0) + 2F_c^2]/3$.

Table 4.1 Crystallographic data of compounds **4.1**-**4.5** and **4.5a** (cont'd)

	4.4	**4.5**	**4.5a**
Formula	$C_{31}H_{30}BNS$	$C_{37}H_{35}BN_2$	$C_{37}H_{35}BN_2$
Fw	459.43	518.48	518.48
space group	P2(1)/c	P2(1)/n	P2(1)/c
a/Å	18.516(6)	7.8712(6)	15.4517(17)
b/Å	7.885(3)	21.2798(14)	13.3461(11)
c/Å	17.269(6)	34.785(3) Å	15.9493(15)
α, deg	90	90	90
β, deg	103.977(6)	94.420(5)	111.807(7)
γ, deg	90	90	90
V/Å^3	2446.7(14)	5809.1(8)	3053.7(5)
Z	4	8	4
D_c/(g cm^{-3})	1.247	1.186	1.128
μ/mm^{-1}	0.153	0.068	0.065
$2\theta_{max}$/deg	54.54	52	50.0
reflns measured	10260	35746	25137
reflns used (R_{int})	5449 (0.1437)	11422 (0.2146)	5366 (0.2517)
final R [I > 2σ (I)]	R_1[a] = 0.0942 wR_2[b] = 0.1232	R_1[a] = 0.0745 wR_2[b] = 0.1336	R_1[a] = 0.1122 wR_2[b] = 0.2367
R (all data)	R_1[a] = 0.2602 wR_2[b] = 0.1721	R_1[a] = 0.2804 wR_2[b] =0.2122	R_1[a] = 0.3241 wR_2[b] = 0.3252
goodness-of-fit on F^2	0.967	0.950	0.879

[a] $R_1 = \Sigma[|F_o| - |F_c|]/\Sigma|F_o|$. [b] $wR_2 = \{\Sigma[w(F_o^2 - F_c^2)]/\Sigma(wF_o^2)\}^{1/2}$.

$\omega = 1/[\sigma^2(F_o^2) + (0.075P)^2]$, where $P = [\max.(F_o^2,0) + 2F_c^2]/3$.

Table 4.2 Selected bond lengths (Å) and angles (°) for compounds **4.1**-**4.5**

	B-N (Å)	B-$C_{chelate}$ (Å)	B-C_{Mes} (Å)	N-B-$C_{chelate}$ (°)	C_{Mes}-B-C_{Mes} (°)
4.1	1.676(4)	1.622(5)	1.633(5) 1.661(5)	94.6(2)	114.6(3)
4.2	1.673(5)	1.633(5)	1.632(5) 1.651(5)	94.9(3)	114.3(3)
4.3	1.668(8)	1.631(9)	1.625(9) 1.649(8)	94.7(4)	113.6(5)
4.4	1.659(6)	1.617(6)	1.632(7) 1.633(7)	94.8(4)	116.2(4)
4.5	1.690(7)	1.609(7)	1.634(7) 1.647(8)	94.6(4)	116.0(4)

4.3 Results and Discussion

4.3.1 Synthesis and Characterization

The heterocyclic organoboron compounds in this chapter can be divided into two groups based on the type of N,C-chelate used: (1) Compounds **4.1**-**4.5** contain a heterocyclic-pyridine group as chelating ring. This group was designed to study the effects imposed by replacing the phenyl group in **2.1** with a heterocyclic ring on the photophysical and photochromic properties on the N,C-chelate organoboron compounds. (2) Compounds **4.6** and **4.7** contain a heterocyclic-phenyl group as chelating ring, namely benzooxazole or benzothiazole. This group was designed to study the effects imposed by replacing the pyridine group in **2.1** with a heterocyclic ring as the source of nitrogen lone pair on the

photophysical and photochromic properties on the N,C-chelate organoboron compounds. These two compounds were synthesized to examine the possible versatility of the photochromic N,C-chelate organoboron compounds.

Compounds **4.1** and **4.2** were prepared according to Figure 4.2. Silylation of position 5 of 2-(2-furyl)pyridine or 2-(2-thienyl)pyridine in THF at -78 °C using LDA afforded the silylated ligands of **4.1L** and **4.2L**, which were purified using column chromatography, yields (44% and 85%) respectively. Compounds **4.1** and **4.2** were prepared via lithiation of the ligands **4.1L** and **4.2L** followed by the addition of $BMes_2F$ with 48% and 47% yields, respectively.

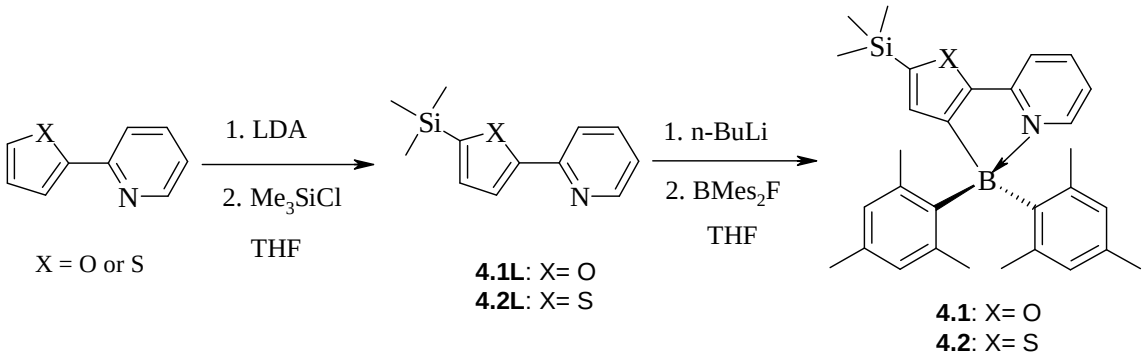

Figure 4.2 Synthesis of compounds **4.1** and **4.2**

Compounds **4.3-4.5** were prepared according to Figure 4.3. Both ligands 2-(benzofuran-2-yl)pyridine **4.3L** and 2-(benzo[b]thiophen-2-yl)pyridine (**4.4L**) were synthesized using a Suzuki-Miyaura coupling protocol of 2-boromopyridine with benzofuran-2-ylboronic acid and benzothiophen-2-ylboronic, respectively. Lithiation of

4.3L, **4.4L**, and **4.5L** followed by addition of $BMes_2F$ produced **4.3**, **4.4**, and **4.5**, in (66, 61, and 39%) yields, respectively.

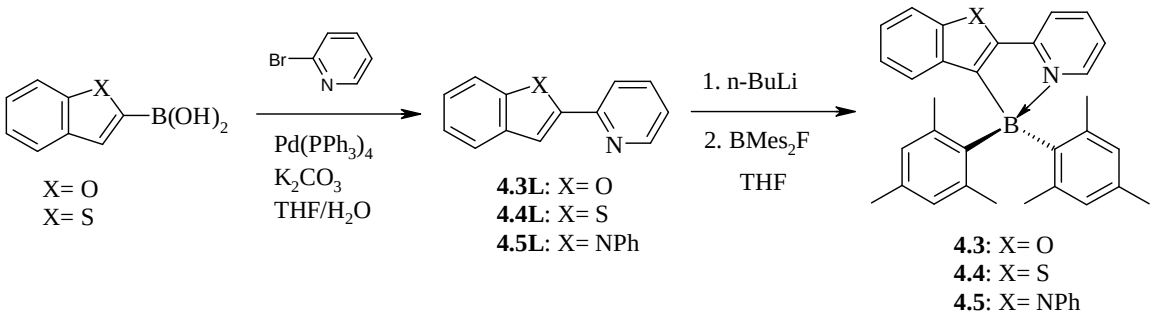

Figure 4.3 Synthesis of compounds **4.3**, **4.4**, and **4.5**

Compounds **4.6** and **4.7** were prepared according to Figure 4.4. Ligands 2-(2-bromophenyl)benzooxazole **4.6L** and 2-(2-bromophenyl)benzothiazole **4.7L** were synthesized using a Suzuki-Miyaura coupling protocol of 2-boromophenylboronic acid with 2-chlorobenzoxazole and 2-chlorobenzothiazole, respectively. Lithiation of **4.6L** and **4.7L** followed by addition of $BMes_2F$ produced **4.6** and **4.7** in (41 and 61%) yields, respectively. All compounds were fully characterized by NMR, HRMS, elemental analysis, and single crystal X-ray diffraction.

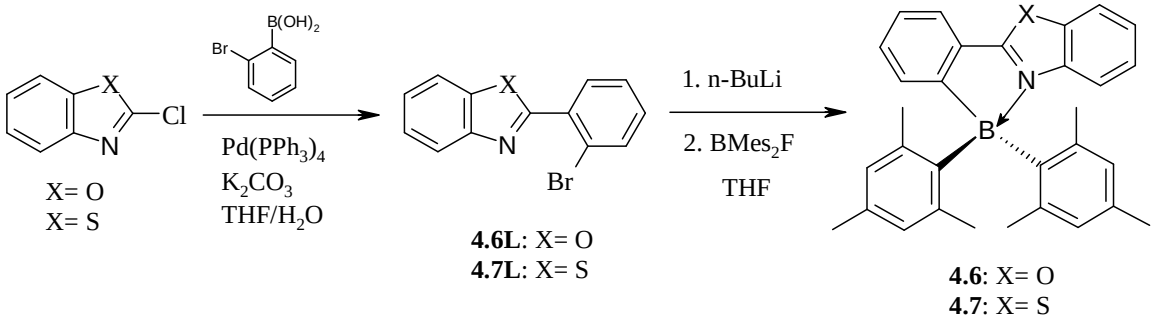

Figure 4.4 Synthesis of compounds **4.6** and **4.7**

4.3.2 Crystal Structures

Crystal structures of compounds **4.1**-**4.5** were determined by single crystal X-ray diffraction as shown in Figure 4.5 - Figure 4.9, respectively. On the other hand, good quality structural data of compounds **4.6** and **4.7** could not be obtained due to disordering of the chelate rings. The important bond angles and bond lengths of **4.1**-**4.5** are shown in Table 4.2. The asymmetric unit of compound **4.5** has two independent molecules which have similar bond lengths and angles except the dihedral angle between the pendant phenyl ring and the indole ring (62.2(4)° vs. 72.7(4)°).

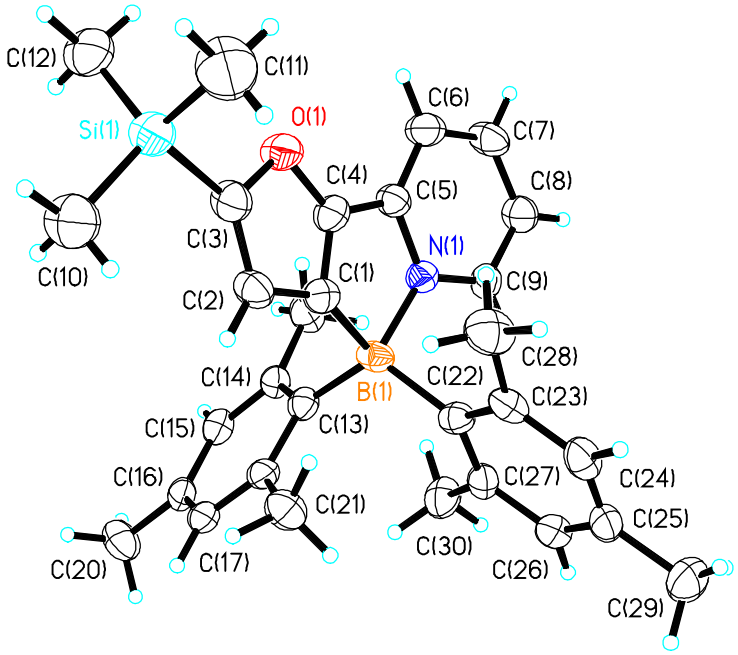

Figure 4.5 Crystal structure of compound **4.1** with 50% thermal ellipsoids

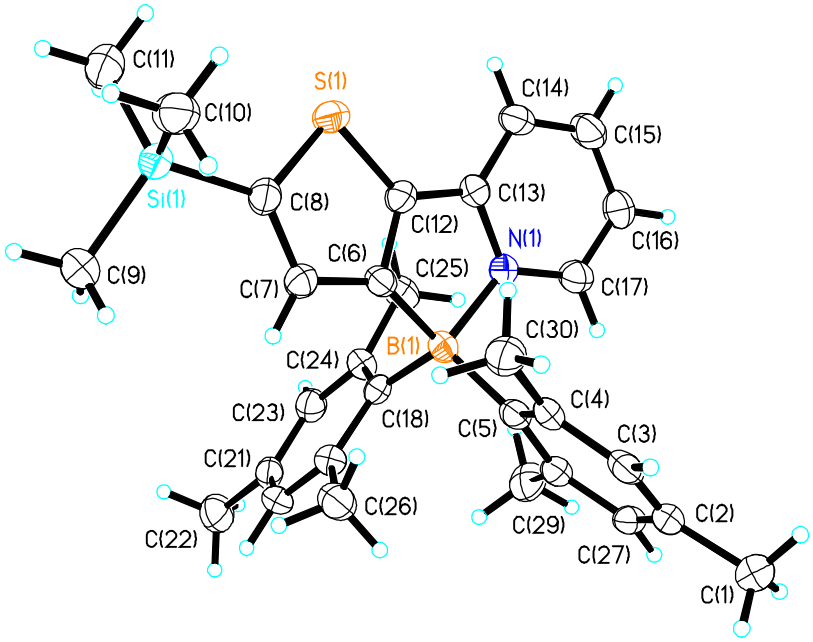

Figure 4.6 Crystal structure of compound **4.2** with 50% thermal ellipsoids

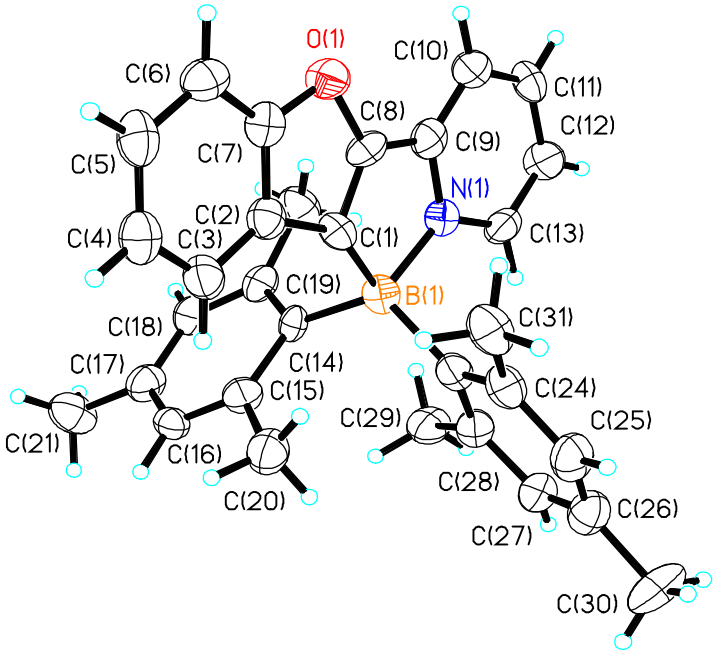

Figure 4.7 Crystal structure of compound **4.3** with 50% thermal ellipsoids

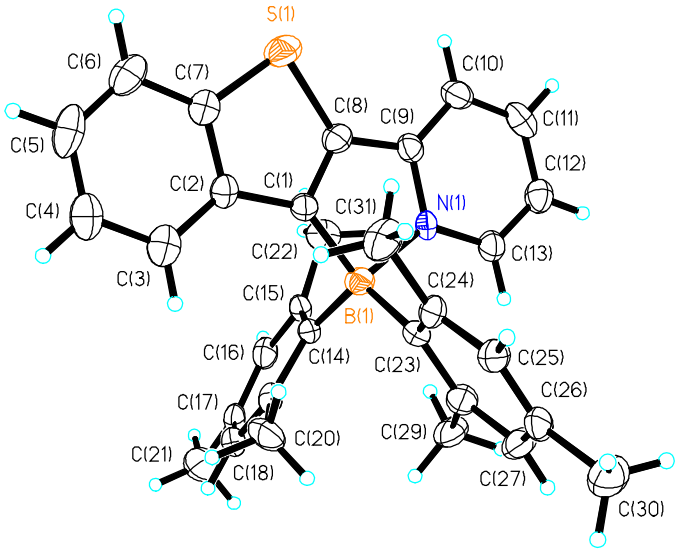

Figure 4.8 Crystal structure of compound **4.4** with 50% thermal ellipsoids

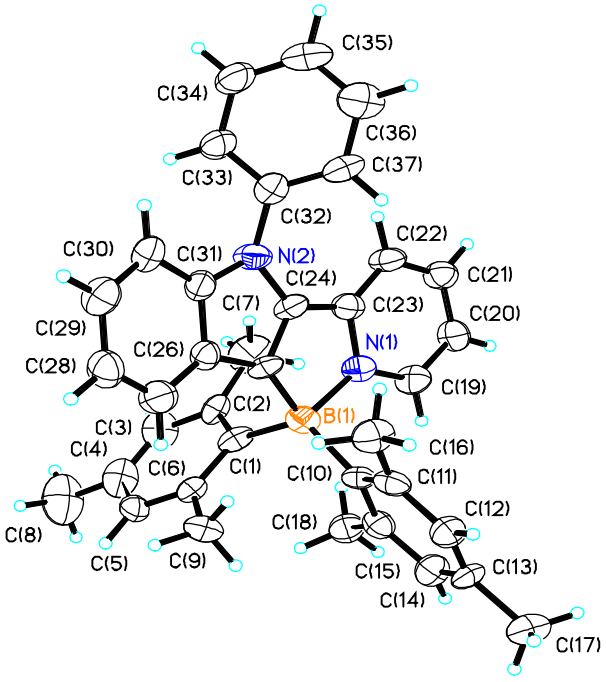

Figure 4.9 Crystal structure of compound **4.5** with 50% thermal ellipsoids

The boron center in compounds **4.1**-**4.5** has a tetrahedral geometry due to the intramolecular N → B coordination, which forces the N,C-chelate back-bone to be co-planar. The N-B-$C_{chelate}$ bond angles of compounds **4.1**-**4.5** are very similar, ranging from 94.6(2)° to 94.9(3)°, while the C_{Mes}-B-C_{Mes} bond angle is ranging from 113.6(5)° to 116.8(3)°. Also, The B-N bond lengths (1.669(6) Å, average), the B-$C_{Chelate}$ bond lengths (1.627(6) Å, average), and the B-C_{Mes} bond lengths (1.642(7) Å, average) are all similar to those of previously reported for sterically congested tetrahedral boron molecules.[12] The five-membered chelate ring (the one containing the boron atom) in all compounds is coplanar with the N,C-chelate rings. Compared to the phenylpyridine based N,C-chelate analogues (**2.1**, **3.1**, **3.3**, **3.4**, and **3.5**) the structures of compound **4.1**-**4.5** have a longer B-N bonds (1.669(1) Å vs. 1.653(6) Å) and similar B-$C_{chelate}$ (1.627(8) Å vs. 1.629(6) Å) and B-C_{Mes} bonds (1.642(5) Å vs. 1.643(8) Å).

The mesityl groups (Mes_1 and Mes_2) in compounds **4.1**-**4.5** are arranged asymmetrically around the boron center with respect to the N,C-chelate ring, where one mesityl group (Mes_1) is closer to the carbon of the N,C-chelate ring, which might be attributed to the steric congestion imposed by the bulky mesityl rings. The Mes_1-$C_{chelate}$ vs. Mes_2-$C_{chelate}$ through-space distances (Figure 4.10) of compounds **4.1**-**4.5** are summarized in Table 4.3. The Mes_1-$C_{chelate}$ distance of compounds **4.1**-**4.5** ranges from 2.559(5) Å to 2.617(5) Å, while the Mes_2-$C_{chelate}$ distance is about 0.3 Å longer and ranges from 2.847(5) Å to 2.901(5) Å.

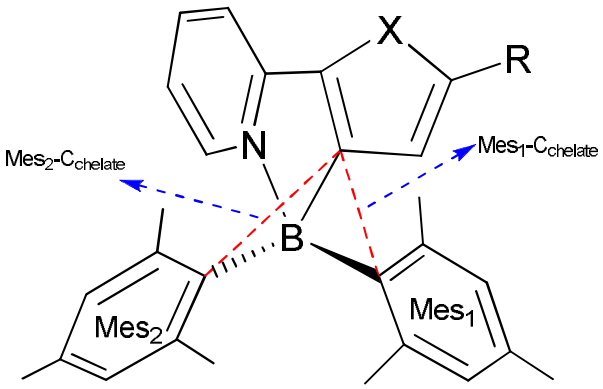

Figure 4.10 Through-space distance: C_{Mes1}-$C_{Chelate}$ vs. C_{Mes2}-$C_{Chelate}$. R = TMS or fused phenyl and X = O, S, or N-Ph.

Table 4.3 Mes_1-$C_{chelate}$ vs. Mes_2-$C_{chelate}$ through-space distances of compounds **4.1**-**4.5**

	Through-space distance (Å) Mes_1-$C_{chelate}$	Through-space distance (Å) Mes_2-$C_{chelate}$
4.1	2.559(5)	2.880(5)
4.2	2.576(5)	2.901(5)
4.3	2.599(5)	2.866(5)
4.4	2.617(5)	2.847(5)
4.5	2.574(5)	2.876(5)

The analysis of the crystal structure packing of **4.1**-**4.5** revealed no significant intermolecular π-π stacking between the aromatic rings, which may be attributed to the presence of the two bulky mesityl groups. Nevertheless, there are partial π-π

intermolecular interactions between the pyridine rings and mesityl rings and between the mesityl rings themselves in compound **4.1**, with the shortest atomic separation distance of 3.95 Å. Also, in compounds **4.2**, **4.3**, and **4.4** there is a similar π-π intermolecular interactions between the pyridine rings and the thiophene, benzofuran, and benzothiophene rings, respectively. The shortest atomic separation distances for these interactions are 4.05 Å, 3.44 Å, and 3.51 Å, respectively; the crystal packing in **4.3** is shown in Figure 4.11. In addition, similar weak π-π intermolecular interactions between the pendant phenyl rings of **4.5** are present with the shortest atomic separation distances of 3.35 Å.

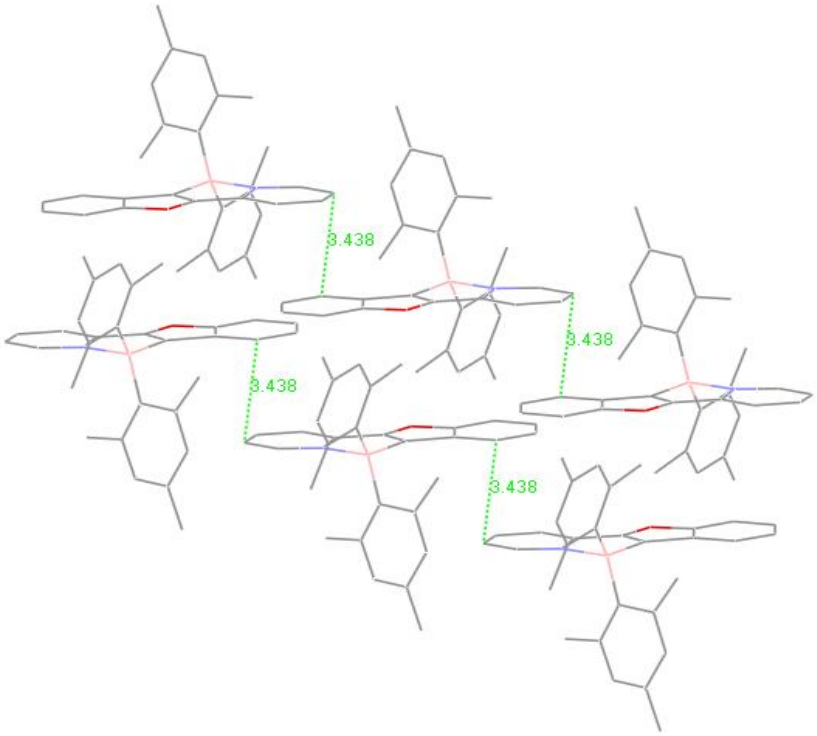

Figure 4.11 π-π intermolecular interactions between the pyridine and benzofuran rings and the shortest atomic separation distances in the crystal lattice of **4.3**.

After many attempts to crystallize the dark isomer of different N,C-chelate compounds, only the dark isomer of compound **4.5** was successfully crystallized. The difficulty in obtaining suitable crystals of the dark isomers is attributed to the following factors: (1) The dark isomers are very soluble in organic solvents both polar and non-polar; (2) Since these photochromic N,C-chelate compounds are of the T-type, they slowly reverse back to the colorless isomer, which in turn starts to precipitate or crystallize out of the solution because they have poor solubility in non-polar solvents. (3) Dark isomers are highly sensitive towards oxygen even in the solid state, which makes their manipulation a very difficult task.

Due to the high thermal stability of the dark isomer of **4.4**, where the thermal reversal process from **4.4a** to **4.4** does not take place unless heating (50°C or higher) is applied, a powder-like micro-crystalline solid was obtained but it was not suitable for single-crystal diffraction study. To enhance the formation of single crystals of the dark isomer, compound **4.5** was prepared, converted to the dark isomer **4.5a**, and successfully crystallized. The dark isomer **4.5a** is similar to **4.4a** in terms of thermal stability. In addition, the extra phenyl group on nitrogen leads to decreased solubility of the dark isomer **4.5a** in hexanes and enhanced the crystal lattice packing.

The crystal structure of **4.5a** is shown in Figure 4.12 and the important bond lengths of **4.5a** are shown in Table 4.1. The B-C and B-N bond lengths of **4.5a** are similar to those of recently reported sterically congested N,C-chelate $BMes_2$ compounds.[12] Compound **4.5** was converted to **4.5a** by suspending **4.5** as powder in degassed hexanes

followed by irradiation of the solution in a UV reactor at 350 nm at room temperature. The yellow solid of **4.5** has poor solubility and bright yellow emission color in hexanes. After, about 2 days of continuous irradiation, the emission color disappeared and there was no solid in the Schlenk flask indicating that **4.5** was converted to **4.5a**, which is soluble in hexanes and doesn't have a considerable emission color. The dark turquoise-green solution was concentrated *in vacuo* and kept at -50°C for about one month, after which dark green-black crystals were obtained and isolated. The crystals were soluble in paraffin oil but they were stable in epoxy glue under air for a few hours, which enabled us to mount a suitable crystal on the diffractometer and collect the diffraction data at 180 K under N_2 successfully.

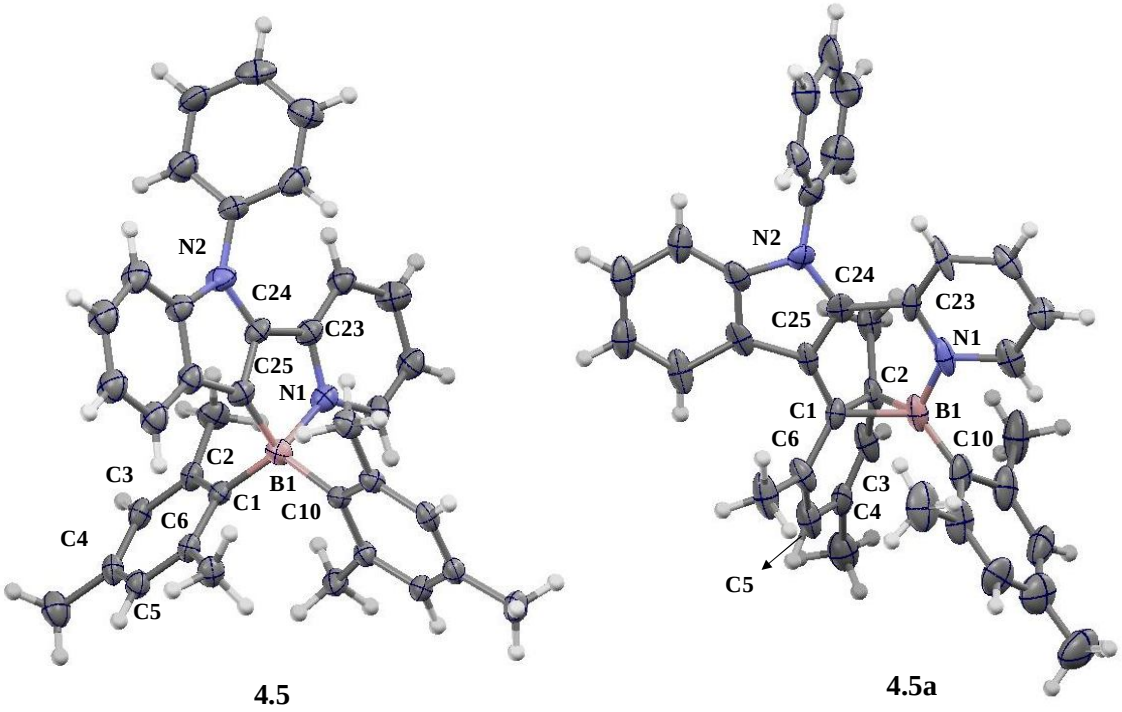

Figure 4.12 Crystal structures of **4.5** and **4.5a** with 30% ellipsoids

The crystal structure of compound **4.5a** proves that the general borabicyclo-[4.1.0]hepta-2,4-diene structure that was proposed in chapter 2 using 2D NMR and computational data was correct. The B(1)-C(1) and B(1)-C(2) bond lengths (1.691(11) Å, 1.644(11) Å), and the C(1)-C(2) bond length of the BCC ring in **4.5a** are very similar to those of **2.1a**, which were obtained using DFT calculations and to those of the BC_2 ring reported by Wilkey and Schuster[13] (Chapter 2).

The C-C bond lengths of the mesityl group, in **4.5**, that was transformed to a cyclohexadiene ring in **4.5a** are summarized in Table 4.4. Within the cyclohexadiene ring, C(1)-C(6) (1.448(10) Å), C(2)-C(3) (1.446(10) Å), and C(4)-C(5) (1.472(11) Å) are longer than C(3)-C(4) (1.312(10) Å) and C(5)-C(6) (1.356(10) Å), which is consistent with the transformation of the mesityl group to a cyclohexadiene group. On the other hand, the C-C bond lengths in the mesityl ring in **4.5** are consistent with a regular aromatic ring with an average C-C bond length of 1.397 Å (Figure 4.12).

Table 4.4 Comparison of C-C bond lengths in the mesityl group affected by photolysis (before (**4.5**) and after (**4.5a**))

	C-C Bond length of **4.5** (Å)	C-C Bond length of **4.5a** (Å)
C(1)-C(6)	1.425(7)	1.448 (10)
C(1)-C(2)	1.411(6)	1.574(7)
C(2)-C(3)	1.391(7)	1.446(10)
C(3)-C(4)	1.394(7)	1.312(10)
C(4)-C(5)	1.374(7)	1.472(11)
C(5)-C(6)	1.391(7)	1.356(10)

In addition, the B(1)-N(1) (1.592(5) Å) and B(1)-C(10) (1.593(5) Å) bonds of **4.5a** are shorter than those of **4.5**, B(1)-N(1) (1.690(7) Å), B(1)-C(10) (1.634(7) Å), which may be attributed to the increased *s* character of the exocyclic bonds of the strained CCB ring, similar to those of cyclopropane rings[14]. Also, the newly formed 6-membered ring composed of B(1), C(1), C(25), C(24), C(23), and N(1) is coplanar with the pyridylindole ring.

Analysis of the crystal structure packing of **4.5a** reveals strong π-π intermolecular interactions between the pyridylindole rings, with the shortest atomic separation distance being 3.40 Å, as shown in Figure 4.13. Also, the N-phenyl ring is oriented towards the

channels in the crystal lattice, which are filled with disordered hexane molecules as shown in Figure 4.14.

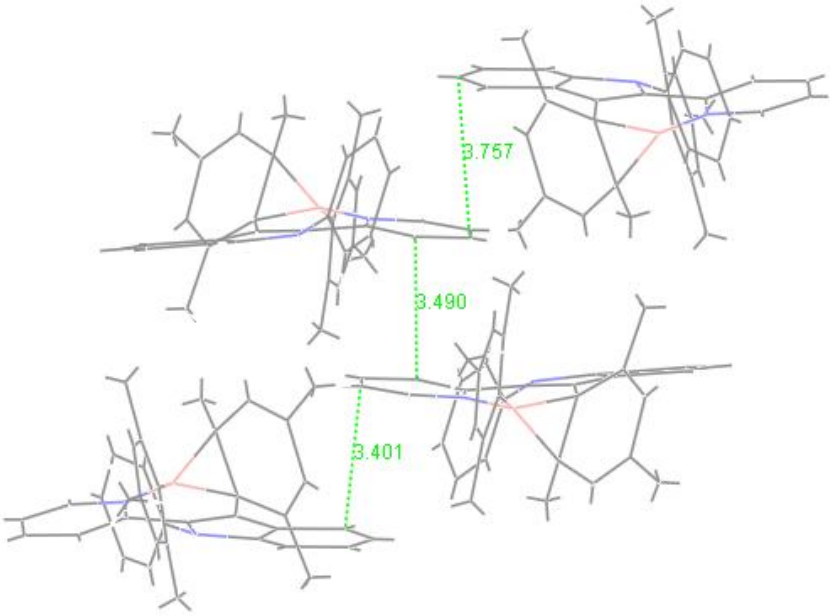

Figure 4.13 π-π intermolecular interactions between the pyridylindole rings and the shortest atomic separation distances in the crystal lattice of **4.5a**.

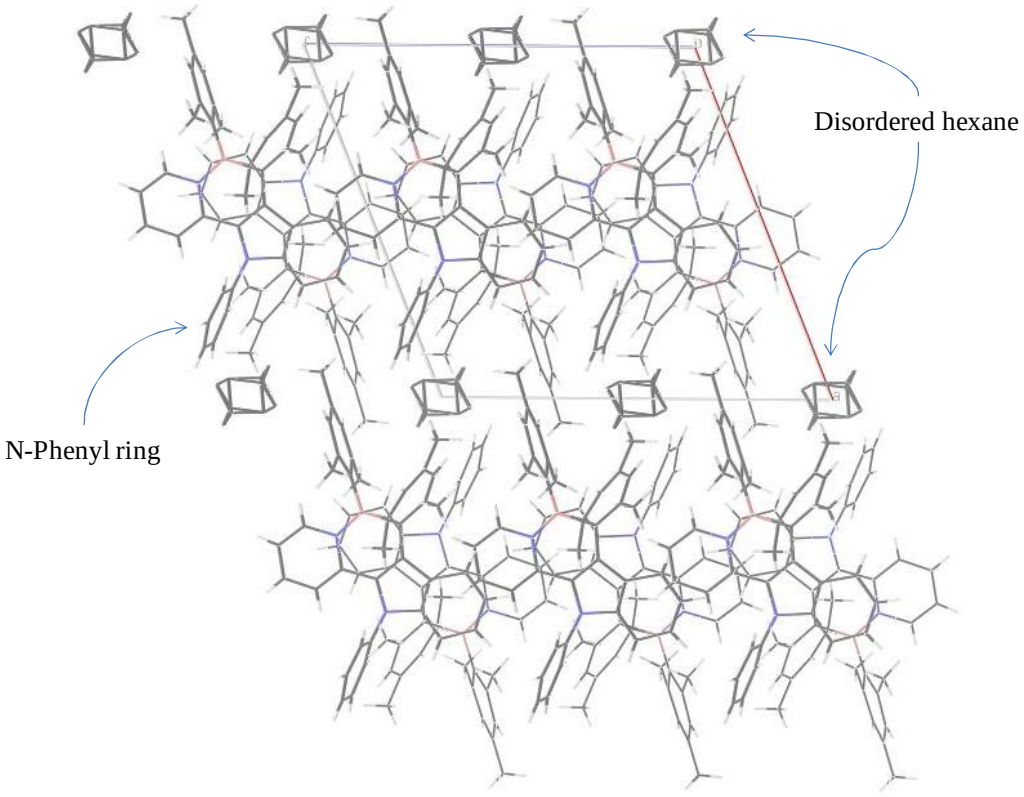

Figure 4.14 Crystal lattice packing diagram of **4.5a** showing the location of the disordered hexane molecules and the N-phenyl group in the lattice: View projected down the *b*-axis

4.3.3 UV-Vis Absorption and Luminescence Properties of 4.1-4.7

The UV-Vis absorption spectra of compounds **4.1**-**4.7** are shown in Figure 4.15 and the λ_{max} of the lowest energy absorption band, the absorption edge (optical energy gap), and the λ_{em} spectra along with fluorescence quantum efficiencies are provided in Table 4.5. All compounds have intense absorption bands in the region 290-400 nm. Compound **4.6**

has no significant absorption in the visible region (400-800 nm), hence it's colorless in solution and in the solid state. On the other hand, compounds **4.1**, **4.2**, **4.3**, **4.4**, **4.5**, and **4.7** have absorption shoulders in the 400-460 nm range; hence they all have a yellow color in both solution and solid states with a distinctively bright color for **4.5**.

Compounds **4.1**-**4.7** have a low energy shoulder band in the 350-480 nm region that can be attributed to a charge transfer transition from one of the mesityl groups to the N,C-chelate, which is supported by DFT and TD-DFT calculations. The HOMO of compounds **4.1**-**4.7** is mainly localized on one of the mesityl legs with variable contribution from the N,C-chelate moieties, while the LUMO is almost entirely composed of the N,C-chelate part.

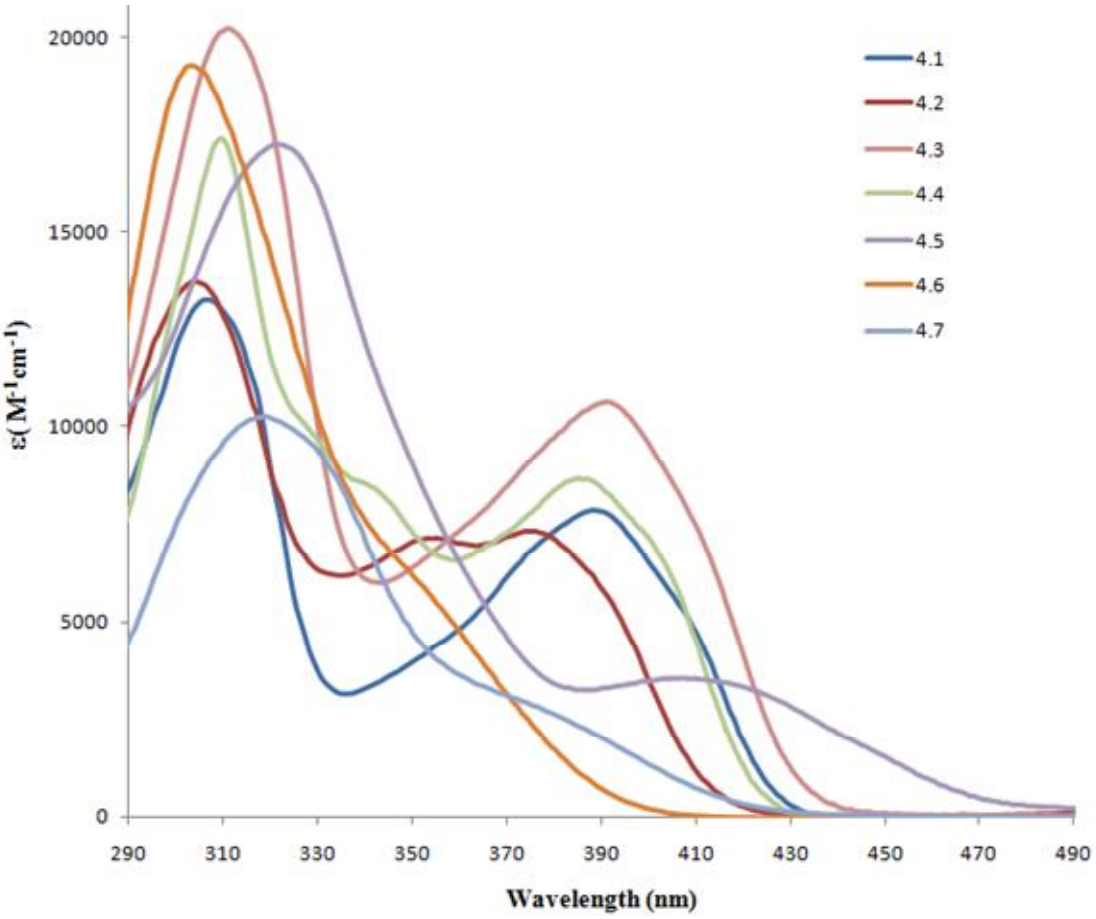

Figure 4.15 Absorption of compounds **4.1-4.7** in toluene (~10^{-5} M)

The optical energy gaps of compounds **4.1-4.7** were estimated using the absorption edge and summarized in Table 4.5. The energy gaps of compounds **4.1-4.7** are very close except for compound **4.5**, which is smaller than all the other compounds, most probably because of the extended conjugation coming from the pendant phenyl group, which is consistent with observed trend in DFT-calculated HOMO-LUMO gaps as shown in Table 4.6.

Table 4.5 Absorption and luminescence data for compounds **4.1-4.7**

Compound	Absorption λ_{max} (nm) (ε, $M^{-1}cm^{-1}$)	λ_{em} (nm)	Optical band gap (eV)	Φ_F in toluene[a]
4.1	388(7900)	450	2.87	0.61
4.2	374(7400)	459	2.95	0.30
4.3	391(11000)	455	2.82	0.72
4.4	386 (8900)	455	2.89	0.30
4.5	403 (3500)	490	2.58	0.32
4.6	355(5500)	460	3.10	0.21
4.7	373(2700)	486	2.95	0.22

[a] Standard reference 9,10-diphenylanthracene (Φ_F = 90%).

Upon irradiation with UV light, all compounds emit a bright blue color except **4.5** and **4.7**, which emit a bright green color, in solution and the solid state with λ_{em} ranging from 450-490 nm, as shown in Figure 4.16. The emission of **4.2** (λ_{em}= 459 nm) is red shifted about 9 nm compared to the oxygen analog **4.1** (λ_{em}= 450 nm), which is similar to the red shift observed for compound **4.7** (λ_{em}= 486 nm) compared to **4.6** (λ_{em}= 460 nm), although it's more pronounced in the latter pair, which can be attributed to smaller energy gaps. The lower emission energy of **4.5** (λ_{em}= 490 nm) compared to **4.3** (λ_{em}= 455 nm) and **4.4** (λ_{em}= 455 nm) can also be attributed to the narrower HOMO-LUMO energy gap in **4.5**.

In toluene, furan-, benzofuran-, and benzoxazole-containing compounds, e.g. **4.1** and **4.3**, are efficient blue emitters with fluorescence quantum yields of 61% and 72%, respectively. In contrast, the thiophene- and benzothiophene-containing compounds, e.g. **4.2** and **4.4**, have relatively lower fluorescence quantum yields (30% and 30% respectively). The lower fluorescence quantum yields of **4.2** and **4.4** can be attributed to the presence the heavy sulfur atom, which can reduce the fluorescence quantum efficiency via the heavy-atom effect e.g. non-radiative decay via intersystem crossing.

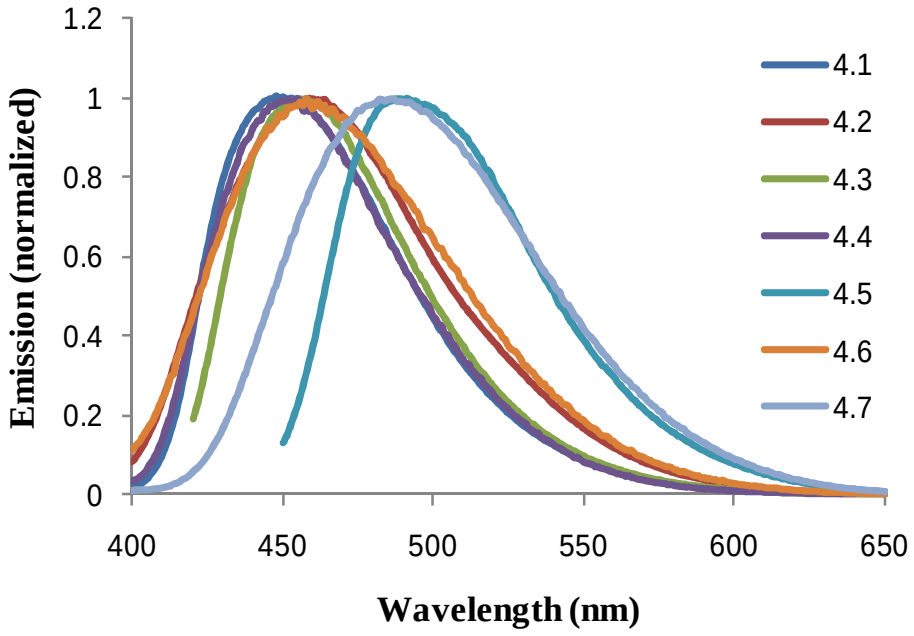

Figure 4.16 Normalized emission of compounds **4.1**-**4.7** in toluene (~10^{-5} M)

4.3.4 DFT Calculations

To further understand the nature of the electronic properties of compounds **4.1**-**4.7**, DFT and TD-DFT calculations were performed on all compounds. The LUMO orbital of all

compounds is mainly dominated by the heterocyclic N,C-chelate ligands π* orbital including the hetero atom with a small contribution from the B-C_{Mes} bonds. The LUMO in compounds **4.1**-**4.5** is more concentrated on the pyridine ring, while the LUMO in **4.6** and **4.7** is evenly distributed over the whole N,C-chelate back-bone. The HOMO of compounds **4.1** and **4.2** is mainly composed of the mesityl group closer to the heterocyclic ring of the heterocyclic-pyridine chelate with contribution from the B-$C_{Chelate}$ bond and small contribution from the furan and thiophene rings as shown in Figure 4.17. Also, the HOMO of compounds **4.3**-**4.5** are similar to those of **4.1** and **4.2** but with larger contribution from the heterocyclic ring, hence they have less charge transfer character than **4.1** and **4.2** (Figure 4.18). In addition, the HOMO of compounds **4.6** and **4.7** is mainly composed of the mesityl group closer to the phenyl ring of the phenyl-heterocyclic chelate with contribution from the B-$C_{Chelate}$ bond and small contribution from the phenyl ring of the N,C-chelate as shown in Figure 4.19

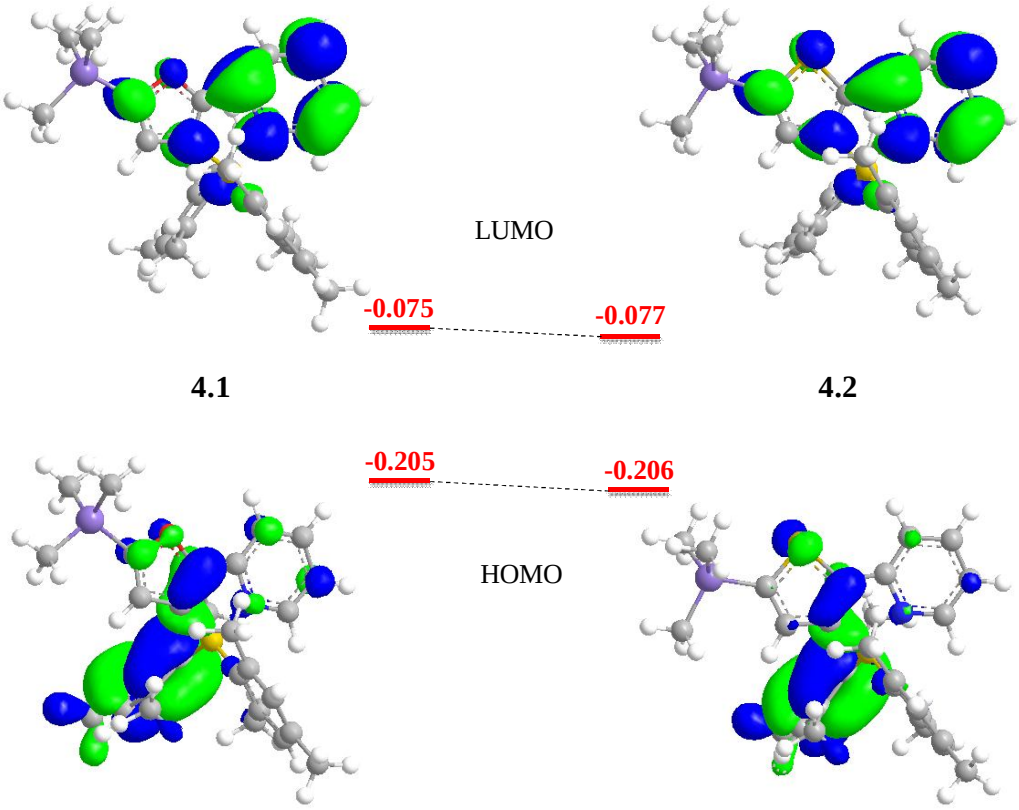

Figure 4.17 HOMO and LUMO diagrams of compounds **4.1** and **4.2** with calculated energy levels shown in Hartree (1 Hartree = 27.2107 eV) and surface isocontour value of 0.03.

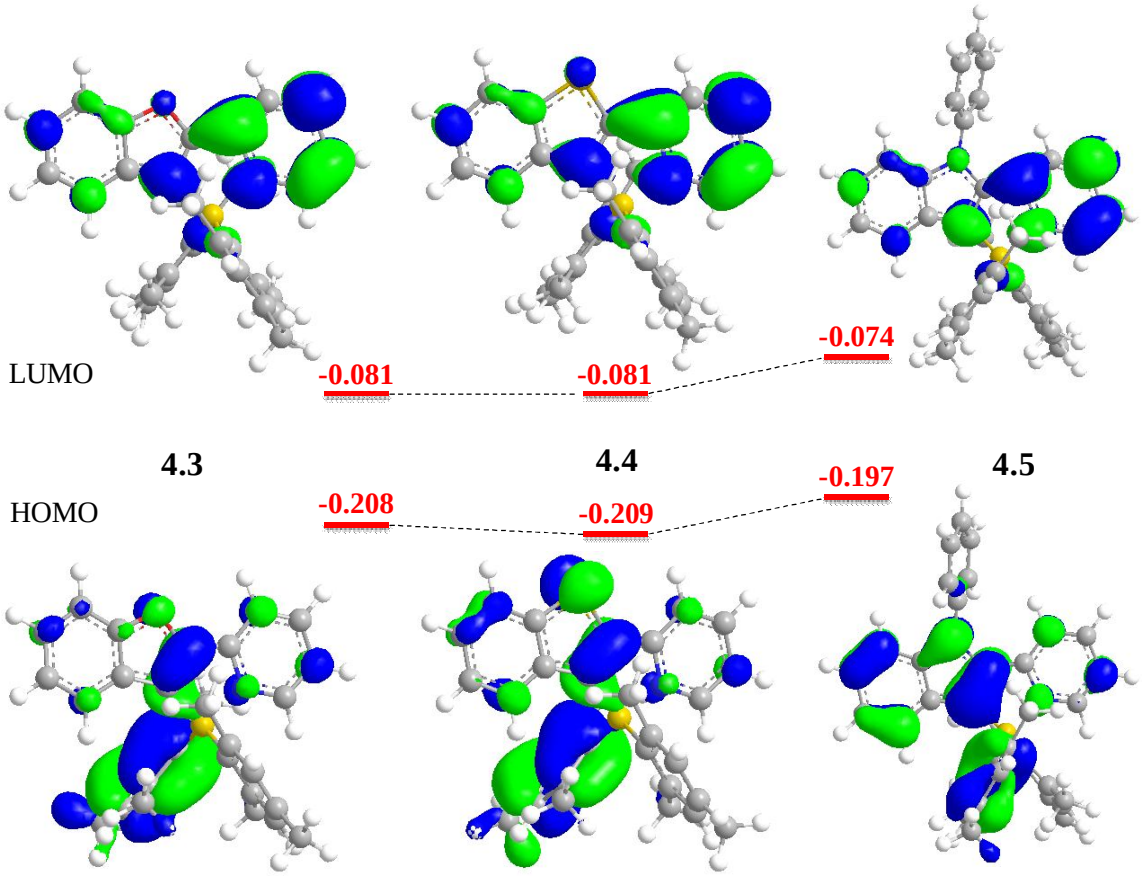

Figure 4.18 HOMO and LUMO diagrams of compounds **4.3**, **4.4**, and **4.5** with calculated energy levels shown in Hartree (1 Hartree = 27.2107 eV) and surface isocontour value of 0.03.

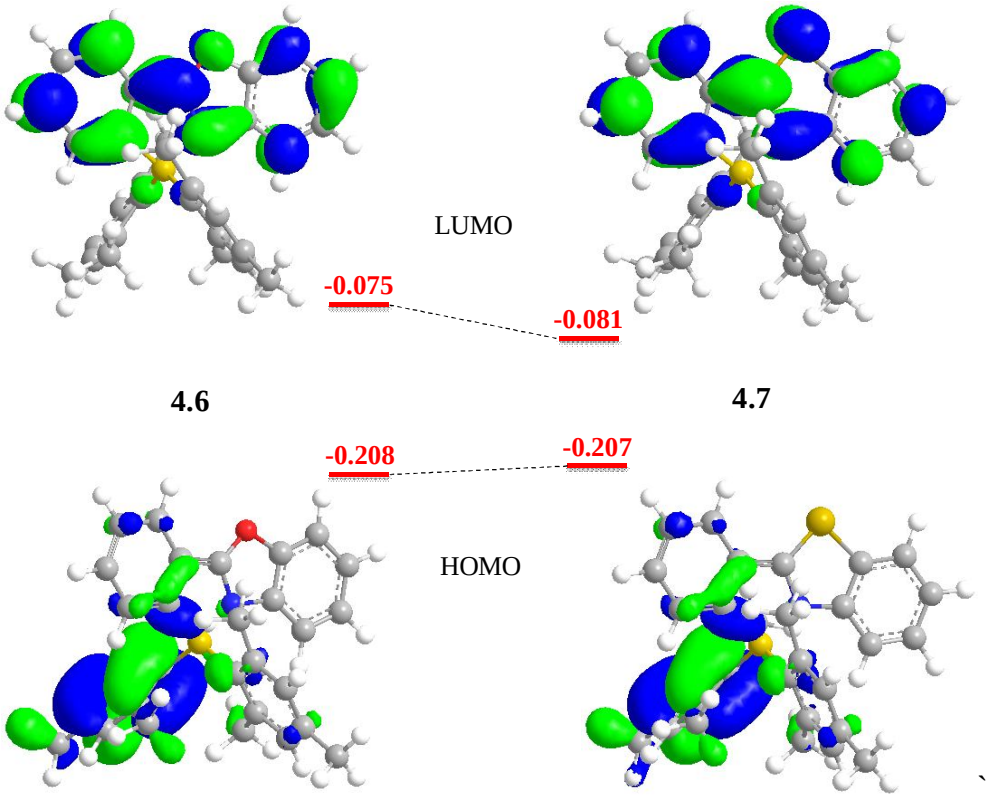

Figure 4.19 HOMO and LUMO diagrams of compounds **4.6** and **4.7** with calculated energy levels shown in Hartree (1 Hartree = 27.2107 eV) and surface isocontour value of 0.03.

DFT and TD-DFT calculations were also performed on the dark isomer **4.5a** using the same basis set used for the other compounds. Compound **4.5a** has similar electronic properties as those of **2.1**., where the HOMO is dominated by the two π bonds of the cyclohexadienyl ring and the 3-memeberd BC_2 ring, while the LUMO is mainly composed of the π* orbital of the N,C-chelate ring as shown in Figure 4.20. The destabilization of the HOMO level resulting from the de-aromatization of the mesityl ring

leads to a smaller HOMO-LUMO gap, which is reflected by the intense low energy absorption band of **4.5a** and the big color change in solution from light yellow (**4.5**) to dark green (**4.5a**). This is also supported by CV data, which shows that the HOMO of **4.5a** is destabilized by about 1 eV compared to **4.5**. This is consistent with all the dark isomers and explains their high reactivity towards oxygen.

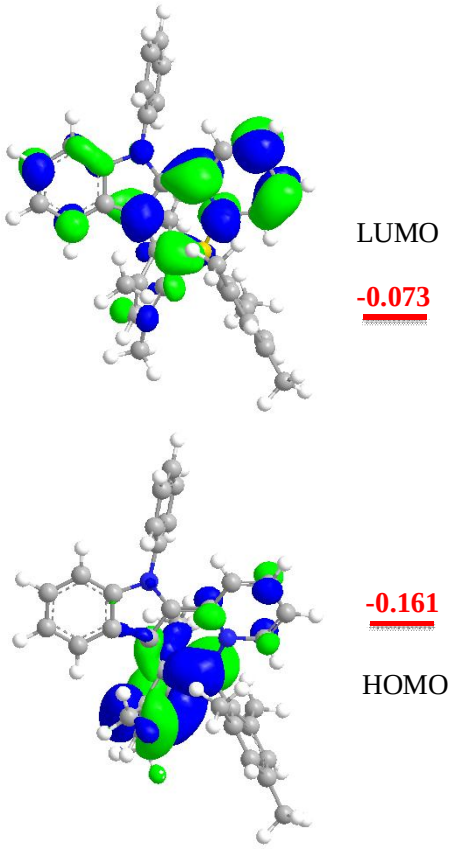

Figure 4.20 HOMO and LUMO diagrams of compound **4.5a** with calculated energy levels shown in Hartree (1 Hartree = 27.2107 eV) and surface isocontour value of 0.03.

The experimental values of the HOMO-LUMO energy gaps, calculated using the optical energy gaps, were compared to those obtained using DFT calculations, Table 4.6. Although the calculated band gap values deviate from those obtained experimentally, the general trends of the HOMO-LUMO band gaps obtained from both methods are consistent.

Table 4.6 DFT-calculated and experimental HOMO-LUMO energy gaps

Compound	MO data			Experimental data
	HOMO (eV)	LUMO (eV)	ΔE_{Calc} (eV)	$\Delta E_{Optical}$ (eV)
4.1	-5.58	-2.05	3.54	2.87
4.2	-5.61	-2.11	3.50	2.95
4.3	-5.66	-2.19	3.47	2.82
4.4	-5.70	-2.19	3.51	2.89
4.5	-5.35	-2.00	3.35	2.58
4.6	-5.65	-2.04	3.62	3.10
4.7	-5.63	-2.20	3.43	2.95

Based on TD-DFT calculations, the lowest energy transition of **4.1**-**4.7** is mainly a HOMO-LUMO transition with oscillator strength (transition probability) values of 0.0321, 0.0256, 0.0322, 0.0212, 0.0455, 0.0264, and 0.0285, respectively, Table 4.7. The HOMO and LUMO orbitals in **4.1**-**4.7** partially overlap around the $C_{chelate}$ moiety, suggesting a possible pathway of a charge transfer interaction.

Table 4.7 Selected data of electronic transitions for compounds **4.1-4.7** calculated using TD-DFT method at the B3LYP/6-311G* level. First excited state is a HOMO→LUMO transition in all compounds (*f* = oscillator strength)

	4.1	**4.2**	**4.3**	**4.4**	**4.5**	**4.6**	**4.7**
Excited State	Transition λ (nm) *f*	Transition λ (nm) *f*	Transition λ (nm) *f*	Transition λ (nm) *f*	Transition λ (nm) *f*	Transition λ (nm) *f*	Transition λ (nm) *f*
1	125→126 423.89 0.0321	129→130 430.06 0.0256	118→119 433.00 0.0322	122→123 428.09 0.0212	138→139 445.38 0.0455	118→119 413.81 0.0264	122→123 444.39 0.0285
2	124→126 391.38 0.0313	128→130 394.97 0.0193	117→119 405.42 0.0429	121→123 409.66 0.0368	137→139 410.88 0.0189	117→119 383.04 0.0116	120→123 401.60 0.0087
3	123→126 378.06 0.0083	127→130 383.80 0.0119	116→119 392.07 0.0054	120→123 389.61 0.0010	136→139 386.73 0.0013	116→119 373.99 0.0110	121→123 397.26 0.0085
4	122→126 359.42 0.0007	126→130 365.15 0.0018	115→119 371.55 0.0490	119→123 377.55 0.0350	135→139 378.22 0.0108	115→119 357.02 0.0023	119→123 378.35 0.0036
5	121→126 359.12	129→131 355.90	114→119 369.39	118→123 371.99	134→139 366.23	114→119 305.65	118→123 325.29

	0.0509	0.0316	0.0076	0.0028	0.0302	0.1911	0.2155
6	125→127 338.37 0.0616	125→130 345.24 0.0917	118→120 343.58 0.0642	122→124 347.04 0.0399	138→140 361.31 0.0455	113→119 294.42 0.2693	117→123 308.91 0.2238
7	124→127 321.18 0.0467	128→131 329.19 0.0284	117→120 330.42 0.0516	121→124 340.21 0.0122	133→139 346.44 0.1589	118→120 277.89 0.0191	122→124 294.78 0.0129
8	123→127 311.04 0.0144	127→131 320.10 0.0176	113→119 321.04 0.0784	117→123 330.12 0.1716	137→140 334.48 0.0724	118→121 277.06 0.0401	116→123 289.57 0.0215
9	122→127 299.94 0.0006	124→130 313.75 0.1076	116→120 319.33 0.0318	120→124 321.98 0.0041	138→141 327.25 0.0138	117→120 267.13 0.0163	122→125 277.03 0.0339
10	121→127 293.43 0.2287	126→131 308.26 0.0011	114→120 306.16 0.0017	119→124 313.83 0.0924	136→140 318.35 0.0097	112→119 266.13 0.0085	120→124 276.44 0.0205

The calculated absorption spectra of **4.1-4.7** and **4.5a** were obtained using TD-DFT calculations at the (B3LYP/6-311G*) level after geometry optimization at the same level of theory using DFT calculations. The TD-DFT-based UV-Vis spectra of **4.1-4.7** are shown in Figure 4.21 - Figure 4.27. The important energy transitions, including the

lowest energy transitions, of **4.1**-**4.7** and **4.5a** are shown on the figures, along with the involved orbital diagrams, oscillator strengths, and the wavelength at which the transition took place. The lowest energy transitions in the calculated UV-Vis spectra for compounds **4.1**-**4.7** follow a similar trend of the emission energies.

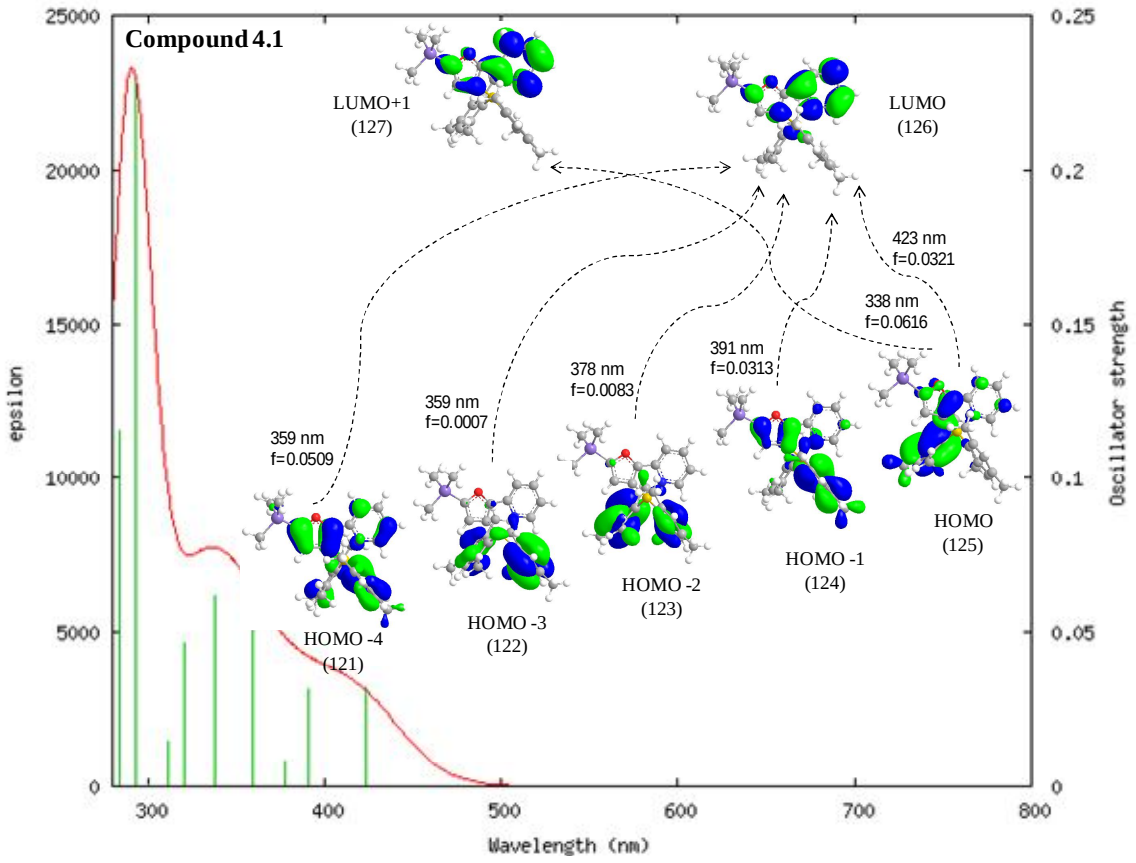

Figure 4.21 Calculated UV-Vis spectrum of **4.1** with characteristic electronic transitions calculated at the TD-DFT (B3LYP/6-311G*) level. Produced using GaussSum[14] program V.2.2.2 with FWHM = 3000 cm^{-1}

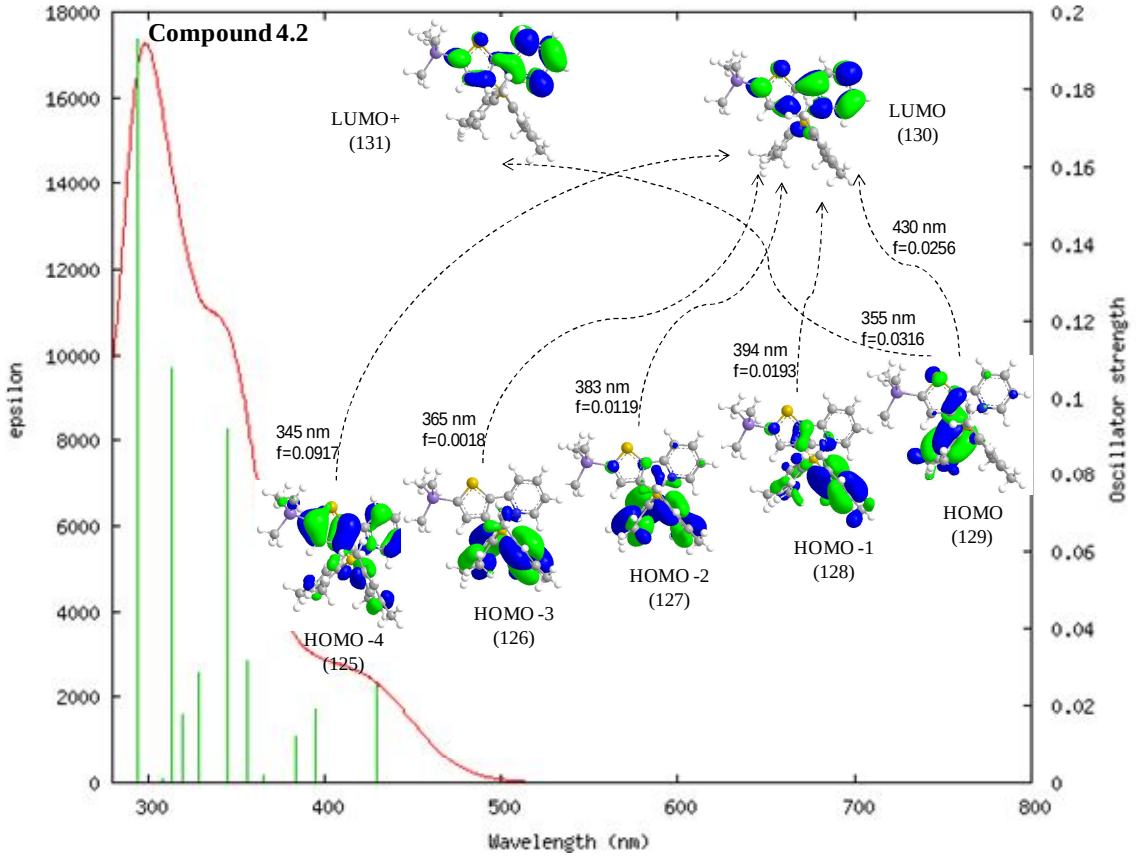

Figure 4.22 Calculated UV-Vis spectrum of **4.2** with characteristic electronic transitions calculated at the TD-DFT (B3LYP/6-311G*) level. Produced using GaussSum program V.2.2.2 with FWHM = 3000 cm^{-1}

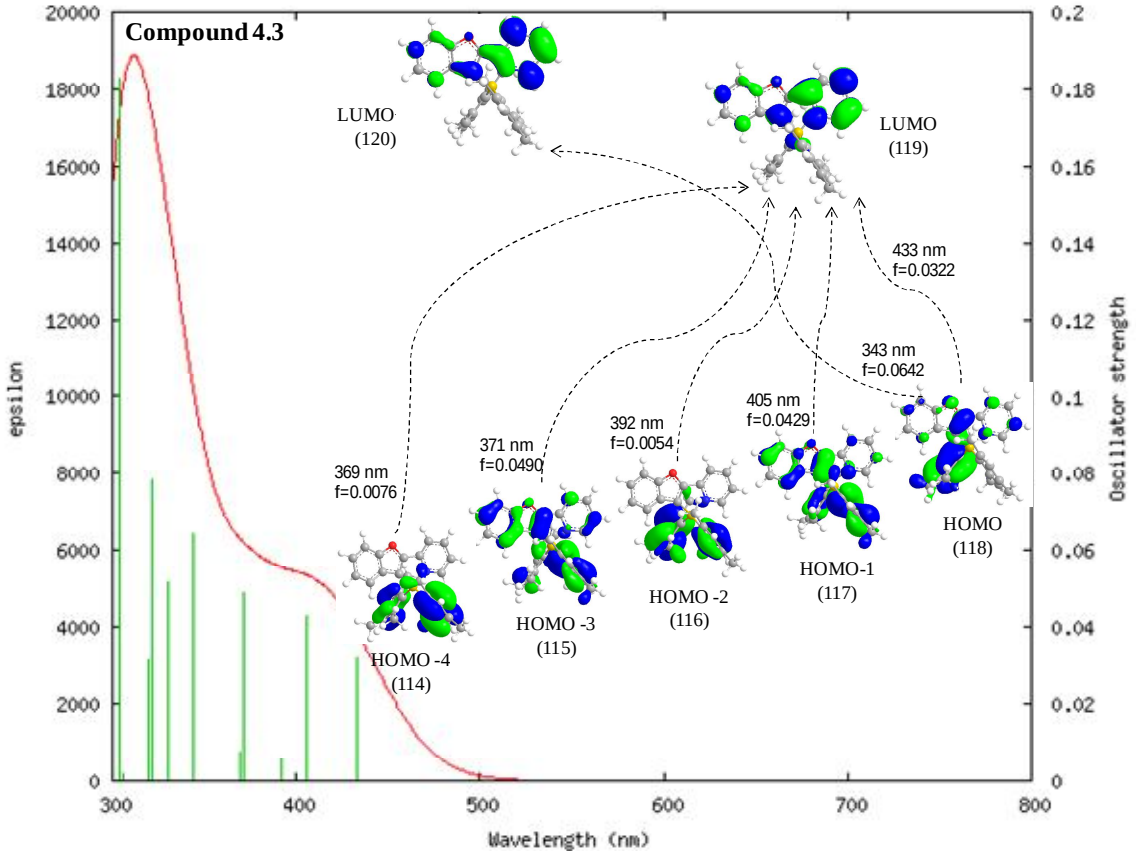

Figure 4.23 Calculated UV-Vis spectrum of **4.3** with characteristic electronic transitions calculated at the TD-DFT (B3LYP/6-311G*) level. Produced using GaussSum program V.2.2.2 with FWHM = 3000 cm^{-1}

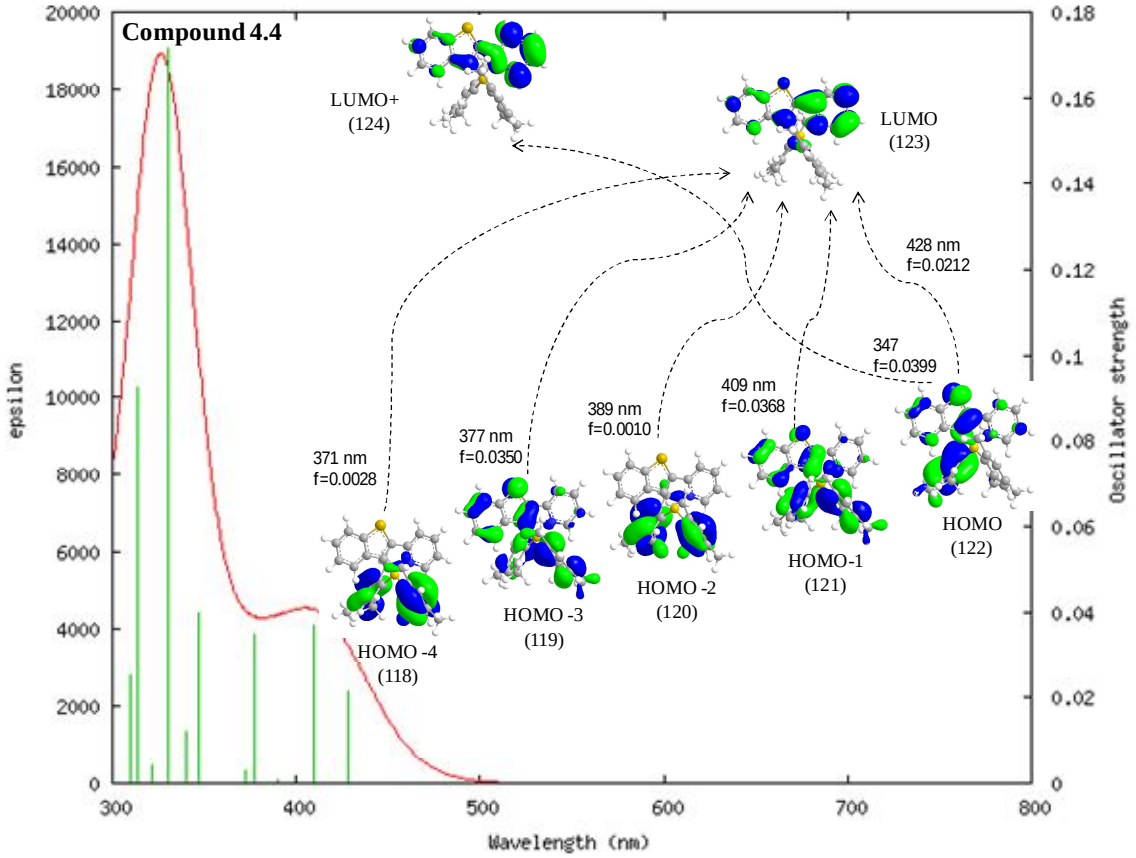

Figure 4.24 Calculated UV-Vis spectrum of **4.4** with characteristic electronic transitions calculated at the TD-DFT (B3LYP/6-311G*) level. Produced using GaussSum program V.2.2.2 with FWHM = 3000 cm^{-1}

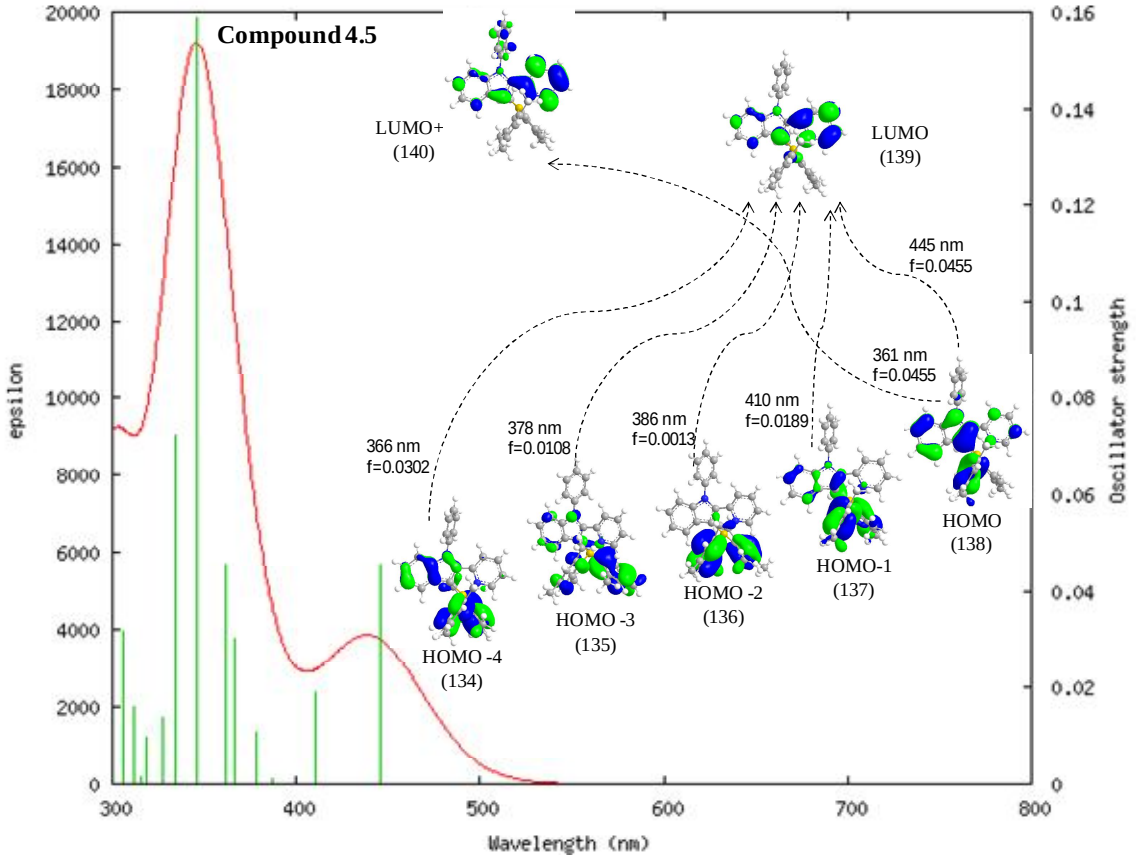

Figure 4.25 Calculated UV-Vis spectrum of **4.5** with characteristic electronic transitions calculated at the TD-DFT (B3LYP/6-311G*) level. Produced using GaussSum program V.2.2.2 with FWHM = 3000 cm^{-1}

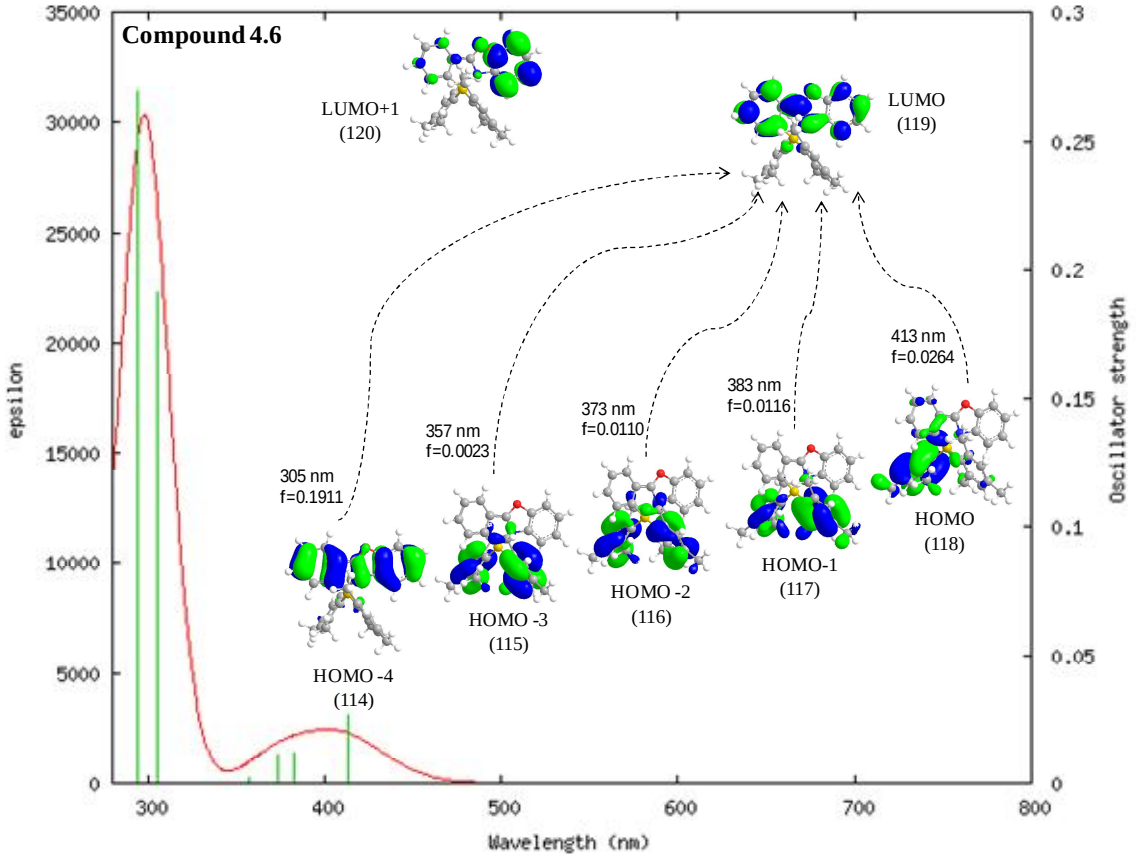

Figure 4.26 Calculated UV-Vis spectrum of **4.6** with characteristic electronic transitions calculated at the TD-DFT (B3LYP/6-311G*) level. Produced using GaussSum program V.2.2.2 with FWHM = 3000 cm^{-1}

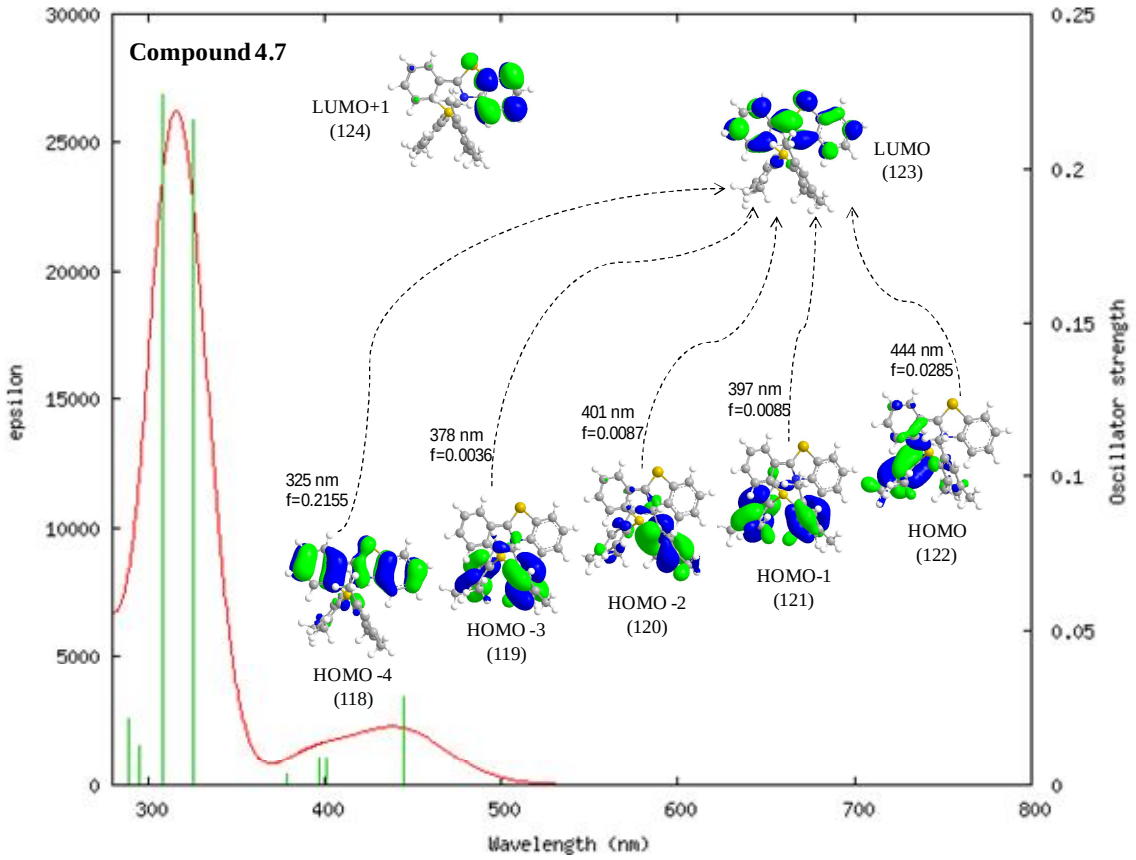

Figure 4.27 Calculated UV-Vis spectrum of **4.7** with characteristic electronic transitions calculated at the TD-DFT (B3LYP/6-311G*) level. Produced using GaussSum program V.2.2.2 with FWHM = 3000 cm^{-1}

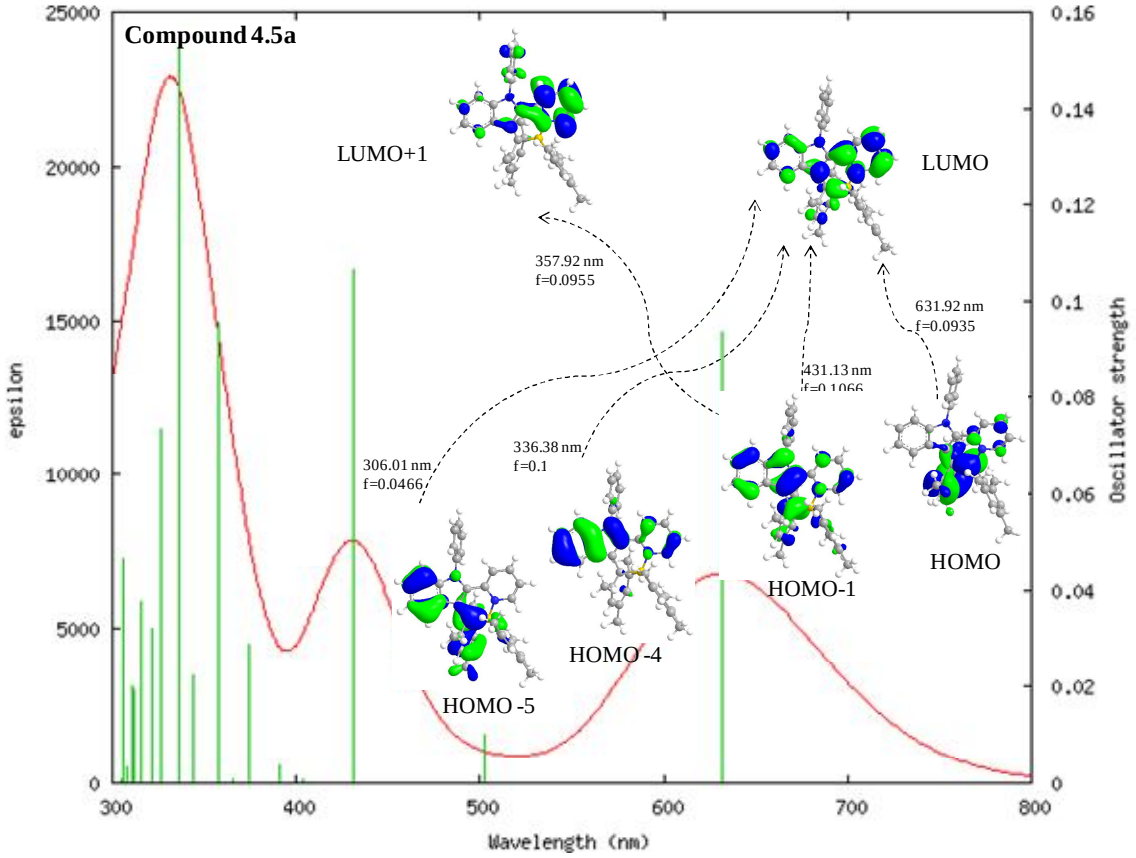

Figure 4.28 Calculated UV-Vis spectrum of **4.5a** with characteristic electronic transitions calculated at the TD-DFT (B3LYP/6-311G*) level. Produced using GaussSum program V.2.2.2 with FWHM = 3000 cm^{-1}

4.3.5 Photochromic Behavior of Compounds 4.1-4.7

Compounds **4.1-4.7** have the same photochromic behavior observed in compound **2.1** and other phenylpyridine-based photochromic compounds, this strongly suggests that photoisomerization process observed is a general phenomenon for π-conjugated N,C-chelate $BMes_2$ compounds. Upon exposure to UV light (365 nm) under nitrogen atmosphere the colorless/yellowish toluene solution changes to dark blue or dark green. The X-ray structure data of **4.1**-**4.7** shows a similar trend to that found in the phenylpyridine-based organoborons in terms of the asymmetric arrangement of the mesityl groups around the boron center. One of the mesityl group is much closer to the $C_{Chelate}$ atom than the other with through-space distances of (2.585 Å vs. 2.877 Å, average), which is attributed to the steric effect of the mesityl groups. Hence, the closer mesityl group is the one expected to be attached to the $C_{Chelate}$ upon irradiation.

The quantum efficiency of the photoisomerization process of **4.1**, **4.2**, **4.5**, **4.6**, and **4.7** determined using the ferrioxalate actinometry was 0.34, 0.77, 0.09, 0.40, and 0.65, respectively. The much smaller photoisomerization efficiency of **4.5** might be attributed to steric effect of the indole group, which is larger in size than furan (**4.1**), thiophene (**4.2**), and benzene (**4.6** and **4.7**). The photoisomerization efficiency of the sulfur-containing compounds **4.2** and **4.7** is larger than those of the oxygen-containing analogues; this might be attributed to better stabilization of the charge transfer state by oxygen, which is more capable of stabilizing extra electron density than sulfur.

The photoisomerization of compounds **4.1**-**4.7** was monitored using UV-Vis and ^{1}H NMR spectroscopy techniques. Upon irradiation of a toluene solution of compounds **4.1**-**4.7** with UV light (365 nm) under an atmosphere of N_2, a new intense broad band appears and grows rapidly (λ_{max} = 566, 587, 598, 628, 606, 600, and 650 nm, respectively) as shown in Figure 4.29 – Figure 4.35).

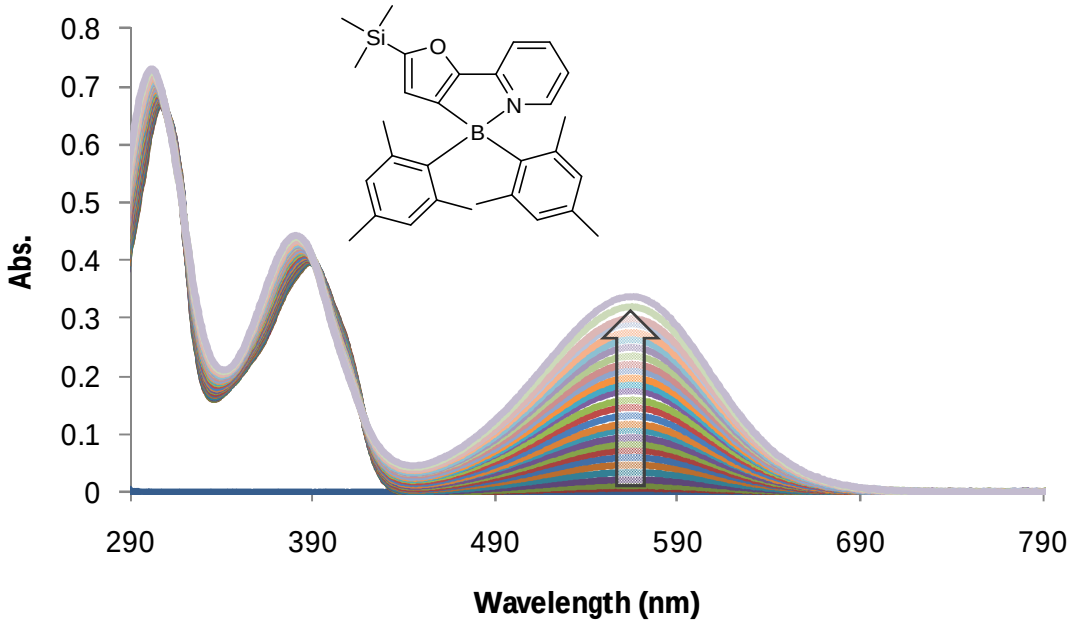

Figure 4.29 UV-Vis spectral changes of **4.1** in toluene upon irradiation by UV light (365 nm) under nitrogen at RT, recorded at ~10^{-5} M with 2 s intervals of UV exposure.

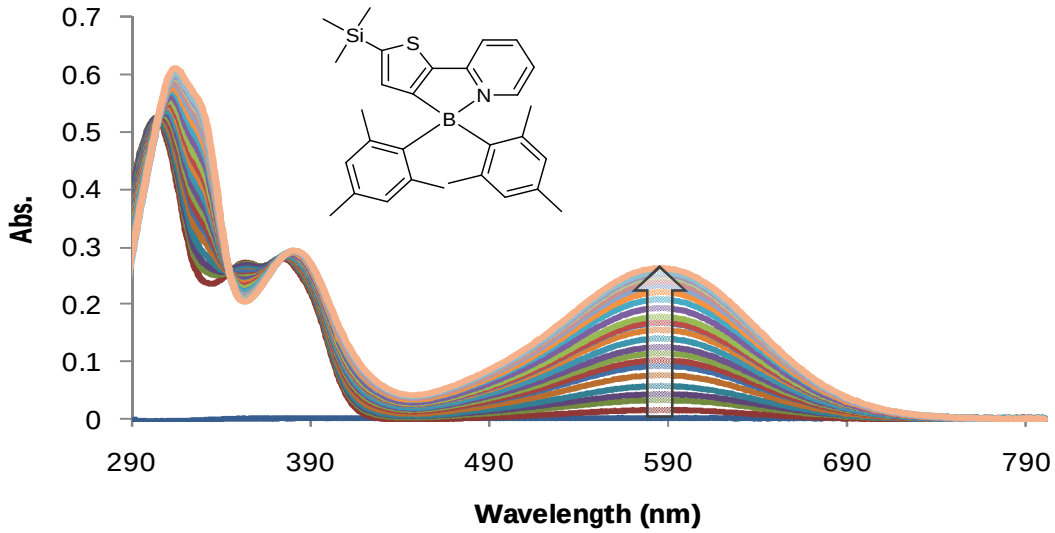

Figure 4.30 UV-Vis spectral changes of **4.2** in toluene upon irradiation by UV light (365 nm) under nitrogen at RT, recorded at ~10^{-5} M with 1 s intervals of UV exposure.

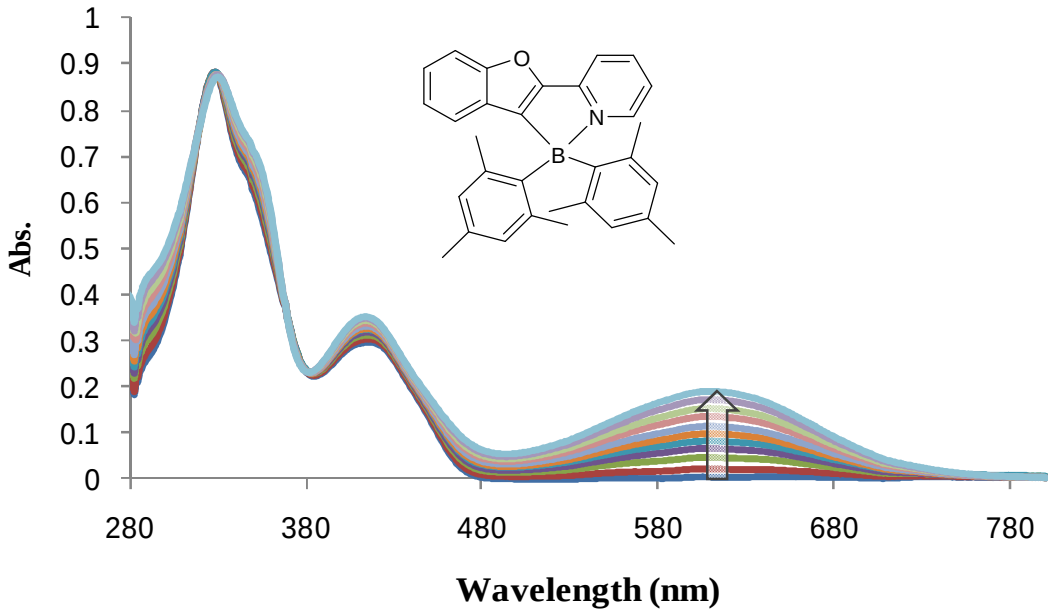

Figure 4.31 UV-Vis spectral changes of **4.3** in toluene upon irradiation by UV light (365 nm) under nitrogen at RT, recorded at ~10^{-5} M with 5-10 s intervals of UV exposure.

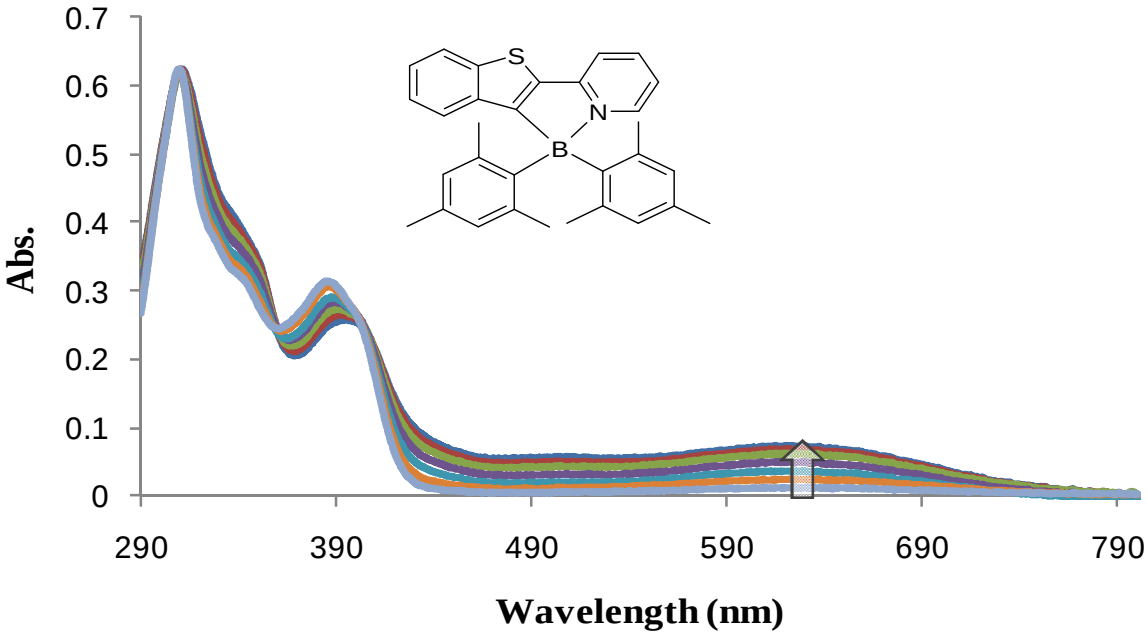

Figure 4.32 UV-Vis spectral changes of **4.4** in toluene upon irradiation by UV light (365 nm) under nitrogen at RT, recorded at ~10^{-5} M with 5-10 s intervals of UV exposure.

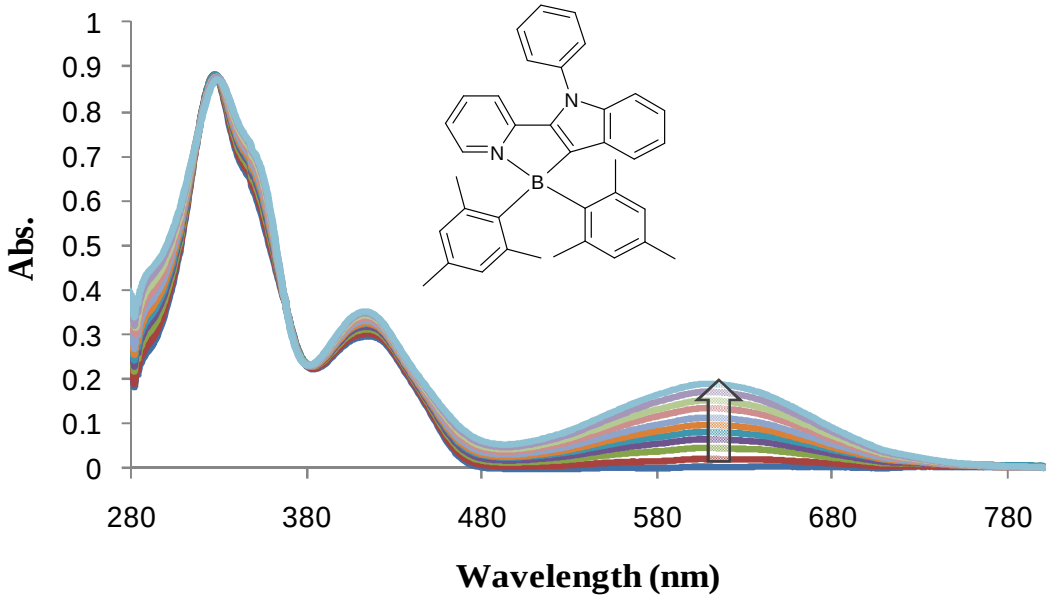

Figure 4.33 UV-Vis spectral changes of **4.5** in toluene upon irradiation by UV light (365 nm) under nitrogen at RT, recorded at ~10^{-5} M with 5-20 s intervals of UV exposure.

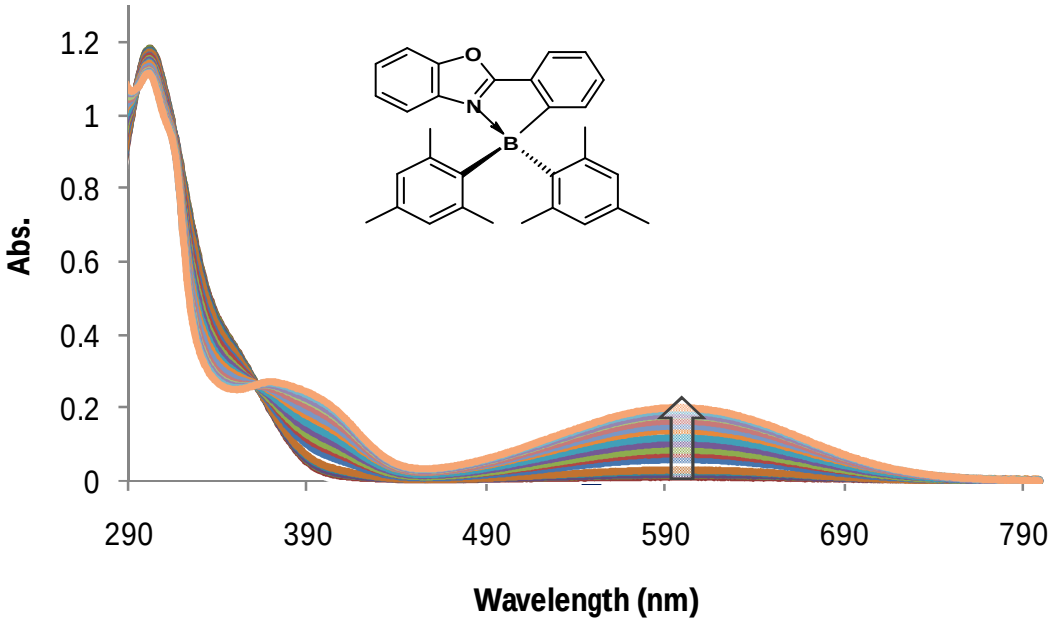

Figure 4.34 UV-Vis spectral changes of **4.6** in toluene upon irradiation by UV light (365 nm) under nitrogen at RT, recorded at ~10^{-5} M with 1 s intervals of UV exposure.

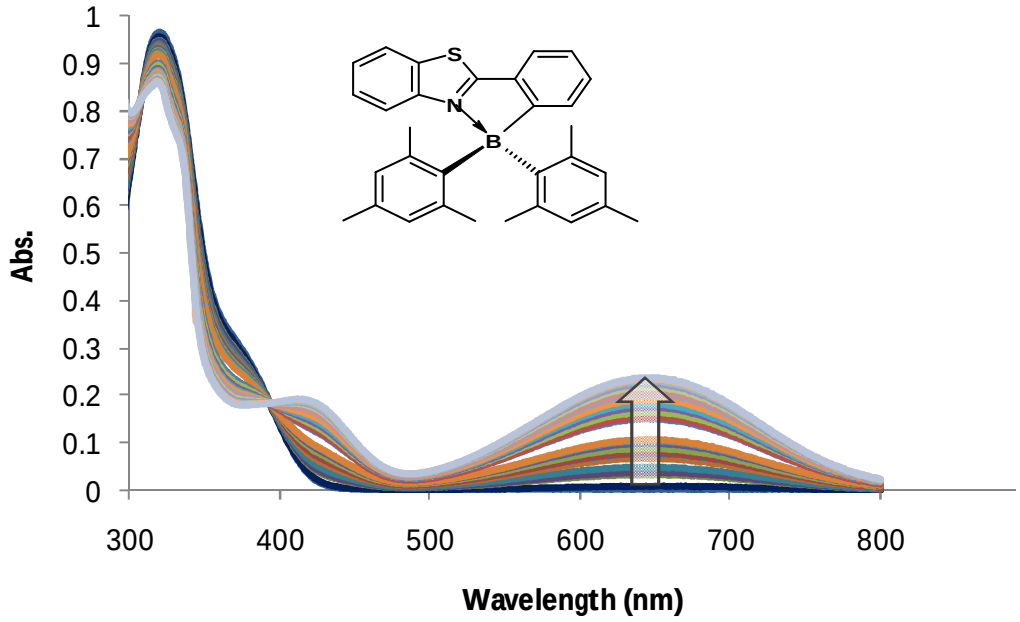

Figure 4.35 UV-Vis spectral changes of **4.7** in toluene upon irradiation by UV light (365 nm) under nitrogen at RT, recorded at ~10^{-5} M with 1-5 s intervals of UV exposure.

The photochromic behavior of **4.1**-**4.7** was also monitored using ^{1}H NMR spectroscopy, Figure 4.36 – Figure 4.42. Upon irradiation of a C_6D_6 solution of these compounds with UV light (365 nm) under N_2, the ^{1}H NMR spectra display a new set of peaks that represent the corresponding dark isomers. Similar to the photo conversion of compound **2.1** to **2.1a** and other phenylpyridine-based organoboron compounds, the singlet representing the four aryl protons of the two mesityl groups (H_{Ar}) splits in to four distinct singlet peaks and the two singlet peaks representing the six methyl groups splits in to six distinct methyl peaks.

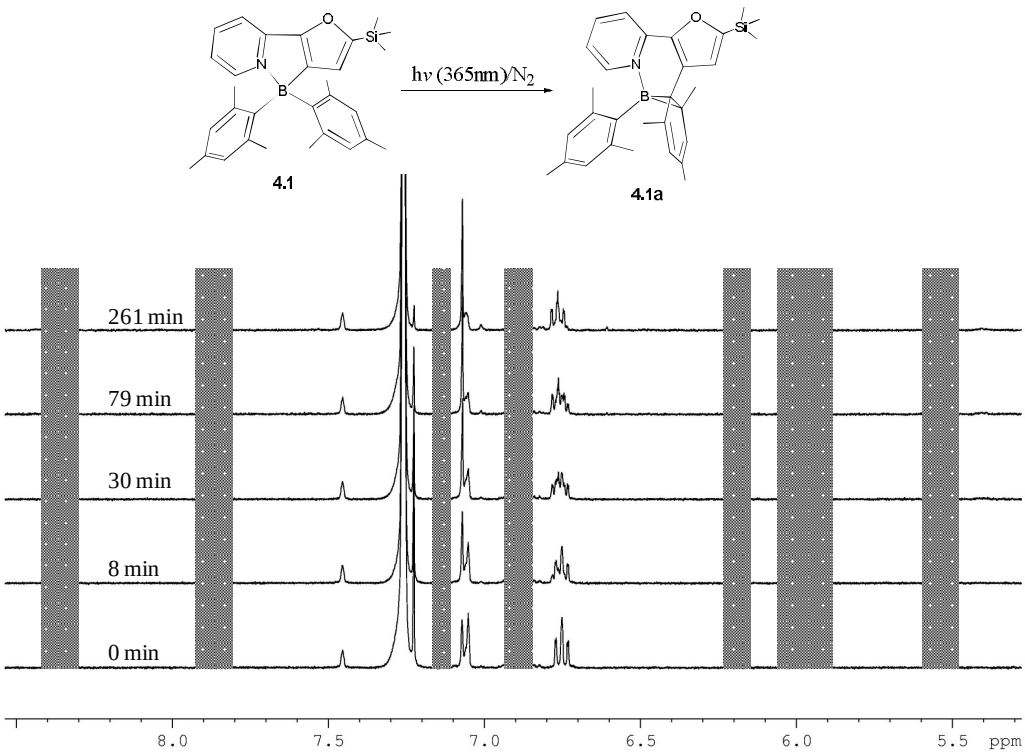

Figure 4.36 ^{1}H NMR spectral changes (aromatic region) of **4.1** in C_6D_6 under N_2 upon irradiation at 365 nm. Violet: **4.1** and green: **4.1a**.

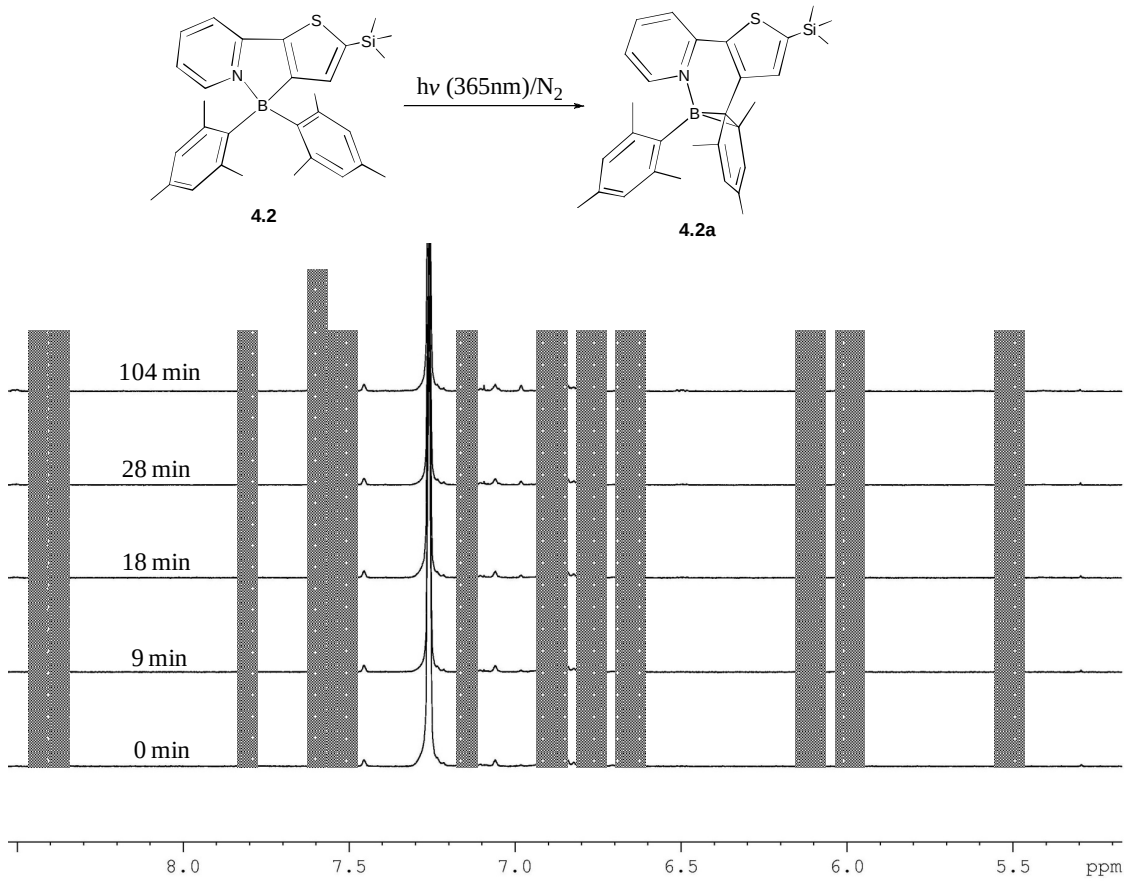

Figure 4.37 ^{1}H NMR spectral changes (aromatic region) of **4.2** in C_6D_6 under N_2 upon irradiation at 365 nm. Violet: **4.2** and green: **4.2a**.

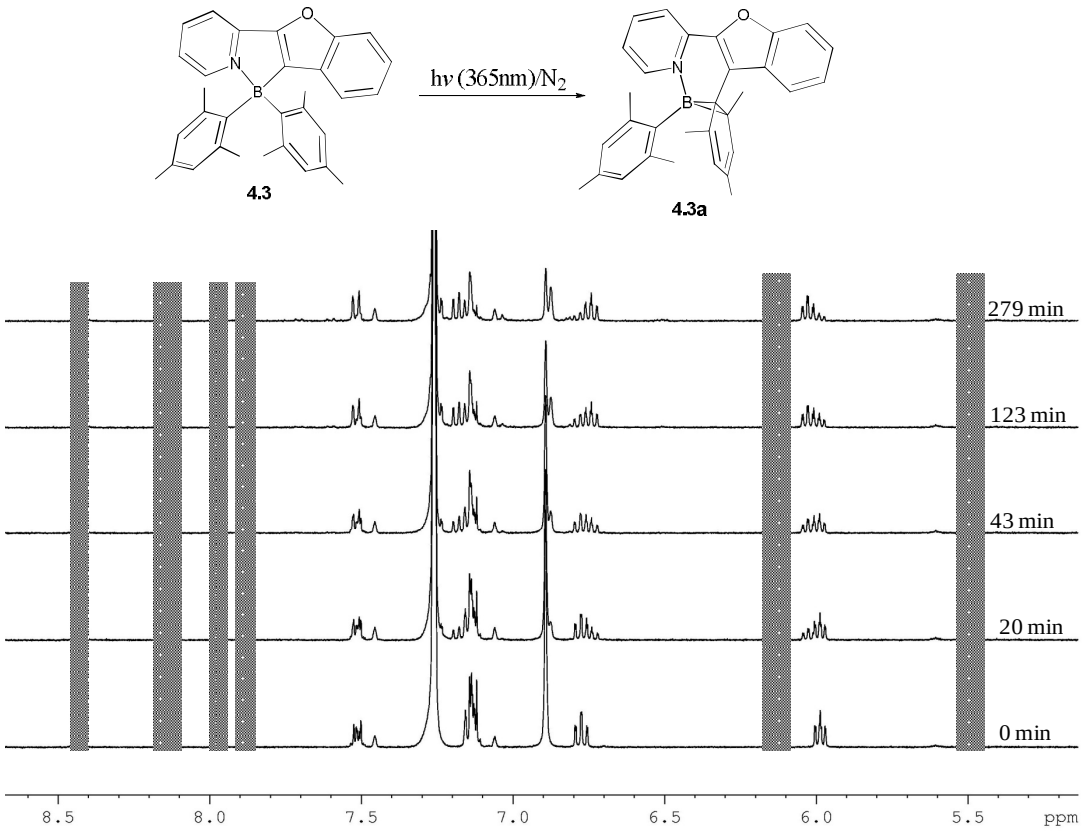

Figure 4.38 ^{1}H NMR spectral changes (aromatic region) of **4.3** in C_6D_6 under N_2 upon irradiation at 365 nm. Violet: **4.3** and green: **4.3a**.

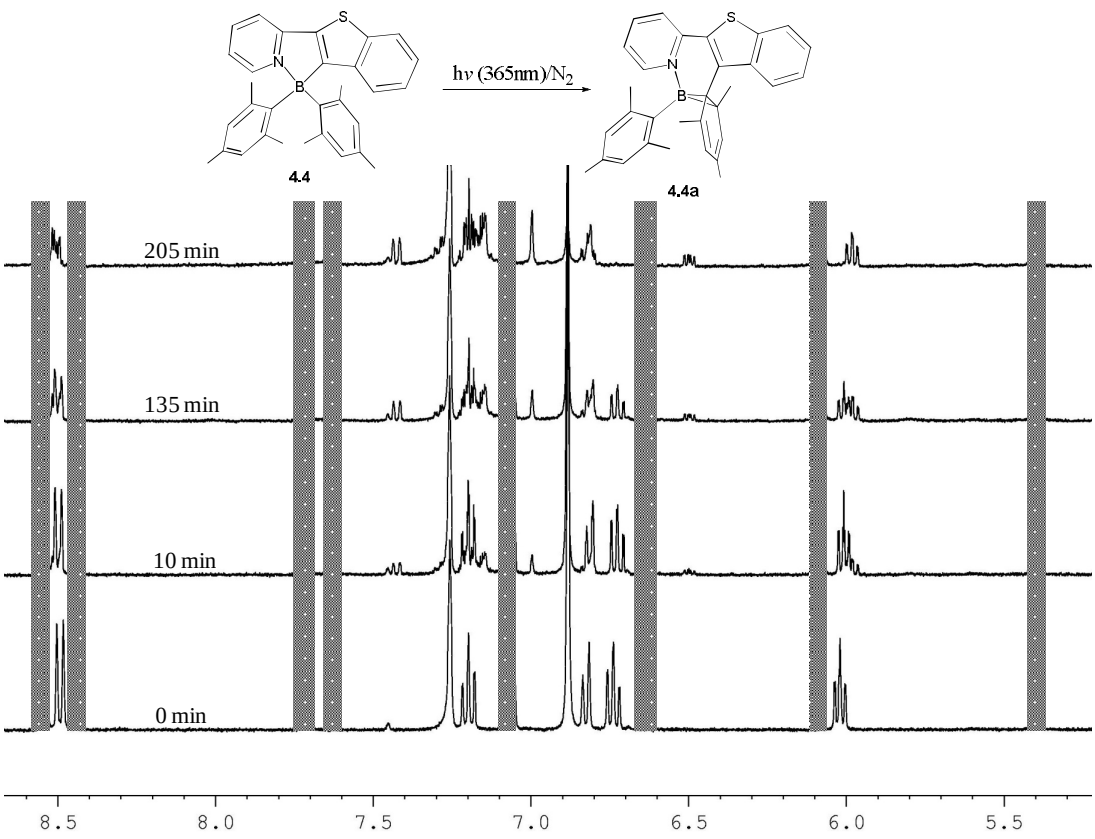

Figure 4.39 ^{1}H NMR spectral changes (aromatic region) of **4.4** in C_6D_6 under N_2 upon irradiation at 365 nm. Violet: **4.4** and green: **4.4a**.

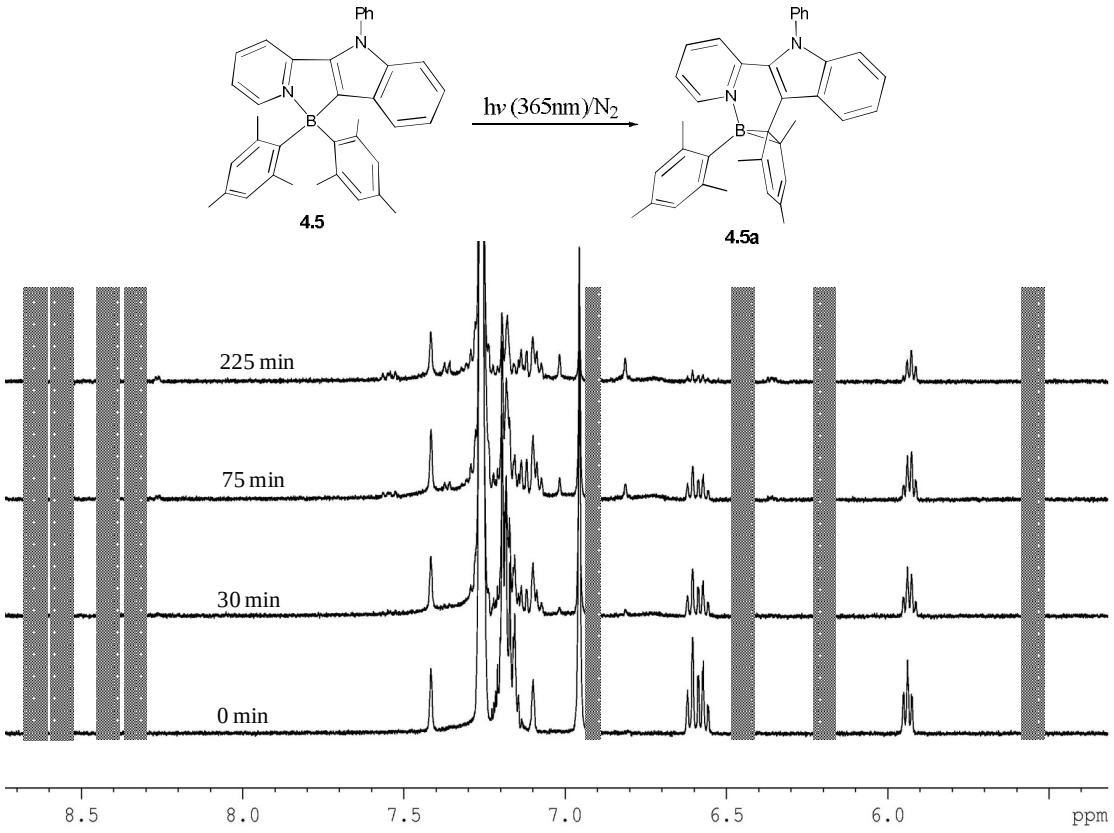

Figure 4.40 ^{1}H NMR spectral changes (aromatic region) of **4.5** in C_6D_6 under N_2 upon irradiation at 365 nm. Violet: **4.5** and green: **4.5a**.

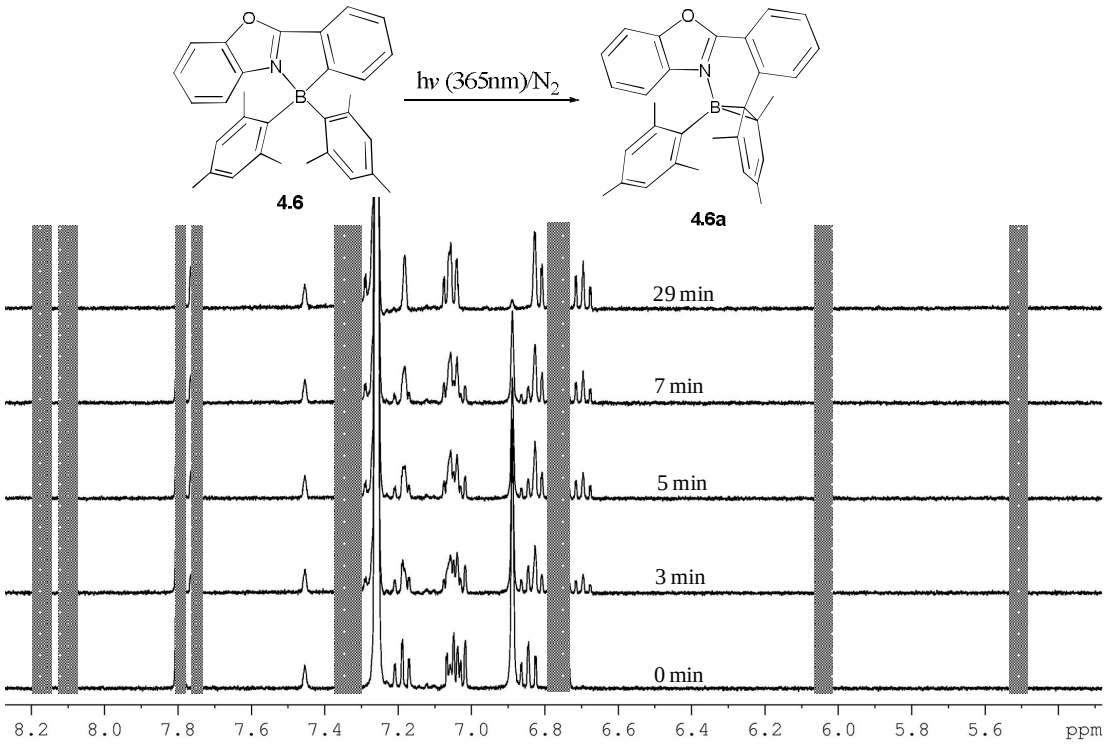

Figure 4.41 ^{1}H NMR spectral changes (aromatic region) of **4.6** in C_6D_6 under N_2 upon irradiation at 365 nm. Violet: **4.6** and green: **4.6a**.

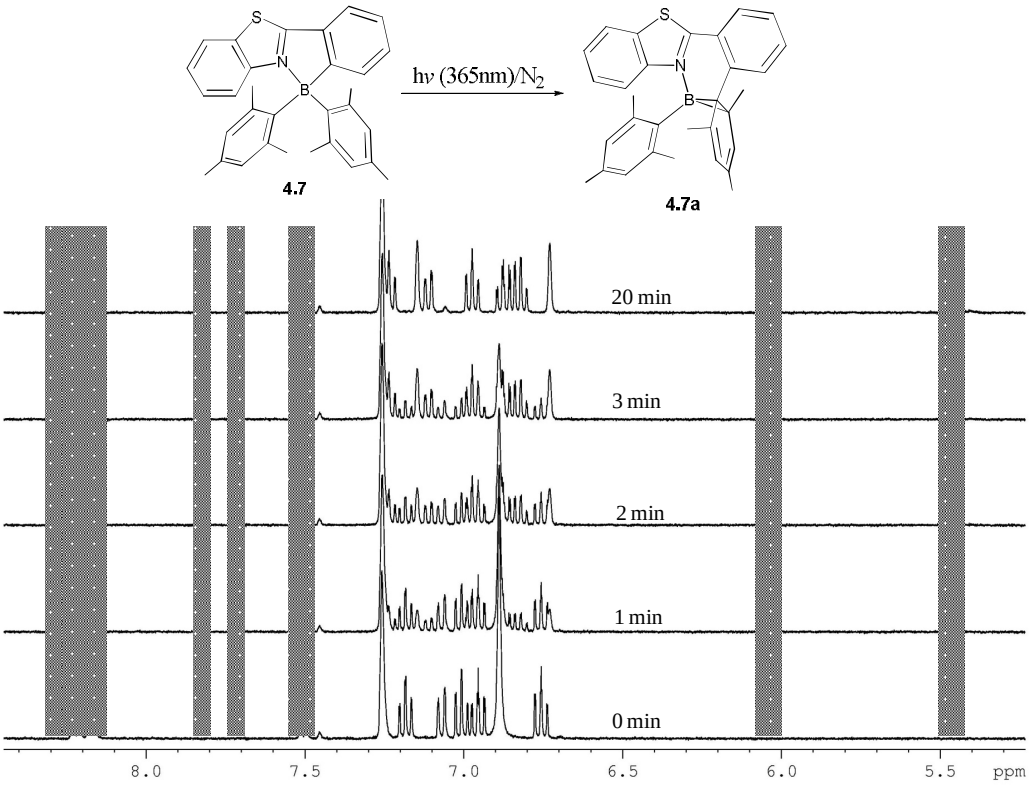

Figure 4.42 ^{1}H NMR spectral changes (aromatic region) of **4.7** in C_6D_6 under N_2 upon irradiation at 365 nm. Violet: **4.7** and green: **4.7a**.

4.3.6 Relative Photoisomerization Rate Studies

The photoisomerization rates of compounds **4.1**-**4.7** relative to compound **2.1** were studied using ^{1}H NMR spectroscopy as shown in Figure 4.43-Figure 4.49. The photoisomerization rate of **4.1** (k(**2.1**)/k(**4.1**) = 5) is slower than that of **4.2** (k(**2.1**)/k(**4.2**) = 0.3), which might be attributed to the relative stabilization of the charge transfer state of **4.1** by the oxygen atom. Similarly, the photoisomerization rate of **4.6** (k(**2.1**)/k(**4.6**) = 1.4) is slower than that of **4.7** (k(**2.1**)/k(**4.7**) = 0.3). On the other hand, the photoisomerization rates of **4.3**, **4.4**, and **4.5** were almost equal (k(**2.1**)/k(**4.3**) = 15), (k(**2.1**)/k(**4.4**) = 15), (k(**2.1**)/k(**4.5**) = 14), which can be attributed to the similar stabilization of the charge transfer state by the greater contribution of the LUMO of the these compounds in the charge transfer state. The faster photoisomerization rates are consistent with the higher photoisomerization quantum efficiencies, which is clearly demonstrated by comparing compound **4.1** vs. **4.2**, where compound **4.2** has a higher photoisomerization quantum efficiency (0.77) compared to (0.34) for compound **4.1**. Similarly compound **4.7** has a higher photoisomerization quantum efficiency (0.65) compared to (0.40) for compound **4.6**.

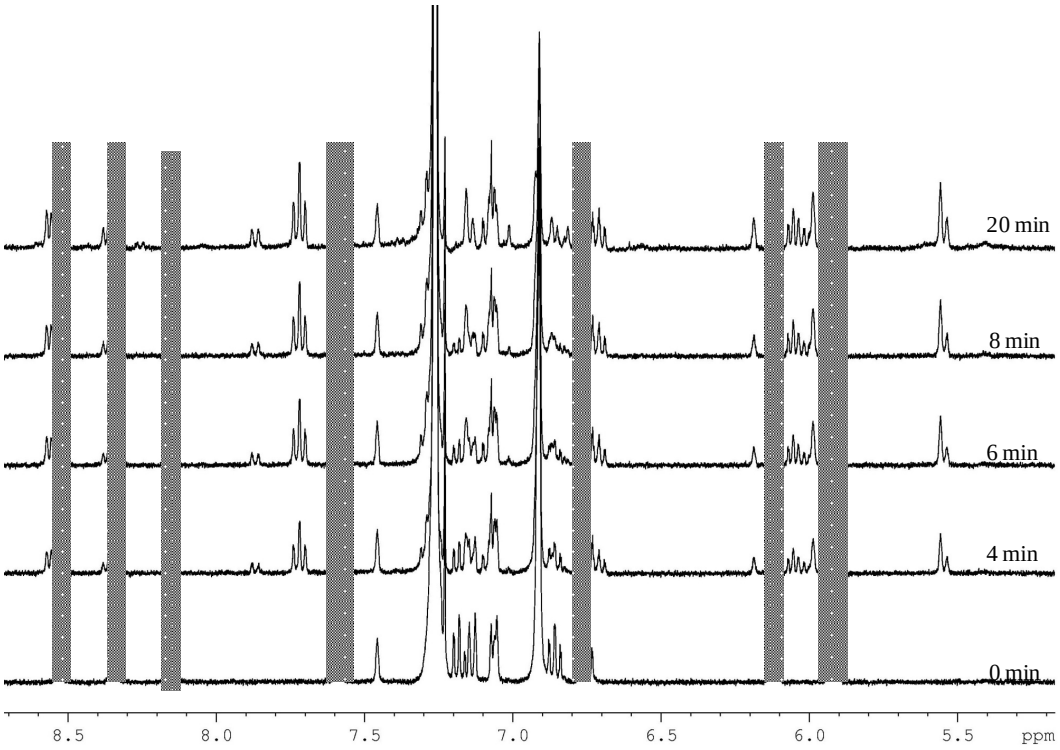

Figure 4.43 ^{1}H NMR spectra of **4.1** and **2.1**(reference) showing the relative conversion rate to **4.1a** and **2.1a** after irradiation with UV (365 nm) in C_6D_6 under N_2 .Color code: **4.1**(Violet) and **2.1** (Orange)

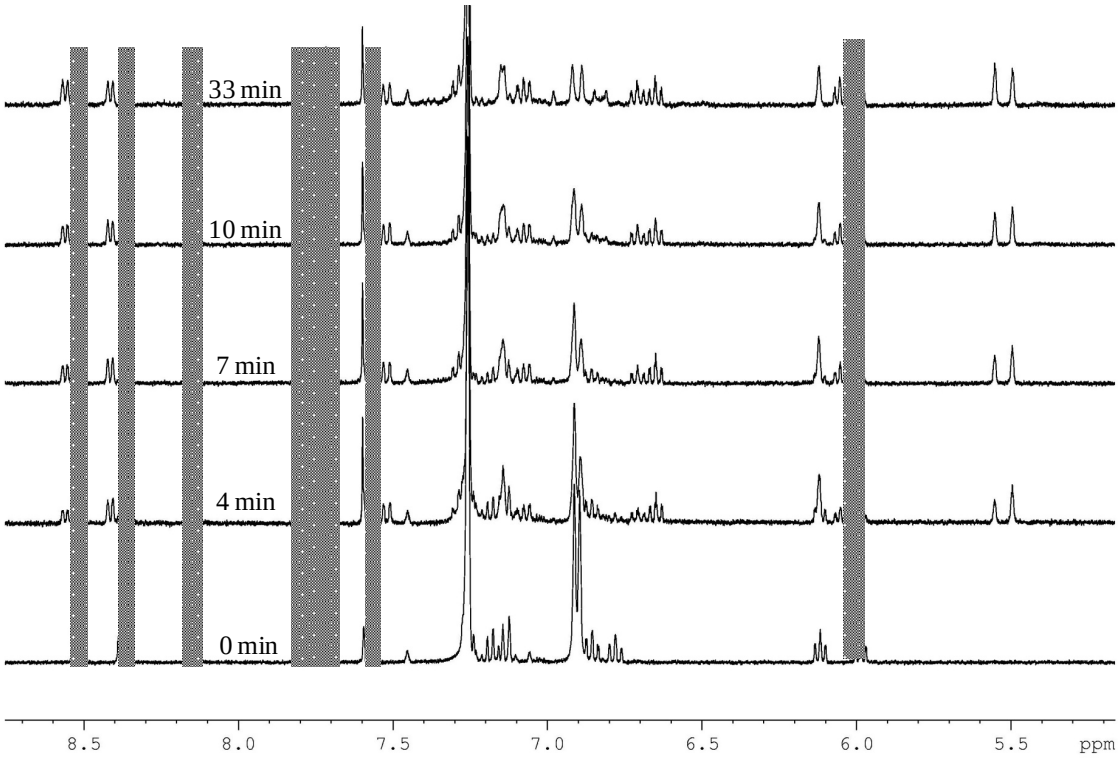

Figure 4.44 ^{1}H NMR spectra of **4.2** and **2.1**(reference) showing the relative conversion rate to **4.2a** and **2.1a** after irradiation with UV (365 nm) in C_6D_6 under N_2 .Color code: **4.2**(Violet) and **2.1** (Orange)

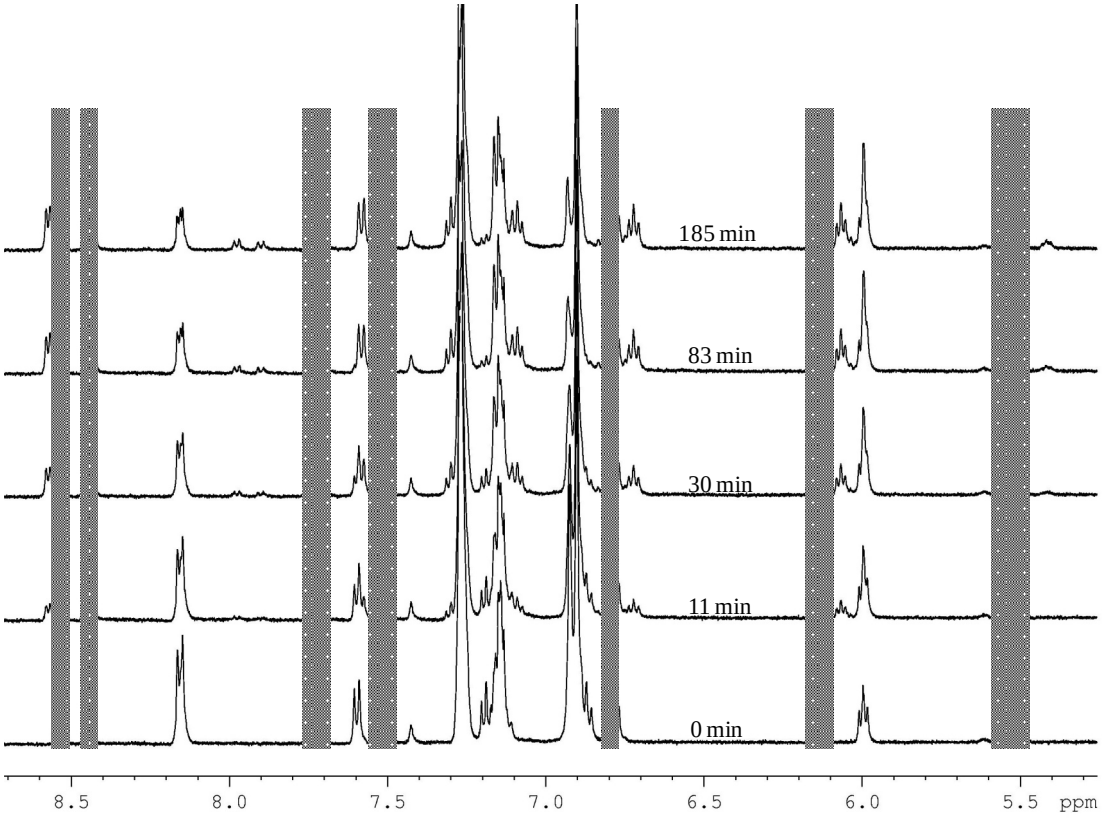

Figure 4.45 ^{1}H NMR spectra of **4.3** and **2.1**(reference) showing the relative conversion rate to **4.3a** and **2.1a** after irradiation with UV (365 nm) in C_6D_6 under N_2 .Color code: **4.3**(Violet) and **2.1** (Orange)

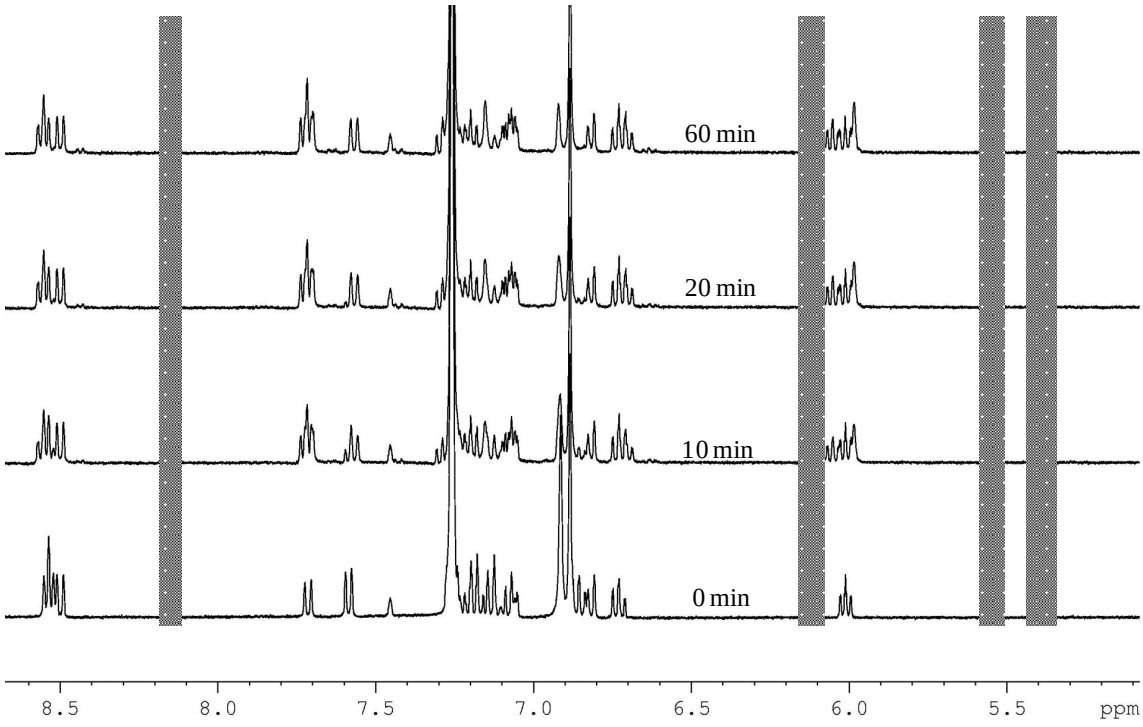

Figure 4.46 ^{1}H NMR spectra of **4.4** and **2.1**(reference) showing the relative conversion rate to **4.4a** and **2.1a** after irradiation with UV (365 nm) in C_6D_6 under N_2 .Color code: **4.4**(Violet) and **2.1** (Orange)

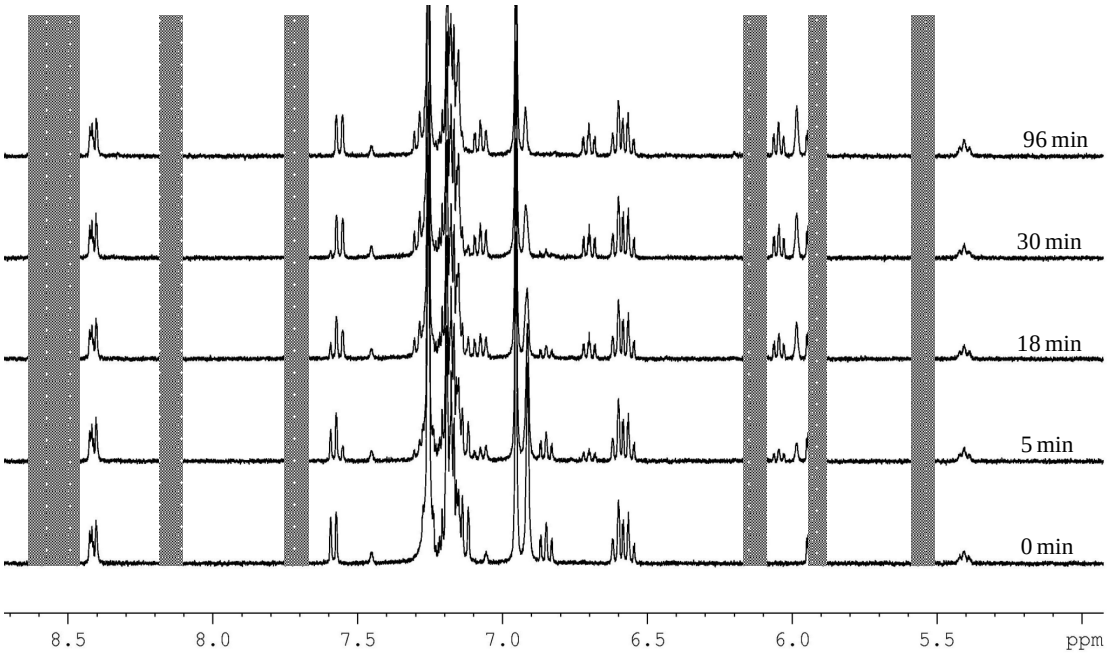

Figure 4.47 ^{1}H NMR spectra of **4.5** and **2.1**(reference) showing the relative conversion rate to **4.5a** and **2.1a** after irradiation with UV (365 nm) in C_6D_6 under N_2 .Color code: **4.5**(Violet) and **2.1** (Orange)

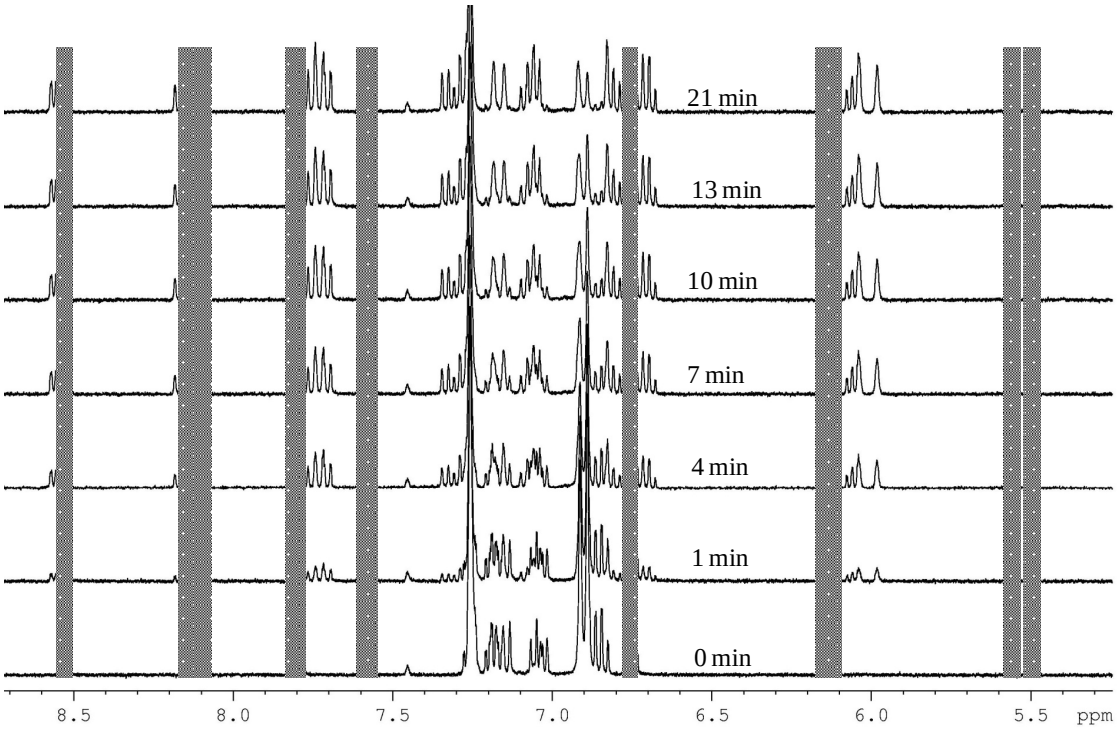

Figure 4.48 ^{1}H NMR spectra of **4.6** and **2.1**(reference) showing the relative conversion rate to **4.6a** and **2.1a** after irradiation with UV (365 nm) in C_6D_6 under N_2 .Color code: **4.6**(Violet) and **2.1** (Orange)

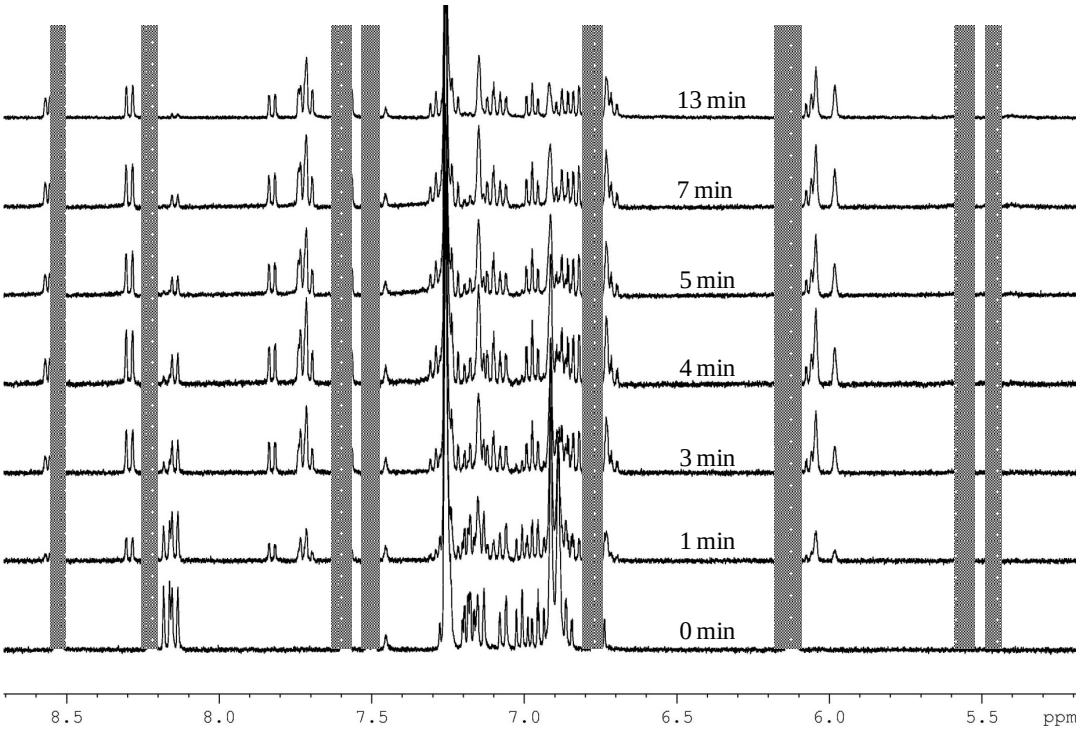

Figure 4.49 ^{1}H NMR spectra of **4.7** and **2.1**(reference) showing the relative conversion rate to **4.7a** and **2.1a** after irradiation with UV (365 nm) in C_6D_6 under N_2 .Color code: **4.7**(Violet) and **2.1** (Orange)

4.3.7 Thermal Reversal of the Dark Isomer to the Light Colored Isomer

The dark isomers of compounds **4.1**-**4.7** show much higher thermal stability compared to their phenylpyridine-based counterparts. The estimated thermal reversal half life of the dark isomer of **4.5** was about 10 hrs at 50°C, while the dark isomers of compounds **4.1**-**4.4** did not show appreciable thermal reversibility upon heating for about 10 hrs. On the other hand, upon heating the dark isomers of compounds **4.6** and **4.7** a new set of singlet peaks appear in the ^{1}H NMR of these compounds indicating different structural rearrangement, which much more pronounced in compound **4.7** as shown in Figure 4.50.

The thermal stability of the dark isomers of **4.1**-**4.5** might indicate that the thermal activation barrier (ΔG*) shown in Figure 1.12 is very high. This requires heating to temperatures higher than 50 °C, which might lead to decomposition of the dark isomer rather than reversing back to the light colored isomer. This was the case when the dark isomer of compound **4.4** was heated up to 70 °C.

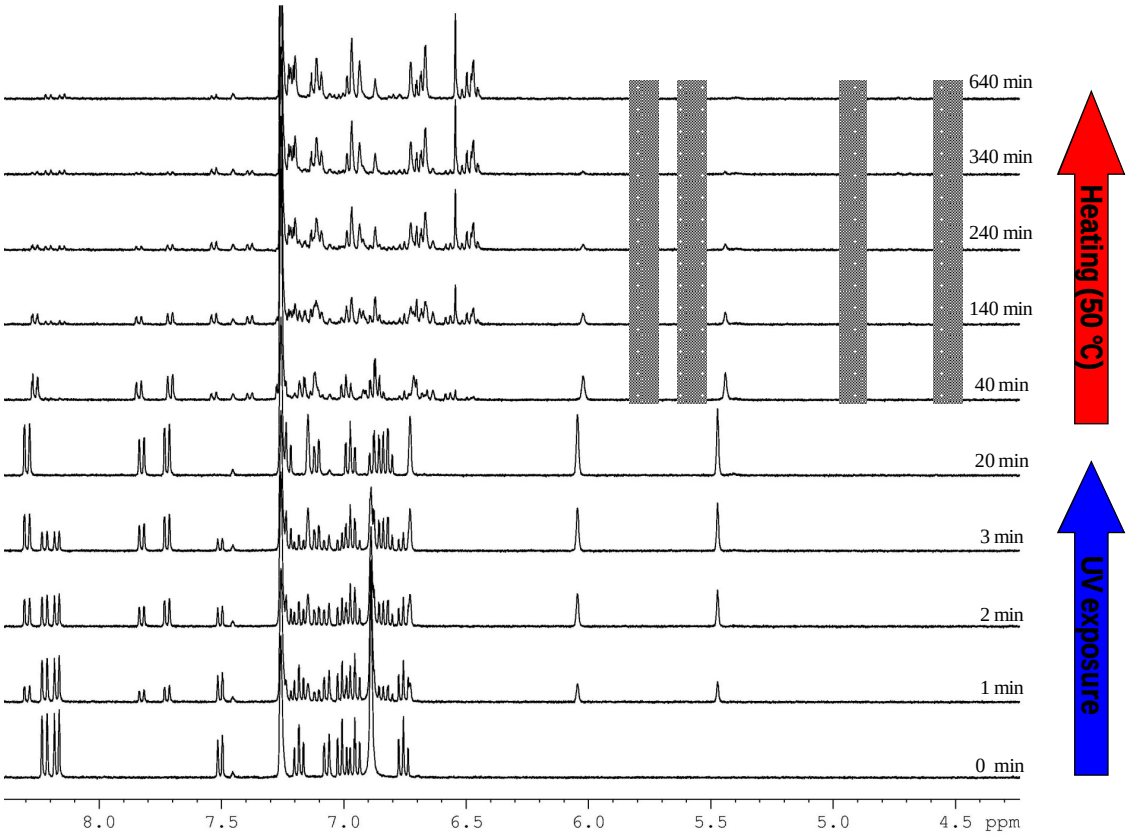

Figure 4.50 Photolysis of **4.7** to **4.7a** and subsequent heating of **4.7a** under nitrogen in C_6D_6 at 50 °C, showing the appearance of new set of singlets (highlighted in blue)

The relative thermal stability of compounds **4.1**-**4.5** might suggest that the dark isomers of these compounds can be reversed back to the light colored isomers using light

instead of heat, which if successful means that these compounds belong to the P-type photochromic system. Similar to diarylethenes, the thermal stability of these photochromic compounds could make them very important candidates for studies related to optical switches and memories applications. Also, the primary attempts to isolate and characterize the new species formed upon heating the dark isomers of compounds **4.6** and **4.7** were not successful.

4.4 Conclusion

Based on the results in this chapter the following conclusions can be made:

(1) The photoisomerization process of N,C-chelate $BMes_2$ compounds is not limited to phenylpyridine-based chelates and can be considered a general phenomenon.

(2) Similar to the phenylpyridine-based $BMes_2$ compounds, the photoisomerization of the heterocyclic-based $BMes_2$ compounds is also initiated by a photo-induced charge transfer from the HOMO localized on the mesityl group closer to the $C_{Chelate}$ to the LUMO localized on the N,C-chelate moiety.

(3) The rate of the photoisomerization process is affected by the steric hindrance of the N,C-chelates (from the C side of the N,C-chelate), which hinders the photoisomerization process.

(4) Oxygen-based heterocyclic N,C-chelates seems to stabilize the charge transfer state and consequently slowdown the rate of photoisomerization.

(5) The heterocyclic-based $BMes_2$ compounds are generally thermally stable (up to 50°C), hence they cannot be considered a T-type photochromic compounds.

(6) The thermal behavior of the dark isomers of benzothiazole and benzooxazole-based $BMes_2$ compounds indicates the presence of different type of structural rearrangement, which could be the scope of a new study.

4.5 References

(1) (a) Bamfield, P. *Chromic Phenomena*; RSC, Cambridge, 2001. (b) Feringa, B. L. *Molecular Switches*; Wiley-VCH: Weinheim, Germany, 2001.

(2) Molander, G. A.; Canturk, B.; Kennedy, L. E. *J. Org. Chem.* **2009**, *74*, 973.

(3) Ribereau, P.; Queguiner, G. *Tetrahedron.* **1983**, *21*, 3593.

(4) Kondolff, I.; Doucet, H.; Santelli, M. *J. Mol. Catal. A: Chem.* **2007**, *269*, 110.

(5) Thomas, S. W.; Venkatesan, K.; Muller, P.; Swager, T. M. *J. Am. Chem. Soc.* **2006**, *128*, 16641.

(6) McCormick, T. M.; Liu, Q.; Wang, S. *Org. Lett.* **2007**, *9*, 4087.

(7) Lee, D.; Choi, M.; Yu, B.; Ryoo, R.; Taher, A.; Hossain, S.; Jin, M. *Adv. Synth. Catal.* **2009**, *351*, 2912.

(8) (a) Demas, N. J.; Crosby, G. A. *J. Am. Chem. Soc.* **1970**, *92*, 7262. (b) Fery-Forgues, S.; Lavabre, D. *J. Chem. Ed.* **1999**, *9*, 1260.

(9) Frisch, M. J.; et al. *Gaussian 03*, revision C.02; Gaussian, Inc.: Wallingford, CT, 2004.

(10) (a) Parker, C. A. Proc. R. Soc. London A 1953, 220, 104. (b) Abdallah, D.; Whelan, J.; Dust, J. M.; Hoz, S.; Buncel, E. *J. Phys. Chem. A.* **2009**, *113*, 6640.

(11) SHELXTL Version 6.14, Bruker AXS, 2000-2003.

(12) (a) Rao, Y. L.; Amarne, H.; Zhao, S. B.; McCormick, T. M.; Martic, S.; Sun, Y.; Wang, R. Y.; Wang, S. *J. Am. Chem. Soc.* **2008**, *130*, 12898. (b) Baik, C.; Hudson, Z, M.; Amarne, H.; Wang, S. *J. Am. Chem. Soc.* **2009**, *131*, 14549. (c) Amarne, H.; Baik, C.;

Murphy, S. K.; Wang, S. *Chem. Eur. J.* **2010**, *16*, 4750. (d) Baik, C.; Murphy, S. K.; Wang, S. *Angew. Chem., Int. Ed.* **2010**, *49*, 8224. (e) Wakamiya, A.; Taniguchi, T.; Yamaguchi, S. *Angew. Chem., Int. Ed.* **2008**, *47*, 834.

(13) Wilkey, J. D.; Schuster, G. B. *J. Am. Chem. Soc.* **1988**, *110*, 7569.

(14) (a) Carey, F. A.; Sundberg, R. J. *Advanced Organic Chemistry*; 3rd Ed.; Plenum Press: NY, 1990; *Part A*, pp: 6. (b) De Meijere, A. *Angew. Chem. Int. Ed.* **1979**, *18*, 809.

Chapter 5

Summary and Perspective

5.1 Summary and Conclusions

The initial goal of this work was to investigate the stability and photophysical properties of N,N- and N,C-chelate 4-coordinate organoboron compounds. The discovery of the photoisomerization of the N,C-chelate organoboron compounds shifted our efforts towards preparing and studying the photophysical and photochemical properties of new N,C-chelate organoboron compounds. It was found that the photoisomerization of the phenylpyridine-$BMes_2$ (**2.1**) was thermally reversible and the photoisomerization process goes through a C-C bond breaking/formation. The structure of the dark isomer was elucidated using NMR techniques, which was supported by DFT and TD-DFT calculations.

The role of the sterically demanding mesityl groups on boron was established by investigating compounds with less bulky substituents on the boron center. It was found that compound **3.6**, which has phenyl groups attached to the boron center instead of mesityl groups, did not have photochromic properties. It was also established that, the photoisomerization process can be influenced by the nature of the substituents on the phenylpyridine chelate ring.

To investigate the generality of the photoisomerization of 4-coordinate N,C-chelate organoboron compounds, a new series of compounds based on heterocyclic N,C-chelate organoborons were synthesized and studied. It was found that these compounds

undergo a photoisomerization process similar to that of phenylpyridine based compounds. The steric demand of the heterocyclic N,C-chelate ring and the nature of the heteroatom were found to have a pronounced effect on the photoisomerization of these compounds.

The research presented in this thesis established that N,C-chelate 4-coordinate organoboron compounds with bulky substituents on the boron center can generally undergo photoisomerization. Both the photoisomerization rate and the color of the dark isomer can be manipulated by the introduction of different types of substituents and N,C-chelates.

5.2 Future Directions

Future directions stemming from this work should focus on preparing substituted derivatives of the heterocycle-based N,C-chelate organoboron compounds to establish the effect of these substituents on the photoisomerization process and the color of the dark isomer. For example, different derivatives of compound **4.7** can be prepared as shown in Figure 5.1.

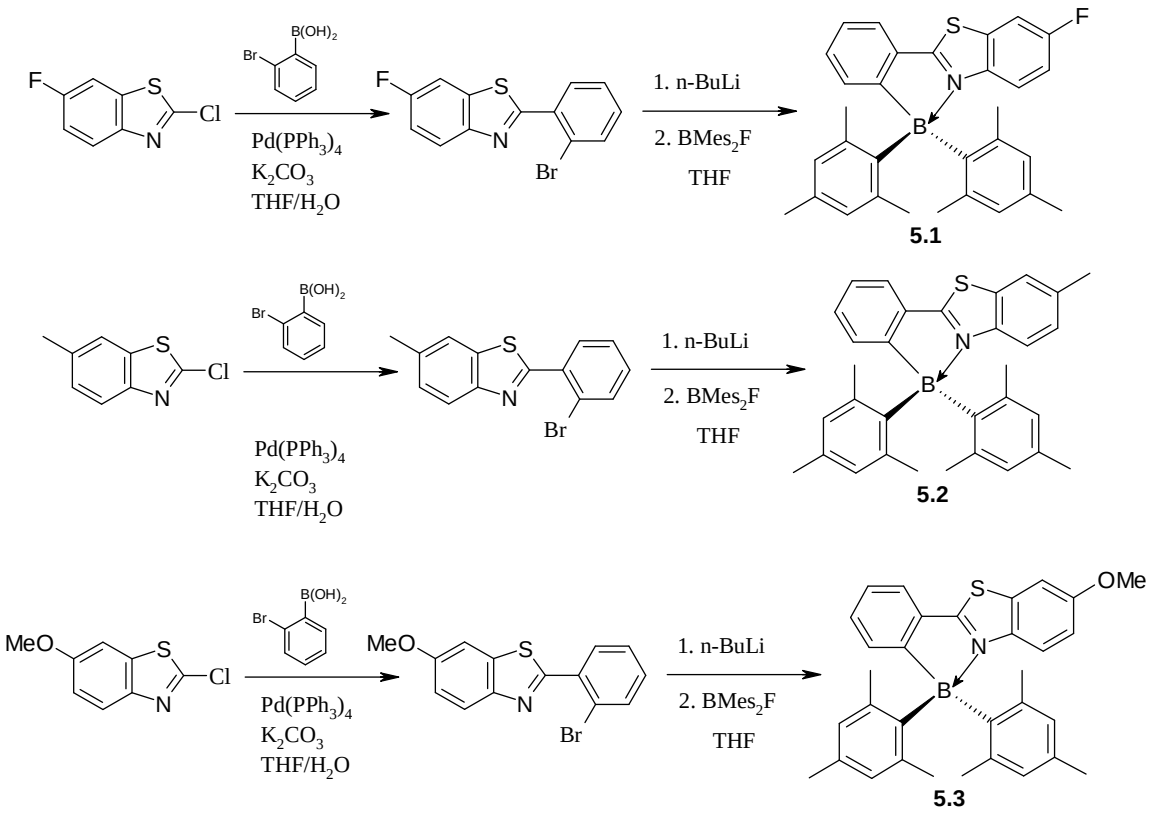

Figure 5.1 Synthetic routes to substituted benzothiazole N,C-chelate organoboron compounds **5.1**-**5.3**.

Our investigation established that for efficient and fast photoisomerization within this class of compounds the HOMO should be localized on one of the mesityl groups and the LUMO should be localized on the N,C-chelate ring. From this prospective DFT calculations can be used as a very useful tool to help predict whether an N,C-chelate organoboron compound can undergo photoisomerization or not.

DFT calculations were performed on compounds **5.1**-**5.3** and the HOMO and LUMO orbitals for all three compounds were found to be very similar to those of compound **4.7** as shown in Figure 5.2, which might further encourage us to prepare these compounds.

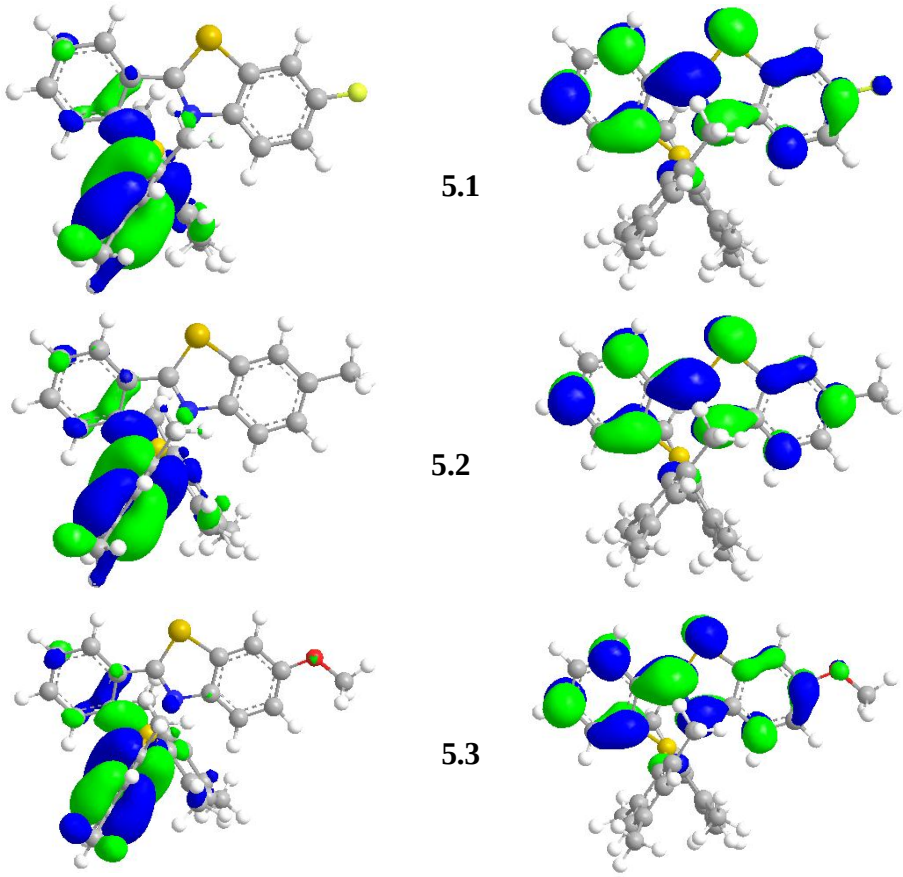

Figure 5.2 HOMO and LUMO orbital diagrams of proposed compounds **5.1**-**5.3**

Derivatives of N,C-chelate organoboron compounds based on bulky substituents other than the mesityl groups could be synthesized to further expand this class of organoborons. For example, compounds **5.4** and **5.5** (Figure 5.3) can be synthesized to further establish that sterically hindered aryl groups are a key factor in the photoisomerization process and to investigate the effect of different bulky aryl groups on the photoisomerization process.

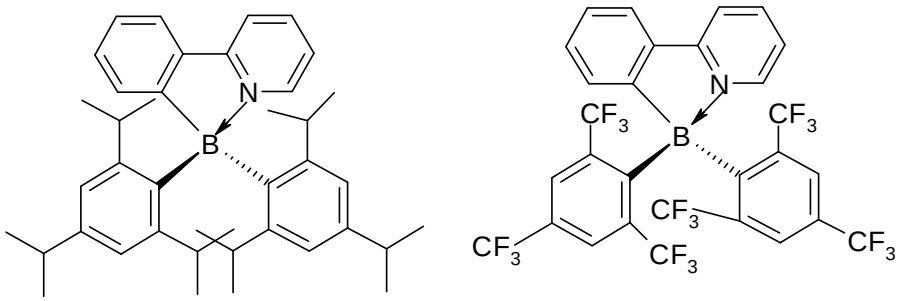

5.4 **5.5**

Figure 5.3 Structures of proposed N,C-chelate organoboron compounds **5.4** and **5.5**

Based on DFT calculations, the HOMO and LUMO of compound **5.4** are similar to those of other photochromic phenylpyridine-based organoboron compounds; hence upon successful synthesis of **5.4** we could expect that it would be photochromic and it would be possible to compare the effect of increasing the steric demand of the aryl groups, CH_3 to *i*-Pr, on the photoisomerization properties. On the other hand, both the HOMO and LUMO of **5.5** are mainly localized on the N,C-chelate ring and it would be expected that this compound will not have photochromic properties.

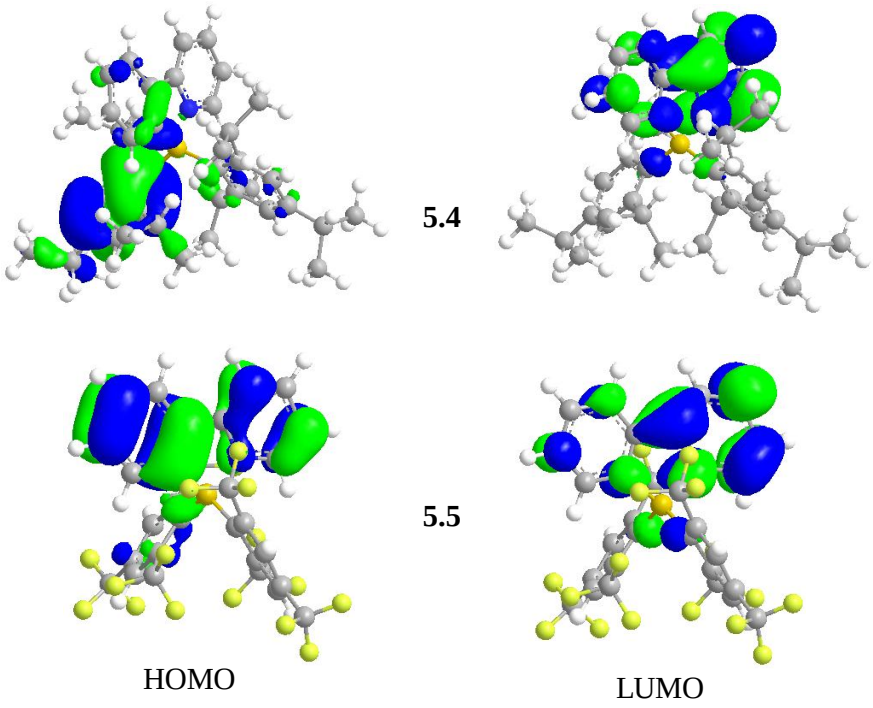

Figure 5.4 HOMO and LUMO orbital diagrams of proposed compounds **5.4** and **5.5**